UNIVERSITY OF SOUTHAMPTON

FACULTY OF ENGINEERING, SCIENCE AND MATHEMATICS

School of Electronics and Computer Science

Space Charge Determination in HVDC Power Cable and its Influence on Electric Field

By

Wilson Choo Chin Tze

Thesis for the degree of Doctor of Philosophy

May 2010

UNIVERSITY OF SOUTHAMPTON

ABSTRACT

FACULTY OF ENGINEERING, SCIENCE AND MATHEMATICS
SCHOOL OF ELECTRONICS AND COMPUTER SCIENCE

Doctor of Philosophy

SPACE CHARGE DETERMINATION IN HVDC POWER CABLE AND ITS INFLUENCE ON ELECTRIC FIELD

by Wilson Choo Chin Tze

Considerable amount of transmission and distribution of electricity is carried out by power cable. At present, most high voltage direct current (HVDC) installation uses traditional (oil-impregnated paper insulation and oil-filled-types) cables which pose a risk of environmental pollution in case of an accident.

Thus, significant advances and usage of polymeric material, notably cross-linked polyethylene (XLPE), have been made as the insulation material for power cables due to its economical production, environmental benefits and its electrical properties. However, unwanted disadvantages to its performance are featured when operated under direct current (DC) application. Such as the accumulation of comprehensive immobile charges in the XLPE, this superimposes to the Laplacian field resulting the changes of electric stress across the dielectric material. Additionally, in most HVDC transmission systems both the presence of temperature gradient across its insulation and bi-directional power flow are also needed to be considered. Space charge existence within the insulation is particularly dangerous in the event of polarity reversal, which has been recognised as the root source of breakdown in the early extruded insulation of commercial DC cables. High electric stresses within the insulation may be created, especially in the case when rated voltage is applied on the cable and with the presence of temperature gradient. Therefore, investigations are needed on both the space charge dynamics and also the accurate determination of electric field across the insulation of a full sized cable.

In this research, space charge accumulation within the polymeric material of a XLPE power cable is measured using a modified pulsed electro-acoustic (PEA) system with a current transformer attached. The presence of these accumulated space charges along with the consideration of conductivity influences the electric field distribution across the insulation material. As it is well known that the conductivity of an insulating material is dependent of both temperature and electric field, the coupled problems impose significant difficulty to know the electric field distribution in HVDC power cables.

In this thesis, scientific contributions have been made towards the research on power cables by allowing both users and cable designers to obtain a much more accurate

calculation of the total electric field. This total electric field calculation is based on the influences of both the variation of the conductivity and the space charge field across the insulation material under its specific temperature gradient. In addition, parameters pertinent to the insulation material of the power cable are obtained based on the hopping model of conduction in dielectric and are utilised in the calculation of the total electric field.

To stage the cables working under a real world HVDC transmission system scenario, experiments on the space charge dynamics of the full sized polymeric insulated cables were conducted by replicating it under the service conditions where both temperature gradient present across its insulation and bi-directional power flow are being considered. The field enhancement obtained within the cable under these scenarios allow us to estimate the lifetime of the power cable which are relatively important towards the power companies in realising the time for replacement of their aging cables.

In the polarity reversal experiments, results have shown that the total electric field is higher during polarity reversal when a 10 ^{0}C temperature gradient is applied across the insulation as compared to the application of no temperature and 20 ^{0}C temperature gradients. Therefore, this higher electric field due to the 10 ^{0}C temperature gradient will stage a higher potential risk due to the amount of heterocharge accumulation adjacent to the outer electrode.

Contents

List of Figures

List of Tables

Definitions and Abbreviations

Symbols	
C	Heat capacity
C_ρ	Heat capacity at a constant pressure
E	Electric field in V/m
k	Boltzmann's constant
T	Temperature (Kelvins)
K	Thermal conductivity
q	Elementary charge
Q	Heat source or a heat sink
u	Velocity field
ε_o	Permittivity of vacuum
ε_r	Relative permittivity
Pa	Pascal
ρ	Charge density (C/m^3)
$\rho(x)$	Space charge density (C/m^3)
φ	Thermal activation energy (eV)
σ	Conductivity

Abbreviations	
ABB	Asea Brown Boveri
ACSR	Aluminium Conductor Steel-Reinforced
ANSI	American National Standards Institute
ASEA	Allmänna Svenska Elektriska Aktiebolaget
Al	Aluminium
AC or ac	Alternating Current
CCV	Catenary Continuous Vulcanisation
CENELEC	Comité Européen de Normalisation Electrotechnique
CV	Continuous Vulcanisation
DC or dc	Direct Current
DCP	Dicumyl Peroxide
EHV	Extra-High Voltage
EPR	Ethylene Propylene Rubber
HDPE	High Density Polyethylene
HV	High Voltage
HVAC	High Voltage Alternating Current
HVDC	High Voltage Direct Current
ICEA	Insulated Cable Engineers Association
ICI	Imperial Chemical Industries
IEC	International Electrotechnical Commission
JEC	Japanese Electrotechnical Committee
LDPE	Low Density Polyethylene
LIMM	Laser Intensity Modulation Method
LIPP	Laser Induced Pressure Pulse
LLDPE	Linear Low-density Polyethylene
MDCV	Mitsubishi Dainichi Continuous Vulcanisation
MIND	Mass Impregnated Non-Draining
MV	Medium Voltage
PE	Polyethylene
PEA	Pulsed Electro-Acoustic
PMMA	Polyethyl Methacrylate

PP	Polypropylene
PVC	Polyvinyl Chloride
PVDF	Polyvinylidene Fluoride
PWP	Pressure Wave Propagation Method
SC	Semi-Conducting
SCLC	Space Charge Limited Conduction
SF_6	Sulfur Hexafluoride
TP	Thermal Pulse
VCV	Vertical Continuous Vulcanisation
XLPE	Cross-Linked Polyethylene

Publications

Conference Item：

1) Xu, Z., W. Choo and G. Chen. (2007). DC Electric Field Distribution in Planar Dielectric in the Presence of Space Charge. In: Proceedings of the International Conference on Solid Dielectrics: 514-517.

2) Chen, G., W. Choo and M. Fu. (2007). Electric Field Determination of Polymeric DC Power Cable in the Presence of Space Charge. In: Proceedings of the International Symposium on High Voltage Engineering.

3) Choo, W. and G. Chen. (2007). Electric Field Determination in DC Polymeric Power Cable in the Presence of Space Charge. In: Proceedings of the IEEE Conference on Electrical Insulation and Dielectric Phenomena: 489-492.

4) Choo, W. and G. Chen. (2008). Electric Field Determination in DC Polymeric Power Cable in the Presence of Space Charge and Temperature Gradient under dc Conditions. In: Proceedings of the 2008 International Conference on Condition Monitoring and Diagnosis: 321-324.

5) Choo, W., G. Chen and S. G. Swingler. (2009). Space Charge Accumulation under Effects of Temperature Gradient and Applied Voltage Reversal on Solid Dielectric DC Cable. In: Proceedings of the International Conference on Properties and Applications of Dielectric Materials: 946-949.

6) Choo, W., G. Chen and S. G. Swingler. (2009). Space Charge Accumulation under Effects of Temperature Gradient on Solid Dielectric DC Cable. In: Proceeding of the 16th International Symposium on High Voltage Engineering.

7) Choo, W., G. Chen and S. G. Swingler. (2010). Temperature Gradient Effect on the Conductivity of an XLPE Insulated Polymeric Power Cable. Submitted to the Proceedings of the International Conference on Solid Dielectrics.

8) Choo, W., G. Chen and S. G. Swingler. (2010). "The Effects of Temperature Gradients and Polarity Reversal on Space Charge Accumulation in XLPE Cable under DC Conditions," Submitted for Publication in IEEE Transactions on Dielectrics and Electrical Insulation.

9) Choo, W., G. Chen and S. G. Swingler. (2010). "Electric Field Determination in Polymeric Cable due to Space Charge Accumulation under DC Conditions under the Effects of Temperature Gradient," Submitted for Publication in IEEE Transactions on Dielectrics and Electrical Insulation.

Acknowledgements

This thesis on Space Charge Determination in HVDC Cable has been completed from findings of three years of research and troubleshooting.

Firstly, I am very grateful and would like to thank my research supervisor Dr George Chen for the chance and opportunity he has given me to pursue this PhD degree and the many long hours taken out of his busy schedules to participate and input to this process. The advice, patience and support given by him have been invaluable to me during the progress of my research.

My heartfelt appreciation and special thanks to my colleague, Dr Zhiqiang Xu, for the kind assistance that she has given me during my research through generously sharing of her viewpoint and suggestions for making this research possible.

I would also like to extend my thanks to the technical support team in the Tony Davies High Voltage Laboratory, Mr Richard Howell, Mr Michael A J Smith, Mr Brian Rogers and Mr Neil Palmer for the excellent assistance they provided to make the research possible and also creating the high voltage laboratory a pleasant atmosphere to work in.

Lastly, not to mention the most important peoples in my life that is my family – my late father George Choo, my mother Maureen Teo, elder brother Jason Choo and fiancée Elaine Pang for being extremely supportive and understanding throughout my studies.

Dad, I love and miss you very much and still think about you to this day. I only hope you are proud of your son, who is doing his best in life and keeps your memory alive.

Chapter 1 Introduction

1.1 Research Background

1.1.1 Developments and Historical Evolution of Power Transmission and Distribution

Exploring of electricity has been done since ancient times and progresses of it were not obtained until the seventeenth and eighteenth centuries. By the late nineteenth century, engineers were able to put electricity to industrial and residential area for usage. The rapid developments of the electrical equipment and technology within this period brought us the advances of electricity as a source of energy that remains the vital backbone of our modern industries which made the world what it is today. For the foreseeable future electrical power demand can be expected to grow as electricity is adapted to a massive and increasing number of applications in our lifestyle habits and also for the sustaining of the growth and modernisation of developing countries.

Energy demand is increasing worldwide, as for the past half century electrical demand has quintuple in some developed countries like United States, Japan and Germany. Nevertheless, the thirst for electricity for developing countries like India and China is getting even higher where China alone is building around two power stations each week to curb the future demands.

In present time, the cost of generation of electrical energy is increasing in a rapid rate due to the increases of oil prices as well as the demand for electricity. This situation suggests to us that this trend is likely to continue and leads us to the conclusion that there will be a greater need for the network performances of a country's power grid to compare favourably internationally. Thus, electrical networks are needed to be ensured

that they continue to meet the increasing stringent needs of the consumers where efforts are made to enhance the generation, transmission and distribution of reliable and quality power energy. With electricity as the life blood of a modern economy; it is becoming more important as we move into the information age. Electricity is transported around by complex of wires and transmission lines known as grid, where power is obtained from different sources and distributed to where they are needed providing a reliable and quality energy source to the consumers.

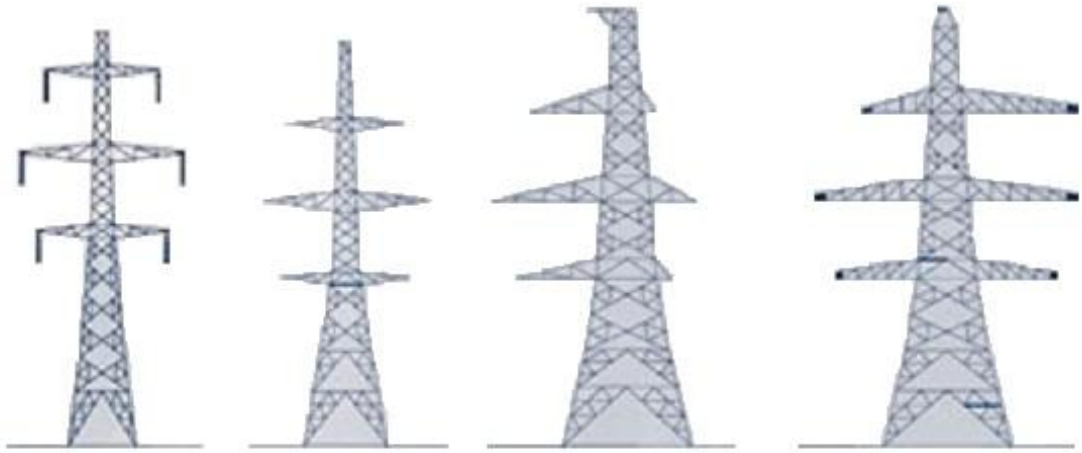

Figure 1-1: Types of overhead-line tower

There are basically two systems for the transmission and distribution of electrical power, namely the overhead transmission lines system and the underground cable system respectively. The overhead transmission lines system delivers electricity by means of a transmission line suspended by structures of poles or towers where units of suspension insulators are used to support the bare conductor (ACSR aluminium conductor, steel-reinforced). In Britain, most of the electric power is transmitted on the 275 kV and 400 kV supergrid. These supergrid conductors are suspended from insulator strings which consecutively are carried on towers about 50 meters high and spaced about 400 meters apart. Each of this tower or pylon usually carries two three-phase lines and one or more smaller shield wires made from steel (high- or extra-high-strength steel, or ACSR with much smaller cross-section than the phase conductors) at the top of the tower for lighting protection. Two main types of tower can be seen and distinguished as illustrated in Figure 1-1: Firstly, the straight-run tower which supports only the weight of the

conductors and insulators; and secondly, the deviation tower for changes in route that also resists some of the conductor tension.

The other system is the underground cable system where electricity is delivered by means of having the high voltage bulk transmission cables circuits placed underground. Methods of installing and laying of the cables underground depend on both the cable voltage classifications and the earth conditions. Four main methods of installing underground cables are illustrated in Table 1-1 [Weedy 1979].

Table 1-1: Methods of installing underground cables.

Underground Cable System	
Direct in the soil	• The cable is laid in a trench which is refilled with a backfill consisting of either the original soil or imported material of lower or more stable thermal resistivity materials.
In ducts or troughs	• Cable installed in ducts buried in the ground with an earth, sand or concrete surround.
In circular pipes	• Cables are drawn through pipes – this has an advantage of further cables installed without excavation.
In air	• Cables installed in tunnels built for other purposes.

At present, the overhead lines transmission system is still the most widely used method of transmitting and distributing of electrical energy throughout the world. The factor contributing to this is that the economic costs for installation and the maintenance of the underground cables is typically 10 times that of an equivalent transmission line, although this ratio decreases with the lower voltages. Secondly, when a cable is buried underground it is placed in a thermal blanket, where they have poor heat dissipation qualities and thus transmission capability is thermally limited and the additional capacitance (~0.22 μF/km) of the ground also results in less efficient power transmission, contrary to overhead line suspended on pylons which are cooled naturally by the surrounding air. Finally, fault detection of an overhead line can be easily detected and repaired at a much reasonable time frame. However, the overhead transmission line system is not absolutely perfect as it does come with some disadvantages like visual pollution, adequate area of clearance is needed for the risk of electrocution due to direct

contact with energised conductor.

Half a century ago, only one percent of the transmission lines in the United States were underground, this situation was mostly valid in the major urban centres. However, in the past two decades underground transmissions and distribution of electricity have gained popularity because of the escalating land prices as population increases leading to the growth of urbanisation. Furthermore, overhead lines would be impossible in the urban area due to safety or aesthetic factors, like the case of Singapore where 100 percent of the transmission of electricity uses underground cable of the range of 6.6 – 400 kV. Secondly, a fully underground transmissions cable system is enclosed within the ground contributing to a reliable and quality transmitting and distributing of electrical power. Such a system protects the system network from negative environmental conditions. Therefore, environmental damaging factors such as icing during winter, strong winds caused by typhoon, lighting strikes, dust and sand factors in desert area, and air-borne pollutants, which normally influence the efficient operation of the overhead line, are eradicated. The negative damage factors vulnerable towards the cables are reduced to damage caused by earthworks and with only one nature disaster that might affect the efficient operation of the underground cable is the damage caused by strong tremors of an earthquake.

1.1.2 Developments and Historical Evolution of DC Transmission

The first commercially generated electricity was a DC electrical power produced by Thomas Alva Edison at the end of nineteenth century. Thus, DC systems were the earliest electricity transmission systems used. However in these early years, DC electrical power was unable to be transmitted over a long distance under the application of a low voltage due to the inherent loss. The difficulty of increasing the voltage for DC systems in this early days led eventually to the popularity of alternating current (AC) systems, pioneered by Tesla and Westinghouse (1890's), which allowed a simpler and a more efficient way of increasing or reducing the voltage using transformers. This development eventually converged to the high voltage AC (HVAC) power system popular today. The main reason for high voltage transmission over long distances is the need to reduce the power loss caused by the resistance of the conductors (I^2R). Without a high voltage the dissipation of energy would make the transmission of electrical

power over long distances impossible. Nevertheless, through the research and development of HV valves, practical manipulation of DC voltages can be achieved. This led HVDC transmission systems attaining more and more popularity recently.

Table 1-2: Summary of direct current (DC) transmission

The use of direct current (DC)	
Economical Advantage	• A critical length of lines above where the use of DC is more economical (for overhead lines a critical distance is 550-750 km, whereas, underground cables are 60 km and above).
Technical Advantages	• Connection of large systems through links of small capacity where DC line is asynchronous or flexible link between two rigid systems (eg. Britain – France cross-Channel link). • Reasonable transmission distances are needed via HVDC cables (limitation of AC cables due to charging current). • Interconnection to AC systems of different frequencies. • Synchronous operation is not necessary and the distance is not restricted by stability. • Corona loss is substantially less than for AC line (less interference with radio and television transmission). • Possibility of monopolar operation (one side of the bipolar line becomes grounded).
Disadvantages	• Difficult conditions for circuit breaking. • Voltage transformation has to be provided on the AC sides of the system. • Rectifier and inverters absorbed reactive power must be supplied locally. • Large filters are needed to prevent harmonics pollution into the systems. • DC converting stations are more expensive than conventional AC stations. • Converters are needed at each end of the line operating as a rectifier (AC to DC) or inverter (power transfer DC to AC) allowing bi-directional power flow.

DC power transmission has several advantages over alternating current (AC) transmission. These advantages include no length limit which is applicable for both overhead lines and underground cables. Secondly, rapid power flow control can be obtained by providing improvements in stability on the connection of HVDC along with the adjoining AC system. Finally, the operating cost is lower due to low conductor loss and no power loss. Further advantages and disadvantages of DC transmission are shown in Table 1-2.

Therefore, electric power HVDC transmission systems are essential and employed for the transmission of electricity. The earliest method of HVDC transmission was designed by Swiss engineer Rene Thury [Donald et al 1978] and with the present form of HVDC transmission technology developed by the Swedish industrial company Allmänna Svenska Elektriska Aktiebolaget (ASEA) in the 1930s, which is now a holding company owning half of Asea Brown Boveri (ABB), who led the beginning of a modern era of power transmission. In 1954, the first commercial modern HVDC started to take place where a DC line began service at 100 kV from Vastervick on the main land of Sweden to Visby on the island of Gotland, covering a distance of 100 km across the Baltic Sea. By 2006, a world's longest submarine cable of 400 kV HVDC is being laid on Murraylink (Australia) with a length of 290 km.

1.2 Research Objective and Aims

The developments in the world of cable technology have stretched for almost 200 years since the first documentation of cables or wires was reported in 1812. Materials used for the insulation of the cable have progressed tremendously throughout the years and with cross-linked polyethylene (XLPE) emerging as the world's preferred insulation for underground power cables.

XLPE material is economically produced providing both cost efficiency in the operation and procurement. One of the reasons for the significant increase of using XLPE as an insulation material is the benefits towards the environment we are living in when

comparing with the older impregnated paper insulation. Furthermore, XLPE insulations have excellent high dielectric strength and electrical resistivity in combination with some excellent physical properties such as resistance to cracking and moisture penetration. However, good dielectric properties may also bring some unwanted drawbacks to its performance under certain work conditions especially under DC conditions. Such as, the low charge carrier mobility and charge trapping within the XLPE insulation give rise to space charge, resulting in localised electric stress enhancement which will contribute to the breakdown of the cable when the threshold level of the cable's insulation is exceeded.

Although investigations on the electric field distribution across the polymeric insulation of the power cables under DC conditions have been made previously, these efforts were insignificant as modest understanding on the formation and accumulation of space charge phenomenon were known besides space charge complexity due to various factors such as the chemical and physical arrangement of the polymeric insulation material, chemical additives, electrodes material and conditions, voltage application, temperature across insulation, aging and so on are also needed to be considered [Mizutani 1994; Takada 1999]. In addition, the method of obtaining space charges measurement under a solid polymeric material is rather difficult due to the ideal of obtaining the measurement in a non-destructively manner.

Following the progress made in non-destructive mapping of space charge distribution in polymeric material, several techniques have been developed and applied not only to plaque samples due to their easy manufacture as well as cable samples. However, the influence of space charge on the electric field distribution in cables so far has been obtained without considering the effects of both temperature and electric field on conductivity. Therefore, this will result in some error in electric field distribution as it is well known that the electric field under DC conditions is determined by conductivity.

A replica of a cable under load conditions was set up and space charge accumulations were being measured and observed. Through the application of these experiments under DC supply, a clearer overview on the underlying theoretical principles and phenomenon of space charge within the insulated XLPE power cable can be obtained. This investigation is needed as it can create a cost effective XLPE insulated cable for the

industries and electric utilities and also providing them with a dependable extended service life.

The general objective of this thesis was to obtain a better understanding of the space charge process and its influence on electric field in HVDC power cables. To reach this objective the following steps were taken:

1. A method of numerically compute the electric field distribution within the polymeric material under the influence of space charge field and the conductivity variation with the temperature and space charge was developed.

2. A measurement technique and the necessary measurement apparatus to measure space charge distribution within the insulation of power cable samples replicating the load conditions was setup, tested and confirmed.

3. Using the developed measurement techniques, measurement setup and computational method the effect of bi-direction power flow over the space charge in HVDC transmission systems was studied.

1.3 Outline of the Thesis

This thesis concentrates on the analysis of accumulation and measurements of space charge obtained from XLPE cables under the application of DC supply. The thesis is divided into 10 chapters as follows:

Chapter 2 ***XLPE Insulated Power Cable***. This chapter gives a brief introduction about the developments and historical evolution of XLPE power cable. The power cable structure and the materials used as its insulation and also the manufacturing process for the production of a XLPE power cable.

Chapter 3 ***Classification and Properties of Polymers and Space Charge***. This chapter introduces the different chemical, physical structure and properties of different

individual types of polyethylene. In addition, principle of space charge formation and the mechanisms that govern these processes are also discussed.

Chapter 4 ***Space Charge Measurement Techniques***. This chapter introduces the different types of techniques that are used for space charge measurements in both polymeric insulating samples and power cable samples. Brief introductions of the working principle as well as the comparisons between various techniques were made. In addition, the modified pulsed electric acoustic (PEA) system for cables is described systematically and also a brief introduction is given on its data processing technique on the geometry and acoustic propagation compensation needed for the signal processing of data due to the cable coaxial geometry.

Chapter 5 ***Electric Field Determination in the Presence of Space Charge and Temperature Gradient using COMSOL***. This chapter introduces the electric field determination in the presence of space charge and temperature gradient in power cable using COMSOL a numerical simulation software package. This allows us to provide a clear overview on the underlying theoretical principles and phenomenon of space charge through the determination of results obtained from the polymeric material, where conductivity together with the influence of space charge field and subsequently electric field distribution within the polymeric material can be considered.

Chapter 6 ***Space Charge Measurements on XLPE Cable with and without Temperature Gradient***. A modified PEA system with a current transformer attached is used to obtain space charge measurements on a commercially available XLPE polymeric insulated power cable under the consideration of both with and without temperature gradient across its insulation. Subsequently, based on the space charge measurements obtained, the total electric field distribution across the insulation is then calculated.

Chapter 7 ***Conductivity of the DC Power Cable's XLPE Insulation Material***. A strip of the XLPE insulation used in the power cable is peeled off. Transient leakage currents of the peeling were then measured and analysed by means of an electric current measuring equipment under controlled temperature conditions. Subsequently, investigation on the conductivity of the XLPE insulation under different temperature conditions can be

obtained based on the initial measurements of leakage current. In addition, parameters of the conductivity equation based on the hopping model of conduction in dielectric are obtained for the calculation of electric field distribution across the XLPE insulation of the cable.

Chapter 8 ***Effects of Temperature Gradient and Polarity Reversal on Space Charge Accumulation in XLPE Cable***. This chapter describes the effects of temperature gradient towards the accumulated space charge within both the degassed and un-degassed cable's XLPE insulation and also the responses of each cable under specific condition towards a polarity reversal. The space charge profiles were then used to derive the before and after the polarity reversal electric stress across the insulation using its own conductivity parameters based on the hopping theory model. Subsequently, the electric stress enhancement is used to estimate the reduction towards the cable's life.

Chapter 9 ***Investigation of Problems Encountered in Space Charge Measurement of Cable when under Temperature Gradient***. In this chapter, we shall discuss the problems encountered during the space charge measurements of the cable's insulation when under the application of temperature gradient. Subsequently, the solution towards this problem will be presented and discussed. In addition, explanation was also made on the experimental failure of the degassed cable when under temperature conditions.

Chapter 10 ***Conclusion and Suggested Future Work***. In this chapter, the whole project is summarised and some further works are suggested.

Chapter 2 XLPE Insulated Power Cable

2.1 High Voltage Direct Current Cable

2.1.1 Developments and Historical Evolution of HVDC Cable

Nowadays, considerable amount of transmission and distribution of electrical power is accomplished by underground power cables through electrical networks, which form an important component of the power system. The large diversity of uses, service conditions, and technological methods associated with the manufacturing and installation of polymeric insulated power cables have resulted in a large number of materials, designs and productions. These materials and designs have undergone impressive developments for the past two centuries as illustrated in Table 2-1 [Orton and Hartlein 2006].

During the last century itself, developments on the insulation of power cable shifted from lead-covered, fluid impregnated paper to polymer based insulation due to the economical cost of manufacturing and maintenance and also environmental concerns towards the insulation used (eg. lead sheath and oil fluid).

Table 2-1: The history of cable developments [Orton and Hartlein 2006]

Year	Developments
1812	First rubber varnish-insulated wires used for detonating a mine – Schilling (Russia).
1850	First subsea telegraphs cable between Dover (England) and Calais (France) and First trans-Atlantic submarine telegraphs cable.
1880	DC cables insulated with jute in "Street Pipes" – Thomas Edison (USA).
1890	10kV tubular cable and paper insulation introduced – Sebastian Ferranti (England).
1900	Natural rubber insulation used on cables.
1925	First pressurised paper cables.
1930	First commercial production of PVC in Germany.
1937	Polyethylene (PE) developed in England.
1942	First application using Polyethylene (PE) in cables.
1954	First DC power transmission cable in Gotland (Sweden).
1963	Invention of XLPE by General Electric Company.
1968	First use of XLPE cables for medium voltage (MV).
1972	Introduction of extruded semi-conducting screens.
1978	Widespread use of polymeric jackets in North America.
1988	First application of 500 kV XLPE cables without joints within a pump storage scheme in Japan.
2000	First application of 500 kV XLPE cables with joints installed under long distance in Tokyo (Japan).
2006	World's longest submarine cable in Basslink (Australia)

2.2 Power Cable Structure and Materials

The design and configuration of a power cable may appear plainly simple. However, technical specification and guarantees associated with the design, starting from the cable conductor and continuing to the protective outer layer, are strictly scrutinised to assure the reliability of its performance during service. A typical XLPE polymeric insulated power cable is shown in Figure 2-1.

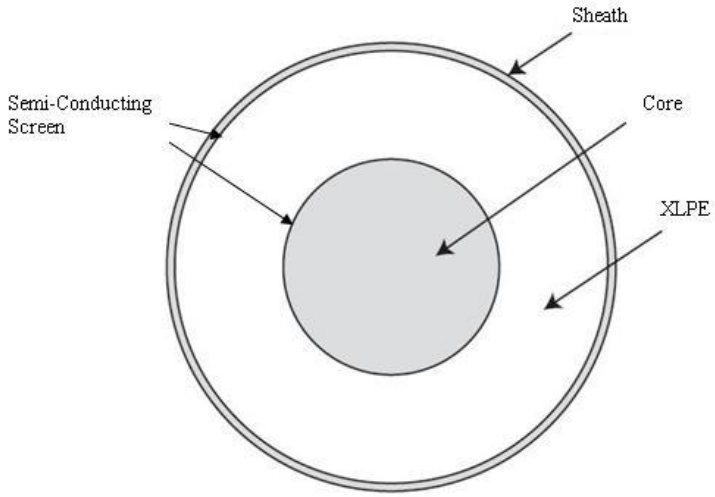

Figure 2-1: Cross-section of a XLPE polymeric insulated power cable

2.2.1 Conductor Materials

Both copper and aluminium materials are widely used as the choice for the conductor of a power cable. However, this choice varies from country to country (UK utilities rationalised aluminium) depending on certain factors. Development in recent years has shown a widespread use of aluminium as the conductor due to the progress made on the effective joints which are in practice subjected to thermal cycling and creep. However, the main reason is that over the years copper prices have been much higher than aluminium in the prevailing market.

Nevertheless, many other detail points (eg. applications) are needed to consider before making the choice between copper and aluminium as both materials have their individual advantages and disadvantages. Comparisons of possible conductor materials are given in Table 2-2.

Table 2-2: Conductor materials used for power transmission cables

Materials	Advantage	Disadvantage
Aluminium	• Inexpensive.	• Both electrical and thermal conductivity is ~60% of copper.
Copper	• High electrical and thermal conductivity.	• Expensive.
Silver	• Slightly better than copper in both electrical and thermal conductivity.	• Extremely expensive.
Sodium	• Extremely inexpensive.	• Safety issues on handling and maintenance. • Poor electrical and thermal conductivity.

2.2.2 Insulation Materials

Power cables are usually named under their insulation system since electrical insulation is a determining factor in the cable design. These materials are used to separate the current carrying conductor from the ground potential. At present, fluid-impregnated paper which has been used as insulation for the past century is commonly found in the underground electrical networks. However, with the developments of polymeric material, extruded polymer insulations are becoming the standard choice for power cables.

2.2.2.1 Paper insulation

At the moment, most present HVDC installations around the world use the traditional oil-impregnated paper insulation. This insulation has provided a satisfactory history at all voltage levels and the common reason for failure is due to the cracked or corroded lead sheath which allows moisture penetration through the insulation. More recently, paper insulations are becoming less popular and are now rarely specified for new

installations due to the environmental issues concerning the lead sheath and the impregnating fluid (eg. oil).

2.2.2.2 Polyvinyl chloride (PVC)

Since its first commercial production in Germany during the 1930s, PVC insulation has been particularly widely used in replacing rubber and paper insulation till the early 1960s due to its properties of being not affected by moisture, therefore, metallic sheath is not required. The lightness, toughness and chemical resistance of its properties also provide easier installations; consequently, they became quickly adopted in industries for installation. However, this trend was set to change ever since the introduction of PE and XLPE as these PE materials boasts better electrical and thermal properties as compared to PVC. Consequently, PVC insulation is now used on power cables with only less than 1 kV rating due to its high failure rate during service.

2.2.2.3 Polyethylene (PE)

PE was first developed in the early 1930s and was further used as an insulation as early as 1943. There is a clear move of cable insulation towards polymeric materials from the traditional paper insulation due to the ease of processing and low production cost of modern polymeric compounds. In addition, its durability, good electrical properties and resistance towards moisture and chemical are also the contributing factors that facilitate the change. Nevertheless, PE also does come with some drawbacks like water treeing growth within the insulation when under electric field exposure in a wet condition and also partial discharge erosion due to poor electrical tracking resistance. But the main disadvantage of all is the maximum operating temperature of PE is 70 ^{0}C, which fluid-impregnated paper insulated has an operating temperature between 80 – 90 ^{0}C. This problem is quickly overcome by the introduction of XLPE to the family of PE where the melting point is greatly enhanced and the thermal capabilities exceeding the rating of insulation using fluid-impregnated paper. Further description on the properties and morphology of PE will be discussed in Chapter 3.

2.2.2.4 Cross-linked polyethylene (XLPE)

Invention on XLPE was made in 1963 at the General Electric Research Laboratory in Niskayuna, New York [Precopio and Gilbert 1999]. It was reported at early 1970s; countries in Europe and Scandinavian as well as Japan had swung towards using XLPE insulated power cables.

The XLPE is a thermosetting material achieved by mixing of LDPE as a base resin and other several additives. These components comprise of water tree retardant package and anti-oxidation package for limiting and minimising the water tree growth and oxidation respectively within the XLPE insulation. Furthermore, additional compound either peroxide or moisture curing compound is added to the blend for the initiation of cross-linking depending on the curing technique used by the cable manufacturer. Through this process, a better thermal performance material with excellent electrical and mechanical properties is achieved. With these enhanced properties, XLPE can be used in a large range of voltage application up to 500 kV. Further description on the properties and morphology of XLPE will be discussed in Chapter 3.

2.2.3 Conductor and Insulation Screens

In a typical construction of a high voltage XLPE cable as shown previously in Figure 2-1. Extrusion of both the inner and outer semi-conducting (SC) screens was done simultaneously together with the XLPE insulation during production giving the final product in a three layer arrangement (SC-XLPE-SC).

Both conductor and insulator SC screens are based on carbon black material manufactured via the absolute and forced combustion of hydrocarbons, which are later scattered within a polymer matrix consisting of organic peroxide for cross-linking and also antioxidant for stability. The concentration of carbon black of a conductor screen is around 30 - 40 percent to achieve the required conductivity at the interface where the conductor screen will have the same electrical potential as the conductor, therefore, providing a uniform field with the insulation. Secondly, the incorporation between the conductor and insulation material portion of the extruded cable is to ensure a smooth

interface between both materials where occurrence of regions with high electric stress is decreased.

On the other hand, the function of the outer SC insulation screen is to ensure a smooth interface with the XLPE material by not having any uneven surfaces between them. Therefore, ensuring the electric field is contained within the core of the cable providing that the outer surface is maintained at ground potential [Burns and Eichhorn et al. 1992].

2.3 Basic Manufacture of a Power Cable

The manufacturing of a power cable consists of many stages and these stages are dependable on what type of cables that are going to be manufactured and its application. There are basically four major types of power cables widely used in the power industries and these underground power cables are distinguished by their insulation as illustrated in Table 2-3:

Table 2-3: Types of underground power cable insulation

Types of Cable's Insulation	**Descriptions**
Polymeric insulation	• LDPE, HDPE, XLPE and EPR etc. insulated.
Paper tape form Self-contained fluid-fill insulation	• Paper or polypropylene paper laminated with biodegradable fluid (refined mineral oil eg. oil-rosin).
Mass-impregnated non-draining (MIND) insulation	• Paper insulation with impregnated MIND compounds (exceptionally low-viscosity poly-butene) that does not flow under service temperature.
High pressured fluid/gas insulation	• Paper insulated with impregnated by high pressure fluid (oil) or gas (SF_6) installed in trefoil pressure pipes.

In this section, focus will be on the manufacturing of a polymeric XLPE insulated power cable since XLPE is presently the most preferred used insulation material for

power cables; and is gradually replacing traditional oil-impregnated paper insulation.

In the process of manufacturing a XLPE insulated power cable, four main stages are associated as shown in Figure 2-2.

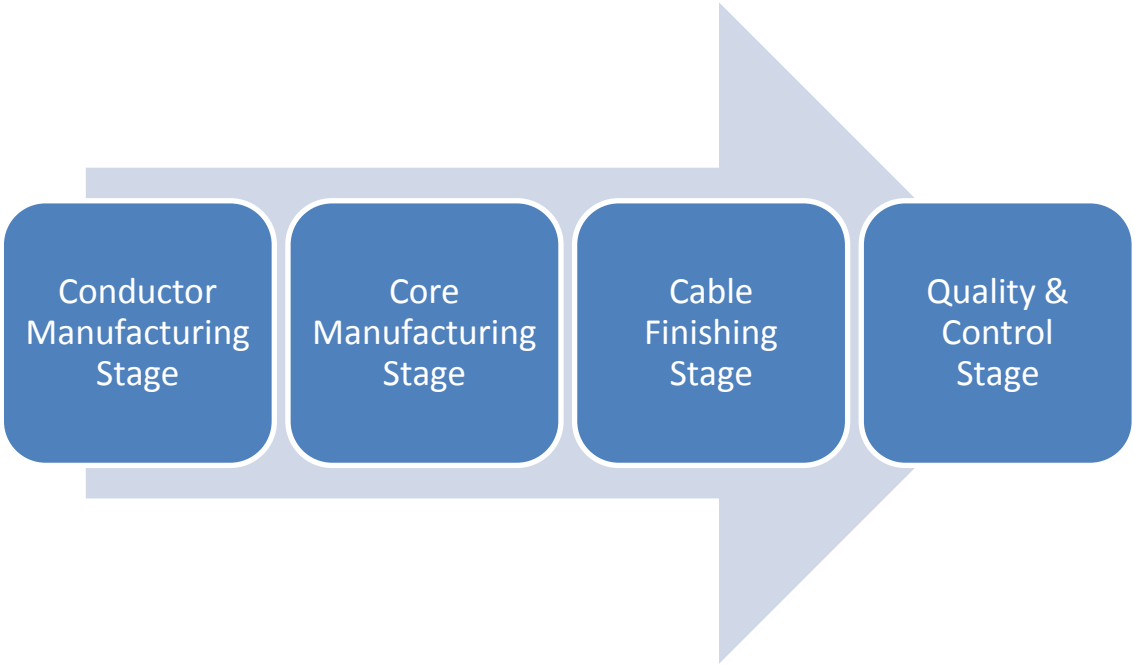

Figure 2-2: Basic process flow of manufacturing XLPE polymeric insulated power cable

2.3.1 Conductor Manufacturing Stage

In some cable manufacturing companies, the production of conductor within the power cables are achieved by two schemes:

1. Fully ready-made metal conductors acquired from metal companies.
2. Acquisition of metals (Copper or Aluminium) rod to draw and strand their own conductor.

For the later scheme, the process embarks by entering of the metal rod into the wire drawing machine. Within this machine, continuous series of dies are used to reduce the diameter of the metal rod to a specific value required where large amount of lubricants are streamed throughout this process. The end product wires are constantly annealed

under steam atmosphere through inductive heating process. Subsequently, these wires are stranded by a conventional practice where a layer of six wires lay over one wire and then succeeding layers, with lay reversal on each layer, leading to an increase of total wires (7, 19 and 37 wires) to form a conductor.

2.3.2 Core Manufacturing Stage

The manufacturing of a cable's core during the whole cable manufacturing process is the most vital and complicated process towards the performance and reliability of the cable during its service life. To produce a quality extruded cable, many sub-stages are needed to work properly and concurrently with each other. The core manufacturing can be divided into 3 main stages as shown in Figure 2-3.

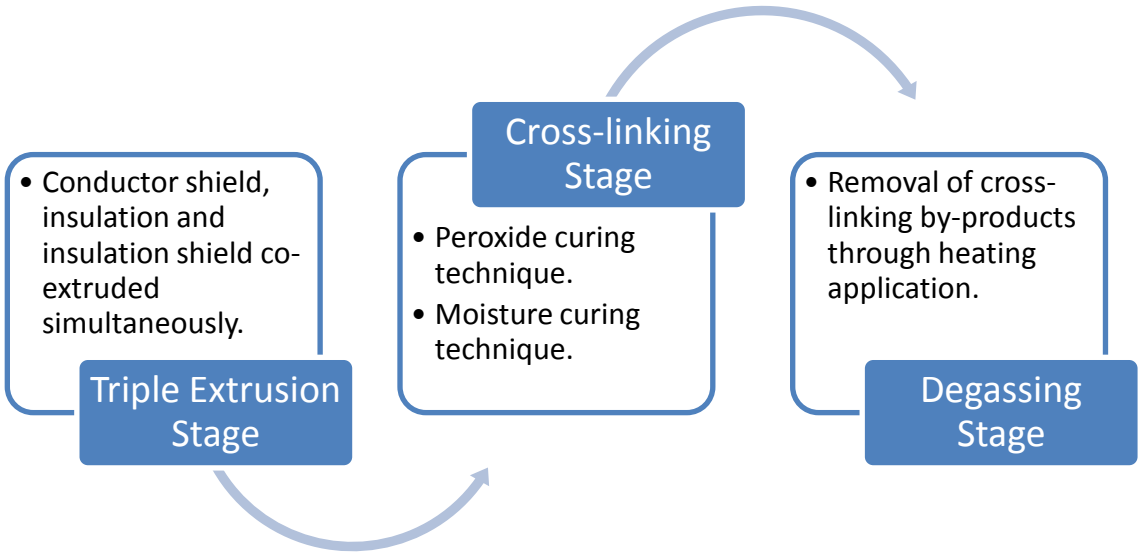

Figure 2-3: Process flow of core manufacturing

2.3.2.1 Triple extrusion stage

The extrusion process occurs when pellets of the polymeric material and semi-conducting materials are fed into the hopper of the extruders. The material is melted within the extruder through a long heated barrel by a revolving Archimedean screw. This melted product is pressurised and flows towards the end of the barrel where the extrusion head is located and where formation of respective cable layers are constructed.

Any speck or impurities that may be present within the melted material are being removed by filters that are found between the end of the screw and the extrusion head [Hampton, Hartlein et al. 2007].

At present, there are two methods implemented by cable manufacturers for a triple extrusion where all three core layers are being formed at once as shown in Table 2-4. For further illustration, drawings of this enhanced and highly sophisticated true triple extruder is shown in Figure 2-4.

Table 2-4: Methods of triple extrusion

Methods	Descriptions
1+2 triple extrusion	• The inner semi-conducting screen is extruded initially. Subsequently, the insulation and outer semi-conducting screen are co-extruded over the inner semi-conducting screen after a short distance of approximate 2 - 5 meters.
True triple extrusion	• The inner SC screen, insulation material and outer SC screen are co-extruded concurrently.

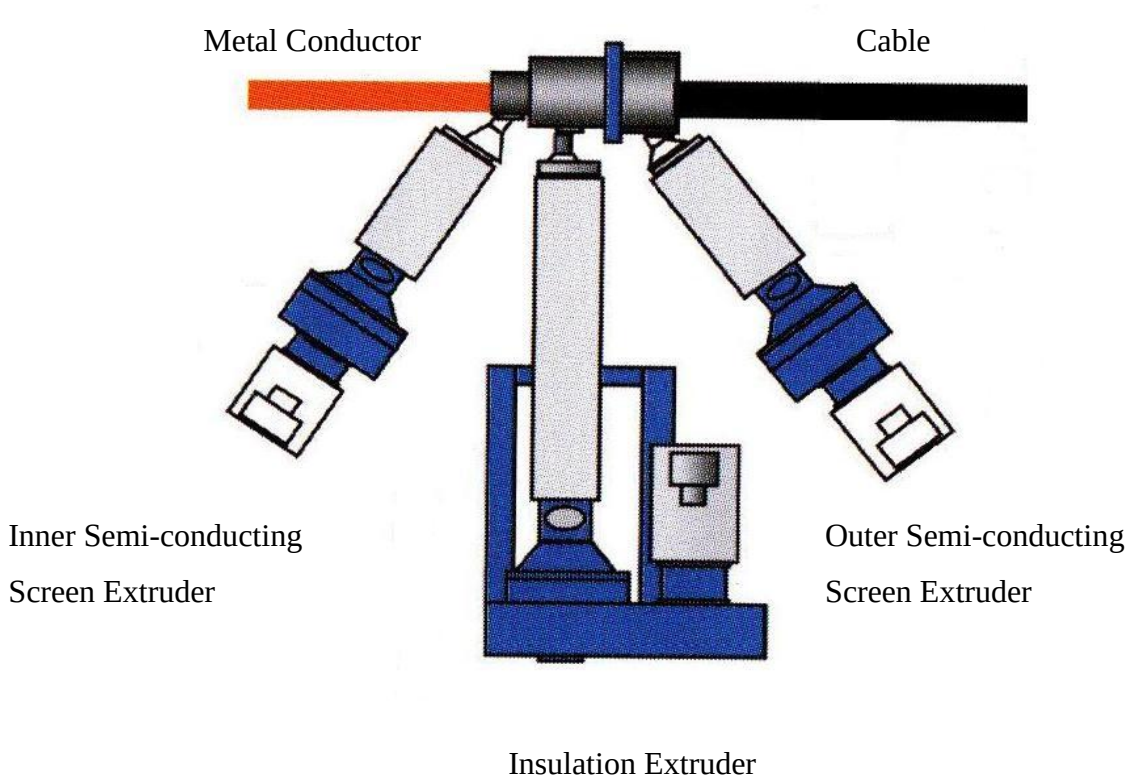

Figure 2-4: Drawing of a true triple extruder

2.3.2.2 Cross-linking stage

After extrusion has been done, the three layer core of the cable is still being uncross-linked, i.e. the polymeric material is still a thermoplastic. Therefore, a curing (vulcanising) process is needed to transform the polymeric material into a thermosetting material through cross-linking. The most commonly used commercial techniques for XLPE cable extrusion and curing are shown in Figure 2-5.

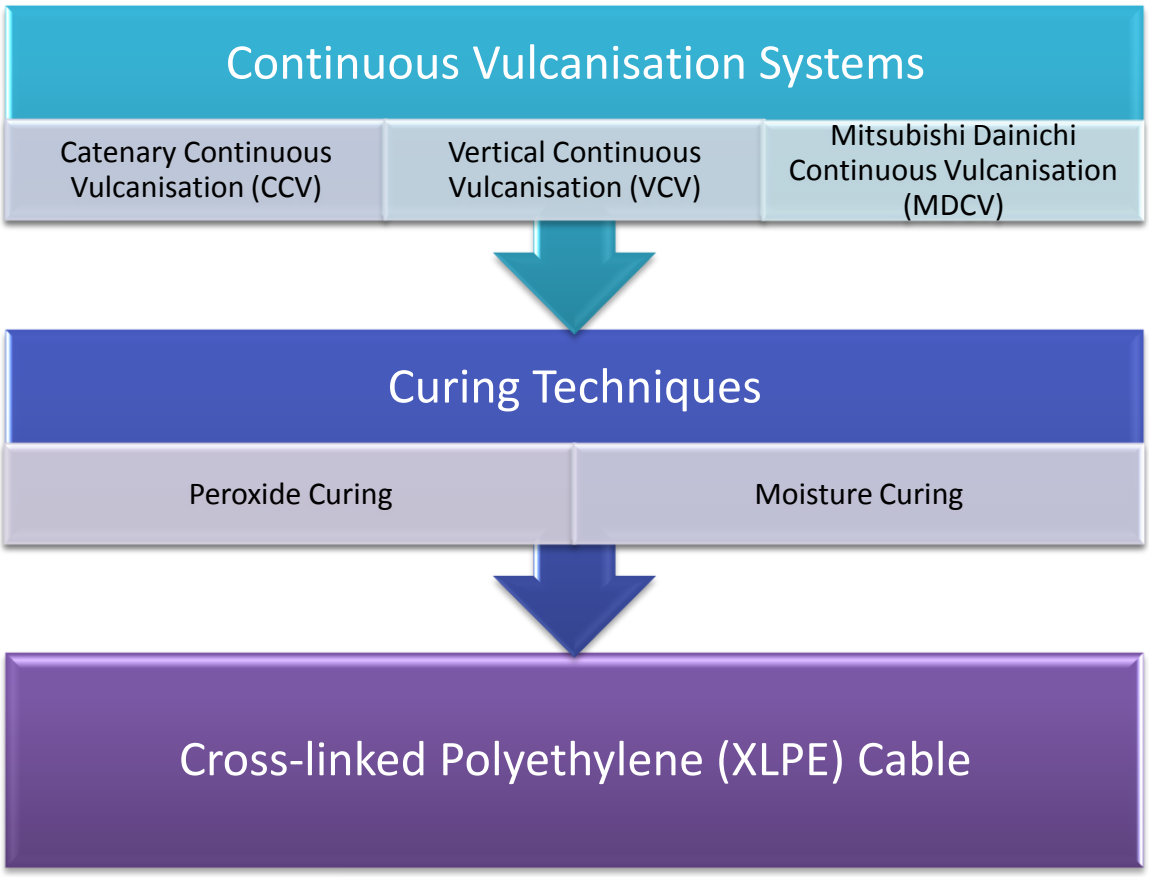

Figure 2-5: Common extrusion and curing techniques on XLPE cable

Catenary and Vertical Continuous Vulcanisation (CCV and VCV)

The CCV system has an arrangement of having the curing tube supported at its ends and acted only on by its own weight. Once the uncross-linked cable has been made by the true triple extruder, the cable goes through a tube that is attached firmly to the extruder head where high pressurised nitrogen gas (dry curing) or steam at a temperature of 300^0C within the tube is admitted for the curing process. The lower part of the tube is filled with water or cooled nitrogen for cooling down the hot cable where normal handling of the cable could be done for drumming [Hampton 1995].

The VCV system has the same working principles of a CCV system. The only difference between them is the configuration of the curing tube where it is vertically placed and the cable is maintained in the centre of the tube through tensioning. Further differences between CCV and VCV systems are illustrated in Figure 2-6 and Figure 2-7 shows the schematic diagrams of a CCV and VCV systems.

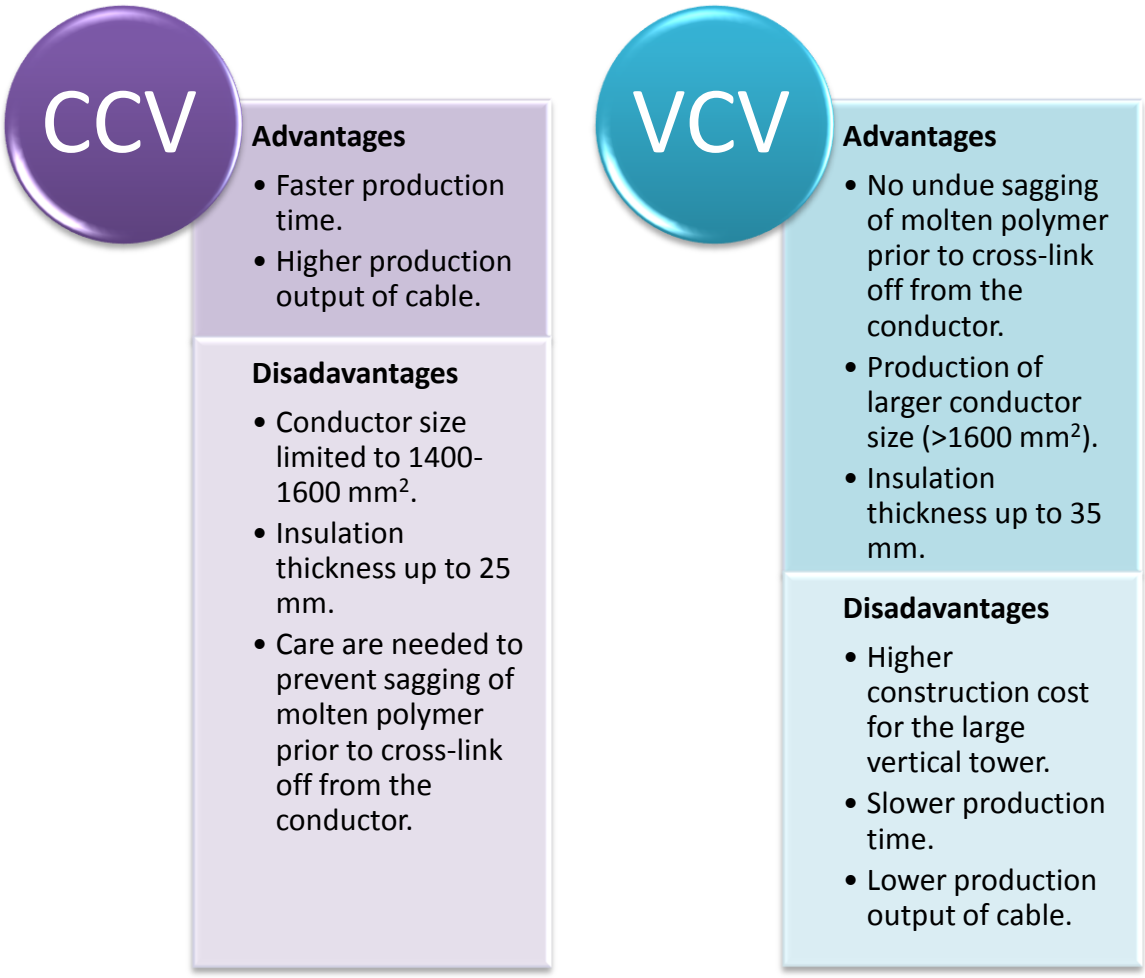

Figure 2-6: CCV and VCV systems advantages and disadvantages

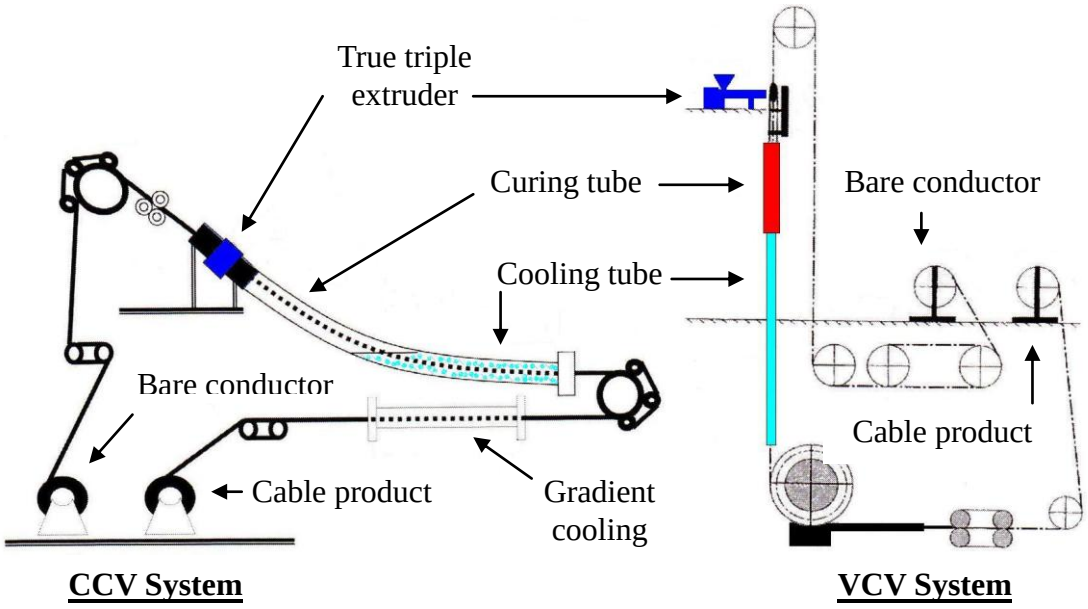

Figure 2-7: Schematic diagrams of a CCV and VCV systems

Mitsubishi Dainichi Continuous Vulcanisation (MDCV)

The MDCV system is also known as Long Land Die process, which is developed by the cooperation of Mitsubishi and Dainichi in the 1970s. The configuration of this system is built compactly and horizontally as shown in Figure 2-8. Curing is done through a heated tube formed by the extension of the die of the extruder, which stretches several meters in length. Curing is achieved by thermal heating of the tube rather than using nitrogen and hot steam methods. This system is normally used for the manufacturing of HV and EHV cables as void formations are eradicated significantly.

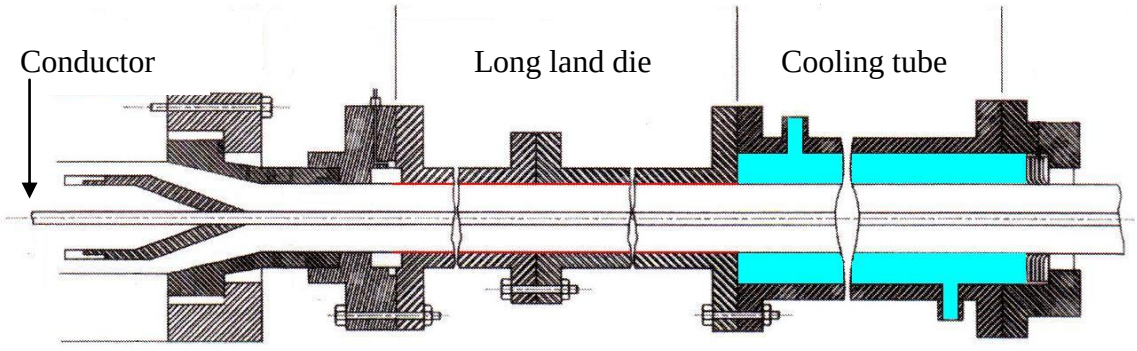

Figure 2-8: Schematic diagrams of a MDCV system

2.3.2.3 Degassing stage

To ensure a long-term performance of insulating material used in cable when put into operation. There is a need for all power cables especially the high voltage (HV) and extra voltage (EHV) cables to have its by-products removed or reduced in content within the insulation, otherwise a series of problems are left within the XLPE matrix [Bamji and Bulinski 1995; Maeno, Hirai et al. 2005]. Since all peroxide-cured cables will retain some of the decomposition by-products (eg. acetophenone, α-methylstyrene, cumyl alcohol and methane) within their structure.

In the industries, different methods are used to degas cables while it is quite common to allow MV cables to degas naturally by storing them for some days (7 days) before shielding and routine testing. For degassing of thick insulated HV and EHV transmission cables, the cables are placed in large heated chambers under moderate temperature between 50 – 80 ^{0}C to remove the volatile by-products and additives.

Nevertheless, the length of duration needed for degassing is determined by additional factors like the construction of the conductor and presence of swelling tapes etc.

2.3.3 Cable Finishing Stage

Once the manufactured cable has finished the degassing phase of the core manufacturing stage, the cable will be led to the cable finishing stage. In this stage, sheathing and armouring (submarine cables) are applied over the insulation of the polymeric cables for better moisture and corrosion protection.

2.3.4 Quality and Control Stage

With all the manufacturing processes done, a series of systems are used for the production tests to ensure the end product cables are designed and produced to meet or exceed the specifications made by the customers. Some of the production tests include conductor examination, dimension check, partial discharge, voids, contaminants and protrusions test. These variety production tests are determined by the cable standards

and specifications prepared by the IEC, ANSI/ICEA, JEC and CENELEC [CENELEC HD620; ICEA Publication S-97-682. 1999; Hampton, Hartlein et al. 2007].

Chapter 3 Classification and Properties of Polymers and Space Charge

3.1 Classification and Properties of Polymers

Polymers are generally used to describe long molecule chains of organic compounds consisting of constructional and replicating units coupled by covalent chemical bonds. This molecule chain length typically consists of thousands or more repeated units of monomers and determines the polymer's strength and durability. Polymers with a shorter chain length of bonded monomers have a lower intermolecular force vice versa a higher intermolecular force is obtained when there is a longer chain length of bonded monomers. This force is required to keep the chains bounded together as when the intermolecular force is high, the polymer material is harder to tear or crack and also a much higher temperature is needed to separate the coupled chains.

Polymers have been widely used since their development in the first half of the 20th century. These new materials have shown us their essential and indispensable usage towards our daily life due to their extraordinary range of properties accessibility. At present, the most widely used polymers are the thermoplastic, which consists of PVC, PE and PP. In general, PE is a term used to specify insulating materials with very different characteristics through different base resins and formulation (cross-linked, antioxidants, etc.). In the electrical industry, highly insulating polymers like XLPE are

used extensively for electrical cable insulation due to their good electrical properties, manufacturing cost and environmental friendliness.

Therefore, with the underlying enormous diversity of polymers and its structural features and properties, relationships between these differences will be introduced in this chapter. In addition, focus will be made on the XLPE polymeric material due to its importance as insulation for power cables. Different cross-linking methods and their impacts shall also be discussed.

3.1.1 Polyethylene (PE)

PE is a polymer that has been rapidly growing since the Second World War due to its stability, easy production and high insulating and minimal loss properties under normal temperature conditions [Jones, Llewellyn et al. 2005]. Ever since its creation by the Imperial Chemical Industries (ICI) Northwich, England in 1933, PE had developed itself as the key wire and cable insulating material for high frequency usage and to a consumer product that is heavily used in the modern world (over 80 million metric tons are produced worldwide every year).

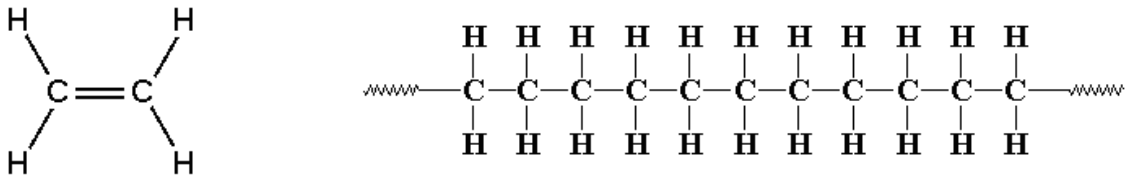

Figure 3-1: Polymerisation from Ethylene to Polyethylene

PE is classified into several different types depending on its branching and density. The mechanical properties of PE depend considerably on elements such as the molecular weight, extent and degree of branching and the crystal structure. Other PE families such as low-density polyethylene (LDPE) with the highest branching occurring, high-density polyethylene (HDPE) are un-branched and linear low-density polyethylene (LLDPE) being short-branched. The PE most extensively used for HV insulation purposes is the cross-linked polyethylene (XLPE) where organic dicumyl peroxide (DCP) is engaged as

a cross-linking agent with a mixture of PE [Ishikawa, Nakamura et al. 1994].

A molecule of PE is basically a long chain of carbon atoms, with two hydrogen atoms attached to each carbon atom [Pascoe 1973; Turton 2000]. The ethene (known commonly as ethylene) molecule, C_2H_4 is CH_2=CH_2. PE is produced through the polymerisation of ethene when two CH_2 that are connected by a double bond is broken, as shown on the left hand side of Figure 3-1.

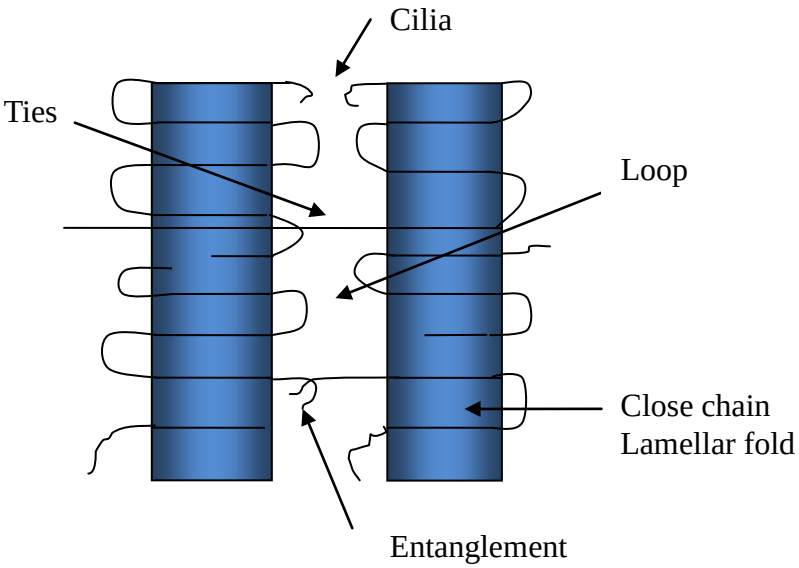

Figure 3-2: Fundamental components of Polyethylene crystalline and amorphous morphology [Lewis 2002b]

PE is a non-polar polymer in a semi-crystalline structure under an ambient temperature [Frutos, Acedo et al. 2007]. PE morphologies are usually created from cooling from a melt phase, polyethylene will consist of structured crystalline lamellae position radially spherulites. Generally, spherulite may have a diameter of approximate 40 μm and consist of a radial array of lamellar crystals separated by less dense amorphous material. The measurement lengthwise of a lamellar crystal is approximately the radius of the spherulite and having a cross-section of approximate 20 μm in the direction of the PE chain (*c* axis) and also 100 nm wide [Lewis 2002b]. The applied temperature along with the conditions of crystallization strongly determines the lamellae structure during solidification [Frutos, Acedo et al. 2007]. Thus, higher temperature is needed to crystallise chains of a longer length and larger spherulites are obtained through a higher molecular weight. In addition, annealing the material subsequently will thicken the lamellae. The key elements of controlling the electrical conduction and setting many of

the breakdown properties of PE are given by the ordered lamellae and their relationship with the disordered amorphous surroundings as illustrated in Figure 3-2 [Lewis 2002b].

3.1.2 Low-Density Polyethylene (LDPE)

LDPE has been used constantly for experimental investigation due to the fact of its simple chemical composition structure. Nevertheless, due to its origin as a semi-crystalline polymer that has both crystalline and amorphous regions. LDPE normally contains approximately 50 – 60 % crystalline with large symmetrical spherulites and both the crystalline and amorphous regions contribute to the complication of its electrical properties. Its maximum melting temperature of crystal is low at approximately 110 ^{0}C. The operational temperature of PE is approximately 70 ^{0}C, which restricts its application as an insulating material for power cables. However, it is widely used in our daily life (sandwich bags, cling wrap and plastic bottles etc.) due to its low crystallinity that contributes to its flexibility and transparency.

3.1.3 Cross-Linked Polyethylene (XLPE)

XLPE usage has been growing steadily since the early 1990s due to its widespread use of it as the insulation for transmission cables. This widespread usage has been due to its high reliability, low dielectric loss and low environmental impact. The material is also a semi-crystalline polymer with both crystalline and amorphous regions. The degree of crystallinity is about 40 % where about half of the molecular mass is arranged in form of crystalline structure, lamellae and spherulites [Carstensen, Farkas et al. 2005].

The incorporation of organic peroxides is a well-established process for cross-linking of PE. Cross-linking method is prepared through the polymer configuration where modification is done on the formation of chemical bonds between the polymer chains. As mentioned earlier in the previous chapter, there are two most widely used XLPE processes named as peroxide curing and moisture curing where the later curing process is further broken down to three methods as illustrated in Figure 3-3:

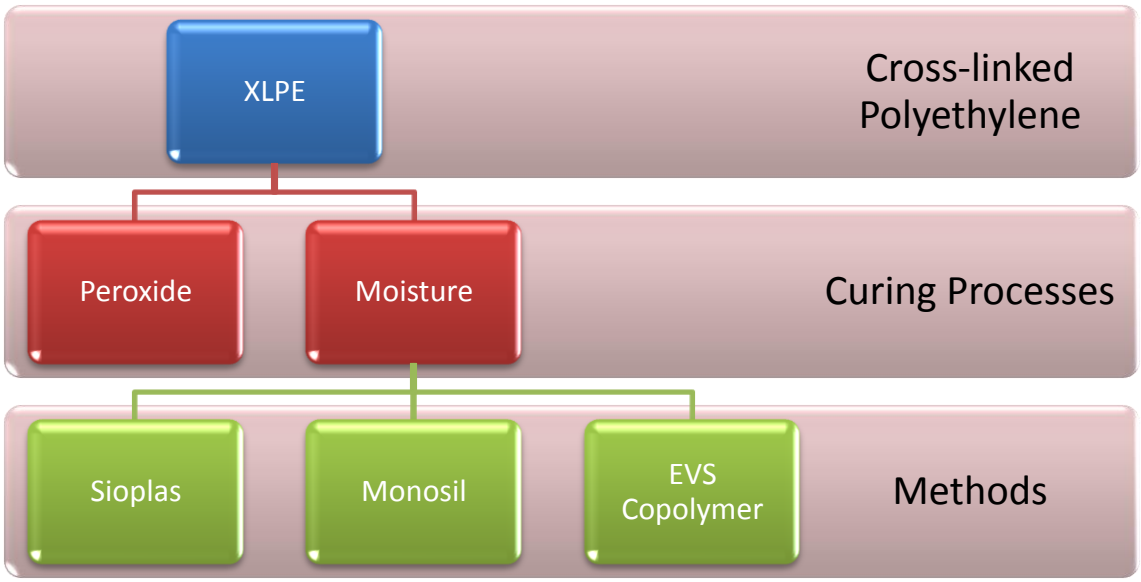

Figure 3-3: XLPE curing processes and methods

3.1.3.1 Peroxide curing

The incorporation of organic peroxides is the most well-established process for cross-linking of PE. Cross-linking method is prepared through the polymer configuration where modification is done on the formation of chemical bonds between the polymer chains. The most commonly used organic peroxide employed as a cross-linking agent is dicumyl peroxide (DCP) whereby activation of the catalyst is triggered thermally [Ishikawa, Nakamura et al. 1994]. Normally, a mixture of 2.5 % of DCP is added into the base polymer (PE) and the initiation of cross-linking reaction is activated only once the curing temperature reaches around 180 ^{0}C. The heated element used for curing may be pressurised steam or with heated nitrogen.

An illustration of a simple cross-linking reaction is shown in Figure 3-4 [Ishikawa, Nakamura et al. 1994]. The results are DCP decomposes to free radicals where cumyloxy radical are produced, followed by abstraction of the hydrogen atom from the polymer backbone to form PE macroradicals, and in the process a variety of reaction products (acetophenone, α-methylstyrene, cumyl alcohol and by-products of DCP) and rearrangement occur among the radical.

In the course of introducing the cross-linking agent, the end product produces smaller

spherulites and thinner lamellae and in XLPE the spherulite structure might not be present and being substituted by lamellar stacks. The XLPE morphology is very much influenced by the existence of interfaces and surfaces within the polymer where columnar, rather than spherulitic expansion, is the preferred mode of crystallisation and by flow patterns in the molten phase [Lewis 2002b]. The existing impurities of cavities or voids of micrometer size at spherulite boundaries are likely to be spread apart and there are reports stating these impurities could act as localised charge trapping centres [Fukuda, Irie et al. 2002].

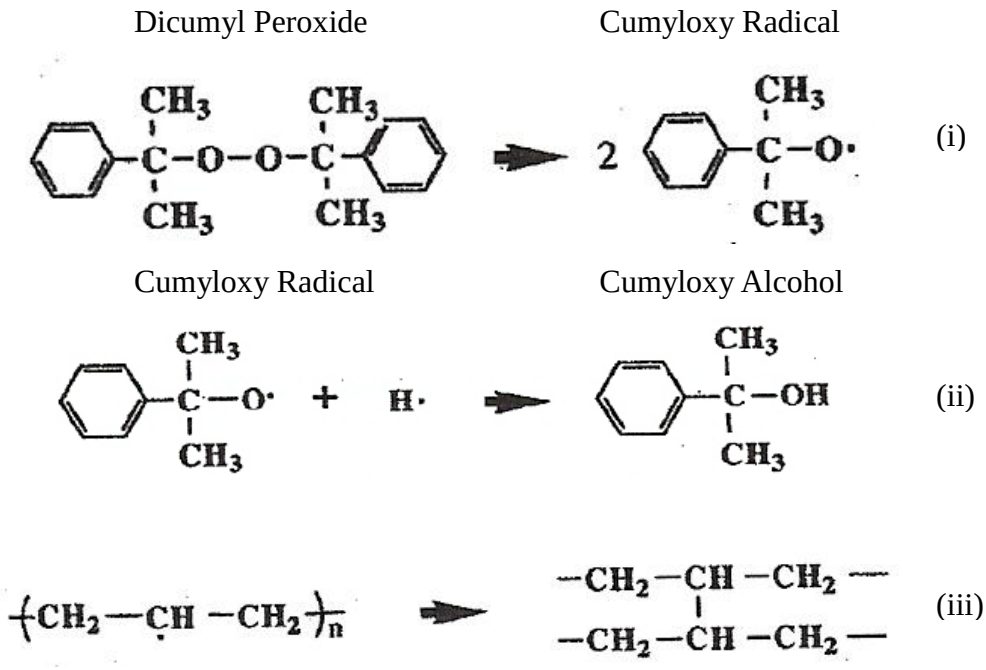

Figure 3-4: Cross-linking reaction (i) Cumyloxy radical product after DCP is heated. (ii) Cumyloxy radical substracts hydrogen atom from PE, producing Cumyl alcohol. (iii) Cross-linked of PE molecules [Ishikawa, Nakamura et al. 1994]

Due to its good thermal performance and its excellent electrical and mechanical properties that is held within the XLPE, it is now commonly used as the insulation material of a power cable where it can tolerate a normal operation of 90 ^{0}C for an indefinite period; during emergency it can withstand 130 ^{0}C up to 36 hours and during short circuit at 250 ^{0}C for a few seconds [Tanaka and Greenwood 1983a; Hanley, Burford at al. 2003]. Care is needed when XLPE undergoes thermal aging at temperatures above its melting temperature (^{0}C) as it will have a great impact on its crystallinity variation [Boukezzi, Boubakeur et al. 2007].

3.1.3.2 Moisture curing

The essential part of moisture curing is the incorporation of the chemically active species onto the base polymer (PE). Three methods can be used to archive this process as follows:

Sioplas (two steps) method

This basic sioplas system was developed in the United Kingdom during the 1970s by Dow Corning. The system consists of two mechanisms where two materials are needed to be prepared first: a cross-linkable graft polymer (0.1 % of Peroxide + LDPE) and catalyst master batch. These two materials are blended together at a fabricating machine and through this process the silane is chemically grafted to the polymer chain. Subsequently, the product is cross-linked by immersion in hot water bath or low pressure steam sauna. An illustration of this method is shown in Figure 3-5.

Monosil (one step) method

A further development of the Sioplas materials has been made by BICC and Maillefer. This process is almost the same as the Sioplas method except for the absence of the separate grafting stage where all the material components (PE, peroxide, silane and stabiliser) are added into the extruder. The silane–grafting reaction takes place at the same time the material is being extruded. Subsequently, the product is cross-linked by immersion in hot water bath or low pressure steam sauna. An illustration of this method is shown in Figure 3-5.

Ethylene vinyltrimethoxysilane (EVS) copolymers method

The EVS method is different as compared to the other two methods due to the silane clusters are inserted into the polymer chain and not grafted onto existing polymer chains. In general, a base polymer (Silane copolymer) is applied where silane insertion process occurs with the polymer reactor. The catalyst and other additives are added at the extrusion stage.

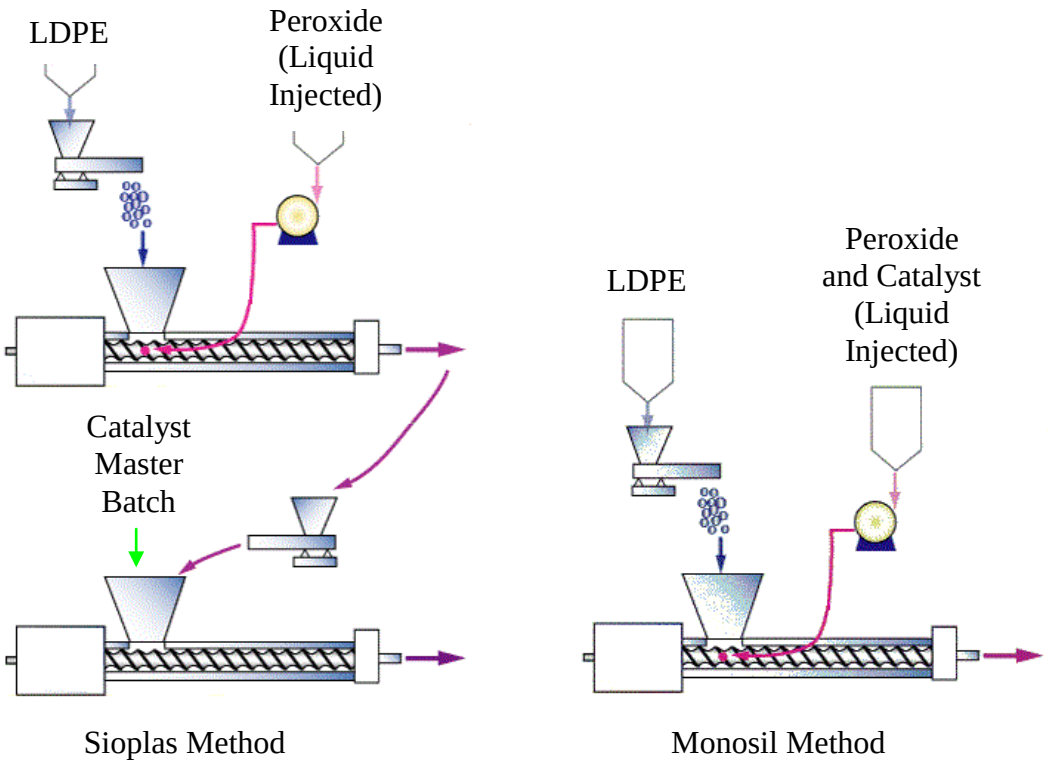

Figure 3-5: Sioplas (two steps) and Monosil (one step) methods

3.2 Classification and Properties of Space Charge

Space charge is surplus of electric charges distributed over a region of space rather than a distinct point. It was firstly used to illustrate the accumulation of electronic charge in the space between the anode and cathode of a vacuum diode, due to electron emission from an electrode.

Space charges occur when the rate of charge accumulation differs from the rate of extraction. This accumulation may be due to generation, drift, diffusion, moving and trapped charge within the volume. Furthermore, charges may be attributed to electrons or ions depending on the mechanism of the charge transfer.

In the context of dielectrics, space charge phenomenon is generally engaged to imply that charges in the dielectric, electrons (negative charges), holes (positive charges), and

ions that are migrating across by the application of voltage that are slow moving or being trapped within the dielectric material. This accumulation of comprehensive immobile charge carrier across the dielectric material which is superimposed to the Laplacian field will result in changes of electric stress of the dielectric material. In the framework itself, it has been concluded that space charge phenomenon is obtained when under electric field due to the following processes

1. The orientation of dipoles (homogeneous) in materials due to electric field and space charge is sharp step function with two peaks at the electrodes.
2. Charge (electrons and holes) injection and extraction from the interface electrodes when application of DC field exceeding 10 kV/mm.
3. Ionisation of impurities within the bulk of the polymeric material assisted by the electric field or from an inhomogeneous polarization [Fu and Chen 2007].

Polymeric insulation shows evidence they have similar properties and characteristic for the formation of traps. The electronic properties within a polymeric material could be interpreted through an energy band diagram [Levy 1968; Pollock 1993]. The energy band diagram illustrated in Figure 3-6 consists of a band gap that separates the valence band and conduction band.

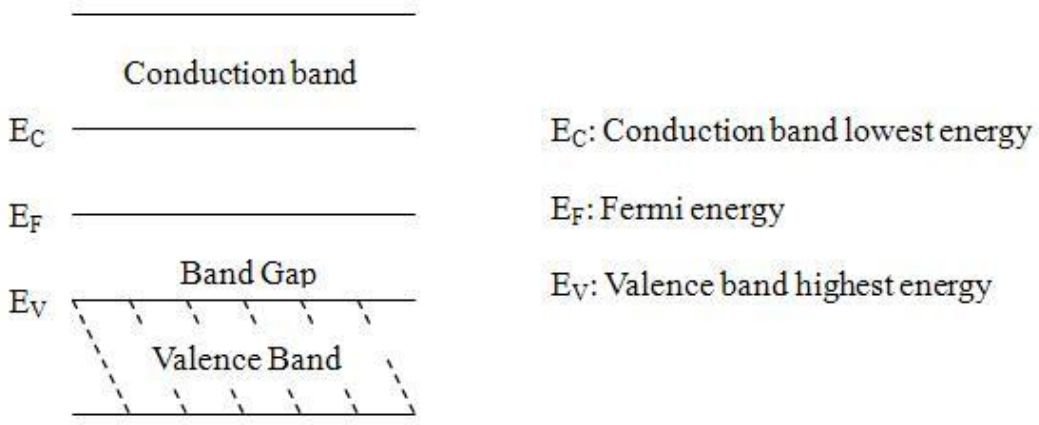

Figure 3-6: Energy band diagram

These bands relate with the deteriorate states where the holes are contained in the vicinity of the valence band and the free moving electrons contained in the vicinity of the conduction band. In reality, there is no existence of a perfect crystal where the physical properties of solid polymers are determined by three factors. Firstly, the

detailed chemistry of the repeat units that make up the polymer chains. Secondly, the defects within each molecule, their length and the gross molecular architecture – the "impurities". Defects and architecture largely determine the extent to which a given polymer is able to crystallise. Crystalline or, more accurately, semi-crystalline are tough ductile solids (eg. polyethylene, polypropylene and nylon). Lastly, the conditions used to convert the base material into the final artefact. Processing conditions can affect the behaviour in two ways, which is through the incorporation of additives or by influencing structural details, in turn, determine properties. The above mentioned factors will modify the deteriorate states of both the valence and conduction bands, which causes the introduction of traps that are characterised by the localised states existing within the band gap that aid to the accumulation of space charge.

3.2.1 Homocharge and Heterocharge

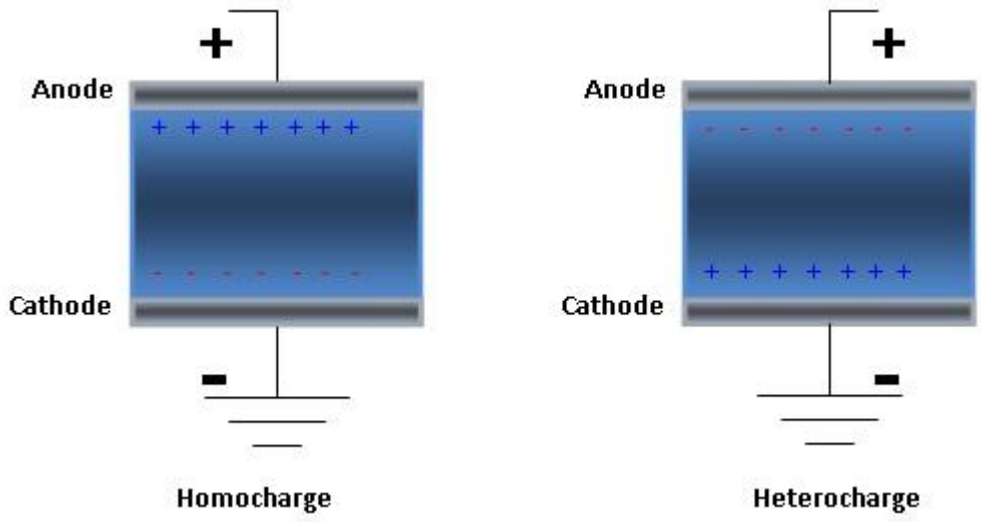

Figure 3-7: Representation of homocharge and heterocharge development near the electrodes

From Figure 3-7, both homocharge and heterocharge are expressed by both the polarity of the electrodes and the polarity of the charges within the material adjacent to the electrodes. The interpretation of homocharge is the accumulation of charge established in the vicinity adjacent to the electrodes which share the same polarity as the electrode (electrons adjacent to cathode or holes adjacent to anode). While, heterocharge are interpreted as the formation or orientations of dipoles or the extraction of opposite

excess charge or basically charges that are formed by the attraction of opposite electrodes (electrons adjacent to anode or holes adjacent to cathode).

Under the regime of DC supply, electric field is dependent of the space charge in addition to the conductivity of the material sample. The consequences of homocharge formation in the sample causes reduction in electric stress between the electrode and material and enhance the electric stress in the middle of the sample material. Whilst, heterocharge formation enhance the electric stress between the electrode and material but reduce the electric stress in the middle of the sample material.

Space charge distribution and formation are widely investigated on low-density polyethylene (LDPE) and cross-linked polyethylene (XLPE) insulation material. It was found that homocharge are normally established in LDPE where no presences of chemical species are found in it. Whilst, heterocharge are formed in XLPE when cross-linking products are present. The decay of space charge was also found to occur at similar time scale of the generation of it. Homocharge built up slowly and the decay rate is slow and possibly slower for a large part of space charge. Whilst, heterocharge built up quickly and decays just as quickly as its generation [Montanari, Laurent et al. 2005; Abou-Dakka, Bulinski et al. 2006; Fu, Chen et al. 2007].

3.2.2 Morphology and Charge Transport

The relationships between the morphology and the electric field distribution of PE are essential to understand the influence of the matrix on charge mobility as since conduction in high electric field during the period of pre-breakdown is recognised as the effect of mechanical strain towards the band structure of the electronic energy.

Electronic ideas of breakdown along with the growing support of molecular modeling had been used on the polymer structures such as PE. However, these ideas deliver inaccurate results due to the uses of primitive quasi-crystalline extended state models for the transportation of charges. Therefore, for the morphology of PE different proposition are made based on the characteristics of electrons, holes and ions transportation.

Research works on the transport of electron have reported that the affinity of electron is negative and in the order of 0.65 eV. This signifies surplus electrons would migrate to a region of lower density intermolecular where the energy is much lower. Electrons that were injected will be channeled into the quasi-vacuum regions at crystalline-amorphous interfaces, and into sub-microvoid spaces and free volume [Serra, Tosatti et al. 1998; Jones, Llewellyn at al. 2005].

Figure 3-8 illustrates the movement of electrons down the energy landscape, where the polarisation reaction within the polymer creates a small region of polaronic energy states in the region denoted as *T*. The efficiency of electron movement across the polymer is determined by a number of factors. These factors comprise of the presence of cross-links, sub-microvoids, tie molecules and polymer structural arrangement of chains (barriers). The polymer structural arrangement establishes the valleys at (i-i) and (ii-ii) along with the polaron traps (T) located adjacent to the valley [Jones, Llewellyn et al. 2005].

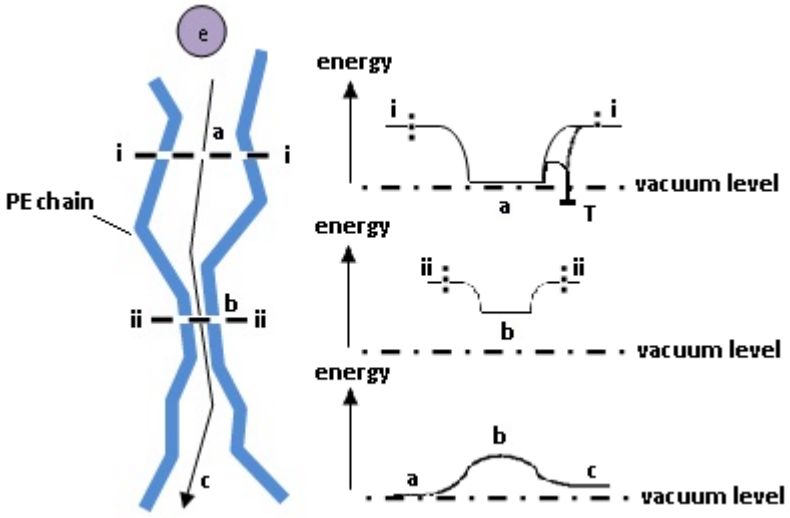

Figure 3-8: Electron movement down the quasi-vacuum energy valley [Jones, Llewellyn et al. 2005]

The transportation of hole (positive charge) shows dissimilarity as compared to the transportation of electron (negative charge) because the hole is confined within the polymer chains and will only arise during electron vacancies in or closely connected with the valence band of the PE molecule. Inter-chain hole transfer is required for long-

range transportation where a reverse resonant tunnelling technique is used by the electrons to move between the valence states of closely connected polymer chains as illustrated in Figure 3-9 where effortless inter-chain tunnelling could be obtained at position (ii-ii) as compared to position (i-i).

Conduction of hole is much more responsive as compared to the conduction of electron due to the requirement of inter-chain tunnelling. Tunnelling of hole can be affected with the increment of electric field as traps are introduced leading to the mobility reduction of hole. Conversely, when the fields are high, encouragement of electron-hole recombination will rise where free volume of chains is exposed in and sub-microvoid spaces. Through the recombination of electron and hole where energy force is released creating the product of luminescence. This luminescence may possibly be reduced by the weakened coulombic attraction and limited spatially due to the formation of polaron.

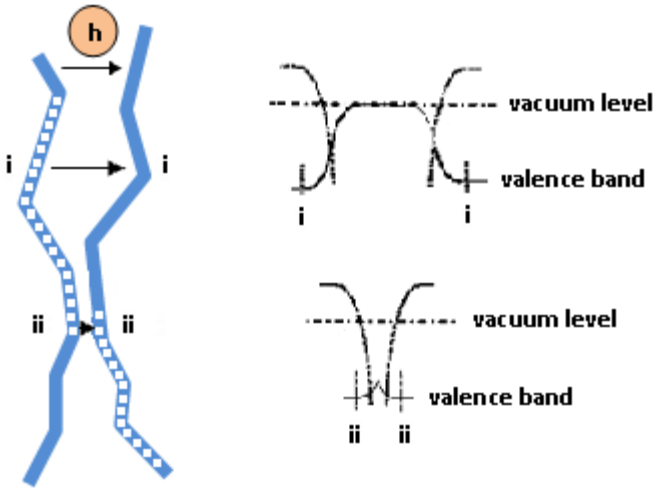

Figure 3-9: Hole movement down the valence bands and across polymer chains through tunnelling [Jones, Llewellyn et al. 2005]

Ionised molecular contaminations coupled by self-trapping polarisation along with polymer adjacent through secondary bonds also do contain within the PE. They are coupled to the amorphous phase, hitting on chain conformation barriers as of electrons [Blaise 1995]. The mobility of ion is field-dependent and determined by the Mott and Gurney law with field–induced charges in morphology.

Through focusing the attention on mechanisms of charge formation due to the processes of both interface electrodes and bulk, further mechanisms that govern these processes

are illustrated in Figure 3-10 and shall be discussed in the later section [Sze 1981; Roland 1979].

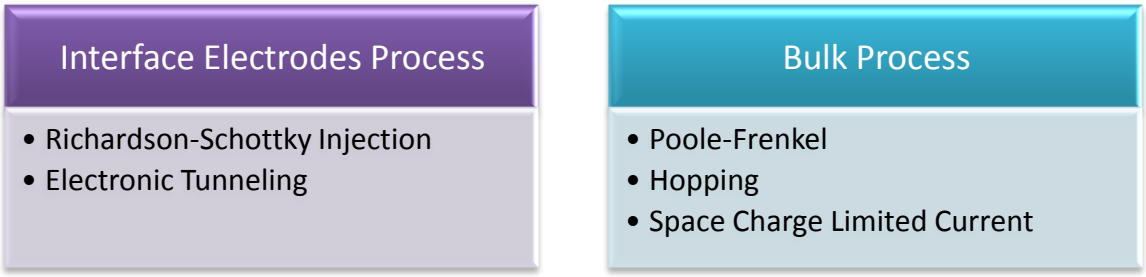

Figure 3-10: Further mechanisms of interface electrodes and bulk processes

3.2.3 Interface Electrode Process

Charge (electrons and holes) injection like electrons from the cathode (hole injection from the anode) is determined by the local electric field. This mechanism may be governed by either Richardson-Schottky injection, which depends on the potential barrier height at the interface, or tunnelling which strongly depends on the width of the barrier [Chen, Tanaka et al. 2004]. Charge injection and extraction can be expected to take place at the interface between electrode and dielectric material. When injection is implemented at the negative or cathode side, a higher amount of electrons will be observed and vice versa an increment of holes when injection is implemented on the positive or anode side. The processes of injection and extraction depend strongly on the interface conditions such as the types of material of electrodes, contact pressure, temperature as well as surface defects of the polymeric material [Fothergill, Montanari et al. 2003; Chen, Tanaka et al. 2004].

To maintain the continuity of polymer current, electrode contacts are necessary for the transfer of electrons at both ending sides. At a cathode edge electrons are thermally triggered to quasi-vacuum states in contact with polymer (region adjacent to the electrode) molecules at energy levels approximately 0.45 eV below the vacuum level, as shown in Figure 3-11. The emission in the above states will cause subsequent transport through the polymer by means of inter-chain states. From the electron transport at the cathode-polyethylene contact, it shows (i) that emission into a quasi-vacuum state, (ii)

emission into a positive ion, (iii) positive hole neutralisation and finally (iv) a hole created in the metal due to electron tunnelling to hole in the polymer chain [Jones, Llewellyn et al. 2005].

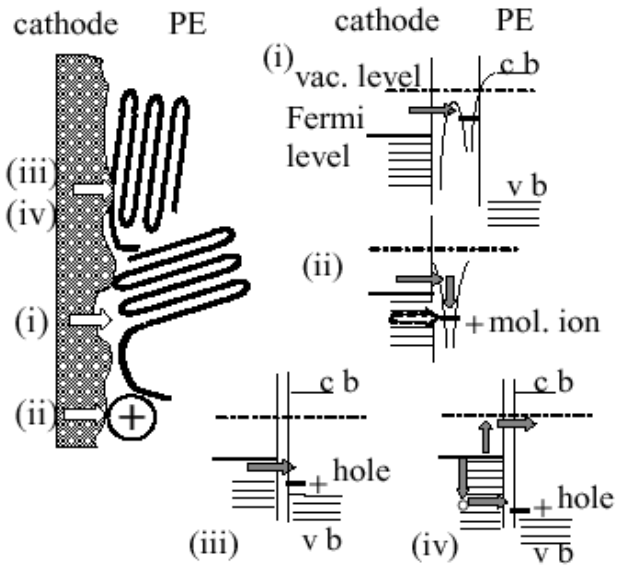

Figure 3-11: Electron transportation at cathode-polyethylene contact [Jones, Llewellyn et al. 2005]

A point needed for consideration is that owing to the natural unevenness on the surface of the cathode, variation of the local field and the concentration of sub-micrometer voids adjacent to the cathode surface increases with the increment of field. As a result, improvement of electron injection to the polymer can be obtained as there is an increment of electron transfer to the quasi-vacuum inter-chain states. In addition, field induced changes in the surface morphology will also influence the electron transfer to positive holes states on polymer chains [Jones, Llewellyn et al. 2005].

Figure 3-12 shows (i) transfer from quasi-vacuum state in polymer, (ii) negative ion neutralisation and finally (iii) generation of Hole in chain. The progression of electron transfer will increase by inputting high electric fields and this process depends on the anode (negative ion) or cathode (positive ion) where the existence of heterocharge arriving at it. The impurity ions will also give rise to the electric field-enhancing heterocharges in the polymer sample [Li and Takada 1992; Jones, Llewellyn et al. 2005].

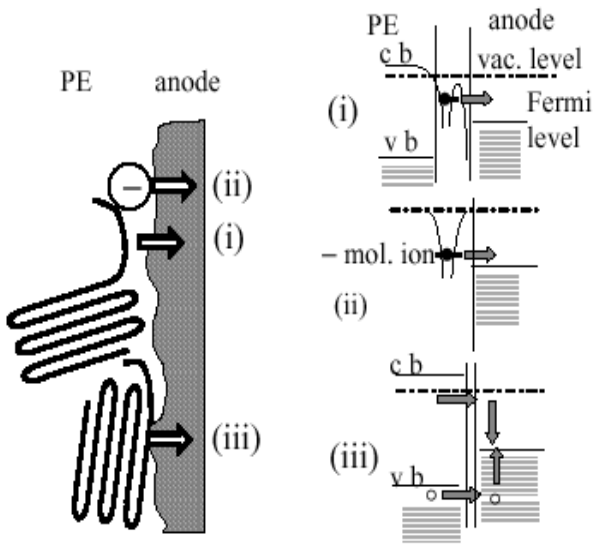

Figure 3-12: Electron transportation at anode-polyethylene contact [Jones, Llewellyn et al. 2005]

3.2.3.1 Richardson-Schottky injection

The Richardson-Schottky injection is an expansion of the thermionic emission occurring from the lowering of the surface potential barrier which comes about by the combination of both applied and image fields.

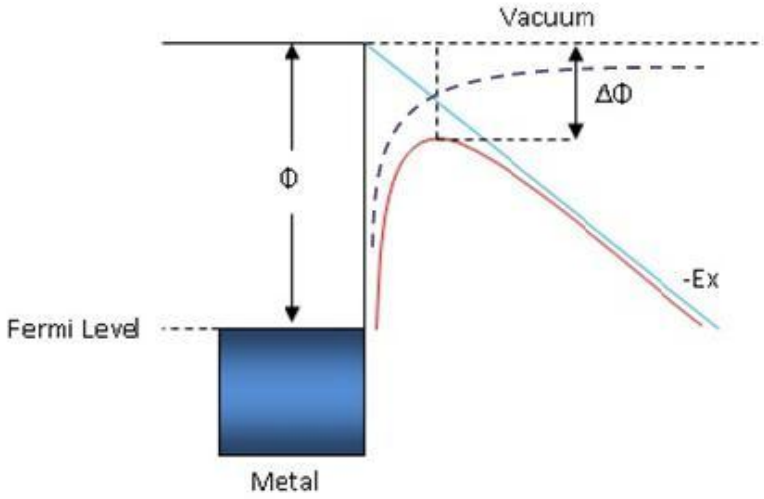

Figure 3-13: Energy diagram for Richardson-Schottky injection

The potential energy diagram showing the cathode interface with an application field E is illustrated in Figure 3-13. The starting point of the potential is at the “vacuum level”

(the potential in eV of an electron, separated to an infinite distance from the cathode).

The potential, V_a, due to the applied field is represented in a straight and declining negative line given that the field E is negative. Consideration is also made on the magnitude of E by letting $E = |E|$, so that

$$V_a = (-Ex) \tag{E3-1}$$

The potential, V_i, owing to the image of the electron in the metal electrode can be calculated by the image charge theorem. If the electron is distance, x, from the interface then the distance separating the electron and the image is $2x$. Therefore, the force of attraction by coulomb's law is

$$F_i = \frac{e^2}{4\pi\varepsilon_o\varepsilon_r(2x)^2} = \frac{e^2}{4\pi\varepsilon_o\varepsilon_r 4x^2} \tag{E3-2}$$

where ε_o is the vacuum permittivity, ε_r is the relative permittivity and e is the electronic charge.

$$\Phi_i = \int_x^\infty F_i(x)dx = \frac{e^2}{16\pi\varepsilon_o\varepsilon_r x} \tag{E3-3}$$

The potential energy of this electron emitted out of the electrode due to the effect is given by $\Phi = -e(Ex)$ and since $V_i = -Ex$. Therefore, we can rewrite it as

$$V_i = \frac{\Phi_i}{e} = \frac{{}^{e^2}/_{16\pi e_o e_r x}}{e} = \frac{e}{16\pi\varepsilon_o\varepsilon_r x} \tag{E3-4}$$

The resultant potential

$$V(x) = V_a + V_i = -(Ex) + \frac{e}{16\pi\varepsilon_o\varepsilon_r x} \tag{E3-5}$$

To find maximum value for potential at stationary point

$$\frac{dV}{dx} = -E - \frac{e}{16\pi\varepsilon_o\varepsilon_r x^2} \tag{E3-6}$$

$\frac{dV}{dx} = 0 \quad =>$

$$0 = -E - \frac{e}{16\pi\varepsilon_o\varepsilon_r x_m^2} \tag{E3-7}$$

where x_m is the maximum stationary point

$$E = -\frac{e}{16\pi\varepsilon_o\varepsilon_r x_m^2} \tag{E3-8}$$

With the consideration of magnitude $E = |E|$ that was made earlier, we could conclude E without regard to its sign as

$$E = \left|-\frac{e}{16\pi\varepsilon_o\varepsilon_r x_m^2}\right| = \frac{e}{16\pi\varepsilon_o\varepsilon_r x_m^2} \tag{E3-9}$$

Thus, from E3-9 the maximum stationary point is derived as

$$x_m^2 = \frac{e}{16\pi\varepsilon_o\varepsilon_r E} \tag{E3-10}$$

$$x_m = \left(\frac{e}{16\pi\varepsilon_o\varepsilon_r E}\right)^{\frac{1}{2}} \tag{E3-11}$$

The maximum attractive potential, V_m, is obtained by substituting E3-11 into equation E3-4 and is written as

$$V_m = \Delta\Phi = \left(\frac{2e}{16\pi\varepsilon_o\varepsilon_r\left(\frac{e}{16\pi\varepsilon_o\varepsilon_r E}\right)^{\frac{1}{2}}}\right) = \left(\frac{eE}{4\pi\varepsilon_o\varepsilon_r}\right)^{\frac{1}{2}} \tag{E3-12}$$

Through utilising the Richardson-Dushman relation for thermionic current density emitted in vacuum without any application field:

$$J_T = AT^2 exp\left(-\frac{\Phi}{kT}\right) \tag{E3-13}$$

By changing Φ into $(\Phi - \Delta\Phi)$,

$$J(E) = AT^2 exp\left(\frac{-(\Phi-\Delta\Phi)}{kT}\right) = AT^2 exp\left(-\frac{\Phi}{kT}\right) exp\left(\frac{\Delta\Phi}{kT}\right) \quad \text{(E3-14)}$$

Therefore, by substituting E3-12 into E3-14, the current density is:

$$J(E) = J_T exp\left(\frac{\Delta\Phi}{kT}\right) = J_T exp\left[\frac{1}{2kT}\left(\frac{eE}{\pi\varepsilon_o\varepsilon_r}\right)^{\frac{1}{2}}\right] \quad \text{(E3-15)}$$

3.2.3.1 Electronic tunnelling

In field emission cathode even at low temperature regardless of the work function, a large electric field from the edge of the cathode aids the tunnelling of electron into the material.

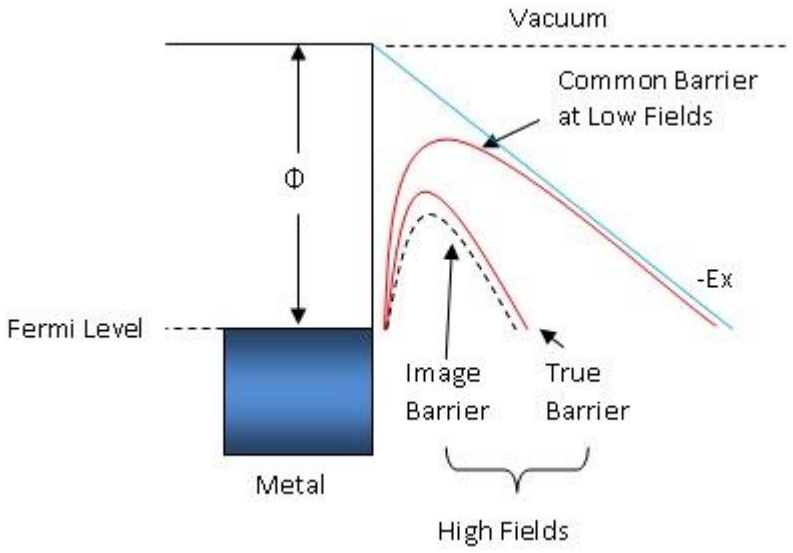

Figure 3-14: Potential energy diagram for tunnel injection of electrons into vacuum

The Fowler-Nordheim equation relates current density to the work function and electric field. The basic idea is that quantum mechanical tunnelling from the adjacent electrode into the insulating material limits the current through the configuration. Once the wave-

like character of the electrons has tunnelled through into the insulating material, these electrons have the freedom of movement within the valence or conduction band of the insulating material. An illustration of this mechanism is shown in Figure 3-14. The calculation of current is based on the Wentzel-Krämers-Brillouin (WKB) approximation, according to which the transmission of a potential barrier for a level of energy.

The current density, *J*, is written using the WKB approximation by assuming the bottom of the valence band is at (-∞) and is given as

$$J = \frac{4\pi me}{h^3}\int_0^{\infty}(W_x - \Phi)exp\left(-\frac{8\pi\sqrt{2m}}{3ehE}W_x^{\frac{3}{2}}\right)dW_x \qquad \text{(E3-16)}$$

where *e* is electronic charge, *h* is Planck's constant, *m* is the mass, *E* is the electric field in V/m, W_x is the top of the barrier height in eV and Φ is the potential barrier height in eV [Lewis 1955a].

Through expanding W_x at the point Φ by using Taylor expansion, the factor $W_x^{\frac{3}{2}}$ can be made into a polynomial of integer powers of W_x about any fixed value of W_x,

$$J = \frac{4\pi me}{h^3}\int_0^{\infty}(W_x - \Phi)exp\left(-\frac{8\pi\sqrt{2m}}{3ehE}\left(\Phi^{\frac{3}{2}} + \frac{3}{2}(W_x - \Phi)\Phi^{\frac{1}{2}} + \cdots\right)\right)dW_x \qquad \text{(E3-17)}$$

The first two terms of the Taylor expansion are only considered as the remaining terms are negligible

$$J = \frac{4\pi me}{h^3}\int_0^{\infty}(W_x - \Phi)exp\left(-\frac{8\pi\sqrt{2m}}{3ehE}\Phi^{\frac{3}{2}}\right)exp\left(-\frac{4\pi\sqrt{2m\Phi}}{ehE}(W_x - \Phi)\right)dW_x \qquad \text{(E3-18)}$$

$$J = \frac{4\pi me}{h^3}exp\left(-\frac{8\pi\sqrt{2m}}{3ehE}\Phi^{\frac{3}{2}}\right)\int_0^{\infty}(W_x - \Phi)exp\left(-\frac{4\pi\sqrt{2m\Phi}}{ehE}(W_x - \Phi)\right)dW_x \qquad \text{(E3-19)}$$

Through using integration by parts, the integral can be calculated as

$$\int_{\Phi}^{\infty}(W_x-\Phi)exp\left(-\frac{4\pi\sqrt{2m\Phi}}{ehE}(W_x-\Phi)\right)dW_x$$

$$=(W_x-\Phi)\left[\frac{exp\left(-\frac{4\pi\sqrt{2m\Phi}}{ehE}(W_x-\Phi)\right)}{-\frac{4\pi\sqrt{2m\Phi}}{ehE}}\right]_{\Phi}^{\infty}-\int_{\Phi}^{\infty}(1)\left(\frac{exp\left(-\frac{4\pi\sqrt{2m\Phi}}{ehE}(W_x-\Phi)\right)}{-\frac{4\pi\sqrt{2m\Phi}}{ehE}}\right)dW_x$$

$$=\left[\frac{exp\left(-\frac{4\pi\sqrt{2m\Phi}}{ehE}(W_x-\Phi)\right)}{\left(-\frac{4\pi\sqrt{2m\Phi}}{ehE}\right)^2}\right]_{\Phi}^{\infty}=\frac{(ehE)^2}{32\pi^2m\Phi} \qquad \text{(E3-20)}$$

Through combining the first portion of E3-17 and the result from E3-20, the final Fowler-Nordheim equation can be obtained as

$$J=\frac{4\pi me}{h^3}exp\left(-\frac{8\pi\sqrt{2m}}{3ehE}\Phi^{\frac{3}{2}}\right)\frac{(ehE)^2}{32\pi^2m\Phi}=\frac{e^3E^2}{8\pi h\Phi}exp\left(-\frac{8\pi\sqrt{2m}}{3ehE}\Phi^{\frac{3}{2}}\right) \qquad \text{(E3-21)}$$

3.2.4 Bulk Process

In addition to electrodes injection process, bulk process also does occur by having charge carriers produced within the bulk of the insulating material when under the application of electric field on the constituent atoms and molecules. This imperfect insulating material contains impurities or chemical species such as residues of cross-linking products and additives that are attached or trapped within it. Consequently, with the application of an external field, these impurities or chemical species will commence indication of polarisation such that additional charge carriers or ions are created within the bulk material; the majority of them would recombine within a short period of time [Maeno, Ohki et al. 2005]. The electrons that did not undergo the recombination would be extracted at the electrode or either deeply trapped during the transfer. The remaining ions, which would be expected to have low mobility, would appear as a stable net positive space charge scattered reasonably even across the bulk sample [Hanley, Burford et al. 2003].

These traps are able to trap both the electrons and holes depending on the energy difference in it. The existence of a band gap implies that, as the temperature increases, the number of carriers increases and, therefore, the conductivity increases [Montanari,

Mazzanti et al. 2001].

Fundamentally, it was suggested there are two different types of trap centres, namely the trapping centres and recombination centres [Kao and Hwang 1981; Solymar and Walsh 1999]. The trapping centre relates to traps that capture the charge carriers where the charge carriers could be simply re-excited in a very short time to re-instate its mobility through thermal excitation. Whilst, recombination centres relates to traps whereby the captured charge carrier have the tendency to create the opportunity for recombination with an opposite sign charge carrier that has fallen into the same trap and experience eradication.

Charge trapping centres can also be expected to be in the form of voids. The propensity of material to trap charges can be explained as a cause of space charge accumulation. When charges are formed within the bulk material, part of the charges is trapped as space charge. There are two main classifications of traps and are classified as shallow and deep traps as shown in Figure 3-15. Shallow traps are generally more common across the material and charges are easily trapped and de-trapped from it without contributing to long lasting of trapping of the charges. As shallow traps have depth range of between 0.15 - 0.3 eV and the residence times of carriers within this sites are of order of 10^{-12} seconds [Meunier, Quirke et al. 2001]. In contrast, deep traps have depth range of between 0.4 - 1.5 eV and residence times of carriers are never-ending [Roy, Segur et al. 2003]. When charges are being trapped, the charges are hard to be de-trapped, which eventually causes a build up of space charge at the location [Ieda 1984; Chen, Tanaka et al. 2004].

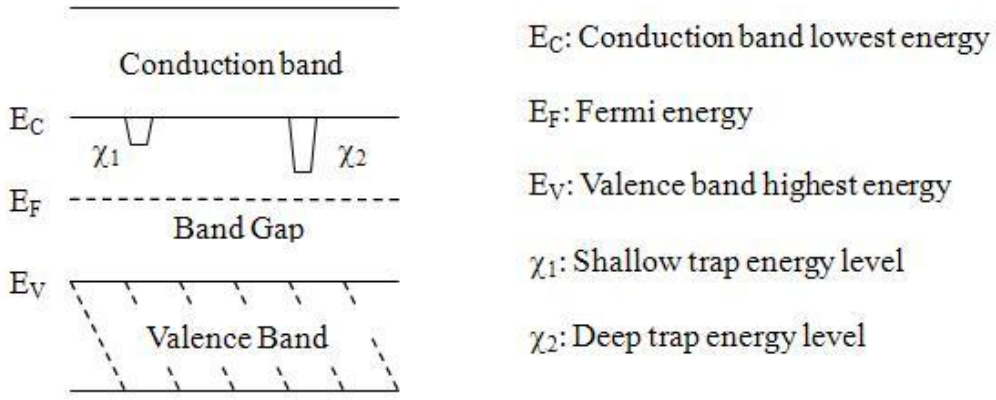

Figure 3-15: Classification of both shallow and deep traps

Through the corresponding information provided, the rate of space charge accumulation and its threshold level depends on the density and depth of the trap distribution. Supported by the traps depth and its nature, it has been proposed that chain defects and or impurities may possibly be accountable for their existence within the material [Ieda 1984].

3.2.4.1 Poole-Frenkel

The Poole-Frenkel effect is fairly equivalent in natural as compared to the Schottky injection. The later mechanism is resulted from the height reduction of the potential barrier at the metal/insulation interface through field induction, whereas, the Poole-Frenkel effect combines the large electric field and the ionisation centre, implies a declination of ionisation energy and consequently the increment of concentration of ionised species under the application of a high field. The energy diagram illustrated in Figure 3-16 shows the potential energies in the plane defined by the ionised centre and the applied field.

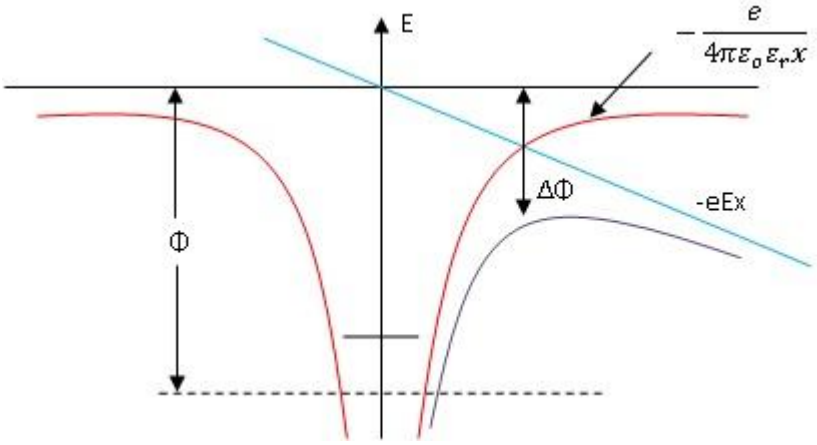

Figure 3-16: Energy diagram for the Poole-Frenkel effect

Through reducing the potential barrier by half, the equation for the new barrier $\Delta\Phi$ is

$$\Delta\Phi = \left(\frac{eE}{\pi\varepsilon_o\varepsilon_r}\right)^{\frac{1}{2}} \qquad \text{(E3-22)}$$

where ε_o is the vacuum permittivity, ε_r is the relative permittivity and e is the electronic charge.

By replacing the new reduced potential barrier stated on E3-22 into the equation of Schottky injection E3-14, the current density can be obtained as

$$J(E) = J_T exp\left(\frac{\Delta\Phi}{kT}\right) = J_T exp\left[\frac{1}{kT}\left(\frac{eE}{\pi\varepsilon_o\varepsilon_r}\right)^{\frac{1}{2}}\right] \quad \text{(E3-23)}$$

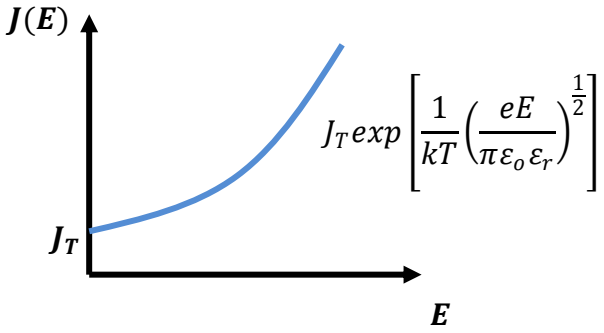

Figure 3-17: The graph of current density versus E

A straight line representing $\log_{10}$ of the current density versus $\sqrt{E}$ is obtained by

$$J(E) = J_T exp\left[\frac{1}{kT}\left(\frac{eE}{\pi\varepsilon_o\varepsilon_r}\right)^{\frac{1}{2}}\right] \quad \text{(E3-24)}$$

$$\ln\left(\frac{J(E)}{J_T}\right) = \frac{1}{kT}\left(\frac{e}{\pi\varepsilon_o\varepsilon_r}\right)^{\frac{1}{2}}\sqrt{E} \quad \text{(E3-25)}$$

$$\ln J(E) = \frac{1}{kT}\left(\frac{e}{\pi\varepsilon_o\varepsilon_r}\right)^{\frac{1}{2}}\sqrt{E} + \ln J_T \quad \text{(E3-26)}$$

With comparison between E3-26 and the linear equation, y = mx + c, it clearly illustrate a straight line when $\ln J(E)$ versus $\sqrt{E}$ and is shown in Figure 3-18.

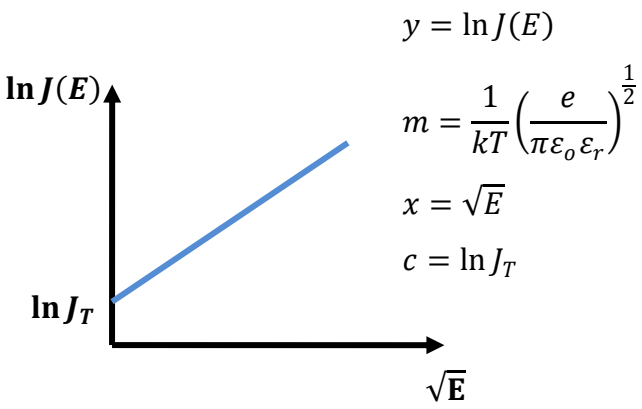

Figure 3-18: The graph of current density versus E through the implementation of $\log_{10}$

3.2.4.2 Space charge limited current

The space charge limited current mechanism results from a current injected into the insulator, where no compensating charge is present. Three assumptions are made in this mechanism

1. The insulation does not possess an intrinsic conductivity. However charges are injected into the insulation through an electrode.
2. Charges injected from the electrode have an identical mobility, μ, which is independent of the local field.
3. The dielectric permittivity, $\varepsilon_o\varepsilon_r$, is unaffected by the existence of the injected charges.

The expression for the steady-state uniform current and Gauss's law are expressed in E3-27 and E3-28 respectively as

$$J = q\rho(x)\mu E(x) \tag{E3-27}$$

$$\frac{dE(x)}{dx} = \frac{q\rho(x)}{\varepsilon_o\varepsilon_r} \tag{E3-28}$$

Substitute $q\rho(x)$ from E3-27 to E3-28 gives

$$\frac{J}{\mu\varepsilon_o\varepsilon_r} = E(x)\frac{dE}{d(x)} \tag{E3-29}$$

By integrating E3-29 from 0 to *x*, while assuming the electric field, $E = 0$, at $x = 0$,

$$\frac{Jx}{\mu\varepsilon_o\varepsilon_r} = \frac{E^2}{2} \tag{E3-30}$$

or

$$E(x) = \sqrt{\frac{2xJ}{\mu\varepsilon_o\varepsilon_r}} \tag{E3-31}$$

Integrate once again from $x = 0$ to $x = d$ with $V(0) = V$ and $V(d) = 0$, it gives

$$V = \int_0^d E\,dx = \sqrt{\frac{2xJ}{\mu\varepsilon_o\varepsilon_r}}\frac{d^{\frac{3}{2}}}{3/2} \tag{E3-32}$$

$$V = \int_0^d \sqrt{\frac{2J}{\mu\varepsilon_o\varepsilon_r}}\,x^{\frac{1}{2}}\,dx \tag{E3-33}$$

$$V = \sqrt{\frac{2J}{\mu\varepsilon_o\varepsilon_r}}\left[\frac{x^{\frac{3}{2}}}{3/2}\right]_0^d \tag{E3-34}$$

$$V^2 = \frac{2J}{\mu\varepsilon_o\varepsilon_r}\left(\frac{4}{9}\right)d^3 \tag{E3-35}$$

or

$$J = \frac{9}{8}\frac{V^2\mu\varepsilon_o\varepsilon_r}{d^3} \tag{E3-36}$$

The above obtained current density equation is also known as “Mott’s relation” which states the maximum or saturation current that can flow through a dielectric material of permittivity, $\varepsilon_o\varepsilon_r$, when electrons of mobility, μ, are injected from the adjacent electrode.

3.2.4.3 Hopping

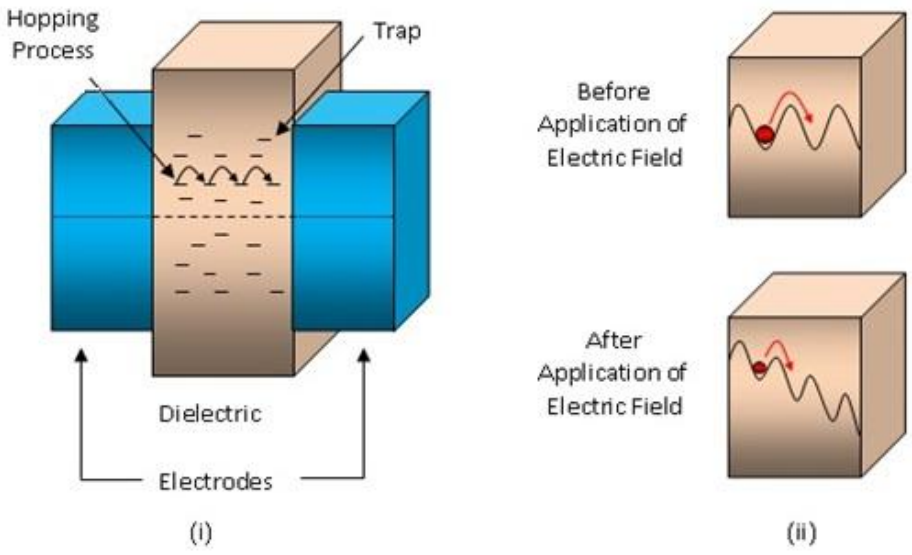

Figure 3-19: Hopping conduction mechanisms: (i) hopping process in the dielectric material and (ii) an array of potential barriers before and after the application of electric field

As mentioned earlier in the section on bulk process, traps existence in the forbidden band leads to the trapping of charges within the bulk of the material. These unoccupied traps (potential well) can be described as a potential well a waiting for a charge to be dropped into as illustrated in Figure 3-19. As soon as a charge has fallen into the trap, the depth of this trap, Φ, will inhibits the movement of the charge. In order for the charge to maintain the migration process through the sample, a hopping mechanism takes place where the charge escapes from one trap to another by means of hopping. Thus, the energy required for a charge to escape a trap corresponds with the height of the trap.

Within the material, a series of traps with depth, Φ, are being separated individually by a distance of, a. The probability per unit time that a charge trapped within the potential well will jump towards the right on to the next trap is given as

$$p = v\, exp\left(-\frac{\Phi}{kT}\right) \tag{E3-37}$$

where v is the frequency (in the order of 10^{12} to 10^{13} Hz), k is the Boltzmann constant

and *T* is the temperature.

Under the application of an electric field, the potential barrier curve is tilted down as illustrated in the figure. This aid the charge by an extra energy of, $eEa/2$, for going the distance from the bottom of the trap to the top of the barrier. Corresponding, the jumping rate of charges to the left is reduced as a higher energy is needed for the same task.

For a single trapping level of depth, Φ, the resulting current is

$$J = v\ exp\left[-\frac{\Phi - \mathrm{eEa}}{kT}\right] - v\ exp\left[-\frac{\Phi + eEa}{kT}\right] \quad \text{(E3-38)}$$

$$= v\left[\frac{\exp\left(\frac{\mathrm{eEa}}{2kT}\right)}{exp\left(\frac{\Phi}{2kT}\right)}\right] - v\left[\frac{exp\left(-\frac{eEa}{2}\right)}{exp\left(\frac{\Phi}{2kT}\right)}\right] \quad \text{(E3-39)}$$

$$= v\ exp\left(-\frac{\Phi}{2kT}\right)\left[\exp\left(\frac{\mathrm{eEa}}{2kT}\right) - exp\left(-\frac{eEa}{2kT}\right)\right] \quad \text{(E3-40)}$$

By using the hyperbolic sine function, $2\ sinh\ x = exp(x) - exp(-x)$, on E3-40. The current density is obtained as

$$J = 2v\ exp\left(-\frac{\Phi}{kT}\right)\sinh\left(\frac{eEa}{2kT}\right) \quad \text{(E3-41)}$$

For a concentration of charges to be considered, the current density will have the form

$$J = 2nevaexp\left(-\frac{W}{kT}\right)\sinh\left(\frac{eEa}{2kT}\right) \quad \text{(E3-42)}$$

where *n* is the charge carrier concentration, *e* the elementary charge, *a* the inter-site distance, and *E* the electric field [Bartnkias and Eichhorn 1983; Roy, Segur et al. 2003].

Chapter 4 Space Charge Measurement Techniques

4.1 Introduction

The importance of understanding mechanisms for the formation and accumulation of space charges within a polymeric insulating material has led to many new measurement techniques to be employed for the measurement and investigation of the space charge phenomenon in the last few decades [Lang and Das-Gupta 1981; Sessler, West et al. 1981; Migliori and Hofler 1982; Maeno, Kushibe et al. 1985].

As mentioned earlier in the previous chapter, these formation and accumulation of charges may be injected from the electrodes or due to ionisation of the impurities held within the bulk sample after the cross-linking process. Once space charge is accumulated within the polymeric insulation material, it will reside through the material bulk for a long period of time. Low charge carrier mobility and charge trapping within polymers present a rise in space charge phenomenon resulting in localised electric stress enhancement [Xu, Choo et al. 2007]. Particularly, the local field may greatly exceed the threshold stress which the material is able to tolerate causing the degradation process, which accelerates the electrical aging of the material and eventually causes a failure [Tanaka and Greenwood 1983a; Zhang, Lewiner et al. 1996]. The deteriorating of the insulating material through electrical aging caused by the initiation and growth of electrical trees is believed to be caused by space charges accumulated within the insulation material [Liu and Liu et al. 1989]. Therefore, a better and reliable technique is needed to measure space charge accumulation within the dielectric samples accurately,

safely and economically.

4.2 Different Techniques of Space Charge Measurement

For the past few decades, a number of different measurement techniques have surfaced in the research field and are now regularly performed in many laboratories throughout the world. These techniques are generalised into two different measurement technique groups, the destructive technique and the non-destructive technique respectively, and are illustrated in Figure 4-1.

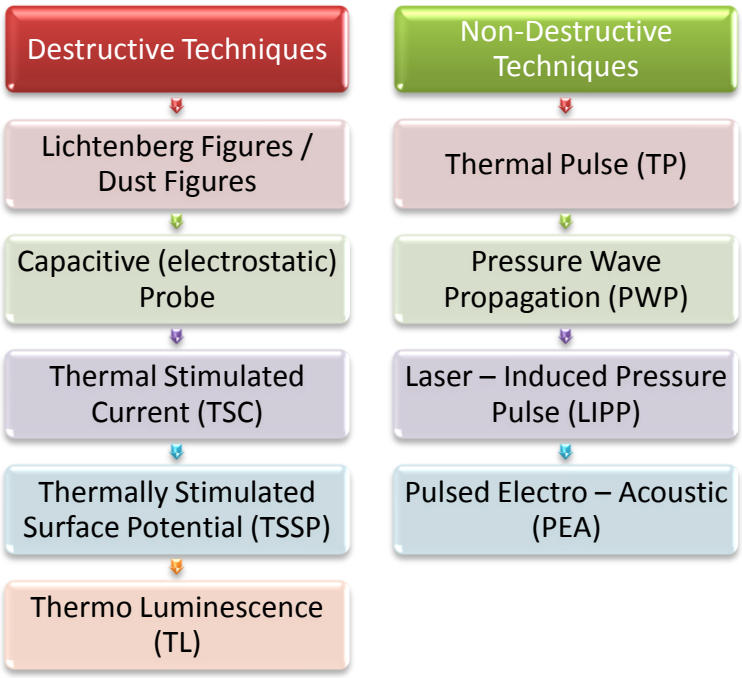

Figure 4-1: Space charge measurement techniques

The destructive techniques for space charge measurements were established in the late seventeen-century and are now obsolete due to the more favoured non-destructive techniques. For illustrative reasons only a short description of these destructive techniques and their working principles will be given in the following paragraphs. The Lichtenberg figures technique is applied by sprinkling charged sulphur powders on the

surface of insulating materials. It was later renamed as dust figures technique and coloured charge polarity sensitive powders are applied on the cut slabs of the insulating material [Toriyama 1961; Ando and Numajiri 1979; Khalil and Hansen 1988; Kawasaki, Arai et al. 1991; Murooka, Takada et al. 2001]. The dust figures technique is simple and relatively cheap, which enables us to visualise the pattern of charge distribution but not able to measure the amount of residual charge. In contrast, the probing technique allows us to roughly estimate the charge pattern and the amount of residual charge but with poor resolution in the order of millimetres. TSC technique is based on a depolarisation (disorientation of the dipoles), on a re-diffusion of the ions, or on a discharge of the sample material by thermal activation (de-trapped charges) and is less sensitive to space charge [Li, Tang et al. 1997; Agnel and Toureille 1997], while, TSSP technique is measured in open circuit conditions under thermal heating [Lee, Lee et al 1988]. Lastly, TL technique consists of a rapid cooling followed by the progressive warming of a pre-illuminated material sample to uncover the different types of charge pairs as successive emission bands. To conclude the destructive techniques, they all acquire the same disadvantages for being destructive and preparation for the experiment can also influence the charge distribution and only qualitatively knowledge is obtained. Therefore, it is less favoured as compared to the non-destructive techniques.

In order to overcome the above-mentioned disadvantages of the destructive techniques, various non-destructive methods have been introduced in the past three decades to study the space charge behaviours. The non-destructive technique is broken down into three groups, namely, the thermal diffusion, the elastic wave propagation and the electric stress group [Holé, Ditchi et al. 2003]. These three groups of non-destructive techniques are based on the same physical effect, where the equilibrium between electrostatic and elastic forces is perturbed. In the thermal group, it uses the diffusion of heat to modify the equilibrium and thus induces an electrical response. The elastic wave propagation group uses the strain produced by the propagation of elastic waves to modify the equilibrium and to induce an electrical signal. Lastly, the electric stress group uses the electrostatic force produced by the application of an external voltage to modify the equilibrium and induces a mechanical response. Although, the three individual groups use different physical means to carry out the measurement to determine the space charge distribution, they have demonstrated that the results obtained are similar. The basic principles and the features of the above mentioned non-destructive techniques

would be briefly explained and compared between the different techniques in the section below. However, depending on the technique used, each type of measurement technique exhibits its own advantages and disadvantages.

Through using these new measurement techniques, it will allow us to obtain quantitatively analysis of space charge distributions and the effects on the insulating material. Consequently, this will also provides us with some key new elements to shed light on the mechanisms of high field phenomenon in insulating material.

4.2.1 Thermal Pulse (TP) Technique

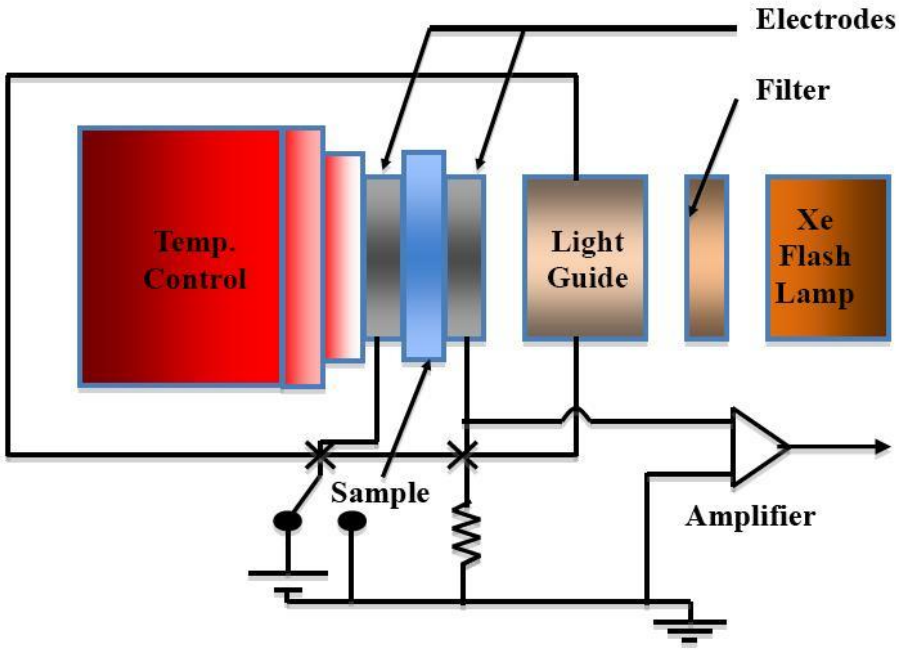

Figure 4-2: Illustration of a thermal pulse (TP) system

The principle of thermal pulse technique utilises the thermal expansion created by a flash lamp or the illumination of a laser to one of the electrode surfaces. The thermal expansion subsequently travels gradually across the sample material. The time scale for TP is approximately 1 ms for 25 μm thick PE sample, which is the thermal relaxation time [Mizutani 1994]. The charge signal is measured through a charge amplifier and the field distribution is subsequently estimated using Fourier coefficients of measured charge transients as shown in Figure 4-2 [Notingher jr, Agnel et al. 2001; Mellinger, Singh et al. 2005]. With comparison to its counterparts, TP signals are not as fast as

LIPP or PEA system's acoustic wave in obtaining results due to the relative slow thermal expansion.

4.2.2 Laser Induced Pressure Pulse (LIPP) Technique

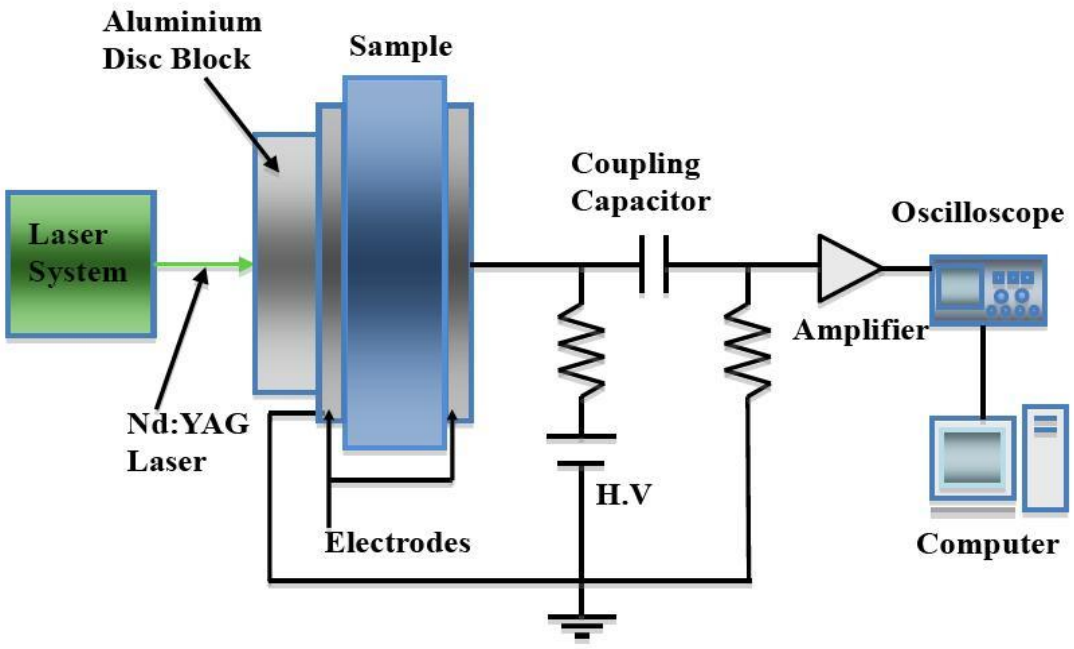

Figure 4-3: Illustration of a laser induced pressure pulse (LIPP) system

In the Laser Induced Pressure Pulse (LIPP) technique, one side of the material sample containing space charge is measured through using a pressure pulse that is generated by the irradiation of a laser pulse (laser ablation) using a Nd:YAG laser, as shown in Figure 4-3 [Mizutani 1994]. With the induced pressure pulse travelling at sound velocity across the sample, a current is induced as a result of non-uniform changes in dimension and permittivity reflecting the space charge distribution. The obtained results show that the induced current is directly proportional to the charge distribution together with the charges on the electrodes [Ahmed and Srinivas 1997].

The LIPP system is applicable to both thin (10 - 100 μm) and thick (1 – 20 mm) samples. Normally a laser pulse width of 100 ps to 10 ns is used, as a strong laser pulse (~300 mJ/pulse) consequence is a strong output current signal that will be observable without any signal averaging [Sessler 1982a; Sessler, West et al. 1982; Malec 2000]. The highest positional resolution of LIPP is approximate 1 μm, making it very useful

towards space charge research in film sample. Nevertheless, as LIPP system's high voltage and detecting circuits are separated by a coupling capacitor, otherwise the amplifier might get damaged due to a surge current in an event of electric breakdown [Takada and Hozumi 2000].

4.2.3 Pulsed Electro-acoustic (PEA) Technique

The history of PEA method was inspired in Japan in 1975 during a lecture under the topics of electrical and magnetic on the theories of electrets microphones and the earphones of audio systems. Voltage supply together with sound wave frequencies were applied to the electrets earphones and there was a short lifespan of the earphone after it was irradiated with an electron beam. From there, it was deduced that the decay of accumulated space charge due to irradiation might have shortened the lifespan of the earphone, which led to the suggestion of space charge measurement and lifespan evaluation [Li and Takada 1994].

From that instant, the research and development on PEA technique for measuring the space charge profile was carried out. In early 1980s, Professor Takada and his research group successfully developed the PEA technique [Takada and Sakai 1983]. Through the application of the PEA technique, existence of periodical charge packets across the material sample can be detected for high fields [Hozumi, Takeda et al. 1998]. This technique is now widely used for the measurement of dynamic space charge distribution in solid dielectric films or plaque samples and also coaxial cable samples. Space charge data were obtained for the first time in the 1990s from the insulation of coaxial cable samples [Fukunaga, Miyata et al. 1990; Fukunaga, Miyata et al. 1991].

The PEA basic principle is schematically represented in Figure 4-4 and the operational principle is based on the Coulomb force law, where an external applied pulse field $V_p(t)$ induces a perturbing force density on the material sample under the existence of resident charges. The perturbation initiates acoustic pressure waves that are then produced at charge layers at both electrodes (q_1 and q_3) and the internal resident charges (q_2) when electrical pulse is applied to the bulk material. The piezoelectric device (PVDF) detects this acoustic pressure wave (p_1, p_2 and p_3) and converts them into electrical signals (V_{s1}, V_{s2} and V_{s3}), where the amplitudes correlate to the local charge density [Ahmed and

Srinivas 1997].

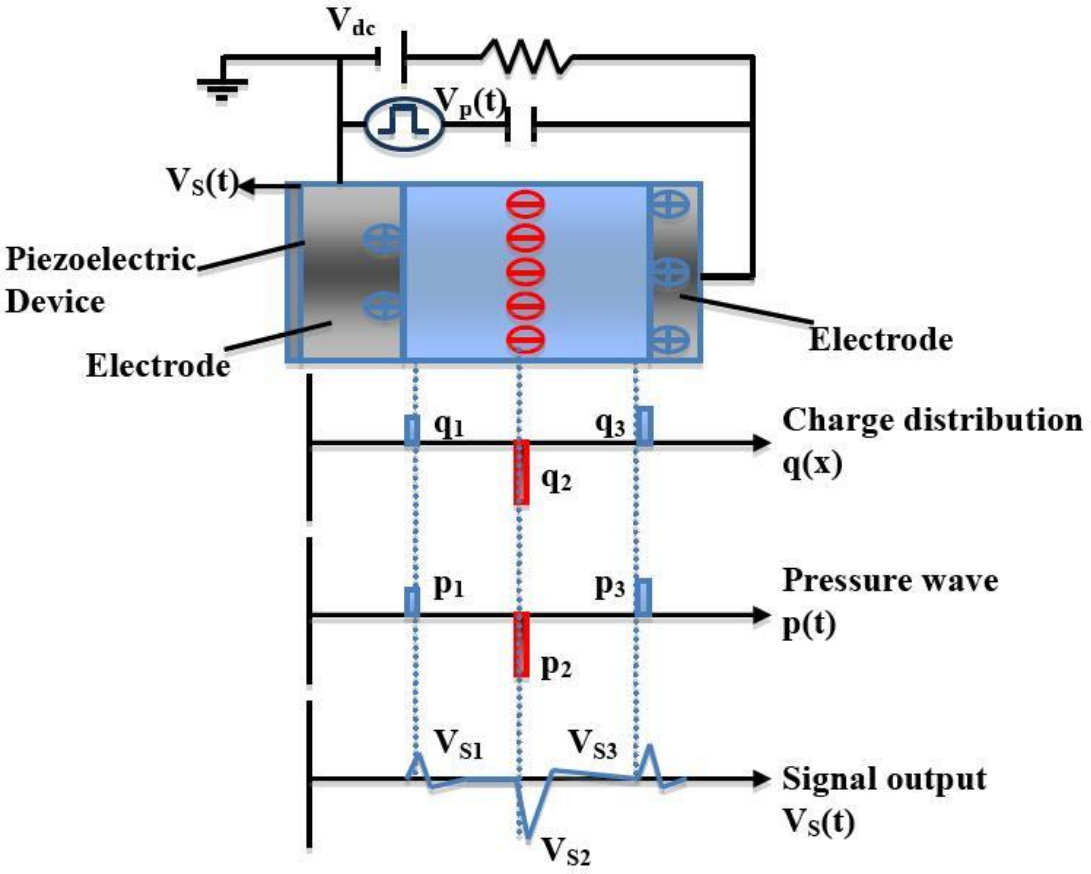

Figure 4-4: Basic principle of PEA technique

4.2.4 Conventional Pulsed Electro-acoustic (PEA) Technique for Cable

The first PEA system used in the early 1990s to measure space charge profiles in cable was based on a conventional design, as shown in Figure 4-5. This conventional design consists of a curved aluminium block used to maintain an intimate contact with the cable outer screen and acts as a buffer to delay noise due to the pulse voltage and a curved PMMA absorber to remove or minimize the reflections of acoustic wave after it reached the acoustic sensor (PVDF) [Hozumi, Okamoto et al. 1992]. Based from the conventional system, it can be seen that there are a couple of problems within the design of this system. There are difficulties to undertake measurements on cables with different radius as modification of aluminium block electrode, acoustic sensor (PVDF) and PMMA absorber is needed to accommodate the changes of cable size. These changes are time consuming and difficult to perform.

In the PEA technique, the pulse width and sensor thickness determines the spatial resolution of the system and the highest positional resolution is approximately 3 μm and 10 μm with or without de-convolution respectively.

The PEA does not have the same disadvantage as compared to LIPP system. In the PEA system, both the high voltage and acoustic detecting circuits are electrically separated via the ground electrode providing damage protection to the amplifier and oscilloscope in the result of an electric breakdown. Therefore, the PEA system is regarded as the safest technique used for research measurement on cable samples through the application of high voltages [Takada and Hozumi 2000].

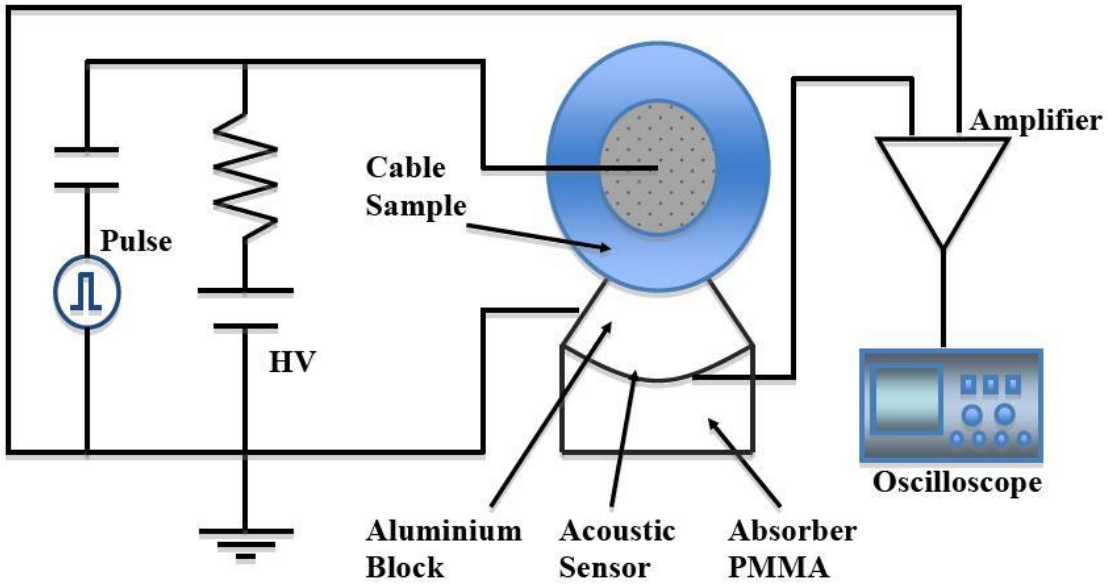

Figure 4-5: Illustration of a conventional pulsed electro-acoustic (PEA) system for cable

4.3 Progression of Pulsed Electro-acoustic (PEA) Technique for Cable

Since the birth of the PEA technique, we have seen the growth and advancement of this marvellous technique after pioneering space charge measurement works are done from plaque to coaxial cable. This technique has shed new lights to researchers, making a

great contribution towards the research and development of electrical insulation technologies throughout the world by allowing researchers in this field to obtain valuable insight overview on the underlying theoretical principles and phenomenon of space charge.

As mentioned earlier, the initial design of the cable PEA system restricts the space charge measurements on cables with different radius due to the curvature electrode. For this reason, a modified and improved PEA system is needed for overcoming this flaw where a flat electrode system was introduced and employed to replace the conventional PEA system. The space charge measuring assembly for a cable shaped sample using a flat lower electrode PEA technique is illustrated in Figure 4-6 [Fu, Chen et al. 2000a].

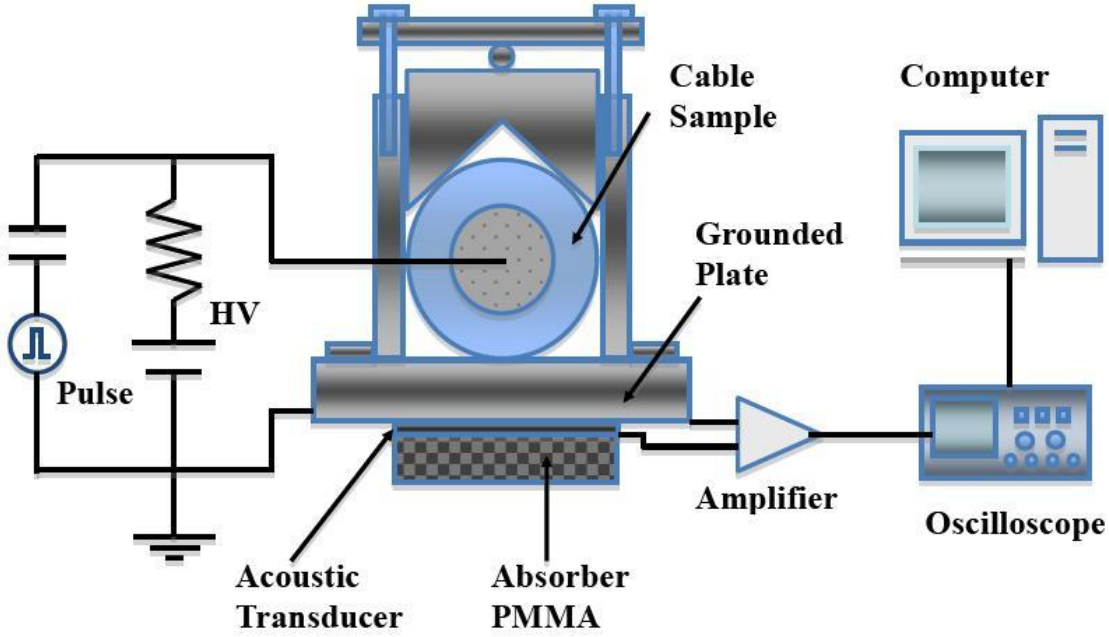

Figure 4-6: Illustration of a modified pulsed electro-acoustic (PEA) system for cable

With this improved system, PEA technique could be employed to any cable sizes. Furthermore, the small contacting area between the cable sample and the electrodes allows high measurement resolution around the angular and axial directions of the cable. Investigations have been done between the enhanced flat electrode system and the conventional curved surface electrode system. Results have demonstrated there is no difference between the obtained measurements when under the same propagation principles of the acoustic wave travelling through the insulation of the coaxial cable [Liu, Takada et al. 1993; Muronaka, Tanaka et al. 1996].

On the other hand, most of the research done on space charge distributions of cable samples were under ambient temperature, where temperature gradient occurring between both the inner and outer insulating material are being ignored. As we know that in the actual service of DC power cables, temperature gradient is present across the insulating material. Therefore, in order for temperature gradient to be taken into consideration a new modified PEA system for cable is required, which allow us to understand the real phenomenon occurring within the polymeric insulating material in power cable samples.

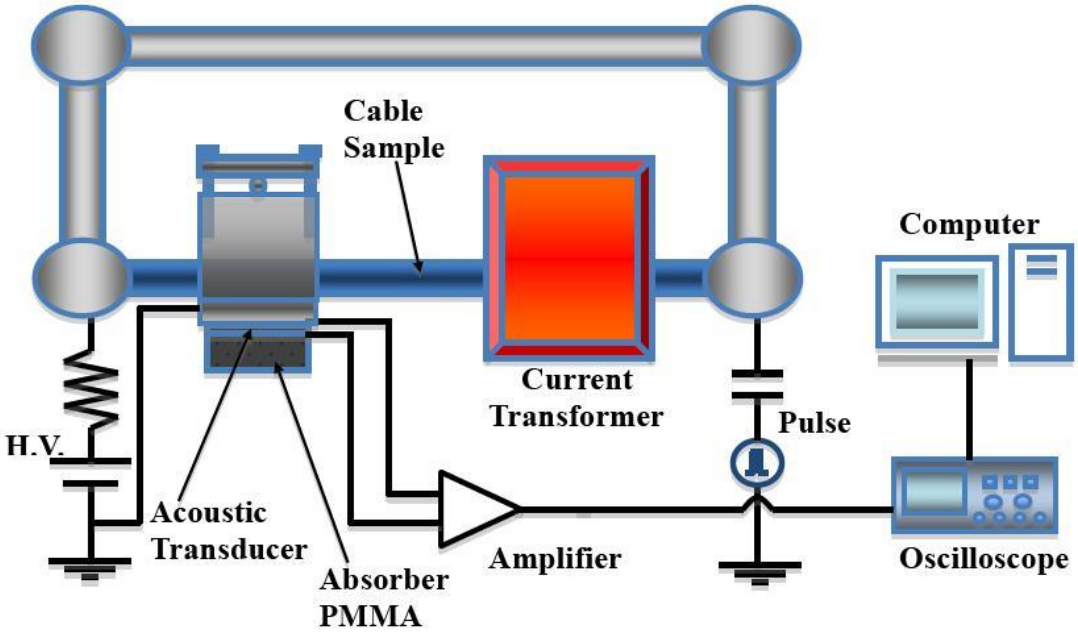

Figure 4-7: Illustration of a modified pulsed electro-acoustic (PEA) system with current transformer for cable

In Figure 4-7, the diagram illustrates the newly modified PEA system with current transformer attached so that temperature gradient can be applied across the insulating material of the cable when space charge measurements are taking place.

The system itself consists of ten important individual components, which are the cable sample itself, HVDC supply, a 20 kΩ resistor, coupling capacitor bank, pulse generator, PEA system, closed-loop aluminium bar, current transformer, oscilloscope and a computer. These components are substantially important, as each individual component

plays a significant role, which enables us to obtain the space charge distributions within the polymeric insulation. The HVDC supply allows us to provide the coaxial cable up to 100 kV of DC application with interchangeable polarity with the 20 kΩ resistor connected in series to limit the current in the case of breakdown. The pulse generator could generate a range of 2 – 10 kV pulse voltage and width of 50 ns simultaneously together with the HVDC applied voltage to the cable core through a coupling capacitor bank.

The basic principles of this modified system is the coaxial cable lies flatly in close contact with the flat ground aluminium (Al) electrode in the PEA system and running through the current transformer, with both ends of the cable cores attached to a HVDC supply and a electrical pulse generator respectively. Once in operation, the current transformer, through induction heating, heats up the cable, where the cable acts as a short circuit due to the connected closed-loop aluminium bar. Space charge measurements are then detected by the acoustic transducer (PVDF) and convert them into electrical signals, where they are fed into a wide band amplifier for amplification. The acoustic transducer and the amplifier are assembled below the ground Al electrode shielded within a box to minimise any noise interference. In the diagram, the amplifier is drawn outside the shielding box for the reason of its presence in the system. The amplified signal is collected by a digital storage oscilloscope (DSO) and this data is then fed into a computer using a general-purpose interface board (GPIB) where further signal processing using LabView program is made.

4.4 Selecting of the PEA's Components

For the construction of a modified PEA system with a current transformer attached, two components within the PEA system need to be selected properly for obtaining an accurate space charge distribution within the polymeric insulation: the acoustic transducer and amplifier components.

4.4.1 Transducer and Amplifier

The calculation of the best resolution for the system is needed in order to select a suitable transducer for the system. As we know from the PEA system that we are using, the pulse generator enables us to produce applied pulse voltage with width of 50 ns to the cable sample. In XLPE, the acoustic waves travel with a velocity of 2.2 μm/ns. Theoretically the best resolution of the system is 110 μm, this value is obtained by multiplying the time when the signal is on with the speed of the acoustic wave in the XLPE medium. Therefore, in order for the PEA system to obtain reasonable spatial resolution for the space charge distributions profile, the applied pulse voltage width should be as narrow as possible.

As mentioned earlier on the previous section, an acoustic wave is generated from the resident charges when pulses are applied to the sample material. The acoustic wave is captured by piezoelectric transducer located below the grounded Al plate. This wave, *p(t)*, is then detected and established as a charge, *q(t)*. From E4-1 [Li, Yasuda et al. 1994; Gallot-lavallee and Teyssedre 2004], it is clear that the electric potential, $v_o(t)$, relates on the thickness of, *d*, rather than the area, *S*, of the transducer if we assume the bandwidth of the transducer response is much wider than the frequency range of the pressure pulse generated. If the bandwidth of the transducer is less than the width of the pressure pulse generated, deconvolution technique must be employed to recover the space charge distribution.

$$q(t) = kp(t)S \tag{E4-1}$$

$$v_o(t) = \frac{q(t)}{C_p} = \frac{kd}{\varepsilon_o \varepsilon_r} p(t) = K_o p(t) \tag{E4-2}$$

where C_p is the transducer capacitance, ε_o the permittivity of free space, ε_r is the transducer's relative permittivity, k is the piezoelectric strain constant, S is the transducer's area and K_o is a constant related with the electro-mechanical coupling property of the transducer.

From E4-2, the transducer's capacitance is used to calculate the output voltage, v_o, of the transducer. As illustrated in Figure 4-7, the transducer output is connected to an

amplifier for the amplification of the signal. Therefore, if the amplifier has a frequency bandwidth wider than the input signal, the amplified output voltage signal, *v(t)*, will be proportional to the pressure pulse, *p(t)*, and is given as

$$v(t) = GK_o p(t) \tag{E4-3}$$

where *G* is the amplifier gain.

To conclude, PVDF film with a very large bandwidth and low, *q*, is chosen as the acoustic transducer utilised in our PEA system. As assumption has been made that the frequency response of both the transducer and amplifier are satisfactorily wider so as the output voltage, *v(t)*, will be proportional to the charge distribution, *q(t)*.

Therefore, the acoustic time of the transducer can be calculated though E4-4 as

$$\tau_a = \frac{d}{\mu_p} \tag{E4-4}$$

where *d* is the transducer's thickness, τ_a is the acoustic time through the transducer and μ_p is the acoustic pressure through the transducer.

Acoustic Pressure Wave

As the pulse generator produce applied pulse voltage of having a width of 50 ns each time. So the frequency range is approximately 20 MHz.

Acoustic Transducer (PVDF)

Transducer thickness, d = 40 μm

Acoustic pressure velocity, μ_p = 2.2 μm/ns

Acoustic time, τ_a = 18.2 ns

The cut off frequency of the transducer function, $(1/\tau_a)$ = ~55 MHz

Amplifier

From the specification of the amplifier attached to our system, it has a very wide band operating range of up to 500 MHz.

In theoretical sense, the acoustic transducer (PVDF) is able to cover the pressure wave due to its higher frequency response. Subsequently, the amplifier is being able to cover the output from the transducer due to its higher frequency response as compared to the acoustic transducer (PVDF). An illustration of the flow is shown in Figure 4-8.

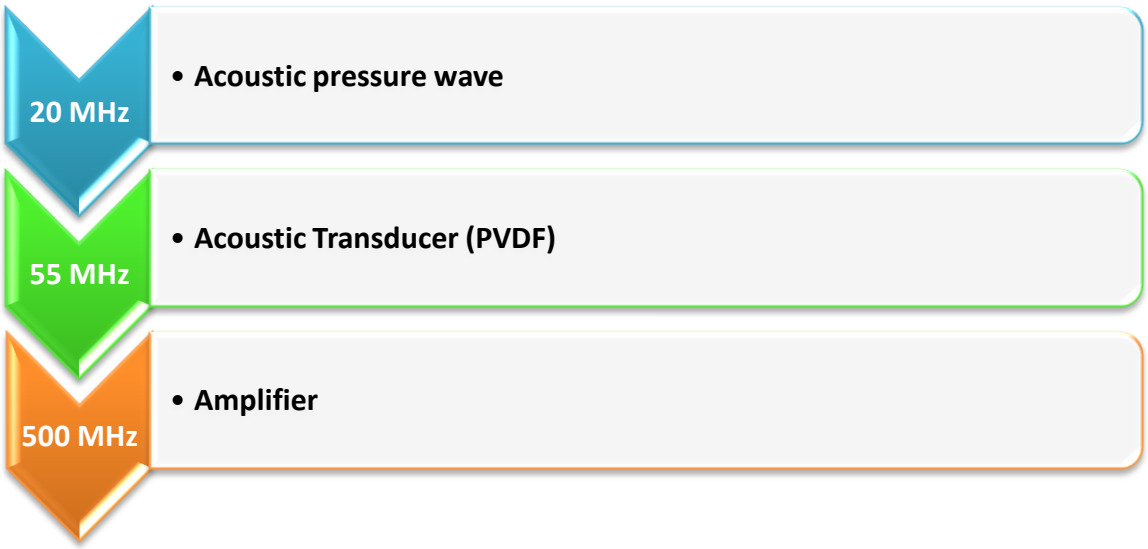

Figure 4-8: Illustration of a frequency response between the acoustic pressure wave, acoustic transducer and amplifier

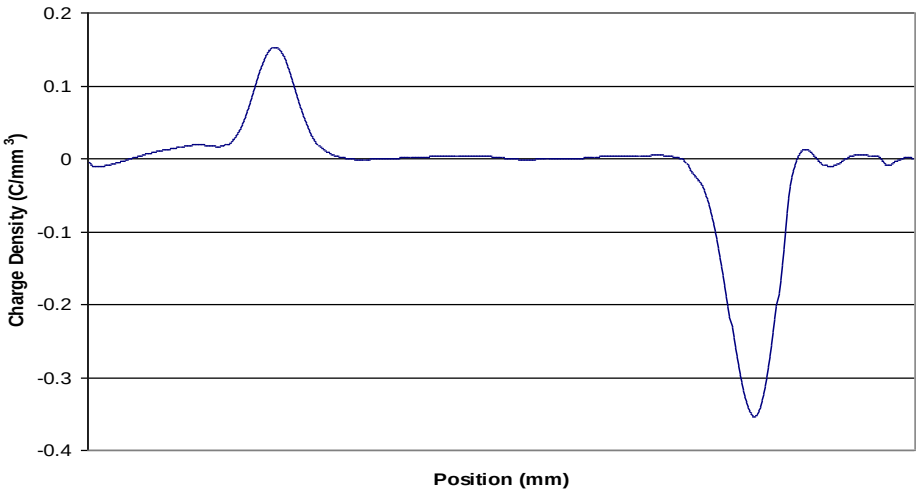

Figure 4-9: Illustration of a theoretical PEA output signal

However in practical case, when the components are connected together and due to the physical characteristic of each individual component, they tend to influence one another. The output signal from the amplifier shows internal charge has already built up when a

low voltage was applied to the sample. In theory the bulk of the sample should remain flat containing no internal charge and the only charges will be the inner and outer interfacial charges due to the applied voltage as illustrated in Figure 4-9.

This distorted or system response signal is the product of the combination of the transducer and amplifier as it operates as a high pass filter with a cut-off frequency that may be in the range of the frequency of the acoustic pressure [Morshuis and Jeroense 1997]. This distortion or system response signal could be misinterpreted as space charge accumulation, thus a deconvolution technique is required to restore the original signal.

4.5 Deconvolution Technique

The deconvolution technique [Maeno, Futami et al. 1988; Liu, Takada et al. 1993] is well established and greatly used in space charge measurements to obtain the recovered signal in the PEA technique. Assumption has been made that the acoustic wave consists of Gaussian distribution expressed as

$$p_1(t) = Ae^{-\alpha(t-\tau)^2} \tag{E4-5}$$

where A is the amplitude of the acoustic wave and a constant for a given sample with fixed thickness, applied DC voltage and pulse electric stress. α is also a constant but it is determined by the system's spatial resolution. Therefore, frequency domains for acoustic wave and electric output is expressed as $P_1(\omega)$ and $V_1(\omega)$ respectively, as shown below

$$V_1(\omega) = H(\omega) \cdot P_1(\omega) \tag{E4-6}$$

With the obtained transfer function of the whole system $H(\omega)$ from E4-6

$$V(\omega) = H(\omega) \cdot P(\omega) \tag{E4-7}$$

The frequency domain of the acoustic pressure wave, $P(\omega)$, could be obtained individually through deconvolution.

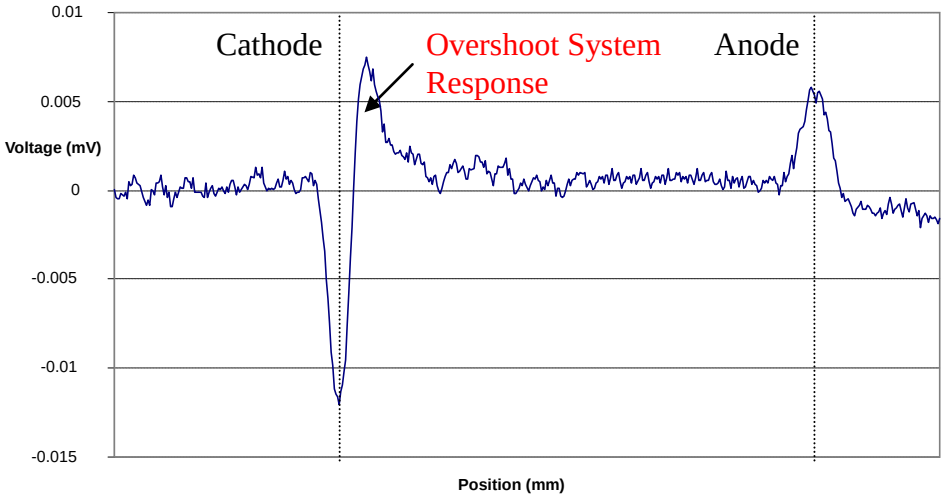

Figure 4-10: Typical PEA output signal

As shown in Figure 4-10, the peak from the outer electrode and the overshoot system response are determined as the reference signal for the calculation of the system transfer function. In the mean time, a "unit impulse time", $\gamma(t)$, is produced at the initial point of the outer electrode peak, expressed by $\delta(t-\tau)$ or $\delta(n-k)$, in continuous and discrete time system respectively.

Fast Fourier Transform (FFT) is applied on the outer electrode interfaces of the range of, $\gamma(t)$, and the reference output signal, $v_1(t)$, as shown below

$$F(\omega) = \int_{-\infty}^{\infty} \gamma(t)\, e^{-j\omega t}\, dt = FFT[\gamma(t)] \qquad \text{(E4-8)}$$

$$V_1(\omega) = \int_{-\infty}^{\infty} v_1(t)\, e^{-j\omega t}\, dt = FFT[v_1(t)] \qquad \text{(E4-9)}$$

Through E4-8 and E4-9, the transfer function of the system can be obtained in the frequency domain as

$$H(\omega) = \frac{V_1(\omega)}{F(\omega)} \qquad \text{(E4-10)}$$

Therefore, from E4-7, the frequency domain pressure wave, *P(ω)*, could be obtained and given as

$$P(\omega) = \frac{V(\omega)}{H(\omega)} \tag{E4-11}$$

Finally, by applying Inverse Fast Fourier Transform (IFFT) on pressure wave, *P(ω)*, the space charge distribution can be obtained. To summarise the whole concept of the process, a flow chart is used for illustration as shown in Figure 4-11.

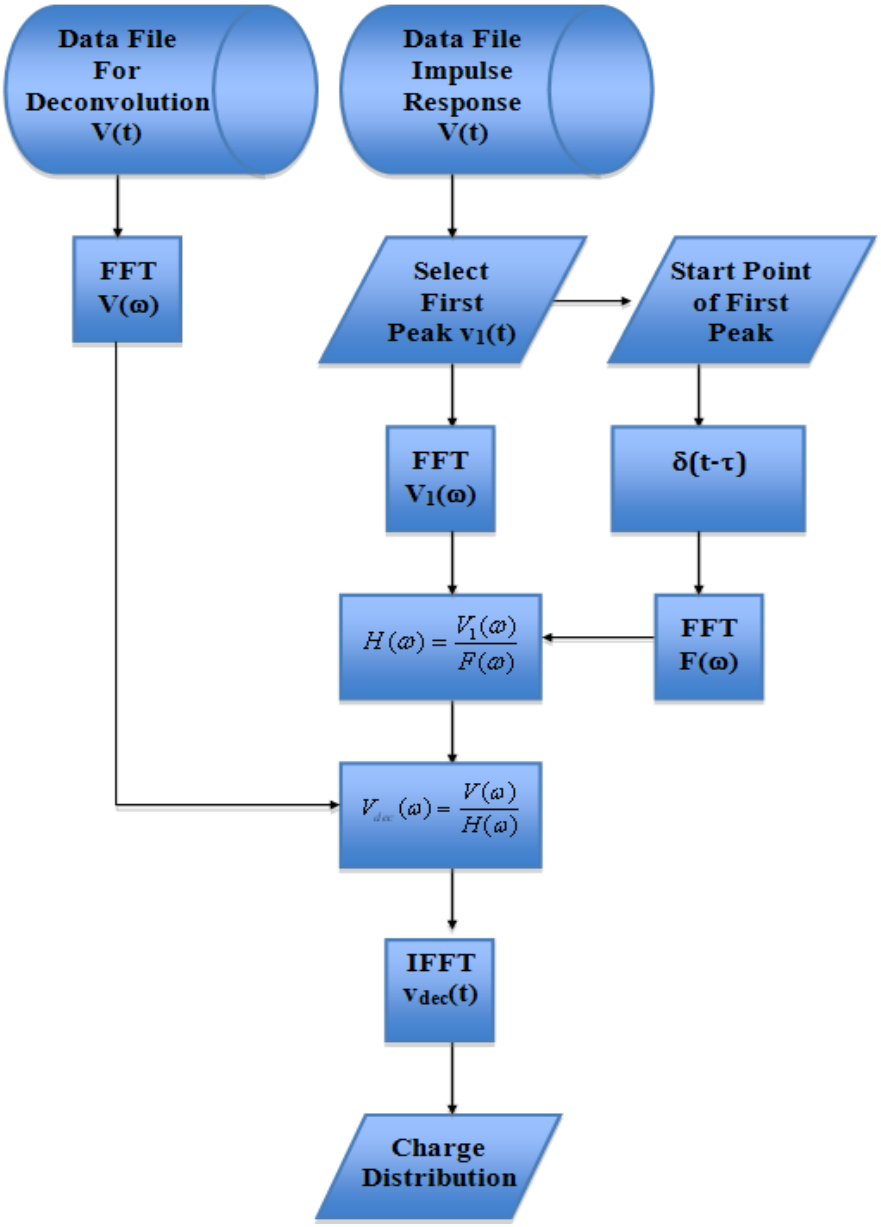

Figure 4-11: Flowchart for deconvolution technique

4.6 Cable's Geometry Compensation

With the coaxial geometry design in power cables, additional compensation are important and needed to be put into consideration if quantitative space charge measurement within the polymeric insulation material are acquired. In reality, polymeric insulation material behaves like a visoelastic medium and due to the coaxial geometry and thick walled insulation of a power cable; factors such as divergence, attenuation and dispersion are needed to be put into consideration [Fu, Chen et al. 2001b].

The main causes of attenuation are due to the absorption and dissipation of the acoustic energy into heat or other forms of energy [Chen, Tanaka et al. 2004]. Conversely, dispersion might be attributed to the scattering of the acoustic waves caused by densely distributed inhomogeneities and frequency dependence of the material constants such as elastic modulus. Consequently, propagation of the acoustic pressure wave through the insulation can strongly influence the resultant measurements [Chen, Chong et al. 2006].

Therefore, in this section we shall discuss on the data processing developed for the compensation of:

1. The divergence of pulsed electric stress and acoustic waves due to the cylindrical geometry of power cable.
2. The attenuation and dispersion of the acoustic waves travelling through the lossy insulating material.

4.6.1 Pulsed Electric Stress and Acoustic Waves Divergence

Through the years of commercial testing in power cables, it is recognised that the performance of insulation is mainly determined by the maximum electrical stress across the material. This maximum stress occurs in the insulation immediately adjacent to the

coaxial cylindrical electrode of the conductor core of a power cable.

Therefore, the electric stress, e_p, due to the external pulse voltage, $v_p(t)$, can be expressed as

$$e_p(t,r) = \frac{v_p(t)}{rIn\left(\frac{b}{a}\right)} \tag{E4-12}$$

where v_p is the external pulse voltage, a is the radius of the inner insulation and b is the radius of the outer insulation [Fu, Dissado at al. 2008].

Thus, the applied pulse will decrease gradually from the inner to the outer insulation. With the non-uniform of applied pulse within the insulation, this means that the stimulating of charges varies within the insulation, where charges located adjacent to the inner electrode are exposed to a higher pulse voltage than those charges located adjacent to the outer electrode, which will then produce a higher acoustic signal as compared to those adjacent to the outer electrode. Therefore, consideration factor of the mentioned event must be taken into account for a quantitatively space charge distribution.

With the space charge measurement taken, assumption was made to assume space charge distribution changes in radial direction. So in the case of acoustic wave equation under cylindrical coordinate, it is given as [Morse and Ingrad 1968; Beltzer 1988]

$$\frac{1}{c^2}\frac{\partial^2 \emptyset(r,t)}{\partial t^2} = \frac{\partial^2 \emptyset(r,t)}{\partial r^2} + \frac{1}{r}\frac{\partial \emptyset(r,t)}{\partial r} \tag{E4-13}$$

where $\emptyset(r, t)$ is the vibration velocity potential in the insulation and c is the acoustic wave propagation velocity.

The solution for the above equation can be written as

$$\emptyset(r,t) = \frac{A}{\sqrt{r}} e^{jk(r-ct)} \tag{E4-14}$$

where A is a constant determined by boundary conditions, c is the acoustic wave

propagation velocity, $\omega(2\pi f)$ is the acoustic wave angular frequency and $k = \omega/c$.

Therefore, the per unit area of the pressure wave that propagate within a cylindrical geometry of a lossy medium at position, *r*, is

$$p(r,t) = \rho \frac{\partial \emptyset(r,t)}{\partial t} = -\frac{j\rho cAk}{\sqrt{r}} e^{jk(r-ct)} \quad \text{(E4-15)}$$

where ρ is the density of insulation when acoustic wave is launched and travels.

The decrease of pressure wave between the inner and the outer insulation can be expressed in the form of

$$\frac{p(b,t+\Delta t)}{p(r,t)} = \left(\frac{r}{b}\right)^{\frac{1}{2}} \quad \text{(E4-16)}$$

where $p(r, t)$ is the acoustic waves produced at radius *r* and $p(b, t+\Delta t)$ is the acoustic waves detected at outer insulation *b*.

To conclude, correction is needed to the coaxial geometry due to the divergent pulse electric stress as the inner electrode acoustic pressure will be (b/a) times larger in value than the outer electrode. Conversely, detection of pressure wave at the outer electrode will be $(a/b)^{1/2}$ times smaller value than the inner electrode due to this effect. Hence, the charge density at the inner electrode will be $(b/a)^{1/2}$ times the actual value and data obtained from deconvoluting have to be corrected by the geometry factor $(b/r)^{1/2}$ [Fu, Chen et al. 2001b].

4.6.2 Attenuation and Dispersion Factors of Acoustic Wave through Lossy Insulating Material and in Cable Geometry

As mentioned earlier, polymeric material acts like a visoelastic medium. Hence, acoustic wave propagating within it will decrease in magnitude gradually and have its shape broaden from place of the origin to the place of detection of the acoustic wave. This event can be expressed in E4-17 through complex form of $k(j\omega) = \beta(\omega) + j\alpha(\omega)$

and results the wave propagation in a lossy medium as

$$p(t,r) = p_o e^{j[k(j\omega)r-\omega t]} = p_o e^{-\alpha r} e^{j[\beta r-\omega t]} \quad \text{(E4-17)}$$

where α is the attenuation factor and β is the dispersion factor.

Through Fast Fourier Transform (FFT) on E4-17, we are able to express the propagation of an acoustic wave in the lossy medium in the frequency domain, which yield into

$$P(\omega,r) = P(\omega,a)e^{-\alpha(\omega)(r-a)}e^{-\beta(\omega)(r-a)} \quad \text{(E4-18)}$$

where *P(ω,a)* is the Fourier transform of acoustic wave at radius *a* and *P(ω,r)* is the Fourier transform of acoustic wave at position *r*.

Through distinguishing both the attenuation, α, and dispersion, β, factors, it allow us to acquire the propagation characteristics. In principle, both factors can be acquired through the pressure wave measurements at inner ($r=a$) and outer ($r=b$) induced surface charge respectively. Magnitudes of both peaks are proportional to the applied electric stress as assumption of no accumulation of space charge within the bulk sample. Therefore, in order to recover the true waveform of both the attenuation and dispersion factors as shown in E4-19 and E4-20. A factor of ($\sqrt{a/b}$) is required to be applied on them as shown below

$$\alpha(\omega) = -\frac{1}{b-a} In \left| \frac{P(\omega,b)}{P(\omega,a)\cdot\sqrt{\frac{a}{b}}} \right| \quad \text{(E4-19)}$$

$$\beta(\omega) = \frac{1}{b-a}|\emptyset(\omega,b) - \emptyset(\omega,a)| \quad \text{(E4-20)}$$

where *P(ω,a)* is the magnitude range of the output signal at inner interface, *P(ω,b)* is the magnitude range of the output signal at outer interface, *ϕ(ω,a)* is the phase range of the output signal at the inner interface and *ϕ(ω,b)* is the phase range of the output signal at the outer interface.

Therefore, the transfer function of the acoustic wave through the cable insulation at position, *r*, can be expressed as

$$G(\omega, r) = \frac{P(\omega, r)}{P(\omega, a)} = e^{-[\alpha(\omega) + j\beta(\omega)](r-a)} \quad \text{(E4-21)}$$

Given the above transfer function, we are able to determine the true waveform from the acoustic transducer output, providing a better understanding of space charge formation within the insulation material of a coaxial design power cable.

Chapter 5 Electric Field Determination in the Presence of Space Charge and Temperature Gradient using COMSOL

5.1 Introduction

For the past few years, polymeric insulation materials using HVDC applications have drawn a high level of interest. Most HVDC installations around the world currently use the traditional oil-impregnated paper insulation and oil-filled-type cables [Rudervall, Charpentier et al. 2000; Hanley, Burford et al. 2003]. Polymeric materials like XLPE have long been the preferred insulation material and are gradually replacing traditional oil-impregnated paper insulation due to their low material and processing costs as well as their excellent high dielectric strength and electrical resistivity in combination with excellent physical properties such as resistance to cracking and moisture penetration [Dissado and Fothergill 1992]. Presently, cross-linked polyethylene (XLPE) insulation has been used, very successfully, for underground transmission and distribution of power, using HVAC transmission. DC power cables are also typically more cost-effective as compared to its counterpart of AC power cable due to the low conductor loss and thinner insulation thickness for the same power rating.

The main reason that prevents the use of polymers as insulation for HVDC cable for the

electricity generation and supply industries lies to the degradation of polymer insulation under high electric stress. This phenomenon is associated with the formation of space charge. In fact, space charge accumulation in polymeric materials under DC regime poses major scientific and technological problems.

In DC field conduction, the formation and movement of space charges within the polymeric material is influenced by both the external electric field (E) and the temperature (T). Hence, to understand the electric field distributions within the polymeric material both of these factors have to be considered in the conductivity of material when under DC field condition. Temperature of the whole polymeric insulation material also varies with its own thermal conductivity (k) and the temperature gradient (T) across it. With the distribution of the space charge obtained from the insulation material, the total field stressing the insulation can be calculated as a sum of the applied ($E_{Applied}$) and space charge field (E_{sc}).

Therefore, due to the complexity of the coupled equations, the total field and conductivity variation along the thickness of the insulation is calculated through a numerical simulation using COMSOL Multiphysics software package, which allows us to provide a clear overview on the underlying theoretical principles and phenomenon of space charge through the determination of results obtained from the polymeric material.

5.2 COMSOL Multi-physics Numerical Modelling

COMSOL Multi-physics software package is a modelling package for the simulation of complex multi-physics problem, which can be described with partial differential equations (PDEs). It is a scientific-software environment for the modelling and simulation of any physics-based system, where a particular strength is its ability to account for multi-physics phenomena through its modern and high-tech solvers that address complex problems swiftly and accurately. Therefore, through using this software package, we are able to construct a simulation that reflects reality depending not only on the accuracy of the geometries and physics but also on the conditions of materials utilised in the real world.

5.2.1 Heat Transfer Module

The effect of heat is ubiquitous and of great importance in the engineering world. Due to this fact, most material properties are temperature dependent, the effect of heat will drive the changes in the properties of the material itself. For instance, the HVDC power cables consist of both the conductor and insulation material. When high voltage is applied to the conductor, thermal energy is generated through the conductor and transferred to the polymeric insulator material. As DC conductivity is a strong function of both electrical field and temperature, it changes accordingly and affects the field grading [Maeno, Kushibe et al. 1985; Xu, Choo et al. 2007].

Heat transfer is described as the movement of energy due to temperature dissimilarity. The three mechanisms that characterise heat transfer are as follows:

1. *Conduction* is heat transfer by diffusion in a stationary medium (solid/liquid) due to a temperature gradient.
2. *Convection* is heat transfer between either a hot surface or a cold moving fluid (liquids and gases) or a cold surface and a hot moving fluid (liquids and gases).
3. *Radiation* is heat transfer via electromagnetic waves between surface A and B with different temperatures T_A and T_B respectively, provided that Surface A is observable to an infinitesimally spectator on Surface B.

The mathematical model of heat transfer implemented in COMSOL through conduction equation

$$\rho C \frac{dT}{dt} - \nabla \cdot (k \nabla T) = Q \qquad \text{(E5-1)}$$

where C is the heat capacity, k is the thermal conductivity, ρ is the density, Q is the heat source or a heat sink, t is the time and T is the temperature.

For a steady-state model, the first part of the equation in E5-1 disappears due to the temperature not changing with time.

For heat conduction and convection in the course of a fluid, a convective term will be

included in the heat equation as

$$\rho C_p \frac{dT}{dt} + \nabla \cdot \left(-k\nabla T + \rho C_p T\mu\right) = Q \quad \text{(E5-2)}$$

where C_p is the heat capacity under a constant pressure and μ is the velocity field.

The heat flux vector is defined by the expression within the parentheses in the equation above. For transport through conduction and convection, the equations are expressed as

$$Q = -k\nabla T + \rho C_p T\mu \quad \text{(E5-3)}$$

where Q is the heat flux vector.

If the heat transfer is by conduction only, Q is determined by

$$Q = -k\nabla T \quad \text{(E5-4)}$$

5.2.2 Electrostatic Module

In the electrostatic application mode, it is normally used on application that involves electrostatic such as high voltage equipments, electronic devices as well as capacitors etc. In COMSOL software package, it uses the application of electric potential, *V*, to model the static electric fields. Through combining the definition of potential with Gauss' law and the equation of continuity, it is possible to derive the classic Poisson's equation.

In particular under static state the electric potential, *V*, is expressed as

$$E = -\nabla \mathrm{V} \quad \text{(E5-5)}$$

$$D = \varepsilon_o \varepsilon_r E \quad \text{(E5-6)}$$

Having a relationship between the two physical quantities *D* and *E* of E5-6 and by

combining both E5-5 and E5-6 together. We are able to represent Gauss' law as Poisson's equation as shown below

$$-\nabla \cdot (\varepsilon_o \varepsilon_r \nabla \mathrm{V}) = \rho \tag{E5-7}$$

where ε_o is the permittivity of vacuum, ε_r is the relative permittivity of the material and ρ is the net charge density.

However, in the cylindrical coordinate, the Poisson's equation [Ida 2004] is expressed as

$$\frac{d^2V}{dr^2} + \frac{1}{r}\frac{dV}{dr} + \frac{1}{r^2}\frac{d^2V}{d\emptyset^2} + \frac{d^2V}{dz^2} = -\frac{\rho(r,\emptyset,z)}{\varepsilon_o \varepsilon_r} \tag{E5-8}$$

where $\rho(r, \phi, z)$ is the charge density at a particular point.

The space charge density, ρ, is dependent on the insulation radius since it only varies with the radial direction. The Poisson's equation is trimmed down to

$$\frac{d^2V}{dr^2} + \frac{1}{r}\frac{dV}{dr} = -\frac{\rho(r)}{\varepsilon_o \varepsilon_r} \tag{E5-9}$$

In cylindrical coordinate, E5-5 becomes

$$E = -\left(\frac{dV}{dr}\hat{r} + \frac{dV}{d\emptyset}\widehat{\emptyset} + \frac{dV}{dz}\hat{z}\right) \tag{E5-10}$$

The charge density is only dependent on the radius. Therefore, with $E = E_{sc}$ and $dV/dr = -E$, E5-9 becomes

$$\frac{dE_{sc}}{dr} + \frac{1}{r}E_{sc} = \frac{\rho(r)}{\varepsilon_o \varepsilon_r} \tag{E5-11}$$

Therefore, by inputting the individual charge densities, $\rho(r)$, obtained across the polymeric insulation into the model of the cable built and solved in COMSOL as shown in Appendix A, we are able to calculate the space charge field, E_{sc}, based from E5-11.

5.3 Expression for DC Conductivity Applied in COMSOL

Under the application of direct current, the electric field is resistively graded. It is recognised that DC conductivity correlates strongly on both electric field and temperature [Weedy and Chu 1984]. The variation in conductivity with temperature of insulation has a major effect on field grading with load as it can be seen that for a small temperature gradient, the electric field distribution is almost uniform. An increase of temperature gradient increases appreciably the degree to which the stress is inverted where the inner interfacial stress is reduced while the outer interfacial stress is increased. However, for the field-dependence of the conductivity, it is normally considered to be a second order effect as the effect is relatively small.

Through the hopping model of conduction in dielectric [Blythe and Bloor 2005], derivation of conductivity could be done from it. The expression of conductivity is well established and is expressed as

$$\sigma(T,E) = Aexp\left(-\frac{\varphi q}{kT}\right)\frac{\sinh\left(B|E|\right)}{|E|} \tag{E5-12}$$

where both *A* and *B* are constants, *E* is the electric field in V/m, *k* is the Boltzmann's constant, *q* is the elementary charge, *T* is the temperature in Kelvin and φ is the thermal activation energy in eV.

The above equation is applied in COMSOL to compute the electric field distribution in cables in the absence of space charge. It was examined that constants *A*, *B* and the thermal activation energy, φ, do varies depending on the types of material used and the condition of it. The parameters can be classified into two groups, good and bad dielectric respectively for XLPE cable [Boggs, Damon et al. 2001]. The expressions for conductivities for both good and bad dielectrics material are specified in E5-13 and E5-14 respectively and are expressed as

$$\sigma_{Good}\left(E,T\right) = 3.2781exp\left(-\frac{0.56q}{kT}\right)\frac{\sinh\left(2.7756\times10^{-7}|E|\right)}{|E|} \tag{E5-13}$$

$$\sigma_{Bad}(E,T) = 3.6782 \times 10^{7} exp\left(-\frac{0.98q}{kT}\right)\frac{\sinh\left(1.086\times10^{-7}|E|\right)}{|E|} \qquad \text{(E5-14)}$$

Under the proposed different dielectric material characteristics, simulations were done on the overall effect on electric field in the presence of space charge where both conductivities parameters are being utilised to obtain an accurate electric field distribution [Choo and Chen 2007].

5.4 Experimental Details

In this experiment, a commercial 11 kV AC XLPE insulated power cable (inner radii = 8.75 mm; outer radii = 11.55 mm; insulation thickness = 2.8 mm) is used. In order to understand the influence of cross-linking by-products (residues) in the space charge formation, this cable did not undergo the degassing process and therefore contains cross-linking by-products.

The cable was then stressed under the application of +80 kV DC supply (anode) for 20 hours and space charge distributions were subsequently measured using the modified PEA system immediately after the removal of the applied voltage as shown in Figure 5-1.

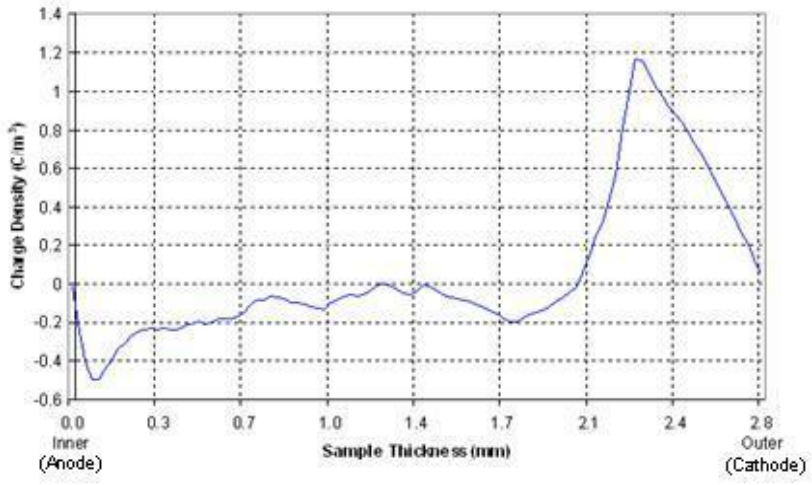

Figure 5-1: Space charge distribution across cable insulation

As illustrated in the above figure, dominating heterocharge formation is obtained in the XLPE insulation. Due to the cross-linking process, there will be formation of by-products such as methane, cumyl alcohol, acetophenone etc. in the XLPE cable. If the cable does not undergo the degassing process these by-products may be present in the material for a long period of time and undergo ionisation process under high electric field. The ionised species will move towards the opposite electrodes to form heterocharge. Due to the extraction of charge at the counter-electrode may be slow and this mechanism might be a potential cause.

In principle, the charge distribution shape and magnitude changes with time. As stressing time increases, both injected negative and positive charges start to move further into the sample and getting closer to each other. Both negative and positive magnitudes increase significantly with the duration of applied voltage [Fu, Chen et al. 2007]. Experiments also revealed that the space charge formed after 20 hours of stressing is very stable, implicating that the charges are deeply trapped [Fu 2002].

Once the space charge distribution, $\rho(r)$, is obtained in the sample material, the electric field, $E_{SC}(r)$, produced by space charge can be calculated based on Poisson's equation represented in E5-11.

Therefore, the total field is obtained by summing the applied field and this field due to space charge and is expressed as

$$E_{Total} = E_{Applied} + E_{sc} \tag{E5-15}$$

5.5 Simulation Results

To summarise the simulation method, the utilisation of both good and bad material parameters as stated in E5-13 and E5-14 respectively are used to obtain an electric field distribution through considering both the influence of space charge field and conductivity [Boggs, Damon et al. 2001].

Three steps have been adopted as follows

1. The calculation of electric field due to space charge based on Poisson's equation.
2. The electric field is being calculated based on the conductivity equation to determine the electric field arisen from the applied voltage.
3. Finally adding both the two fields together to form the total electric field as indicated in E5-15.

5.5.1 Good and Bad Parameters Simulated Results without Consideration of Both Temperature Gradient and Presence of Space Charge

Through using COMSOL, the simulated results of both good and bad dielectric parameters under an application of +80 kV DC supply to the cable considering the field-dependent conductivity, where no occurrences of temperature gradient on the conductivity and space charges are being considered, are shown in Figure 5-2 and Figure 5-3 respectively.

In both figures, the voltage distribution decrease gradually from 80 kV to 0 V from the inner interface to the outer interface as in principle, the outer interface of the insulation lies flatly on the grounded flat electrode of the PEA system. Conductivity distribution within the insulation is also shown in both Figure 5-2b and Figure 5-3b, where conductivity is slightly linear and it also does decrease gradually from the inner to outer interface when space charge accumulation within the cable is ignored. Electric field distribution within the cable's insulation is approximately 29.1 kV/mm to 28.1 kV/mm and 29.9 kV/mm to 27.4 kV/mm at the inner interface to outer interface of the insulation for both good and bad material parameters respectively.

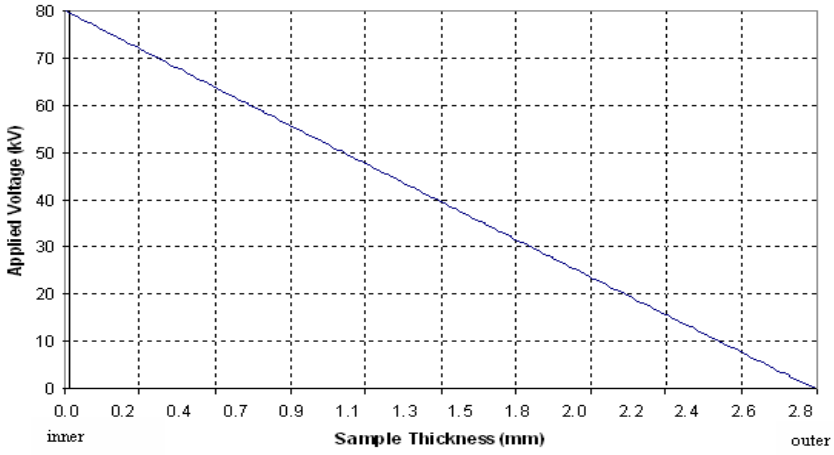

(a) Voltage distribution

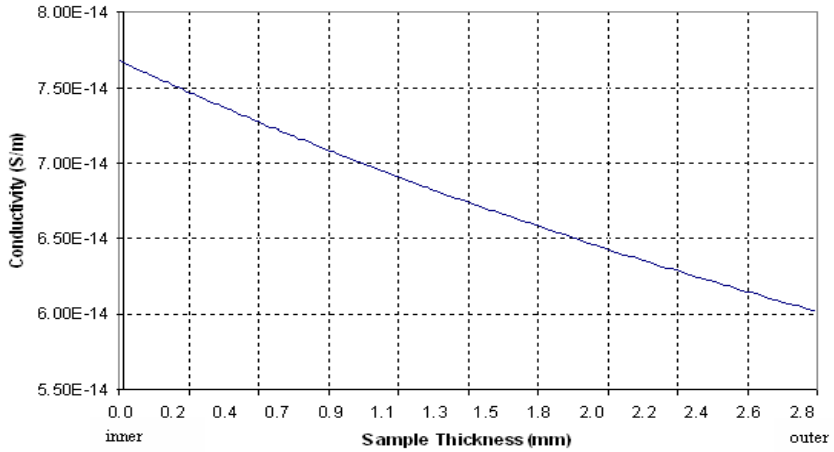

(b) Conductivity distribution

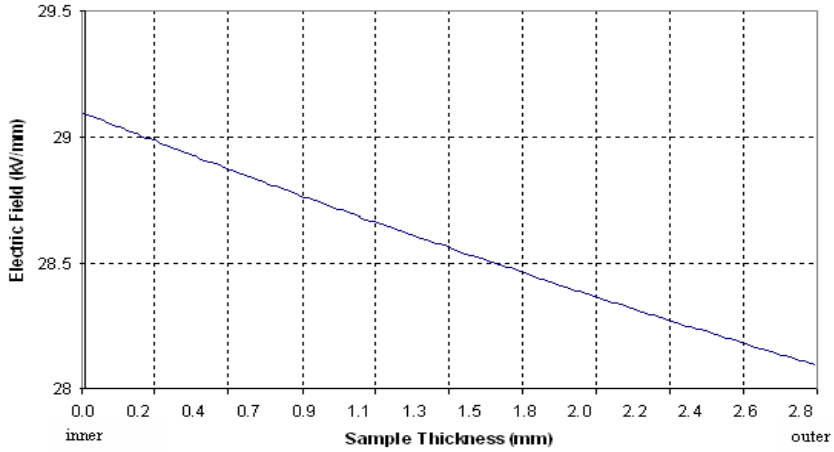

(c) Electric field distribution due to applied voltage

Figure 5-2: Simulation results considering the field-dependent conductivity when 0K temperature gradient T_{inner} = 295K and T_{outer} = 295K without the presence of heterocharge for good parameters

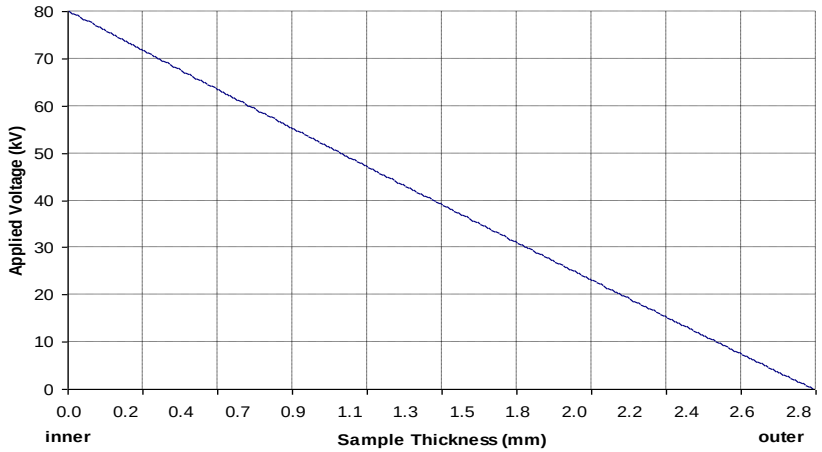

(a) Voltage distribution

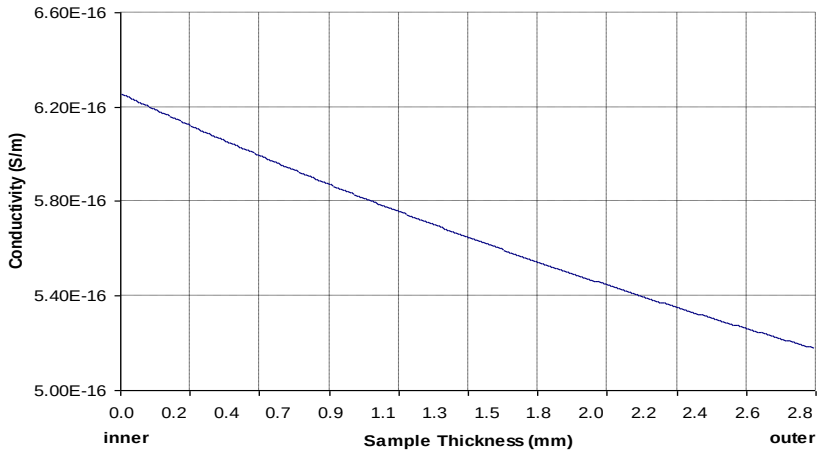

(b) Conductivity distribution

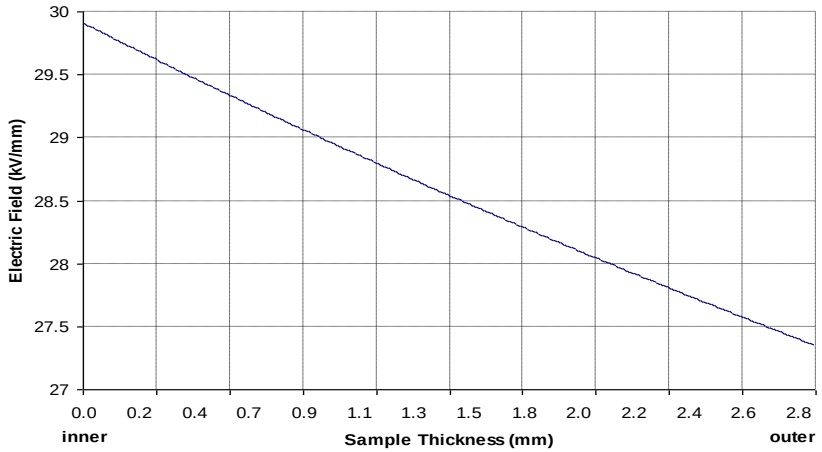

(c) Electric field distribution due to applied voltage

Figure 5-3: Simulation results considering the field-dependent conductivity when 0K temperature gradient T_{inner} = 295K and T_{outer} = 295K without the presence of heterocharge for bad parameters

5.5.2 Good and Bad Parameters Simulated Results with Consideration of Temperature Gradient but without the Presence of Space Charge

With the exclusion of the presence of space charge within the insulation and the classification of both good and bad parameters previously inserted to the program. A new factor of temperature gradients of 30 K and 50 K occurring between the insulation are being considered in the program.

The presence of temperature gradients within the XLPE insulation of the cable will alter the results obtained as compared to the results shown in section 5.5.1, when no occurrences of temperature gradient on the conductivity and space charges are being considered within the insulation.

From the results obtained for both good and bad dielectric parameters, it can be seen respectively from both Figure 5-4a and Figure 5-5a that, with the consideration of temperature gradients, the voltage distribution within the insulation tends to deviate to non-linearity at the middle of the bulk sample. This deviation becomes severer with the increases of temperature gradient and it can also be observed that when the insulation material possesses the classification of bad parameters, the deviation to non-linearity from the inner interface to the middle of the bulk is also much severe as compared to the classification of good parameters. Conductivity distributions within the insulation are also observed for both good and bad parameters, where the conductivity increases when temperature gradient increases, as shown in Figure 5-4b and Figure 5-5b respectively. With the presence of temperature gradient on the conductivity, the electric field distribution, due to applied voltage, is completely changed, as illustrated in Figure 5-4c and Figure 5-5c for good and bad parameters respectively as compared to Figure 5-2c and Figure 5-3c in section 5.5.1. It can be seen that the maximum stress appears at the outer screen, and the value of this stress increases as the temperature gradient across the insulation increases.

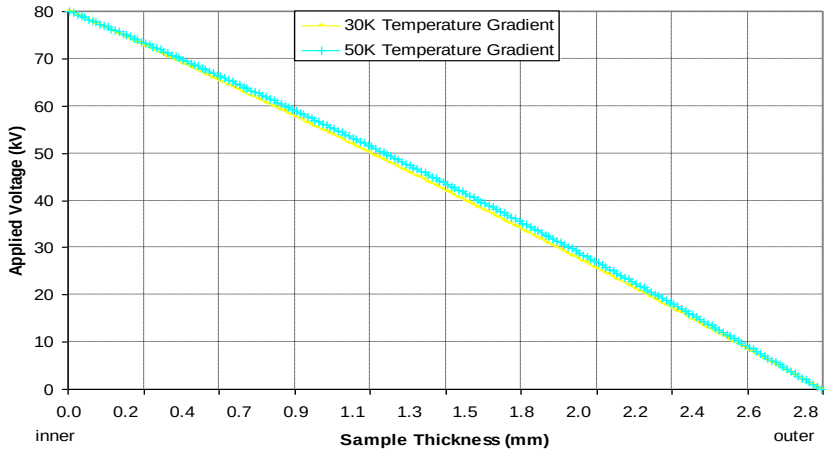

(a) Voltage distribution

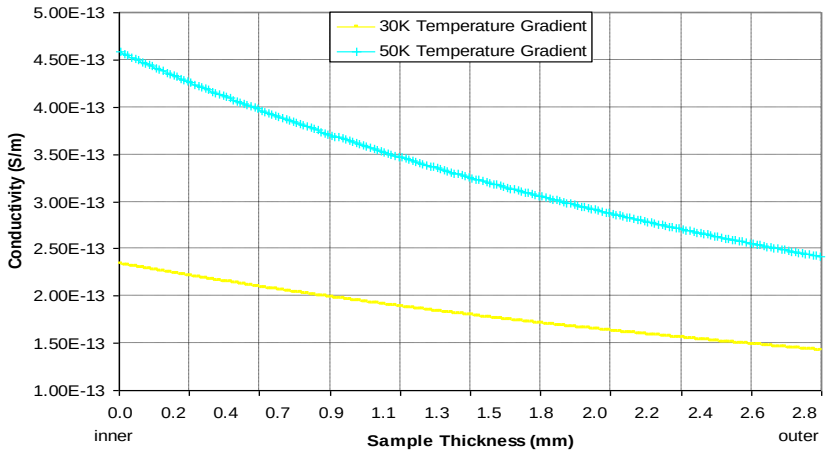

(b) Conductivity distribution

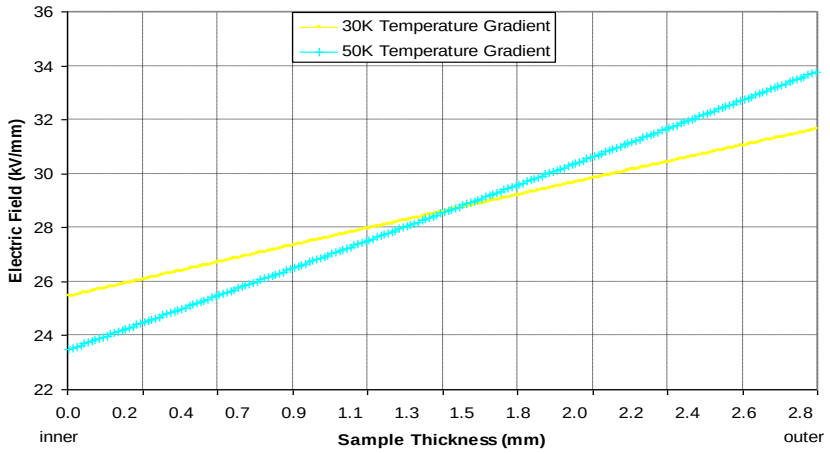

(c) Electric field distribution due to applied voltage

Figure 5-4: Simulation results considering both field and temperature gradient dependent on conductivity and T_{outer} = 295 K without the presence of heterocharge for good parameters

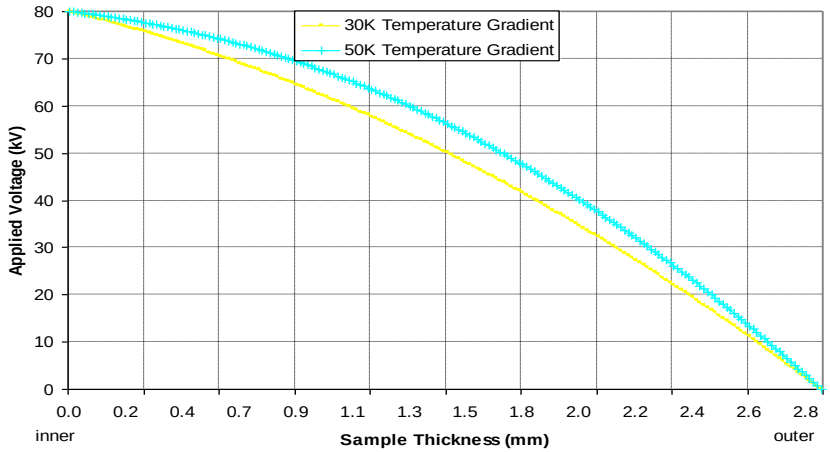

(a) Voltage distribution

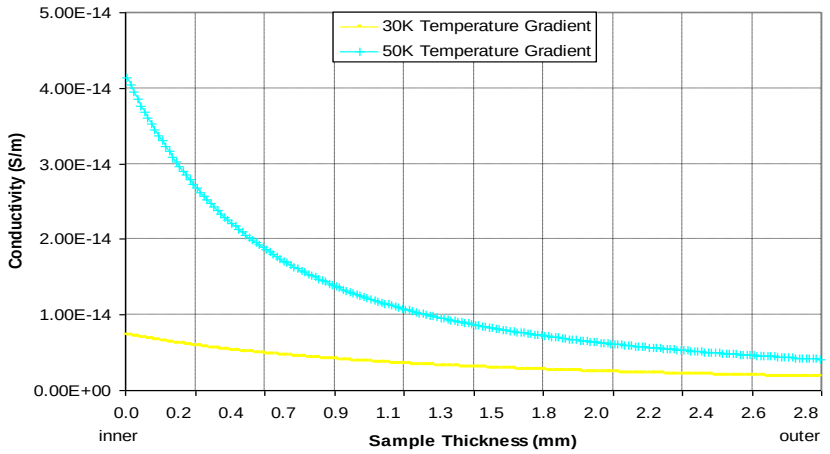

(b) Conductivity distribution

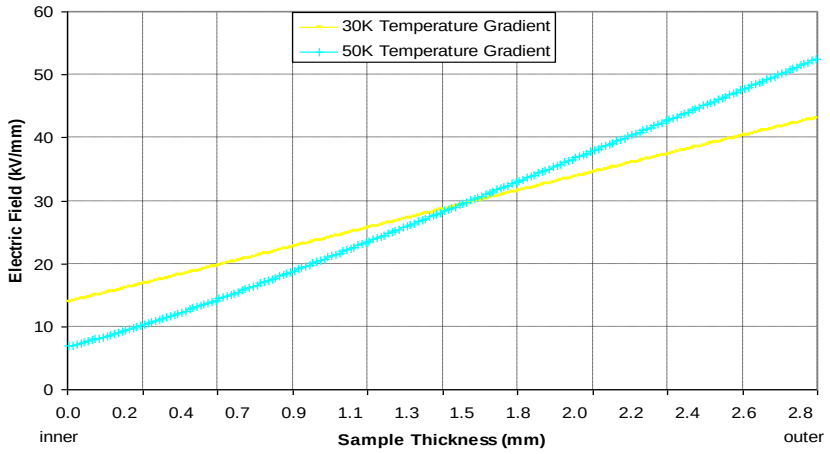

(c) Electric field distribution due to applied voltage

Figure 5-5: Simulation results considering both field and temperature gradient dependent on conductivity and T_{outer} = 295K without the presence of heterocharge for bad parameters

5.5.3 Good and Bad Parameters Simulated Results without Consideration of Temperature Gradient but with the Presence of Space Charge

With the insertion of individual space charges accumulated across the insulation as shown in Figure 5-1 after an application of +80 kV supply for 20 hours on the power cable into the simulated one dimension drawing of the cable in COMSOL. This presence of heterocharges accumulation within the XLPE insulation of the cable will alter the results, as shown in Figure 5-6 and Figure 5-7.

In Figure 5-6, the results illustrate the profiles of having good parameters for the insulation material, where there is no temperature gradient occurring within the insulation but with the presence of space charge accumulated within the insulation. With the consideration of the space charge field, it can be seen clearly from Figure 5-6a that with this accumulated space charge, the voltage profile deviates to non-linearity at the region adjacent to the interface. Conductivity of the insulation sample is no longer linear due to the consideration of space charge field, as shown in Figure 5-6b. The maximum conductivity of 1.08×10^{-13} S/m occurs at the outer interface. The total electric field distribution as illustrated in Figure 5-6c, shows that high stresses are located at both inner and outer interfaces with the higher stress located at the outer interface. The higher interfacial stress adjacent to the cathode is due to the higher amount of heterocharge accumulation as compared to the vicinity adjacent to the anode.

Whilst in Figure 5-7, the results illustrate the profiles of having bad parameters for the insulation material. The results obtained are similar to those using good material parameters, where the voltage profile deviates to non-linearity at the region adjacent to the interface and conductivity of the insulation sample is no longer linear due to the consideration of space charge field.

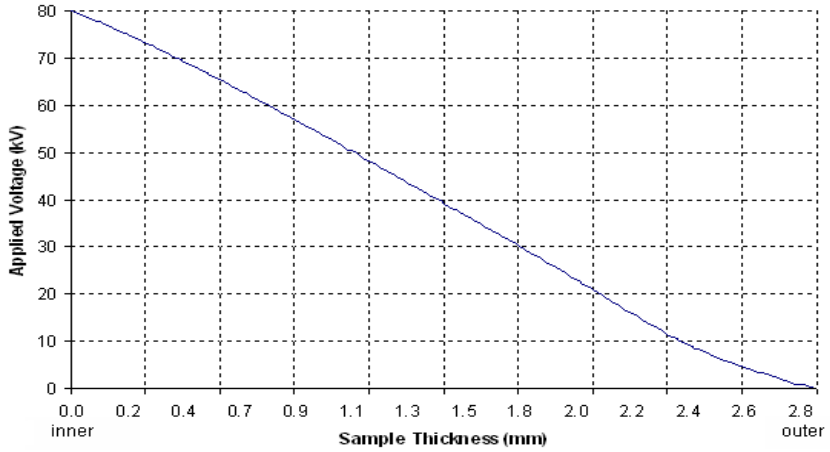

(a) Voltage distribution

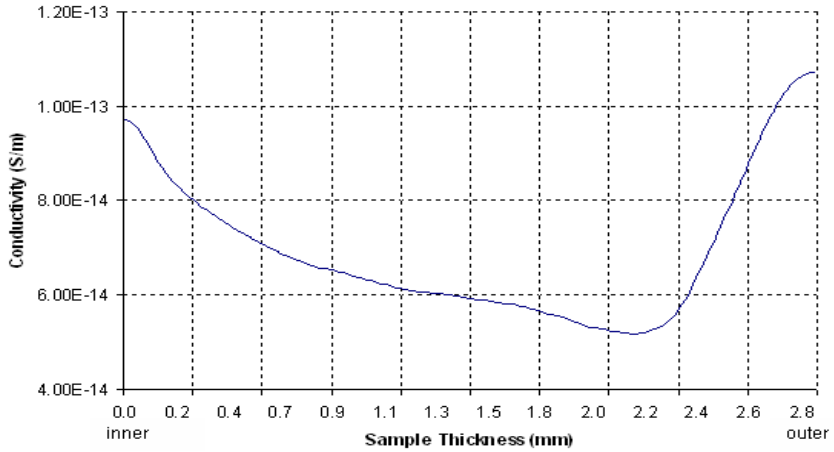

(b) Conductivity distribution

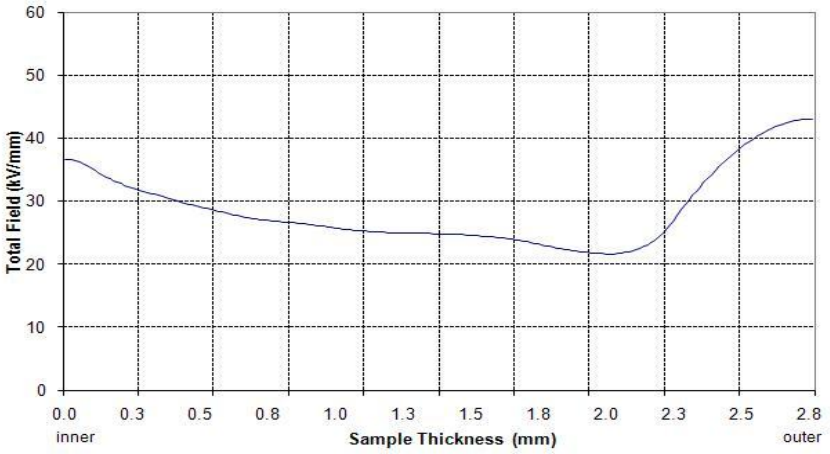

(c) Total electric field distribution in cable

Figure 5-6: Simulation results considering the field-dependent conductivity when 0K temperature gradient T_{inner} = 295K and T_{outer} = 295K with the presence of heterocharge for good parameters

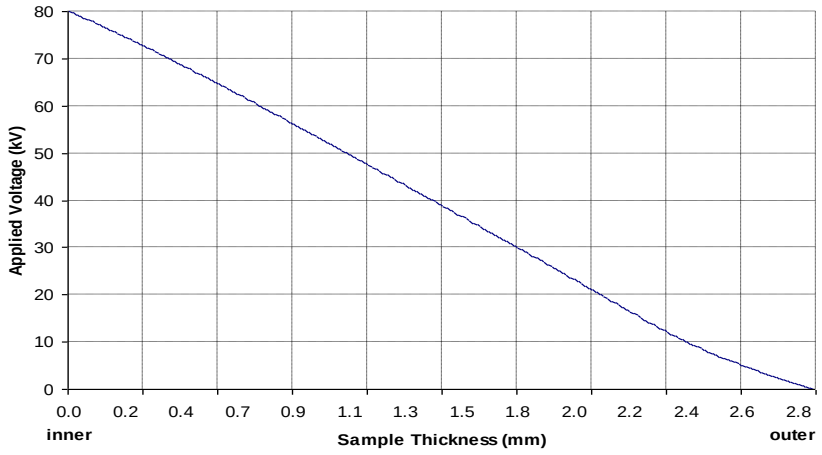

(a) Voltage distribution

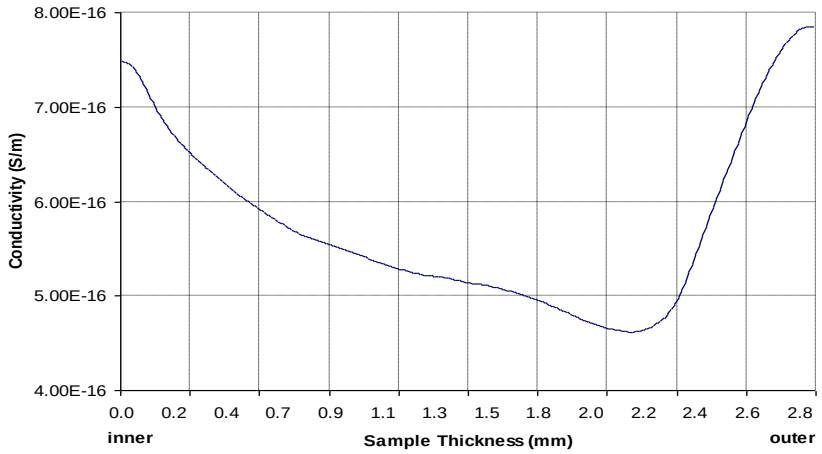

(b) Conductivity distribution

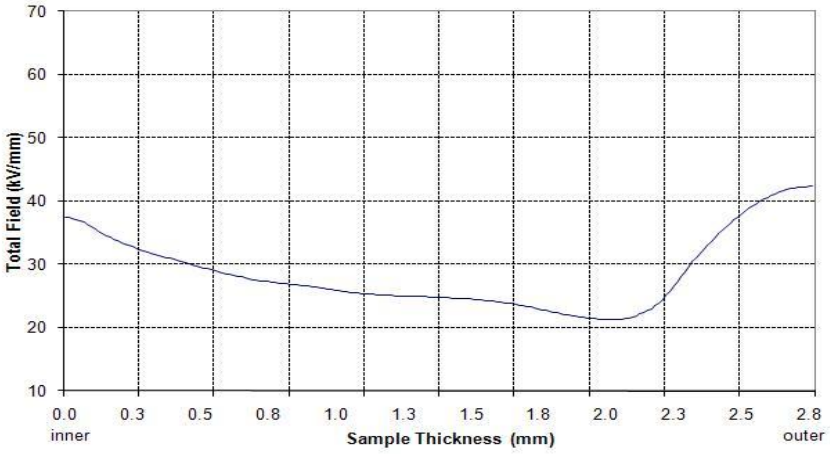

(c) Total electric field distribution in cable

Figure 5-7: Simulation results considering the field-dependent conductivity when 0K temperature gradient T_{inner} = 295K and T_{outer} = 295K with the presence of heterocharge for bad parameters

5.5.4 Good and Bad Parameters Simulated Results with Consideration of Temperature Gradient and with the Presence of Space Charge

When both temperature gradient and space charge accumulation were to be considered between the inner and outer interface of the XLPE insulation of the power cable. The simulated results for good parameters are illustrated in Figure 5-8, where Figure 5-8b clearly shows that there is an increase in conductivity distribution when temperature gradient increases. Therefore, in Figure 5-8c when temperature gradient increases from 30 K to 50 K, it shows that the total electric field distribution due to applied voltage actually decreases at the inner region and tends to increase at the middle of the sample towards the outer interface of the insulation material.

In the case for bad parameters, it is observed that when both temperature gradient and space charge accumulation are considered between the inner and outer interface within the XLPE insulation of the power cable, the voltage profile deviates more to non-linearity between the inner interface and the middle of bulk sample, as shown in Figure 5-9a. In Figure 5-9b, the conductivity distribution drops rapidly between the inner interface and the middle of bulk sample and tends to settle down after the middle bulk sample. Similarly, the total electric field distribution across the insulation are obtained and shown in Figure 5-9c and comparisons are done between the results obtained using the good parameters. The bad parameters total electric field distributions show a lower inner interfacial stress and a much higher outer interfacial stress as compared to using the parameters of a good dielectric material. The interfacial stresses under bad parameters show that when temperature gradient increases from 30 K to 50 K, the inner interfacial stress drops further to 15 kV/mm, whereas the outer interfacial stress rises to a much higher value of 67 kV/mm.

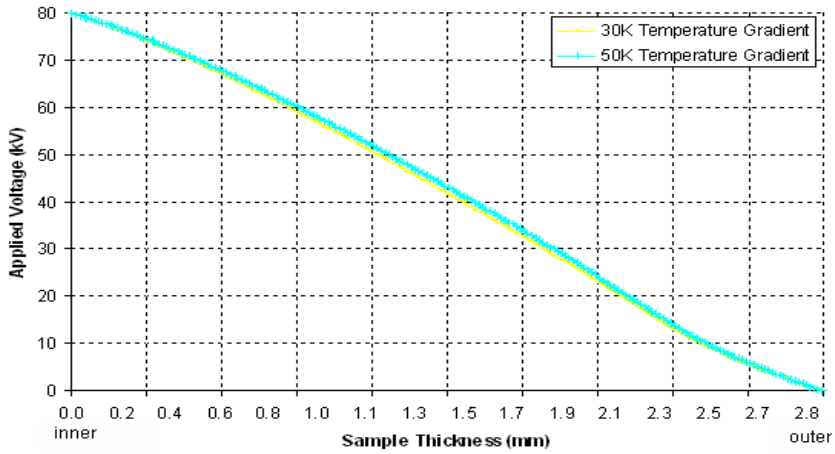

(a) Voltage distribution

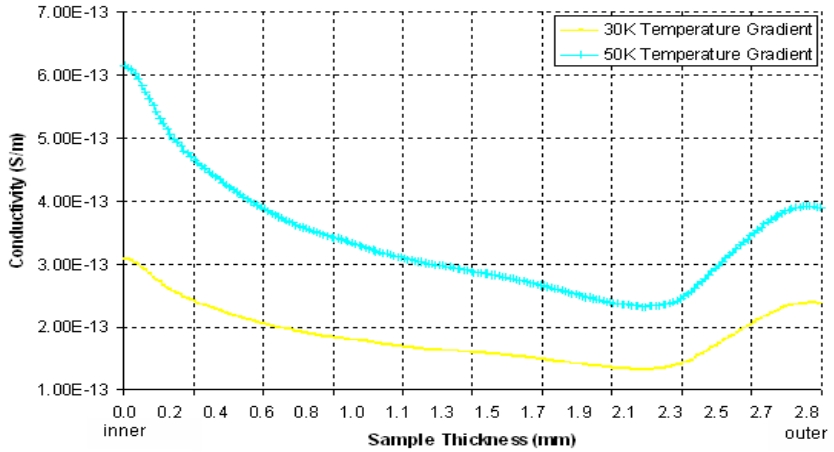

(b) Conductivity distribution

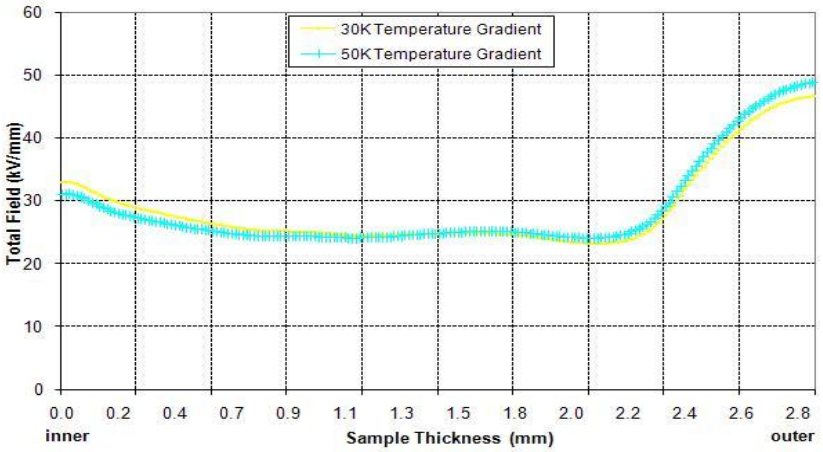

(c) Total electric field distribution in cable

Figure 5-8: Simulation results considering both field and temperature gradient dependent on conductivity T_{outer} = 295K for good parameters

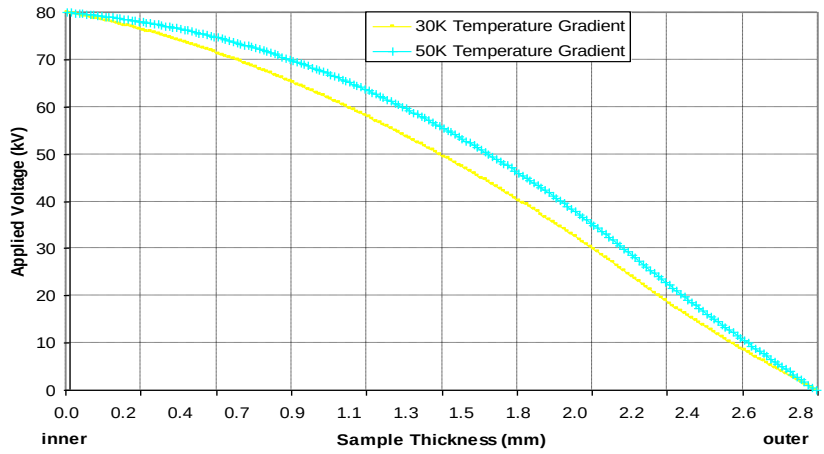

(a) Voltage distribution

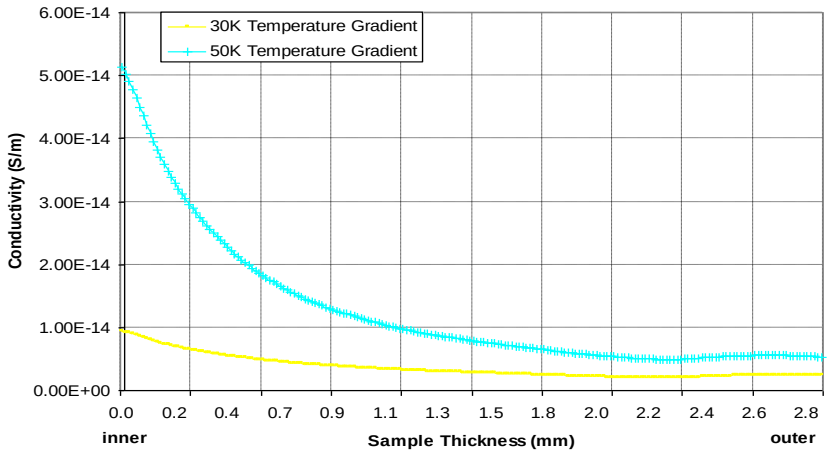

(b) Conductivity distribution

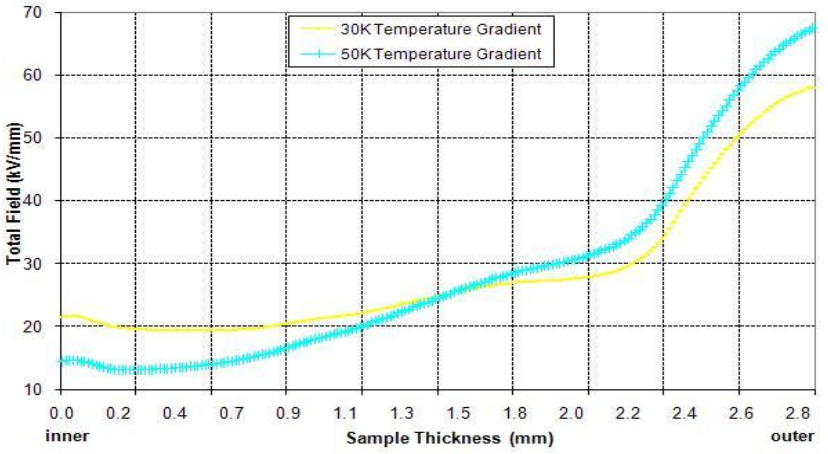

(c) Total electric field distribution in cable

Figure 5-9: Simulation results considering both field and temperature gradient dependent on conductivity T_{outer} = 295K for bad parameters

5.5.5 Simulated Results of Total Electric Field Distribution for Both Good and Bad Parameters

The total electric field is obtained through summing the applied field and the space charge field as expressed in E5-15. Therefore, a comparison of the total electric field distribution within the XLPE insulation of the cable has been made in this section.

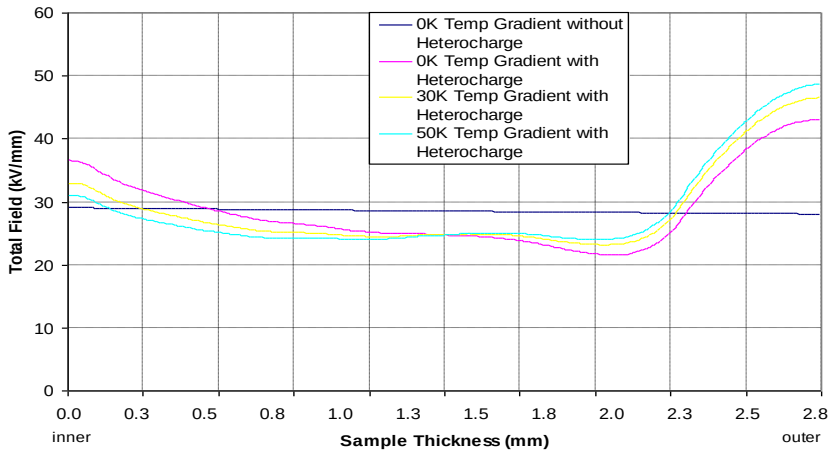

Figure 5-10: Total electric field distribution in cable with T_{outer} = 295K based on good parameters

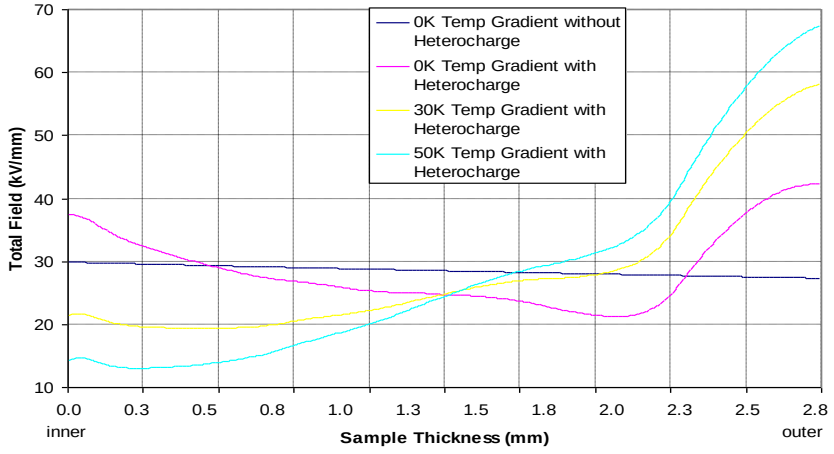

Figure 5-11: Total electric field distribution in cable with T_{outer} = 295K based on bad parameters

Illustrations on the total electric field distribution for both good and bad parameters of a dielectric material are being used and illustrated in both Figure 5-10 and Figure 5-11 respectively. It clearly shows that, when the conductor of the cable is heated, the

maximum stress occurs at the outer region adjacent to the screen of the cable. With the increment in temperature gradient within the insulation material, the stress at the inner region tends to decrease further and the stress at the screen of the cable tends to increase higher.

5.6 Discussion

Our simulation results suggest there is no significant difference when no temperature gradient is considered. These results could be explained by the fact that the final value of conductivity which is determined by the space charge field is the same for both cases considered – good and band dielectric. Nevertheless, when temperature gradient is considered, it has been shown that there is a significant difference in the computed results for the good and bad dielectric parameters. Hence, as illustrated in Figure 5-10 and Figure 5-11 where good and bad dielectric parameters results in terms of total electric field are compared when temperature gradients are considered, it can be concluded that there is not much variation in terms of stress when good parameters are adopted, as compared with a significant variation when bad parameters are assumed.

Table 5-1: Comparison of Simulated Results of Good and Bad Material Parameters

	With Space Charge	**30K Temperature Gradient**	**50K Temperature Gradient**
Good Parameters	53%	66%	73%
Bad Parameters	55%	112%	146%
Between Good and Bad Parameters		20%	28%

The difference in the total electric field in terms of temperature gradient for 30 K and 50 K are 20 % and 28 % respectively between good and bad dielectric materials, as illustrated in Table 5-1. From the simulation results we obtained, it can be suggested that bad dielectric parameters, as indicated in E5-14, shows stronger temperature dependence.

5.7 Conclusion

We have measured space charge across the insulation in a DC power cable after an application of +80 kV for 20 hours using the PEA technique. In this experiment, heterocharge is accumulated in the XLPE dielectric material of the cable due to the influence of cross-linking by-products (residues) in the space charge formation as the cable did not undergo the degassing process and, therefore, contained cross-linking by-products.

COMSOL Multi-physics software package is used to accurately determine the total electric field distribution across the insulation of the power cable by considering the influences of both the variation of the conductivity and the space charge field across the insulation material under a specific temperature gradient. The results indicate that when a cable is heated, the maximum stress occurs at the outer region adjacent to the screen of the cable and the value of this stress increases with the increase value of temperature drop across the dielectric material. Comparisons were also made between good and bad dielectric parameters, with temperature gradients being considered. It shows that there is not much variation in terms of stress when good parameters are adopted as compared with bad parameters adopted, where significant variation were observed.

Bulk space charge accumulation, caused by non-uniform conductivity due to temperature gradient and electric field, is therefore essential to both cable designers as well as the users.

Chapter 6 Space Charge Measurements on XLPE Cable with and without Temperature Gradient

6.1 Introduction

There is a worldwide demand for electricity, which is growing annually in every developing country. The requirement for bulk-power transmission is not only emerging for systems providing dense urban areas but also in meshed transmission networks, where electric power companies are upgrading their installed capacity in response to factors such as network stability requirements and transmission de-regulatory policies. Also, the increasing importance of environmental considerations in designing and constructing new lines has stirred the requirement for efficient HV and EHV underground transmission cable systems that offer high power ratings and stability with reduced transmission losses.

Cable manufacturers have been manufacturing and delivering HV XLPE insulated cables for the past thirty-five years and in terms of material production, handling and development tests made on the insulating materials. The usage of super clean EHV XLPE insulating high grade compounds are used for the manufacturing of the insulating material and an on-line melt inspection system is utilised to screen the cleanliness of the

insulating compounds. In fact, comprehensive regimes of measurements are needed to ensure the reliability, in particular, with regards to the cleanliness and homogeneity of the insulation and the smoothness of the interfaces with the extruded semi-conducting shields.

As a precondition for an excellent long-term service performance of an XLPE power cable, space charge measurements can be made on the polymer insulation to acquire additional quality assurance.

In this chapter, the space charge measurements were taken on the XLPE power cable both with and without temperature gradient consideration within its insulation. This investigation allows us to understand the space charge phenomenon within the insulation of the power cable with consideration of its service temperature.

6.2 Experiment Details

In this experiment, space charge measurements were taken from a 11 kV AC XLPE insulated power cable, under an average room temperature of 18 ^{0}C, by means of a modified PEA system with a current transformer attached as shown in the earlier chapter's Figure 4-7. An application of 80 kV DC supply is applied on to the cable and different temperature gradients across the insulation are considered to simulate the conditions when under service conditions. A numerical simulation using COMSOL Multi-physics software package has been used to determine the electric field distribution of XLPE power cable in the presence of space charge.

6.2.1 Sample Preparation

The 11 kV XLPE insulated power cables (inner radii = 5.8 mm; outer radii = 9.2 mm; XLPE insulation thickness = 3.4 mm; cross-section of stranded aluminium conductor = 95 mm^2) used in these experiments were contributed by commercial company Prysmian Cables & Systems.

The as-received roll of cable is being cut and prepared as illustrated in Figure 6-1. Both ends of the outer semi-conducting are stripped back exposing part of the conductor cores allowing high voltage and applied pulse voltage to be attached onto it. Stress relief rings were also used at the screen cuts to reduce the possibility of failure of the insulation due to the long duration of testing the cable sample.

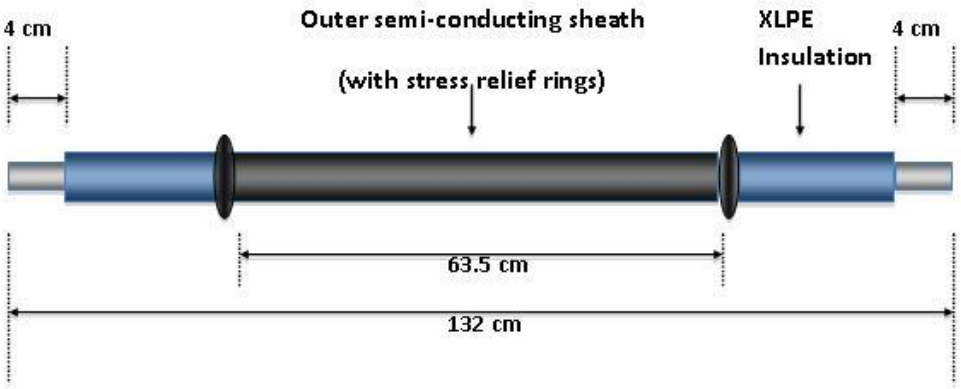

Figure 6-1: Illustration of a prepared cable for experiment

6.2.2 Temperature Gradient Setup

In this experiment, temperature gradient is generated across the insulation material through induction heating using a current transformer, where the cable aluminium core is heated and a radial temperature gradient is generated across the insulation material. The temperature distribution across the XLPE insulation can be calculated as a function of the radius, *r*, and is expressed as

$$T(r) = T_{outer} + \frac{T_{inner} - T_{outer}}{\ln(r_{outer} - r_{inner})} \ln\left(\frac{r_{outer}}{r}\right) \quad \text{(E6-1)}$$

where T_{inner} and T_{outer} indicates the inner and outer temperature screen of the conductor respectively.

Table 6-1: Temperature gradient across the insulation using 250A induced current

Hour	Ambient Temperature (^{0}C)	Inner Temperature (^{0}C)	Outer Temperature (^{0}C)	Temperature Gradient (^{0}C)
0	18	18.4	18.4	0
1	18.6	48.4	39.5	8.9
2	19.2	49	39.7	9.3
3	19.8	50.7	41.3	9.4
4	20.2	52.2	41.3	10.9
5	20.4	52.4	41.2	11.2
6	20.7	54.1	43.8	10.3
7	20.9	54.3	44.3	10
8	20.8	55.2	45.1	10.1
9	20.3	55.3	44.8	10.5

Table 6-2: Temperature gradient across the insulation using 350A induced current

Hour	Ambient Temperature (^{0}C)	Inner Temperature (^{0}C)	Outer Temperature (^{0}C)	Temperature Gradient (^{0}C)
0	17	17.3	17.3	0
1	17.6	80.6	64.6	16
2	18	83.9	64.7	19.2
3	18.8	84.8	65.3	19.5
4	19.2	84.9	65.3	19.6
5	19.4	86	66.2	19.8
6	19.7	86.8	66.7	20.1
7	19.9	88.7	68.5	20.2
8	19.8	89.4	69.4	20
9	19.8	89.6	69.2	20.4

In order to obtain the desired temperature gradient across the insulation, a dummy cable is firstly utilised which is quite similar to the one as shown in Figure 6-1 but with a portion of the XLPE insulation removed at the centre, exposing the cable core. An

induced AC current is then applied to the cable core through a current transformer and temperature measurements were taken on the interfaces of the inner and outer insulation of the cable, as shown in Table 6-1 and Table 6-2.

Through an induced current of 250 A and 350 A, stabilised temperature gradients of ~10 ^{0}C and ~20 ^{0}C are obtained across the insulation respectively after 2 hours of induction heating, where the outer semiconductor of the cable is cooled through natural convection cooling by the ambient temperature.

6.2.3 Experimental Setup

Three as-received cables were prepared into the specification illustrated in Figure 6-1 and the cables did not undergo the degassing process; therefore, cross-linking by-products are contained within the insulating material. In addition, results obtained through the experiments are accurate and repeatable as the cables are from the same batch obtained directly from the cable manufacturer.

Three different test conditions were then setup for each of the cable samples as follows:

1. No temperature gradient across the insulation at under ambient temperature.
2. A 10 ^{0}C temperature gradient across the insulation.
3. A 20 ^{0}C temperature gradient across the insulation.

In both test conditions, for 10 ^{0}C and 20 ^{0}C, the cable is first heated up through the current transformer 2 hours prior to obtain the desired stabilised temperature gradient before starting the experiment and the current transformer is remained on throughout the experiment measurements. A DC voltage of +80 kV was then applied on the 11 kV XLPE cables and space charge measurements of both voltage on and off were taken on specific time during the 9 hours of stressing. Subsequently, removal of the application voltage is done through short-circuiting of both electrodes where charge decaying measurements were taken.

6.3 Experiment Results and Discussion

As mentioned earlier, as the cable did not undergo the degassing process, cross-linking by-products such as methane, cumyl alcohol, acetophenone etc. are still present within the XLPE insulation [Andrews, Hampton et al. 2006]. These by-products may be present in the material for a long period of time and influence the space charge distributions within the material. Some of the by-products enhance electron (or hole) injection from the electrode and, as a result, formation of homocharge is observed. Heterocharge formation is obtained from ionic carriers supplied from some impurities. It has been observed that homocharge is formed in degassed XLPE and heterocharge is formed in as received XLPE [Li and Takada 1992]. Furthermore, similar observation has been reported on the results for increasing cross-linking by-product concentrations in XLPE and it is suggested that these impurities may become charged and migrate to the counter electrode under DC stress [Suh, Hwang et al. 1994]. Therefore, these cross-linking by-products present from the cross-linking reaction will undergo ionisation process under a high electric field and these ionised species will move towards the opposite electrodes to form heterocharge. Nevertheless, at high electric field accompanied with a higher temperature, the amount of charges tend to increase due to the higher injection rate and also having a higher mobility leading to the enhancement of the transportation of charges. Therefore, the observed heterocharge formation is due to the resultant effect of both scenarios, as shown in the results in Figure 6-2 to Figure 6-4.

6.3.1 Space Charge Profiles of XLPE Cable with No Temperature Gradient across the Insulation at under Ambient Temperature

In the first test condition, space charge distributions were obtained from the modified PEA with no temperature gradient across the insulation and are illustrated in Figure 6-2. The voltage on space charge profile presented in Figure 6-2a shows homocharge formation begins to accumulate where negative space charge starts to form within the sample adjacent to the cathode and a large amount of heterocharge builds up in the XLPE insulation vicinity adjacent to the anode (inner electrode) after the first hour of

poling. Furthermore it was observed that positive charges tend to accumulate around the middle of the sample towards the cathode (outer electrode) after 3 hours of poling.

This rapid accumulation rate of negative charges within the sample can be explained through negative charge being much easily trapped as compared to positive charge. It is also evident through the observation of the relatively higher increment rate of negative charges in each cable sample prior to being cancelled out by the positive charges. Other reasons could be more negative charges are injected into the insulation samples than positive charges or it could be a combination of both scenarios. For the build up of positive charge around the middle of the sample towards the outer electrode, this may be due to the difficulty of trapping positive charge and consequently these positive charges will not be trapped in the region of the anode but rather will be attracted to the region of the cathode where they are cancelled out or recombine with the accumulated negative charges. A steady space charge accumulated state within the bulk of the sample is obtained at 3 hours of poling as the barrier height of both anode and cathode will increase due to the accumulated charges adjacent to them, which lead to the fall of injection and extraction rates where they equal to the charges transportation rate.

In the volts off measurement when the external voltage is temporarily off, as illustrated in Figure 6-2b, it was found that portions of negative slow moving charges are been trapped adjacent to the vicinity across both anode and cathode. Slow moving positive charges are also observed accumulating within the centre part of the sample. Based from the observation, it is evident that the charges contributed by both ionisation of by-products and injection from electrodes are slow moving charges, which are permanently trapped across the insulation material.

Additionally, a space charge decay test was done after the cable was stressed for 9 hours by having the inner and outer electrodes short-circuited. Measurements were taken at certain time intervals between the 24 hours of the decay test and are presented in Figure 6-2c. The space charges that are accumulated within the insulation material seem to hold up at a rather long period of time for at least 18 hours. The sign of decay was observed after 18 hours of decaying, where measurements recorded during the 24th hour of decay show minimum amount of positive charges with ~0.1 C/m^3 density left in the centre of the insulation and ~0.2 C/m^3 of negative charges density are left adjacent

to both anode and cathode respectively. A point to note from the results in Figure 6-2 is a decrease in thickness of 0.2 mm of the cable's XLPE material. This effect was caused by the tightening of the cable sample between the electrodes and the cable sample may have been sandwiched too tightly.

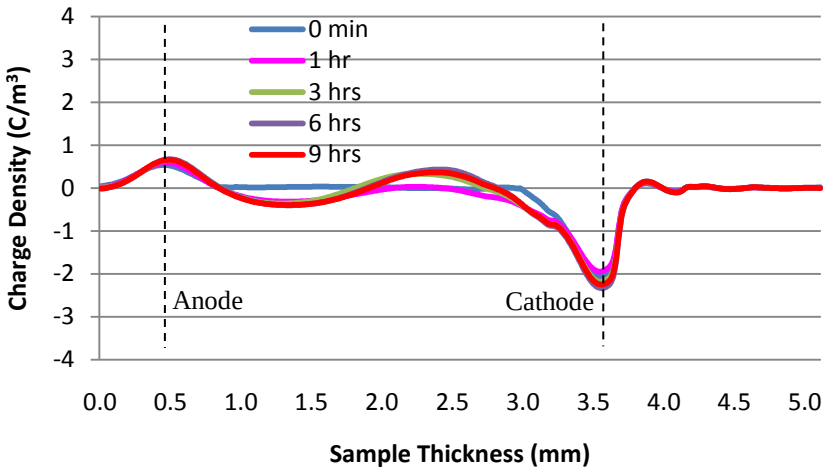

(a) Volts on

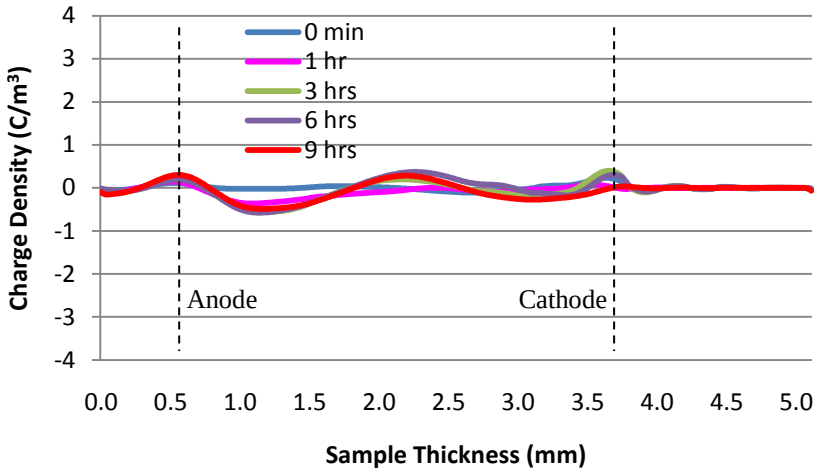

(b) Volts off

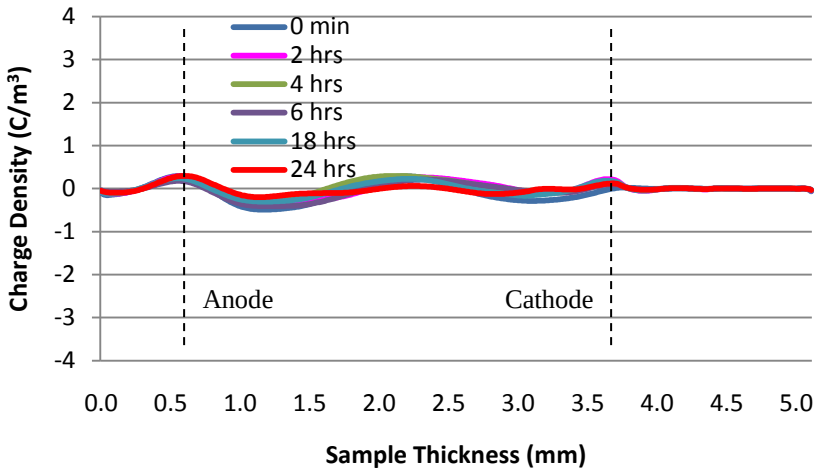

(c) Space charge decay

Figure 6-2: Space charge profiles for (a) volts on, (b) volts off and (c) decay at ambient temperature with T_{outer} = ~18 ^{0}C

6.3.2 Space Charge Profiles of XLPE Cable with 10 ^{0}C Temperature Gradient across the Insulation

Figure 6-3 shows the result when 10 ^{0}C temperature gradient is applied across the power cable insulation when replicating it under service condition. At the voltage on measurements as illustrated in Figure 6-3a, it is observed that only negative charges are formed initially on the first hour of poling in the vicinities adjacent to the both electrodes across the sample with the largest concentration located in the vicinity adjacent to the anode. As mentioned earlier, space charge formation within the cable insulation are caused by the ionisation process due to the residue of by-products leftover from cross-linking process and the injection of charges from both anode and cathode respectively. The development of charges observed on the first hour depends mainly on the mobility of electrons travelling across the sample. As it shows, the mobility of electrons is high enough to ensure the electrons liberated by ionisation of impurities close to the cathode, and those electrons injected from the cathode are fairly rapidly transported towards the anode due to a higher mobility leading to the higher arrival than extraction in the anode region. Furthermore, positive charge injection behaviour is also observed at the anode vicinity where it became more obvious after 1 hour of poling. As it clearly shows the positive charges are attracted to the cathode vicinity, where it

cancels out or recombines with the accumulated negative charges, leading to a decrease in negative charges adjacent to both electrodes. After 3 hours of poling, heterocharge formation begins to take form in the vicinity adjacent to the cathode and this positive charge increases with the duration of application voltage applied to the cable. Migration of the positive charge moving further into sample is also observed under 10 ^{0}C temperature gradient due to the enhancement of mobility with comparison to no temperature gradient across insulating material, as shown in Figure 6-2a.

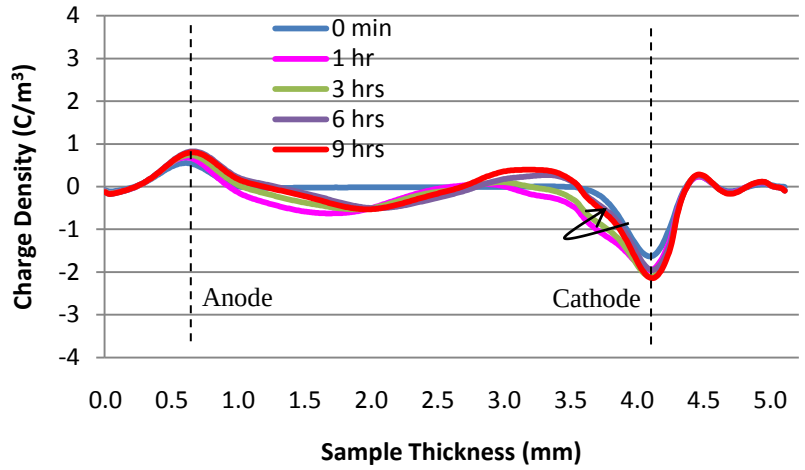

(a) Volts on

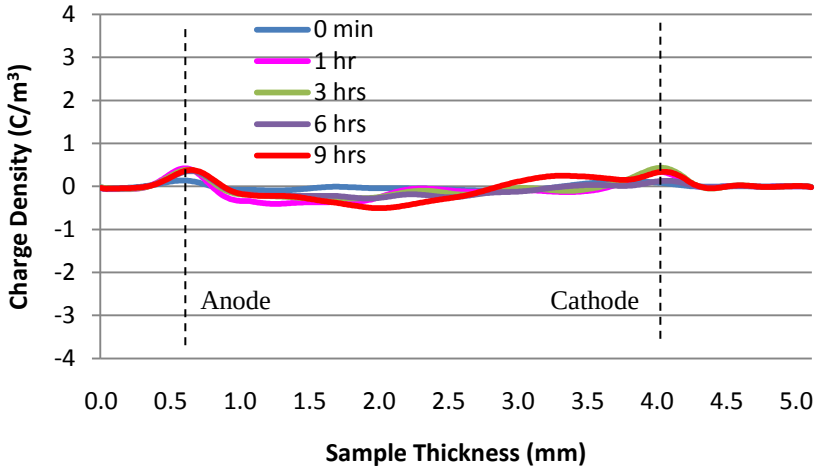

(b) Volts off

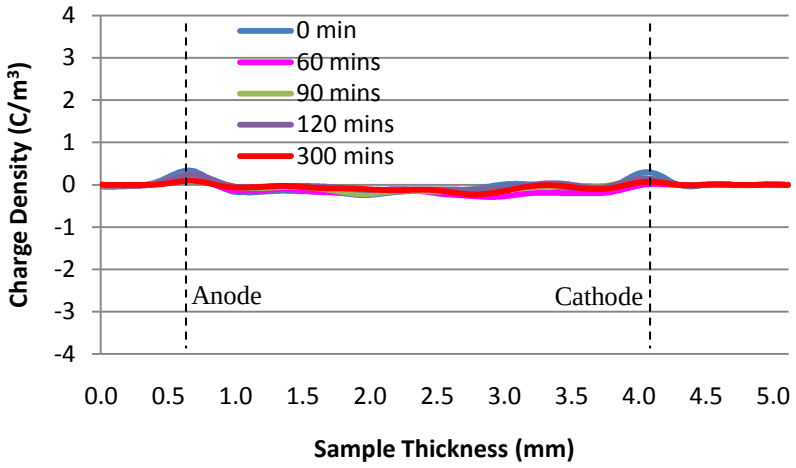

(c) Space charge decay

Figure 6-3: Space charge profiles for (a) volts on, (b) volts off and (c) decay with 10°C temperature gradient and with T_{outer} = ~45 ^{0}C

In the volts off measurement illustrated in Figure 6-3b, only packets of slow moving negative charges are observed being trapped across the sample, where the main portion of the negative charges spread across from the anode vicinity to the middle of the sample, and small packets of it are visible from the middle of the sample to the cathode vicinity. Slow moving positive charges that were previously observed in the middle of the sample under no temperature gradient across the insulation were not accumulated on the same location as measured before. The disappearing of this positive charge may be due to the enhancement in mobility of the positive charge, which enables them to advance to the adjacent of the cathode, whereby; the positive charge cancels out or recombines with the accumulated negative charge or is extracted out by the cathode. Therefore, with the applied temperature gradient across the insulation, no positive slow moving charges were observed due to the enhancement of mobility for both positive and negative slow moving charges, leading to no permanently trapped positive charges.

In the charge decaying profile for 10 ^{0}C temperature gradient as shown in Figure 6-3c, the charges show a quick decay rate and the charges almost diminish in 2 hours after the removal of applied voltage. By the 5th hour of decay, it shows only a small stretch of ~0.2 C/m^3 of negative charges in the middle of the insulation and also in the vicinity adjacent to the cathode.

6.3.3 Space Charge Profiles of XLPE Cable with 20 ^{0}C Temperature Gradient across the Insulation

Under a temperature gradient of 20 ^{0}C across the insulation material, the results obtained are illustrated in Figure 6-4. With comparison to the result between Figure 6-3a and Figure 6-4a, of 10 ^{0}C and 20 ^{0}C temperature gradient respectively, it shows that with an additional increase in temperature gradient the amount of charges do increase across the sample material. Thus, the high temperature enhances the injection and little changes are done on the relative injection barriers. It has also been reported, an average increase for positive and negative mobility is about 3 and 6 times larger respectively on doubling the temperature [Delpino, Fabiani et al. 2007].

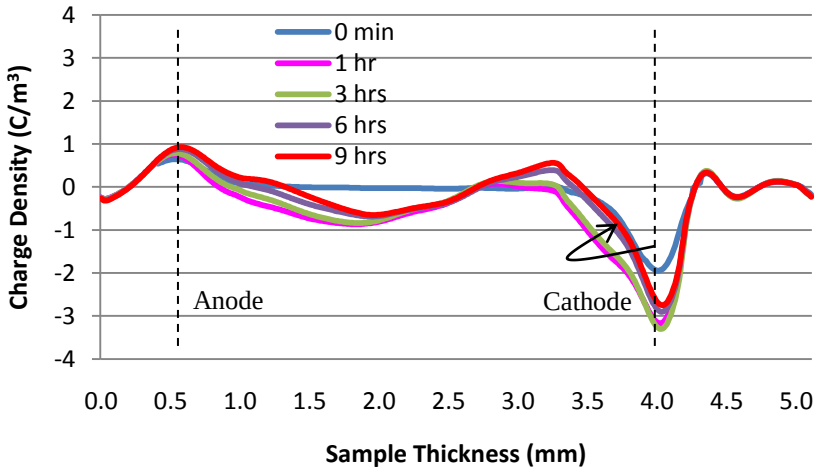

(a) Voltage on

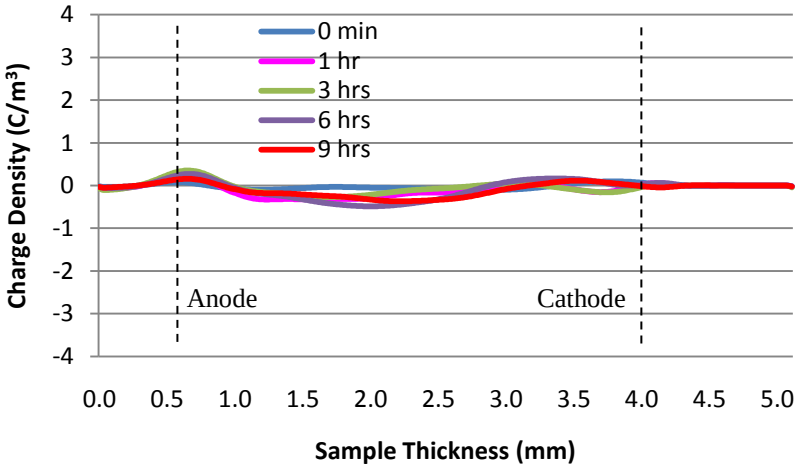

(b) Voltage off

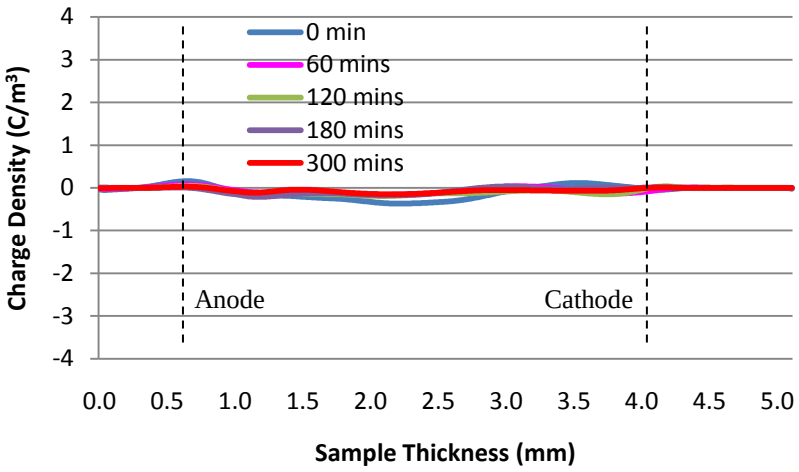

(c) Space charge decay

Figure 6-4: Space charge profiles for (a) volts on, (b) volts off and (c) decay with 20°C temperature gradient and with T_{outer} = ~69 ^{0}C

The voltage off measurements also tend to show that slow moving positive charges are now visible in the vicinity adjacent to the cathode after 3 hours. There were no sign of slow moving positive charges in both the voltage off profiles of ambient temperature and 10 ^{0}C temperature gradient in Figure 6-2b and Figure 6-3b respectively. Hence, by doubling the temperature gradient across the insulation, it led to the enhancement in mobility of the positive charge. These positive charges, with an enhanced mobility, are all attracted and trapped to the adjacent of the cathode, whereby, the arrival rate of it is much more than the negative charges and they could cancel out or recombine and even be extracted out by the cathode. Therefore, positive charges are visible during the voltage off measurements.

In the space charge decay profile, decaying rate was extremely rapid when 20 ^{0}C temperature gradient is present across the sample material as charges were observed to have been diminished within an hour of decay. The rate of decay was twice as fast as compared to the 10 ^{0}C temperature gradient across the sample material.

Due to the existence of temperature gradient across the insulation material, additional complexity is introduced to the space charge dynamics. According to the theory, the build-up of the induced charges on the cathode should lead to a decrease in negative charges or an increase of positive charges adjacent to the outer electrode. Surprisingly,

however, with the increasing temperature gradient, the electrode adjacent negative charges decrease with the increase of the induced charges on the cathode, as shown in Figure 6-4a, with comparison to both Figure 6-2a and Figure 6-3a. Specifically, the charge very close to the cathode is decreasing, while the space charges closer to the middle of the sample seem to be more consistent. This phenomenon could not be explained from simple electromagnetic theory. In view of the fact that the decrease with temperature is restricted to the area close to the colder electrode and, interface phenomenon was not included in the theory [Holbøll, Henriksen et al. 2000].

The basic explanation for this phenomenon can be explained if we were to imagine that the cable insulation consists of a series of parallel capacitors and resistors connected under DC application and with the consideration of temperature gradient across the insulation material. The resistivity through the insulation material will increase across from the inner to the outer of the insulation material, when a temperature gradient exists. In addition, the formation of homocharge in the vicinity of the cathode results in the electric field reduction. The conductivity of an insulating material increases with the electric field. The lower electric field in this region leads to an increase in resistivity. As the voltage distribution under DC condition is governed by resistivity. Therefore, voltage drop across the region increases. This increased voltage drop can be reflected by an increase in the amount of charge accumulated on the paralleled connected capacitor. This will lead to an increase in measured charge on the cathode. Similarly, if the homocharge moves away, the induced charge peak will decrease. This phenomenon is unique to the DC cable and become obvious with a higher temperature gradient.

6.3.4 Total Electric Field Distribution in Cable

In the present simulation, we have utilised the parameters from good and bad material, as stated in E5-13 and E5-14 respectively, to obtain an accurate electric field distribution through considering the influence of space charge field and conductivity [Choo and Chen 2008].

By applying the space charge distribution measurements, $\rho(r)$, obtained from the different conditions of temperature gradients after 9 hours of stressing into E5-11, the electric field, $E_{sc}(r)$, produced by space charge at 9 hours of stressing is obtained.

Consequently, classifications of both good and bad parameters as mentioned earlier are applied under an application of 80 kV based on the conductivity equation, where the electric field is determined based on the applied voltage.

Figure 6-5 illustrates the total electric field distribution across the cable's insulation, where considerations were made to the influences of both the effects of temperature and electric field on the conductivity of the insulating material. In our experiments, all three different temperature conditions produced heterocharge formation. It is also straightforward to understand that heterocharge will result in interfacial stress enhancement and also stress reduction in the centre of sample. Therefore, during the 9 hours of positive stressing with no temperature and 10 ^{0}C temperature gradient across the insulating material, heterocharge raises the interfacial stresses at the inner and outer interface to 40 kV/mm and 20 kV/mm for no temperature gradient and 41 kV/mm and 28 kV/mm for 10 ^{0}C temperature gradient respectively. When under 20 ^{0}C temperature gradient the inner interfacial stress is reduced to 36 kV/mm while the outer interface stress increases to 33 kV/mm. With the increment of temperature gradient, the stress at the inner interface doesn't seems to fluctuate much between no temperature and 10 ^{0}C temperature gradient but a reduction of ~9 % is observed once 20 ^{0}C temperature gradient is applied. Subsequently, the stresses at the outer interface have shown to increase to ~41 % and ~68 % with the increment of temperature gradient of both 10 ^{0}C and 20 ^{0}C applied to the insulation respectively. Furthermore, the electric stress in the middle of the insulation is reduced to a certain extent and the position of it tends to move towards the outer interface when there is an increment of temperature gradient applied across the insulation.

The simulation results in Figure 6-5 are all based on parameters from a good dielectric material. Conductivity equation E5-13 indicates that it has stronger field dependence, which means when there is a small variation in electric field, the conductivity changes significantly. This therefore results in a stronger modification of the electric field and less of temperature dependence as it was observed that the inner interfacial stresses does not change much between no temperature and 10 ^{0}C temperature gradients.

Conversely, if we choose the parameters for a bad dielectric material by using equation E5-14, one should expect there will be less field modification but stronger temperature

dependence. The total electric field distribution based on parameters from a bad dielectric material is illustrated in Figure 6-6. From the results it shows that with the increment of temperature gradient across the insulation, the inner interface stress tends to decrease and the outer interface stress tends to increase. The decreases of the inner electric stress are ~10 % and ~30 % and increases of ~65 % and ~114 % at the outer electric stress for both 10 ^{0}C and 20 ^{0}C temperature gradients respectively with contrast to the electric stress of no temperature gradient. Thus, within the insulation a lower electric stress is observed at the inner interface and a higher electric stress at the outer interface when a 20 ^{0}C temperature gradient is applied across the insulation.

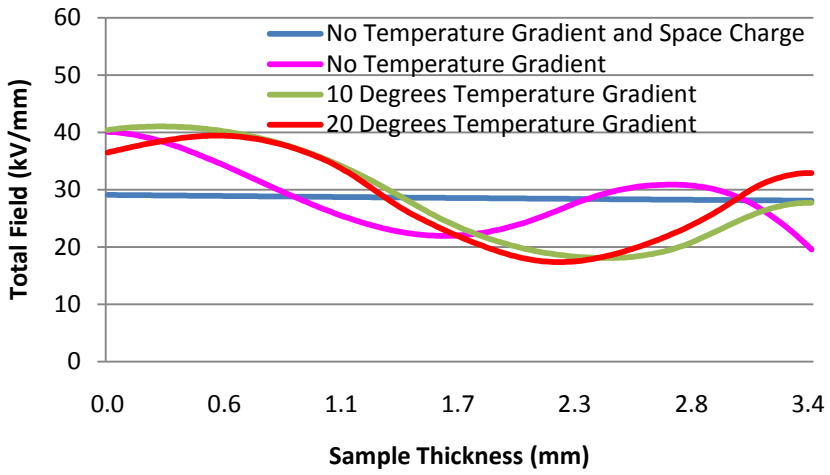

Figure 6-5: Total electric field distribution in cable based on Good Parameter

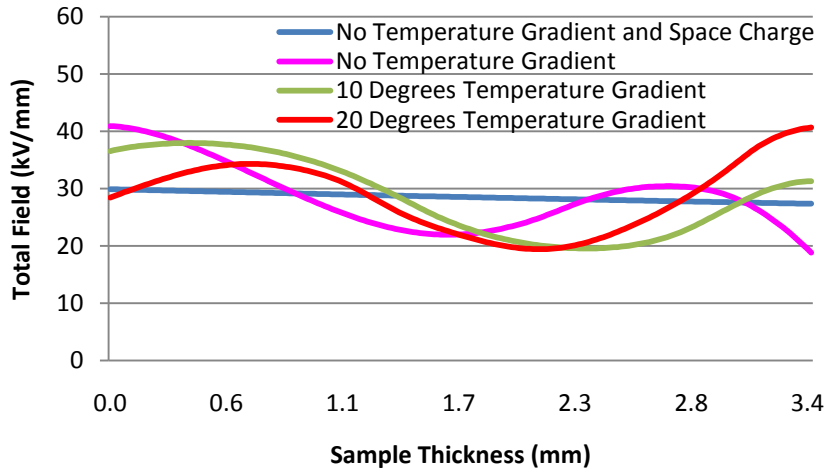

Figure 6-6: Total electric field distribution in cable based on Bad Parameter

Subsequently, comparisons were also made on the total electric field obtained through using both good and bad parameters. No significant difference is found between the

results of no temperature gradient due to the final value of conductivity of the material. However, when temperature gradients are applied across the insulation, it shows a significant difference between the results. In the case for 10 ^{0}C temperature gradient comparison between good and bad parameters, the difference between the inner and outer interface stress is approximately ~9 % and ~12 % respectively. For the 20 ^{0}C temperature gradient, the results difference is ~21 % and ~20 % between the inner and outer interface stress respectively.

6.4 Conclusion

When considerations are made by having the existence of temperature gradients across the insulation material of a rated voltage DC cable, additional complexity will be done on space charge dynamics. At higher temperature, the injection barrier height changes little but injection is enhanced leading to a higher amount of charges. The accumulation of space charge is much more rapid under temperature gradient. Conversely, it may happen that by increasing the temperature of the cable insulation the charges will have a higher mobility and the neutralisation of space charge is also faster. Furthermore, negative charges seem to be always travelling faster than the positive charges when under the same temperature [Delpino, Fabiani et al. 2007]. Therefore, it is clear that injection and transport of charges are enhanced upon the increase of temperature.

The electric field distribution in the DC power cable through considering the influences of both the effects of temperature and electric field on the conductivity of the insulating material is determined. The results indicate that with an increase of temperature gradient, the maximum stress occurs at the outer region adjacent to the screen of the cable and the value of this stress increases with the increase value of temperature drop across the dielectric material. The determined value of having a maximum total electric stress occurring at the outer interface of the insulating material is mainly dictated by the space charge field rather than the applied field; where it is dependent on the amount of heterocharge accumulated adjacent to the outer electrode.

Finally, the presented results clearly show that space charge distributions in commercial

XLPE cables with increasing temperature gradients across the insulating material is not a simple phenomena. The charge distribution is affected by the thermal gradient and this affect the conductivity across the insulation. It is obvious that this is a coupled problem hence only solving the Poisson's equation disregarding the temperature effect on charge distribution will not suffice, as demonstrated throughout our work. However, further investigation is needed to clarify if the outer electrode and the semi-con/insulation interface play an important part in this phenomenon.

Chapter 7 Conductivity of the DC Power Cable's XLPE Insulation Material

7.1 Introduction

Knowledge is the base of technology and its application. Since XLPE is extensively used in the manufacturing of power cables, the electrical conduction of this polymeric insulation material is of considerable commercial interest. It is recognised that the electrically charged particles movement through a medium is identified as electrical conduction where an electric current movement is represented by the charge. The charge transportation may result as a response to the electric field, or the consequence of a concentration gradient of current density. The physical parameters governing this transportation depend upon the material itself.

Generally in a dielectric material, charges are bound and not free to migrate so that the conductivity is ideally zero. Based on the conditions and the amount of traps within the polymeric material itself, it is said that the traps control the conductivity of the insulation material. With the higher amount of charges being trapped leads an increase of conductivity [Montanari, Mazzanti et al. 2001]. The higher the value of conductivity of the insulation, the shorter time for the charges to be accumulated. In addition, temperature conditions are also needed to be considered. With a higher temperature, the time duration is decreased for a minimum value in conductivity to be reached. Under

higher temperature, the efficiency of diffusion and decomposition of cross-linking by-products are enhanced, making the process of hopping conduction between traps more efficient for shorter times [Frutos, Acedo et al. 2007; Goshowaki, Endoh et al. 2007].

As a result, researchers now strive to translate the accumulated knowledge of space charge dynamics and its relationship with transient current.

7.2 Experiment Details

In this experiment, the transient leakage currents of a XLPE polymeric insulation material of the power cable were measured and analysed by means of an electric current measuring equipment under controlled temperature conditions via an oven. Electric field stress of ranges 12.33 kV/mm to 51.22 kV/mm were applied to the XLPE insulation sample at different temperature conditions.

7.2.1 Sample Preparation

An un-degassed commercially available 11 kV XLPE insulated power cables contributed by Prysmian Cables & Systems was used in this experiment. The XLPE samples were peeled from the cable itself using a microtome machine equipped with a specially designed knife to get the optimum surface smoothness. The cable's XLPE insulation was peeled to a thickness of 90 μm with an area of 4 cm by 4 cm.

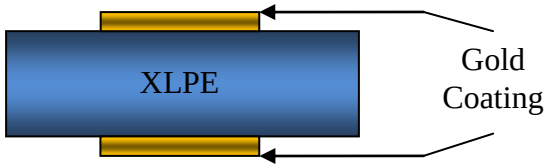

Figure 7-1: Sketch of XLPE sample with gold coating at both top and bottom interface

Subsequently, the peeled XLPE samples were inserted into Sputter coater equipment (Emitech K500X) where a thin layer of gold was coated at both the top and bottom

interface of the sample to improve the contact between the sample and the electrodes, as illustrated in Figure 7-1.

7.2.2 Experimental Setup

The specifically prepared XLPE sample peeling was inserted into the electric current measuring equipment as illustrated in Figure 7-2. The conduction current was measured by applying an initial stress of 12.33 kV/mm and then increasing the stress in steps to a maximum of 51.22 kV/mm. The conduction currents for each applied voltage were recorded using a pico-ammeter (Keithley 486 pico-ammeter). In order to maintain a constant current measuring conditions and applying different temperature conditions onto the sample, the electrodes were set up and placed within an oven (Sanyo Gallenkamp OMT Oven).

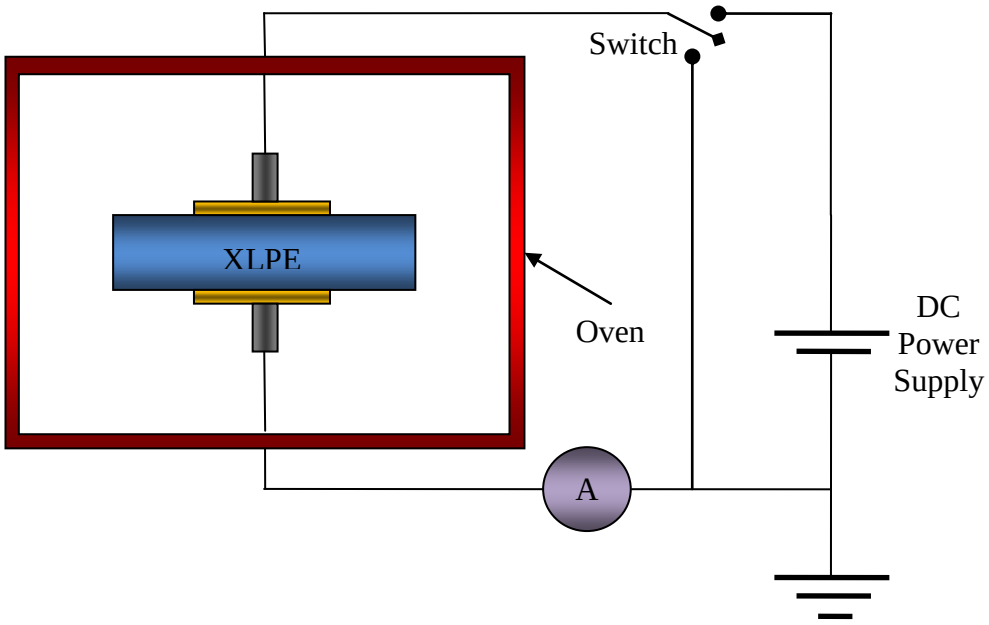

Figure 7-2: Electric current measuring equipment

In this experiment, a positive DC voltage is applied across the XLPE cable sample for 3600 seconds under a controlled temperature condition where the transient leakage current is then measured at an interval of 20 seconds. Under each individual electric field strength, seven different constant temperature conditions are applied to obtain the transient leakage current, as shown in Table 7-1.

Table 7-1: Transient leakage current test conditions on XLPE peel

		Applied Electric Field Strength (kV/mm)					
Temperature Conditions (^{0}C)	**30**	12.33	23.44	34.56	40.11	45.67	51.22
	40	12.33	23.44	34.56	40.11	45.67	51.22
	50	12.33	23.44	34.56	40.11	45.67	51.22
	60	12.33	23.44	34.56	40.11	45.67	51.22
	70	12.33	23.44	34.56	40.11	45.67	51.22
	80	12.33	23.44	34.56	40.11	45.67	51.22
	90	12.33	23.44	34.56	40.11	45.67	51.22

7.3 Experiment Results and Discussion

From the change of electric current against time curves obtained, it is observed that they generally decreases as one might expect from the response of a dielectric material under the application of DC voltage. As when DC high voltage is applied to the XLPE sample, the electric current from the test will decrease from an initial high value and decay to a fixed value. The electric current is generally divided into three components; the charging current, polarisation current and the conduction current. The charging current component is required for charging the capacitance of the sample and the value decreases rapidly with time. The measurement of the charging current is not important to the test as it only distorts the electric current. The polarisation current is caused by the polarisation and accumulation of charges within the XLPE material under the application of DC voltage. This polarisation current is normally small and will also decrease rapidly with time. Both components normally mask the true reading of the electric current. Nevertheless, the last component which is the conduction current is dependent on the applied DC voltage and the resistance of the XLPE material.

Figure 7-3 to Figure 7-9 show the results of conduction current measurements in the XLPE peel at different controlled isothermal conditions. They show a decrease in current with the duration of the applied voltage, where the current approaches a constant value after about 3000 seconds. With consideration of this factor, the measurement of

conduction current was continued for an additional 600 seconds and in each experiment, the value of conduction current measured at 3400 seconds as the leakage current. From the obtained results, transient current peaks are observed occurring within the first 2000 seconds after the application of DC voltage, as shown in Figure 7-3 to Figure 7-9. This transient current peak becomes more obvious when a higher DC voltage is applied across the sample material. In addition, with the increment of the controlled isothermal condition, the transient current peaks can be observed at a much lower applied voltage and it also tends to shift further to left of the curve i.e. occurring at a faster time.

With the increment of isothermal condition, it is shown in the results that the electric current increases with the applied controlled temperature. If we were to imagine the insulation sample consists of a parallel capacitor and resistor connected under DC application and with the consideration of the temperature in the insulation material. The resistivity through the insulation material will decrease when temperature increases. Subsequently, due to the decrease of resistance, more charges are allowed to pass through the material, therefore, leading to the increment of electric current. Nevertheless, once the situation 60 ^{0}C and with the electric stress set as more than 40.11 kV/mm, as shown in Figure 7-6 to Figure 7-9, the electric current tends to increase immediately once voltage is applied across the insulation, where it reaches its maximum value within 400 seconds. In Figure 7-10, further evidence can also be related to the situation of temperature condition setting more than 60 ^{0}C as it show the decrease in mobility of charges when higher electric field is applied due to the changes done on the morphology of the material. This conduction current peak may be explained by the build up of charges by the injection of carriers from the electrodes to the XLPE peel. It has been reported that the transient space charge limited current is related to the meeting of positive and negative charge fronts in the presence of both positive and negative carriers [Vlastós 1989, Lau and Chen 2006].

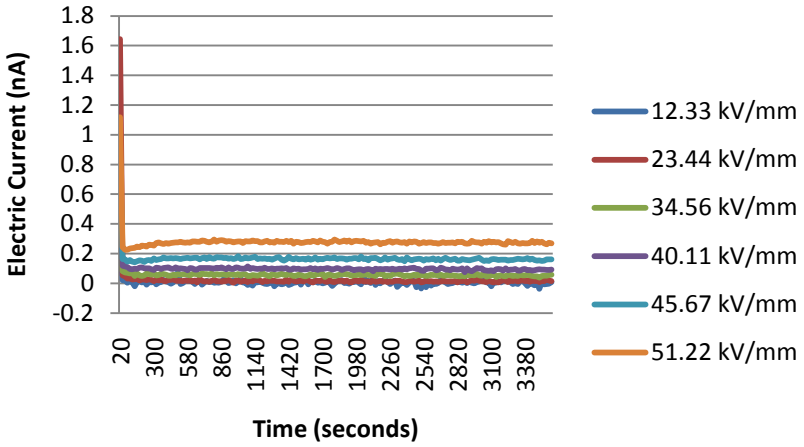

Figure 7-3: Change of electric current with lapsed time at isothermal 30 ^{0}C

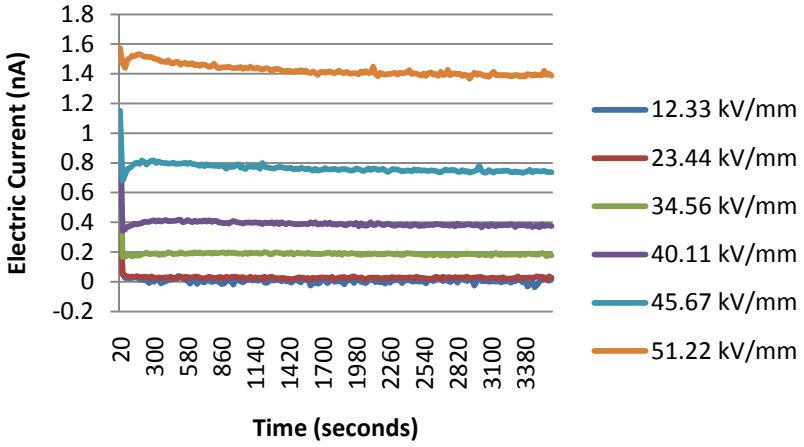

Figure 7-4: Change of electric current with lapsed time at isothermal 40 ^{0}C

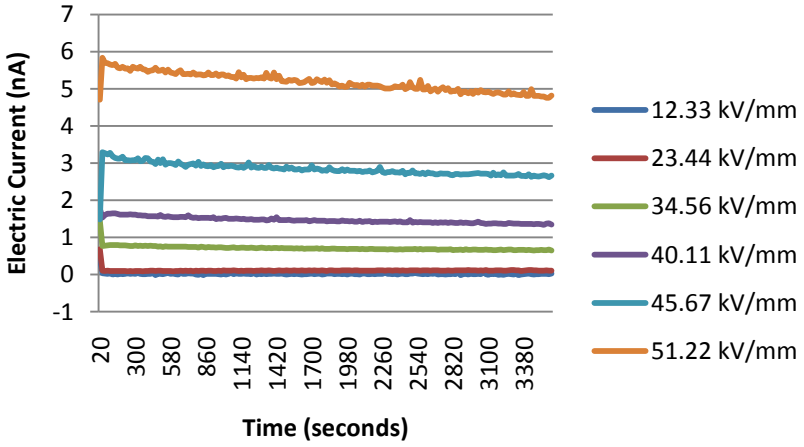

Figure 7-5: Change of electric current with lapsed time at isothermal 50 ^{0}C

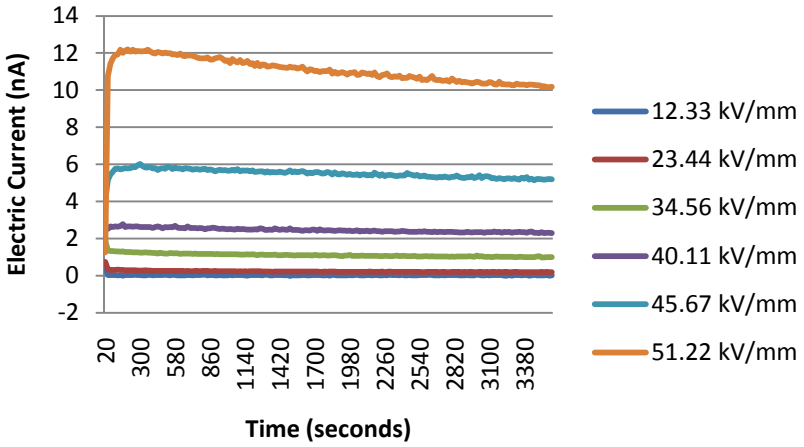

Figure 7-6: Change of electric current with lapsed time at isothermal 60 ^{0}C

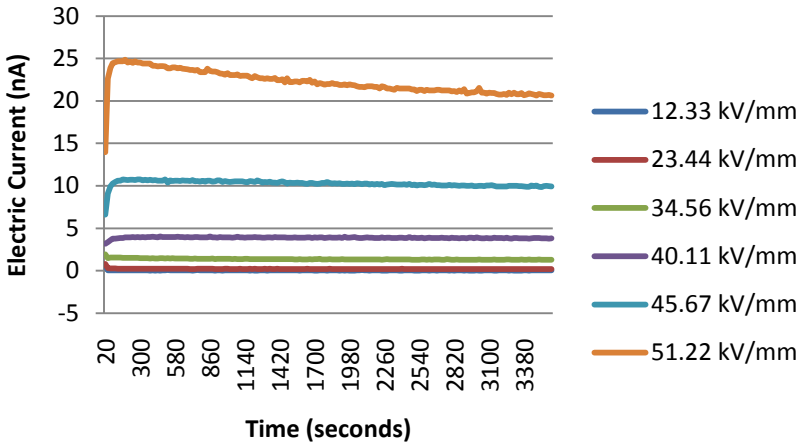

Figure 7-7: Change of electric current with lapsed time at isothermal 70 ^{0}C

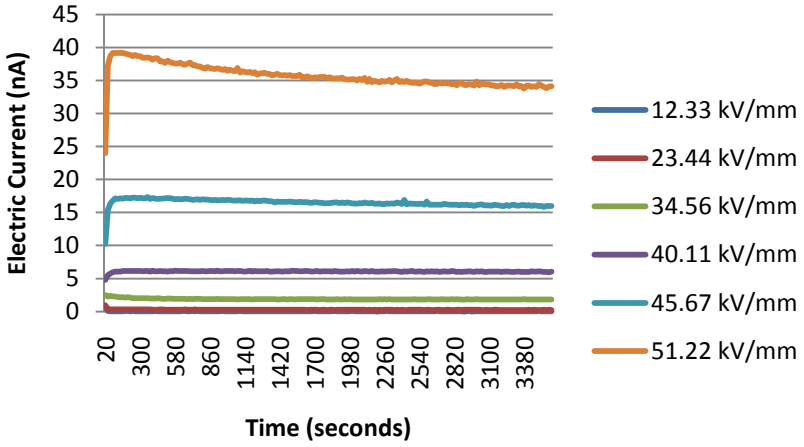

Figure 7-8: Change of electric current with lapsed time at isothermal 80 ^{0}C

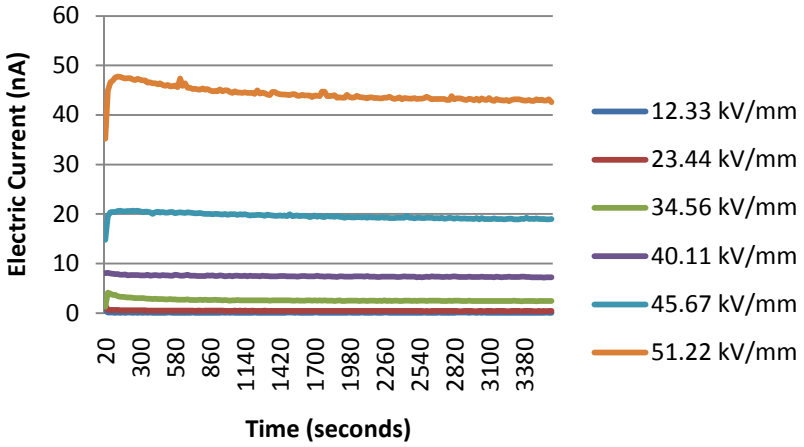

Figure 7-9: Change of electric current with lapsed time at isothermal 90 ^{0}C

With the transient current peaks showing correspondences to the space charge limited current (SCLC), mobility of carriers, μ, can be obtained by

$$\mu = \frac{0.786 \times d^2}{t_p \times V} \qquad \text{(E7-1)}$$

where d is the thickness of sample, t_p is the time which the current peak arise and V is the application voltage [Many and Rakavy 1962].

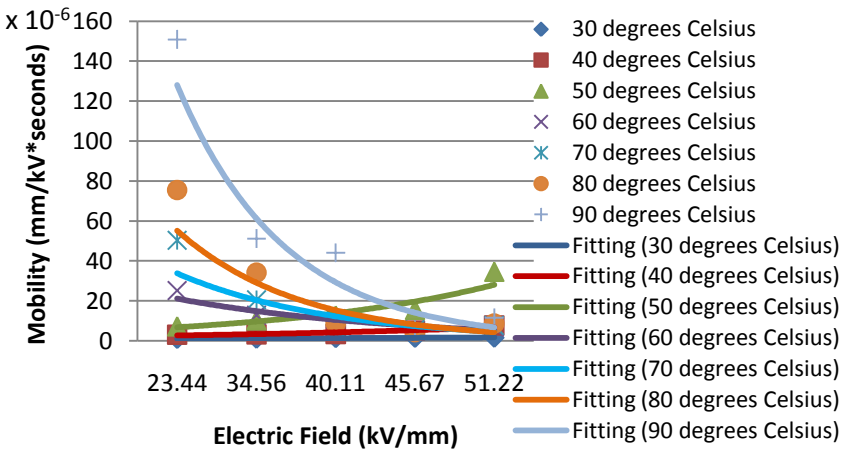

Figure 7-10: Electric field dependent of carrier mobility under different temperatures

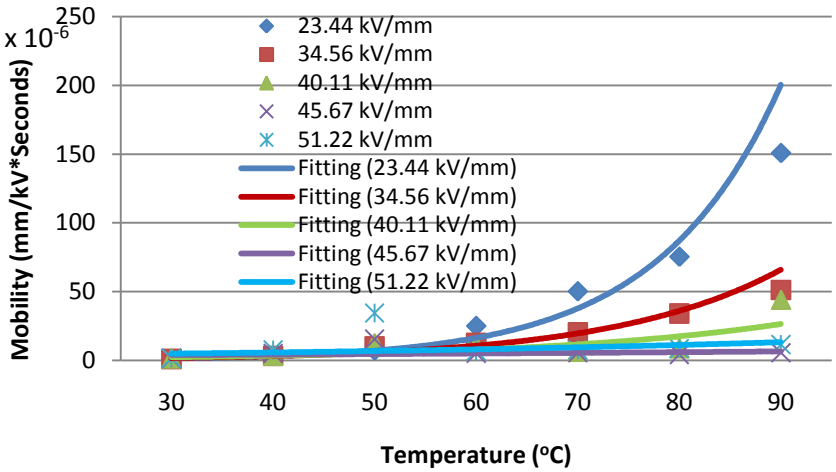

Figure 7-11: Temperature dependent of carrier mobility under different electric fields

The resulting mobility of carrier generally tends to increase with the application of both electric stress and temperature, as illustrated in both Figure 7-10 and Figure 7-11. However, under the application of 90 ^{0}C the mobility of the carriers tends to decrease with the increment of applied field and this inclination was being observed when the temperature was increased to 60 ^{0}C, as illustrated in Figure 7-10. The increment of temperature from 60 to 90 ^{0}C may have inevitably annealed the material resulting in a change of its morphology due to the modification of the microstructure of the material. The modification and movement of the crystallinity of the material may have hindered the movement of the charges leading to the decrement of carrier mobility.

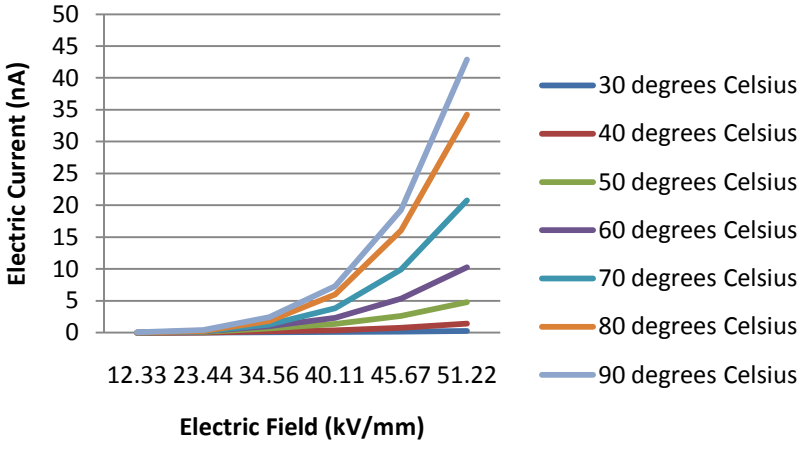

Figure 7-12: Electric current vs. applied electric field

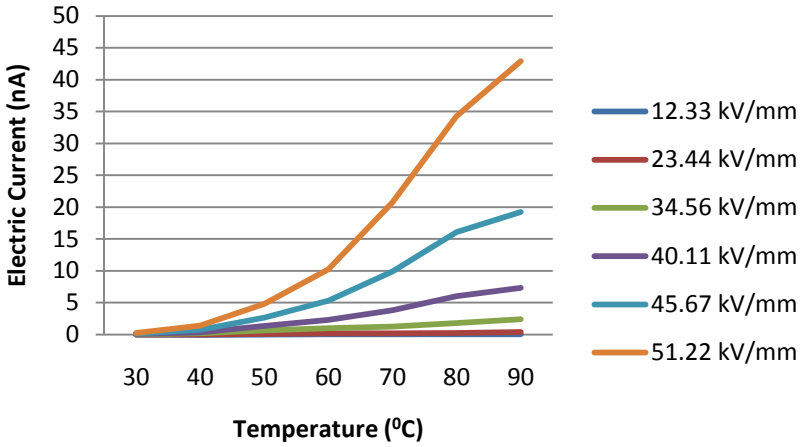

Figure 7-13: Electric current vs. temperature

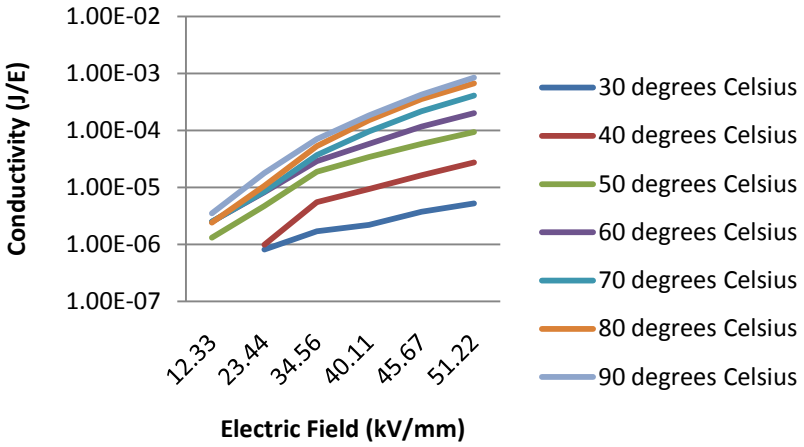

Figure 7-14: Conductivity vs. applied electric field

In both Figure 7-12 and Figure 7-13, it shows the direct relationship that the electric current is dependent on both temperature and the applied field. Large increment in electric current can be observed once temperature reaches 40 ^{0}C and it is evident that the current flowing at 40 ^{0}C will be greater in value if a higher voltage is applied across the sample.

Figure 7-14 shows the relationship between conductivity calculated from the results of the leakage current measurements in Figure 7-12. From this figure, it is observed that the conductivity of the XLPE peeling is the greatest at 90 ^{0}C and is twice the order of magnitude against the XLPE peeling when under 30 ^{0}C.

7.4 XLPE Material Parameters

With the description of conductivity as a function of field and temperature, as illustrated in equation E5-12, the parameters of the peeled XLPE insulated power cable material's thermal activation energy, *A* and *B* constant values can be determined through the current density measurements obtained in the experiments.

Under an application field of 23.44 kV/mm and influence of temperature ranging from 30 ^{0}C to 90 ^{0}C, the temperature dependence of conductivity of a peeled XLPE sample is shown in Figure 7-15. Furthermore, a linear least squares approach is used to find a line that fits the data points for the calculation of the activation energy for the material.

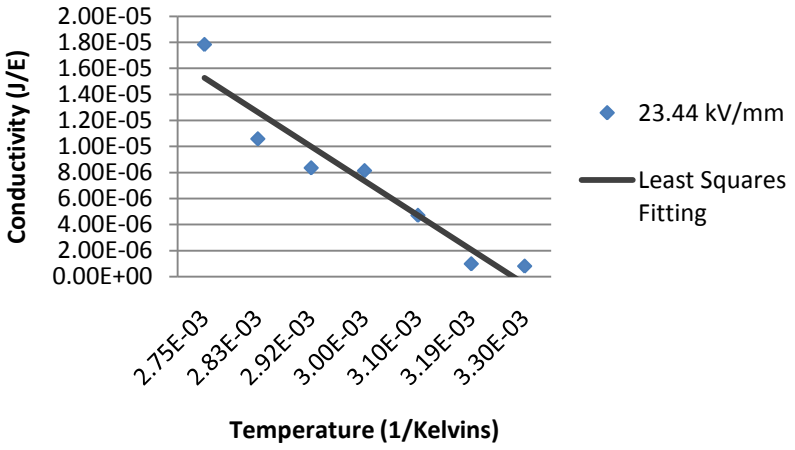

Figure 7-15: Relative temperature dependent conductivity of the XLPE material

The activation energy is obtained through two data points using the least squares fitting line from Figure 7-15 and is calculated as

$$7.6 \times 10^{-6} = Ae^{\frac{-\emptyset q}{k_B(333)}} \quad \text{(E7-2)}$$

$$4.8 \times 10^{-6} = Ae^{\frac{-\emptyset q}{k_B(323)}} \quad \text{(E7-3)}$$

Through dividing equation E7-2 by E7-3, the activation energy could be obtained as

$$1.583 = e^{\left(\frac{-\emptyset q}{k_B(333)}+\frac{\emptyset q}{k_B(323)}\right)} \quad \text{(E7-4)}$$

$$\ln 1.583 = \frac{10(\emptyset q)}{(323\times333)k_B} \quad \text{(E7-5)}$$

$$\emptyset = 0.425732829\ eV \quad \text{(E7-6)}$$

The activation energy of 0.43 eV obtained from our XLPE peeling has the same activation energy value as reported by other authors [Kon, Mizutani et al. 1994]. Under the variation of conductivity with applied electric field (Figure 7-14), the constant B value is computed approximately using two data points namely 23.44 kV/mm and 34.56 kV/mm of the applied field. The conductivity values for each of this two points are illustrated in Table 7-2 for temperature ranging from 30 ^{0}C to 90 ^{0}C. More details on the computation of B are given in Appendix B.

Table 7-2: Computation of constant value of B under different applied temperature

	Applied Field (23.44 kV/mm)	**Applied Field (34.56 kV/mm)**	
Temperature (^{0}C)	**σ_1**	**σ_2**	**B**
30	8.042 x 10^{-7}	1.686 x 10^{-6}	1.008 x 10^{-7}
40	9.825 x 10^{-7}	5.453 x 10^{-6}	1.890 x 10^{-7}
50	4.711 x 10^{-6}	1.882 x 10^{-5}	1.594 x 10^{-7}
60	8.144 x 10^{-6}	2.880 x 10^{-6}	1.484 x 10^{-7}
70	8.357 x 10^{-6}	3.691 x 10^{-5}	1.685 x 10^{-7}
80	1.059 x 10^{-5}	5.297 x 10^{-5}	1.797 x 10^{-7}
90	1.784 x 10^{-5}	7.024 x 10^{-5}	1.581 x 10^{-7}

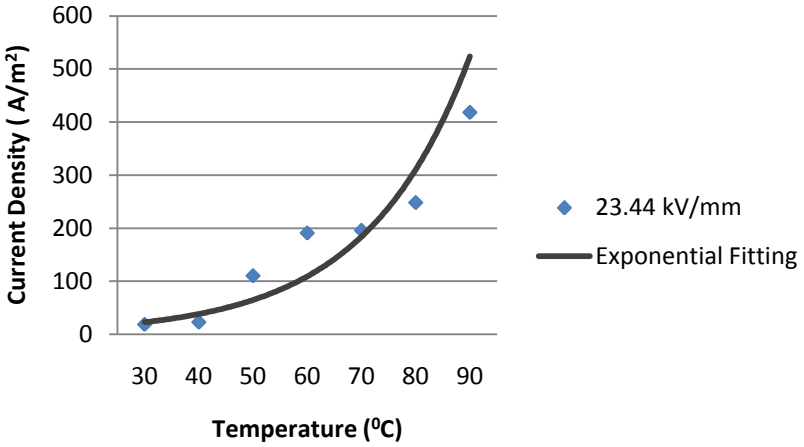

Figure 7-16: Current density against temperature of the XLPE material at 23.44 kV/mm

The variation of current density with temperature under the application of 23.44 kV/mm of electric field as shown in Figure 7-16 was fitted to equation E7-7 as

$$J(T) = Dexp\left(\frac{-\emptyset q}{k_B T}\right) \tag{E7-7}$$

where the constant D value will be calculated. In addition, the variation in current density with applied field is fitted to equation E7-8 as

$$J(E) = C\sinh(B|E|) \tag{E7-8}$$

where constant value of C is obtained. As a result, the overall current density can be described as

$$J(E,T) = Aexp\left(\frac{-\emptyset q}{k_B T}\right)\sinh(B|E|) \tag{E7-9}$$

Since $J^2 \propto A \propto CD$, constant value of A can be determined by the multiplication of both equations E7-7 and E7-8 as

$$A = \frac{C \times D}{J} \tag{E7-10}$$

Thus, the constant values used in the conductivity equation for the peeled XLPE material in equation E5-12 could be obtained and illustrated in Table 7-3.

Table 7-3: Computation of constants value of *C*, *D* and *A* under different applied temperature

	Constants		
Temperature (^{0}C)	**C**	**D**	**A**
30	3.585	2.272×10^8	4.322×10^7
40	0.549	1.649×10^8	3.928×10^6
50	5.267	4.850×10^8	2.313×10^7
60	11.783	5.297×10^8	3.270×10^7
70	7.558	3.527×10^8	1.361×10^7
80	7.359	2.971×10^8	8.810×10^6
90	20.551	3.404×10^8	1.673×10^7

7.5 Conclusion

The influence of temperature on electric conduction under the application of DC voltage has been studied on a commercial XLPE insulated power cable peeling. The results highlight the complexity of electric conduction in the XLPE peel and confirm that this conduction relies strongly on both the application of high electric field and temperature.

For low applied field and low temperature condition, the initial current, which is due to mainly the orientation of dipoles of the XLPE sample, will exponentially decay and reach its final value. When under moderate applied field and temperature condition, the conduction current will decrease initially followed by an increase that passes through a well defined peak value and then decay in a exponentially manner. This well defined current peak is shifted to the left (shorter time) when the applied field and temperature increase [Vlastós 1989]. The carrier mobility can be obtained from this current peak and this mobility is electric field and temperature dependent. It was also pointed out that with the increment of temperature towards 60 ^{0}C to 90 ^{0}C, this may have initiated the movement of crystallinity within the XLPE material leading to the obstruction on the movement of the charge carrier.

Through these current density measurement results of the cable's XLPE insulation, we are able to determine the conductivity parameters of the hopping model of conduction in dielectric. Subsequently, this conductivity equation is used in the next chapter to calculate the electric field distribution across the XLPE insulation of the cable when under the application of DC voltage.

Chapter 8 Effects of Temperature Gradient and Polarity Reversal on Space Charge Accumulation in XLPE Cable

8.1 Introduction

In most HVDC transmission systems, bi-direction power flow is a common and necessary operating mode. The presence of space charge within the polymeric insulated material of the power cable is especially dangerous during polarity reversal and is commonly recognised as the primary cause of failures of the early commercial DC cables with extruded insulation [Zhang, Lewiner et al. 1996]. Through the exchanging roles of rectifier (sending end) and inverter (receiving end), polarity voltage reversal is enabled. In the presence of space charge due to the low mobility of charge carrier, high electric stresses within the insulating material may be created superimposed to the Laplacian field, which results the changes of electric stress within the dielectric material itself. Furthermore, additional complexity will be made on space charge distribution when existence of temperature gradient in the insulation of a fully rated voltage DC cable is considered.

As a result, a modified PEA system is employed to perform space charge measurements across an XLPE extruded cable in order to understand the dynamics of space charge

injection/accumulation under the conditions when rated voltage is applied on the cable during service; and the response of it during polarity reversal in different temperature gradients consideration across the insulation.

8.2 Experiment Details

In this experiment, the setup process is similar to the experiment in Chapter 6, where a modified PEA system with a current transformer attached is used to measure the space charge distribution across the insulation material of the coaxial cable.

The 11 KV XLPE insulated power cables (inner radii = 5.8 mm; outer radii = 9.2 mm; XLPE insulation thickness = 3.4 mm; cross-section of stranded aluminium conductor = 95 mm^2) samples used in these experiments were a later manufactured batch of cables contributed by Prysmian Cables & Systems as compared to the sample previously used in the experiments in Chapter 6. However, these cables samples were being cut and prepared in the same manner as in Chapter 6.2.1.

The temperature gradient across the insulation material of the power cable is also generated through induction heating where the same induced current of 250 A and 350 A is applied on the current transformer due to the cables having the same specifications size.

8.2.1 Experimental Setup

Seven as-received cables were prepared into the specification illustrated in the same manner in Chapter 6.2.1. In addition, six of the XLPE cable samples did not undergo the degassing process; therefore, cross-linking by-products are contained within the insulating material. In contrast, one of the XLPE cable was degassed in a vacuum sealed oven at 101.325 kPa and 90 ^{0}C temperature for 120 hours to remove any cross-linking by-products that are retained after the manufacturing process of the cable.

Nine different test conditions were then setup for each cable sample as follows:

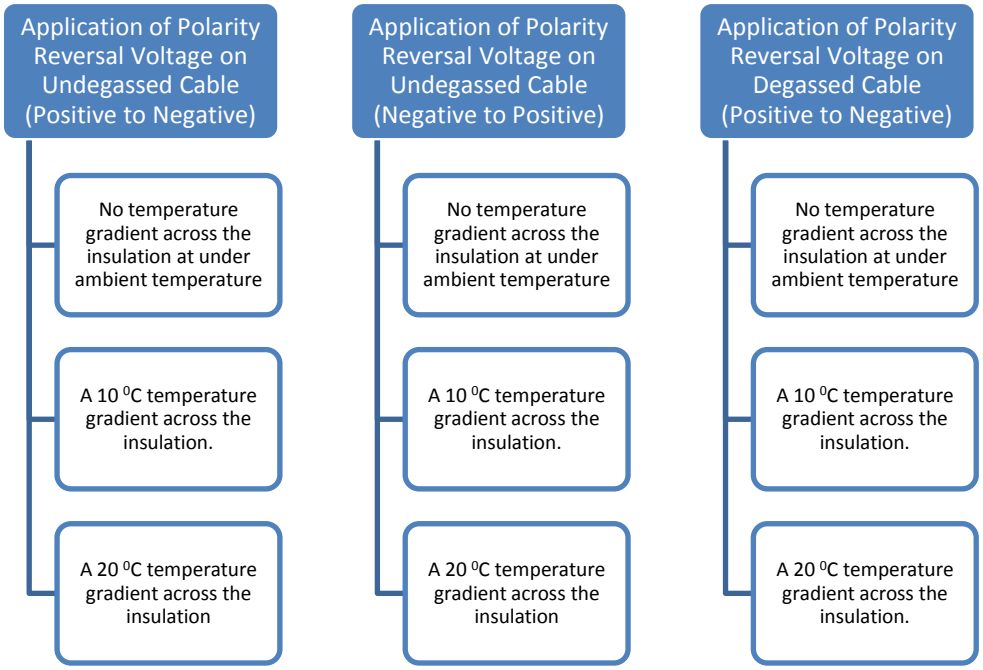

Figure 8-1: Test conditions on each different application voltage and temperature gradient

In both test conditions, for 10 ^{0}C and 20 ^{0}C, the cable is first heated up through the current transformer 2 hours prior to obtain the desired stabilised temperature gradient before starting the experiment. The current transformer is kept on throughout the experiment measurements.

A DC voltage of 80 kV was then applied on the 11 kV XLPE cables for 9 hours and space charge measurements were taken at different stressing periods. With the space charge accumulation distributed across the insulation after the 9 hours of initial polarity voltage, the external initial voltage supply was switched off and the XLPE insulated power cable was then short-circuited to release the surface static charge.

Subsequently, polarity reversal voltage is then stressed on the cable and space charge measurements were once again taken at different stressing periods. The whole implementation of voltage polarity reversal procedure took less than one minute.

8.3 Experiment Results and Discussion

8.3.1 Un-degassed Cable (Positive to Negative Voltage Polarity Reversal)

8.3.1.1 Ramp Test

A rapid ramp test was done on the cable sample prior to its appropriate experiment test condition. The test was done between a range of 0 V – 80 kV rapidly within a minute, where at each interval of 10 kV, magnitudes of both inner and outer insulation interface charges were recorded. The purposes of this test is to examine the formation of any fast charges during the process of increasing the voltage and also to determine the threshold level of voltage applied on the insulation, in which space charge starts to form within the insulation. As it corresponds that the XLPE conduction mechanism is of ohmic type at low applied voltage and turning into a space charge assisted conduction mechanism at high applied voltage exceeding the threshold level of the material. In summary, a linear proportional relationship is obtained between the induced charge at the electrode and the applied voltage when no space charges are formed within the insulation, whereas, a non-linear relationship is formed when space charges are developed within the insulation. An illustration of the ramp test is shown in Figure 8-2.

In the ramp test results as shown in Figure 8-3, it clearly states that no space charge formation are observed forming within the insulation material when the applied voltage was ramped up from 0 kV to +70 kV for all three test conditions. Heterocharge formations are observed at both anode and cathode (inner and outer electrode respectively) and it clearly shows that both lines of the anode and cathode appear to deviate from the straight line after +70 kV applied voltage. Additionally, it is observed that the degrees of deviation from the linear tendency increases with the increase temperature gradient applied across the insulation material.

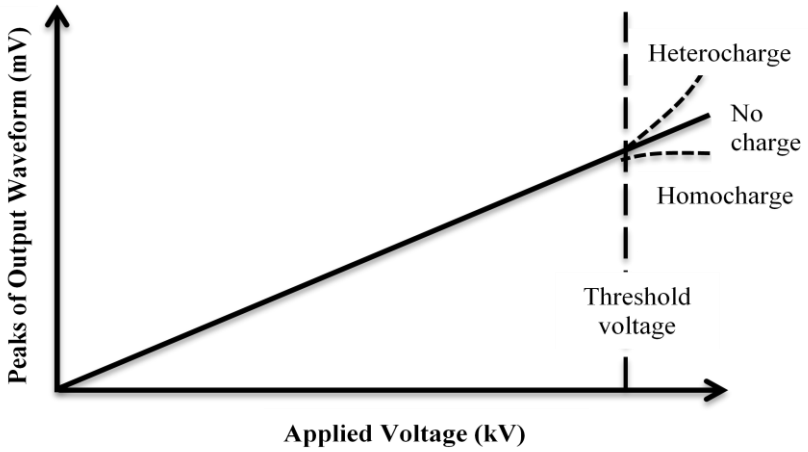

Figure 8-2: Illustration of a ramp test

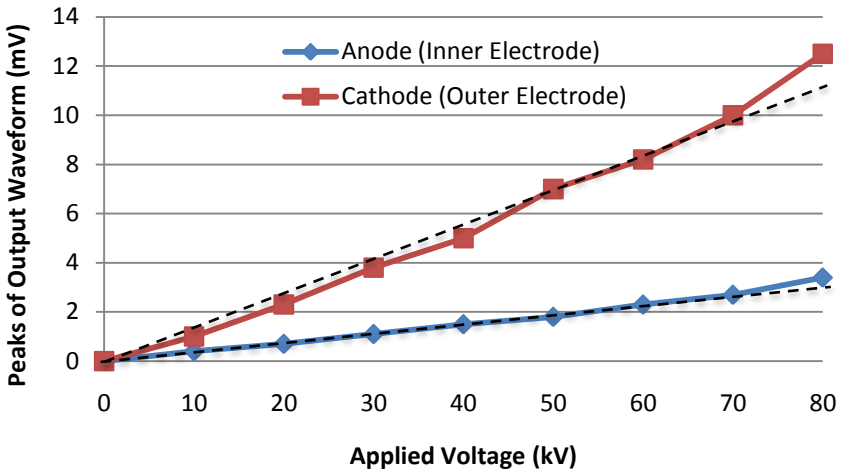

(a) No temperature gradient

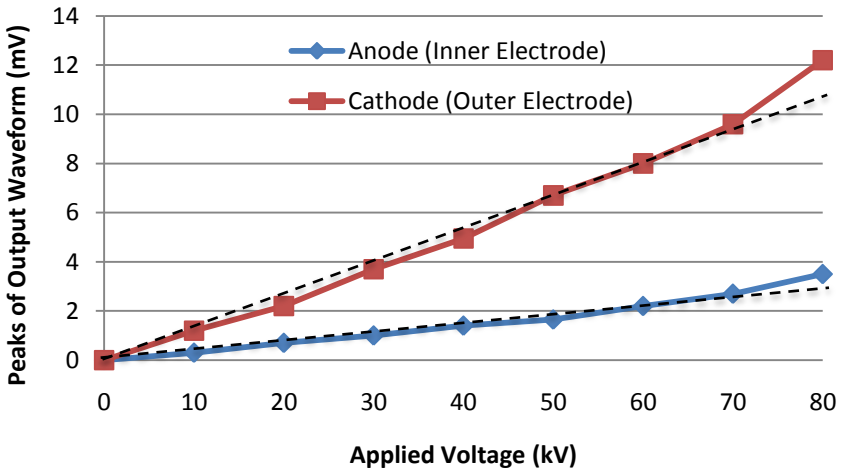

(b) 10 ^{0}C temperature gradient

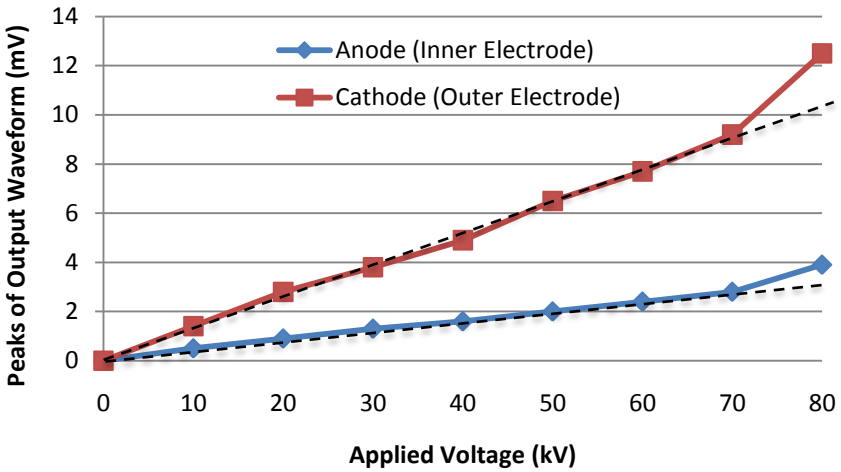

(c) 20 ^{0}C temperature gradient

Figure 8-3: Ramp test profiles for (a) no temperature gradient, (b) 10 ^{0}C temperature gradient and (c) 20 ^{0}C temperature gradient

8.3.1.2 DC Aging Test

Space charge distributions are obtained through using a modified PEA system with a current transformer attached, as illustrated in Chapter 4 Figure 4-7. The voltage on space charge profiles for no temperature gradient, 10 ^{0}C and 20 ^{0}C temperature gradients across the XLPE insulation material of the cable, are presented in Figure 8-4a, Figure 8-4b and Figure 8-4c respectively.

Under the application of +80 kV poling voltage, heterocharge can be seen forming immediately (0 minutes) in the vicinities adjacent to the anode and cathode, as shown in Figure 8-4a, Figure 8-4b and Figure 8-4c respectively. From the comparison between no temperature, 10 ^{0}C and 20 ^{0}C temperature gradients in Figure 8-4, it is observed that the amount of heterocharge formed adjacent to the electrodes tend to increase gradually with the increment of temperature gradient across the insulation material. This observation is coherent with the results obtained from the ramp test results in Figure 8-3, where heterocharge formations are observed once 70 kV of poling voltage is applied across the conductor of the cable.

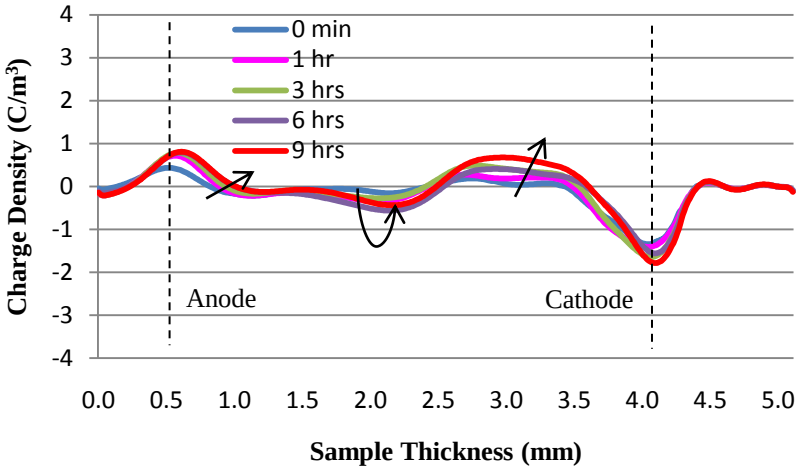

(a) No temperature gradient

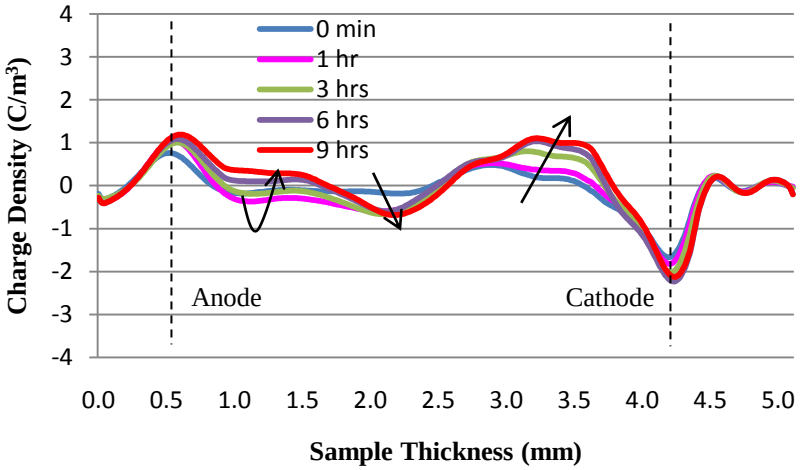

(b) 10 ^{0}C temperature gradient

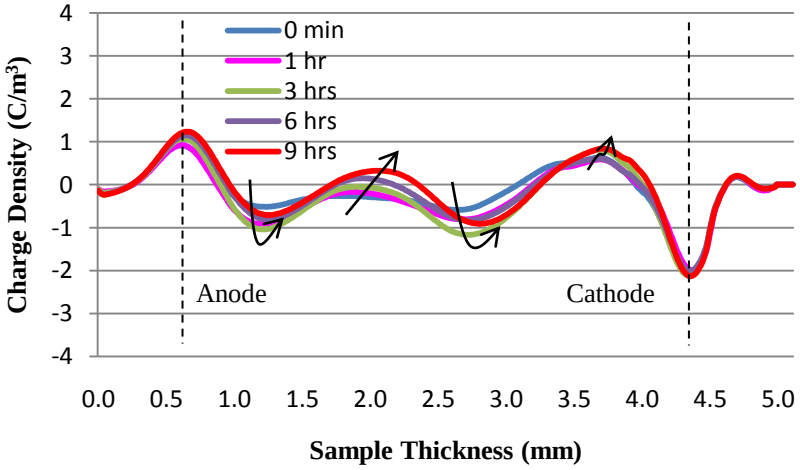

(c) 20 ^{0}C temperature gradient

Figure 8-4: Voltage on space charge profiles with aging time under the application of +80 kV

Therefore, it is evident that cross-linking by-products such as methane, cumyl alcohol, acetophenone etc. are still present within the XLPE insulation of the cable as degassing process was not being applied to the cable sample prior to the experiment. These by-product residues from the manufacturing process of the XLPE may be present within the material for a long period of time and these residues will undergo ionisation process when under a high electric field. Thus, under the influence of the high electric field these ionised species will move towards the opposite electrodes to form heterocharge.

Nevertheless, at high electric field accompanied with a higher temperature, the amount of charges across the insulation material tend to increase due to the higher injection rate and also having a higher mobility leading to the enhancement of the transportation of charges. Therefore, the observed heterocharge formation is due to the resultant effect of both scenarios.

The overall space charge distributions in Figure 8-4a and Figure 8-4b are quite similar in shape to each other except for in Figure 8-4b where there is a much higher accumulation of charges across its insulation due to the temperature gradient. In addition, homocharges are observed accumulating and gradually increasing in the region adjacent to the anode after 6 hours of poling. The purging of the initial 6 hours of negative charges might be due to the extraction by the anode and also the injection of positive charge where it cancels out or recombines with the accumulated negative charges. In view of the situation, the inner interface current seems to be triggered with higher activation energy than the currents in the bulk.

When 20 ^{0}C temperature gradient is applied across the insulation as shown in Figure 8-4c, it clearly shows the injection and transportation of charges increase with the temperature. As it has been reported, an average increase for positive and negative mobility is about 3 and 6 times larger respectively on doubling the temperature [Lim and Fleming 1999]. In Figure 8-4c it also illustrates that the amount of homocharge adjacent to the anode that was accumulated at 10 ^{0}C after 6 hours of poling has moved further into the sample. Furthermore, heterocharge is again observed forming adjacent to the anode throughout the 9 hours of poling as the removal of charge carriers by the anode is slower than the transit rate in which the negative charges are injected from the cathode.

8.3.1.3 Polarity Reversal Test

After 9 hours of poling with positive voltage, the external voltage supply is switched to negative to simulate the event of bi-directional flow of power. Space charge measurements were once again taken at different stressing periods as illustrated in Figure 8-5. From the results obtained, space charge profiles that were previously accumulated at 9 hours of application voltage (+80 kV) were immediately overrun at 0 minutes by negative charges when the external voltage polarity was reversed to -80 kV. This application of negative stress introduces the infiltration of a huge amount of negative charges into the insulation material, which at an instant totally eliminated the previous accumulated space charge when under positive supply. This overrun effect by negative charges can be observed clearly from both no temperature and 10 ^{0}C temperature gradient across the insulation material, as shown in Figure 8-5a and Figure 8-5b respectively.

With the increment of temperature gradient across the insulation material as shown in Figure 8-5, it is observed that this immediate overrun of negative charges at 0 minutes tends to decrease with the increasing temperature gradient across the insulation due to the increase of mobility of both positive and negative charges enhanced by the temperature gradient. By having a higher mobility rate of positive charges, the initial overrun negative charge tends to decrease in density due to the faster cancelling effect from the positive charge.

In addition, we could see that immediately after voltage reversal, negative charge dominates across the insulation material first followed by the positive charge, where the latter gradually increases its pace after the negative charge has done so. This event is clearly illustrated in Figure 8-5, where it shows the rapid advancement and cancelling effect of the positive charge when temperature gradient across the insulation is increased.

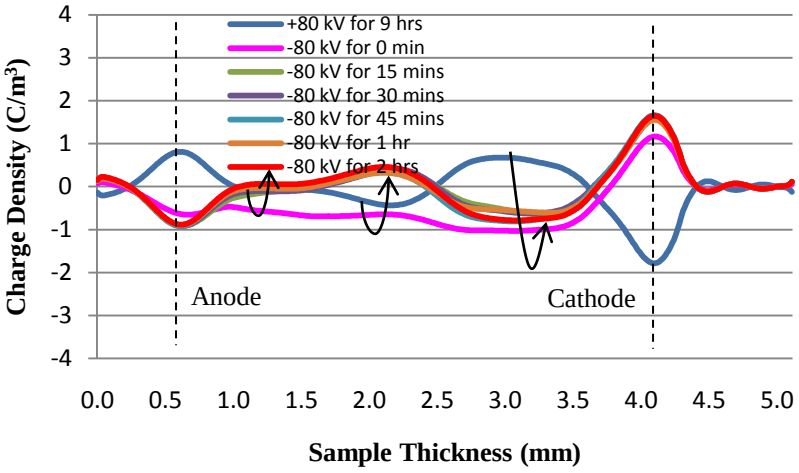

(a) No temperature gradient

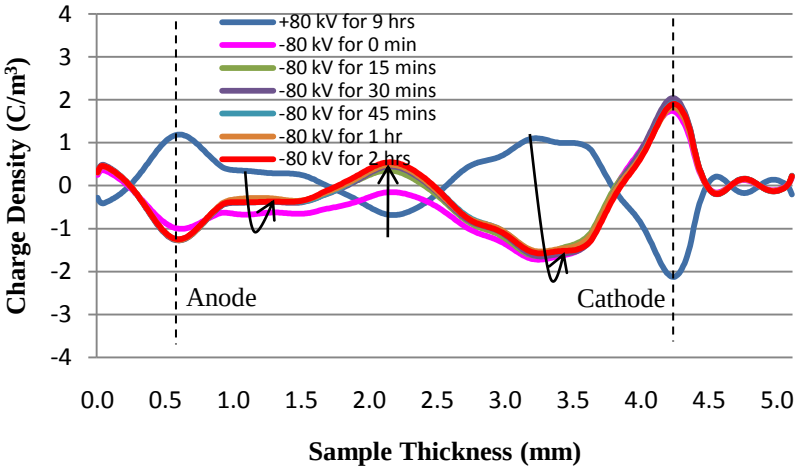

(b) 10 ^{0}C temperature gradient

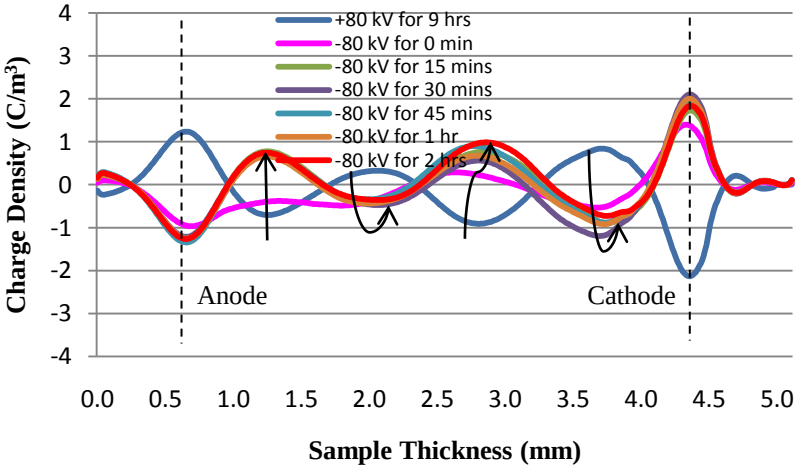

(c) 20 ^{0}C temperature gradient

Figure 8-5: Voltage on space charge profiles with aging time under the application of voltage reversal -80 kV

"Mirror Image Effect" space charge accumulation is observed when a polarity reversal is applied on the previous state of charge distribution under +80 kV for 9 hours of poling. Such "Mirror Image Effect" charge distributions means that the charges obtained under an opposite polarity is almost identical to the charge distributions obtained under positive polarity, but of an opposite polarity.

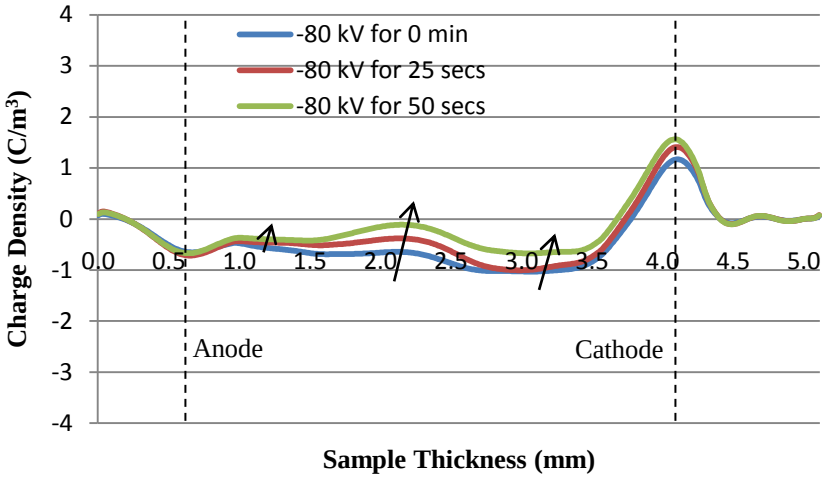

(a) No temperature gradient

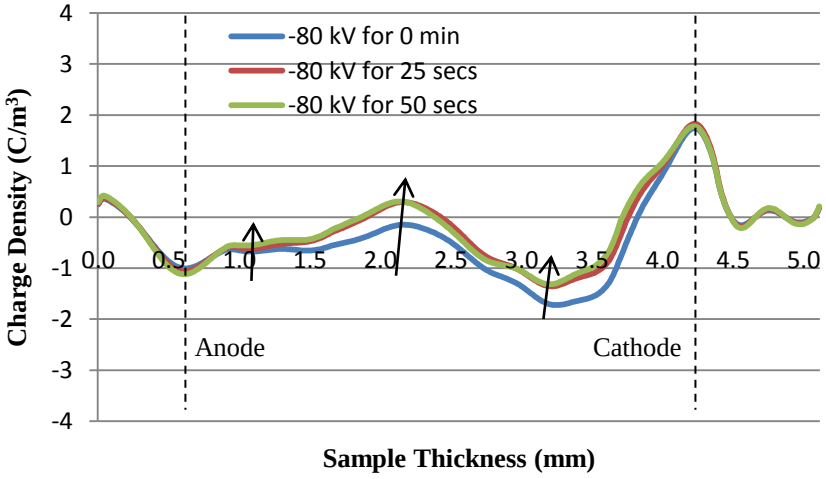

(b) 10 ^{0}C temperature gradient

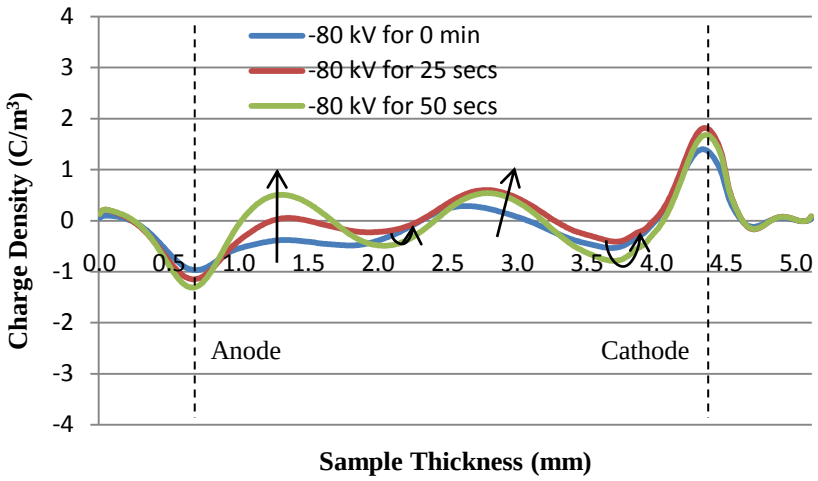

(c) 20 ^{0}C temperature gradient

Figure 8-6: Voltage on space charge profiles within a minute of aging time under the application of voltage reversal -80 kV

To further analyse the investigations on the immediate consequences on polarity reversal, space charge measurements were also taken within the first minutes when the external voltage polarity was reversed to -80 kV, as shown in Figure 8-6. As mentioned earlier, a large amount of negative charges are spread across the insulation immediately (0 minutes) after polarity reversal, as illustrated in both Figure 8-6a and Figure 8-6b. This scenario may indicate that the positive charge has a low mobility and the mobile group of charges is the negative. Furthermore, it is observed that with an increase temperature gradient applied across the insulation, the duration for the time to reach a steady state "Mirror Image Effect" formation decreases. As the results illustrated in both Figure 8-6b and Figure 8-6c show, space charge distribution starts to take the form of a "Mirror Image Effect" formation at 50 seconds for a temperature gradient of 10 ^{0}C and 25 seconds for a temperature gradient of 20 ^{0}C. These whole events indicate that the activation energy of negative charges is indeed higher than positive charge and also having a higher temperature gradient across the insulation increases the mobility of both the positive and negative charges.

8.3.1.4 Total Electric Field Distribution in Cable during Polarity Reversal

As mentioned earlier, the presence of space charge within the insulation of a polymeric

power cable is hazardous during polarity reversal leading to the cable failure in service. A direct insight of DC electric stress distribution in cable geometry during the event of polarity reversal is obtained by allowing charge accumulation within the polymeric insulated cable under different service temperature gradient across its insulation material.

The hopping model of conduction in dielectric is utilised for the calculation of the total field under the effects of both temperature and field dependence. The parameters for the XLPE insulation material were obtained from Table 7-3 in Chapter 7 and based on these parameters, under each different temperature gradient across the insulation; the total electric field is calculated and presented in Figure 8-7.

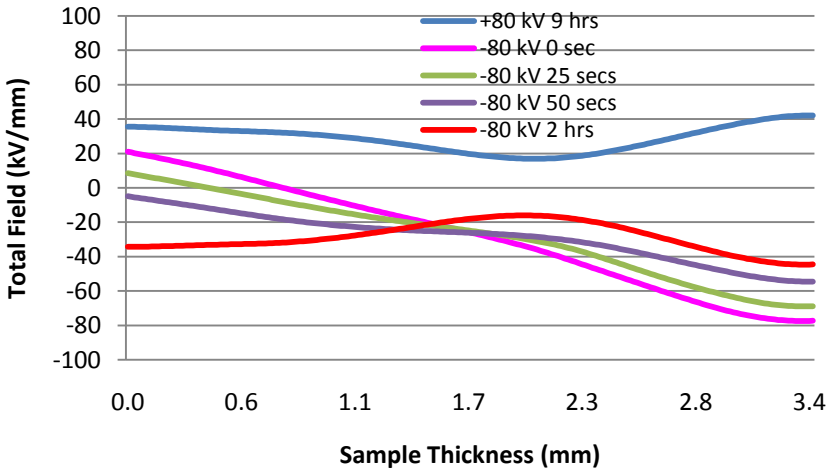

(a) No temperature gradient

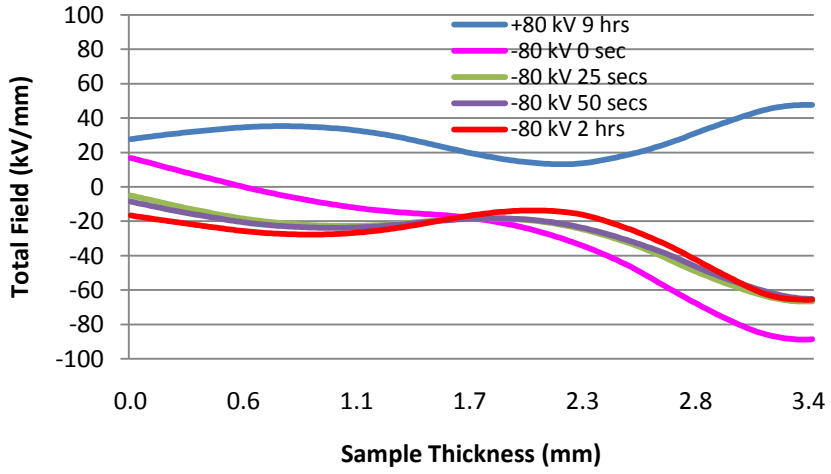

(b) 10 ^{0}C temperature gradient

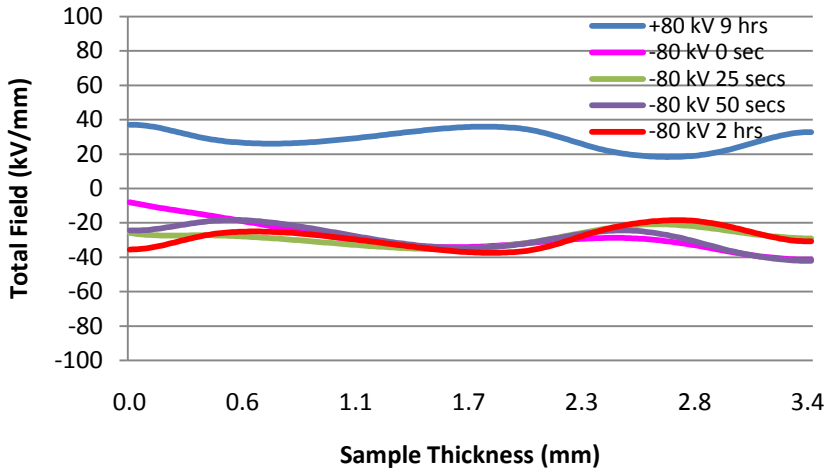

(c) 20 ^{0}C temperature gradient

Figure 8-7: Total electric field distribution during polarity reversal in cable based on own parameter (Positive to Negative)

Based on the insulation own parameters, Figure 8-7 shows the results of the total electric field distribution under different temperature gradient conditions during polarity reversal. Under no temperature gradient across the insulation, as illustrated in Figure 8-7a, heterocharges are formed in the vicinities adjacent to both electrodes after 9 hours of +80 kV of stressing leading to the interfacial stress at both inner and outer interface at 35.5 kV/mm and 42 kV/mm respectively, whereas, a reduction of electric stress is located at the centre of the XLPE material. Immediately after polarity reversal (0 seconds), it is observed that the inner interfacial stress decreases to 21 kV/mm and outer interfacial stress increases to -77.3 kV/mm due to the massive initiation of negative charges once the negative voltage is applied (-80 kV). Between the negative aging periods from 0 to 50 seconds, a decrement of electric stress is shown at both inner and outer interface where it decreases to a value of -4.8 kV/mm and -54.5 kV/mm respectively as negative charge within the insulation is reduced by the advancement and cancelling effect of the positive charge. Subsequently, a mirror image of the total electric field is formed, similar to the one under +80 kV of applied stress, due to the identical final distribution of charge density within the insulation except for the opposite polarity sign.

With the consideration of 10 ^{0}C temperature gradient across the insulation as shown in Figure 8-7b, it is observed that the outer interfacial stress at 47.6 kV/mm is greatly

higher as compared to the inner interfacial stress at 27.7 kV/mm due to the higher amount of heterocharge accumulated adjacent to the electrodes. It is observed at 0 seconds immediately after the polarity reversal, the interfacial stress at the inner electrode decrease to 16.8 kV/mm and the outer interfacial stress to -88.65 kV/mm. In addition, the outer interfacial stress tends to stabilise within 25 seconds of polarity reversal whereas the inner interfacial stress tends to increase gradually towards its final value of -16.7 kV/mm at 2 hours. With comparison between the results of no temperature gradient and 10 ^{0}C temperature gradient across the insulation as shown in Figure 8-7a and Figure 8-7b respectively, the total electric stress profiles across the insulation look similar but when under a 10 ^{0}C temperature gradient, a higher interfacial stress is located at the outer interface and a much lower interfacial stress occurs at the inner interface.

Subsequently, when 20 ^{0}C temperature gradient is applied across the insulation, the results obtained is quite different from what we expected based on the results of both no temperature and 10 ^{0}C temperature gradient, as shown in Figure 8-7a and Figure 8-7b respectively. In Figure 8-7c, it is observed at the instant after polarity reversal (0 minutes); the inner interfacial stress immediately drops towards -8 kV/mm with the outer interface stress at -41.4 kV/mm. In addition, the final total electric stress profile shows the inner and outer interface stress to be -35.5 kV/mm and -30.7 kV/mm even though a higher temperature gradient is applied across the insulation material. The reason for the difference in results may be due to the number of large portions of positive charge accumulated across the sample causing a reduction in electric stress at the outer electrodes.

8.3.2 Un-degassed Cable (Negative to Positive Voltage Polarity Reversal)

8.3.2.1 Ramp Test

Implementing the same ramp test procedure as mentioned earlier, with the exception of applying a negative voltage. The results shown in Figure 8-8 correlates with the results for all three temperature conditions in Figure 8-3 where space charge formation are not formed when the applied voltage was applied between 0 kV to -70 kV along with the formation of heterocharge at the cathode once the applied voltage reached -80 kV.

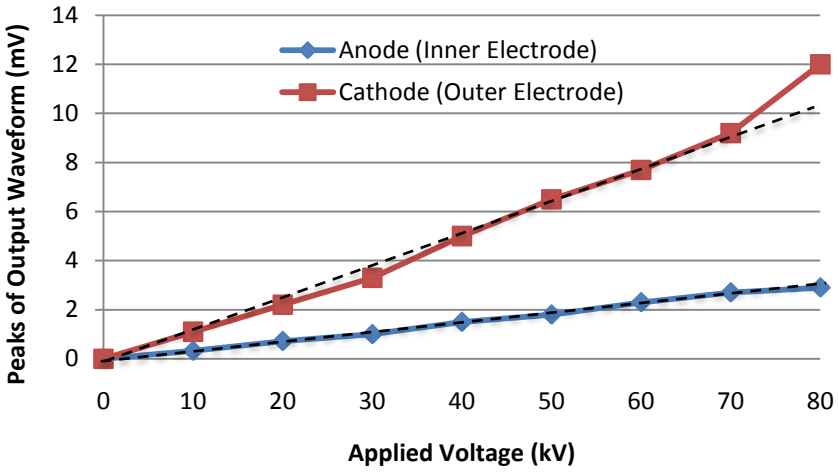

(a) No temperature gradient

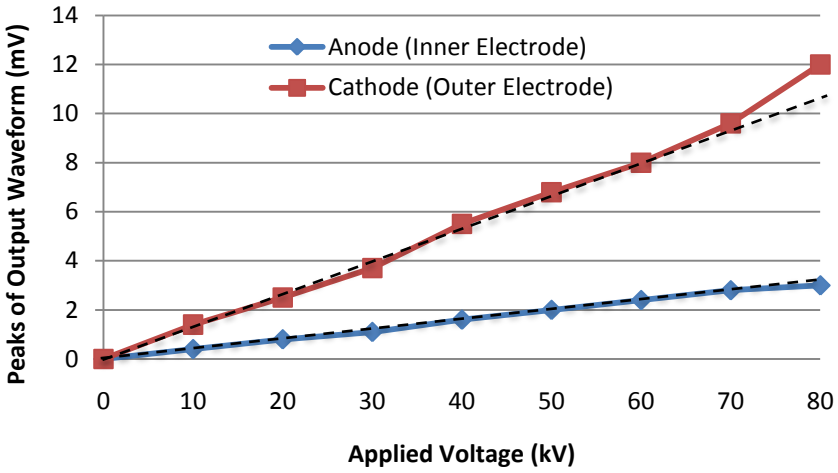

(b) 10 ^{0}C temperature gradient

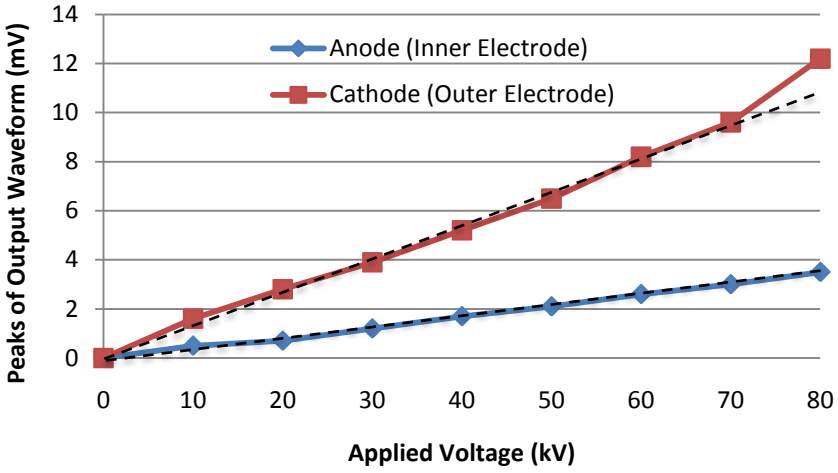

(c) 20 ^{0}C temperature gradient

Figure 8-8: Ramp test profiles for (a) no temperature gradient, (b) 10 ^{0}C temperature gradient and (c) 20 ^{0}C temperature gradient

It was also observed that with the application of negative voltage, there is no charge formed at the anode area for both no temperature and 20 ^{0}C temperature gradient. However, a very small amount of homocharge is formed at 10 ^{0}C temperature gradient. This minimum amount of homocharge formed may be due to the injection enhancement at the anode. In addition, the formation of heterocharge in the vicinity of the cathode for all three temperature conditions are formed by the rapid migration of the injected electrons across the insulation where it cancels out the holes at the cathode region while awaiting to be extracted.

8.3.2.2 DC Aging Test

The results for un-degassed XLPE cable samples under negative DC aging tests over a period of 9 hours are illustrated in Figure 8-9. All test conditions show under the application of -80 kV at 0 minutes, negative charges are distributed across the XLPE insulation with heterocharge accumulated adjacent to the cathode and with little or no homocharge forming near the vicinity of the anode. These results are consistent with the ramp test results obtained prior to the DC aging. Furthermore, these cables did not undergo the degassing process, therefore, the separation of existing and field generated charge species within the material are also an inevitable source for the formation of heterocharge.

Under no temperature gradient across the insulation material, as shown in Figure 8-9a, it can be clearly observed that both negative and positive charges evolve under the first 3 hours of stressing where the initial broadly distributed negative charge at 0 minutes were converted into heterocharge formation in the vicinity adjacent to both electrodes. With the difficulty of trapping the positive charges, they migrate from the cathode towards the anode where it is cancelled out or recombines with the accumulated negative charge leading to the increment of positive charge over the stressing period.

With increment of temperature gradient towards 10 ^{0}C, the charge profile illustrated in Figure 8-9b show that small broadly distributed negative charges are spread across the insulation at 0 minutes. Within 1 hour of stressing, positive charge seem to have saturated across the material leading to the rest showing on the negative charges

formation. With the increasing stressing period towards 9 hours, there is a build up of negative charges adjacent towards the anode's heterocharge, heading towards the centre of the bulk. Furthermore, negative charges adjacent to the vicinity of the cathode tend to decrease during the initial hour of stressing due to holes penetration into the sample where they partly compensate or recombine with the initial negative charges.

When temperature gradient is increased to 20 ^{0}C, two sets of larger and broader distribution of negative charges are located in the middle of the bulk as well as the vicinity adjacent towards the cathode. Evidently, it can be observed that positive charge tends to move towards the anode as a packet of positive charge begins to form between the two sets of distributed negative charges. In addition, the large and broad negative charges at the centre of the bulk tend to decrease due to entry and build up of positive charges towards its position.

Therefore, with the increment of temperature gradient the results show a relationship with the earlier results obtained in section 8.3.1.2 where both positive and negative charges have different mobility which tend to increase with the increment of temperature.

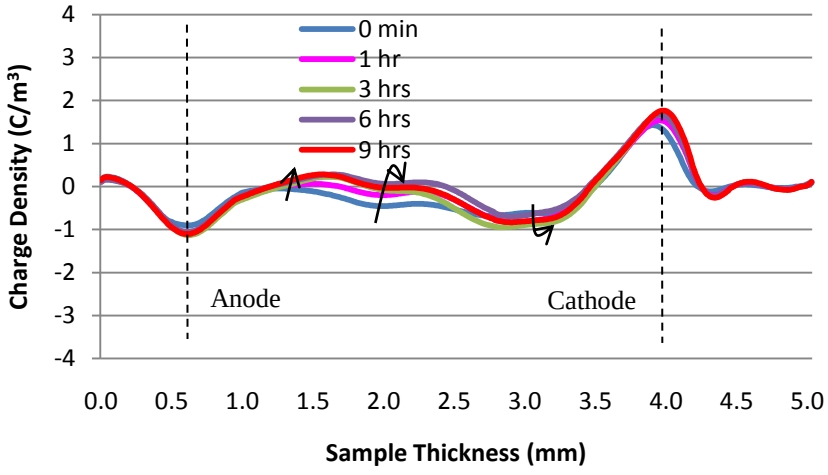

(a) No temperature gradient

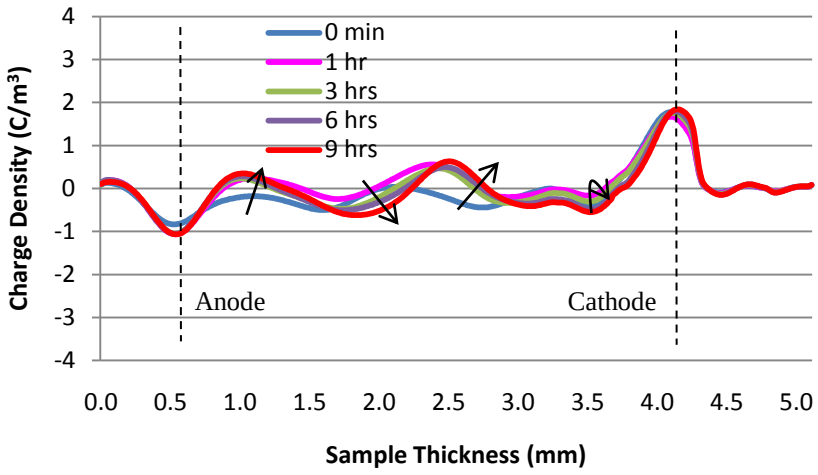

(b) 10 ^{0}C temperature gradient

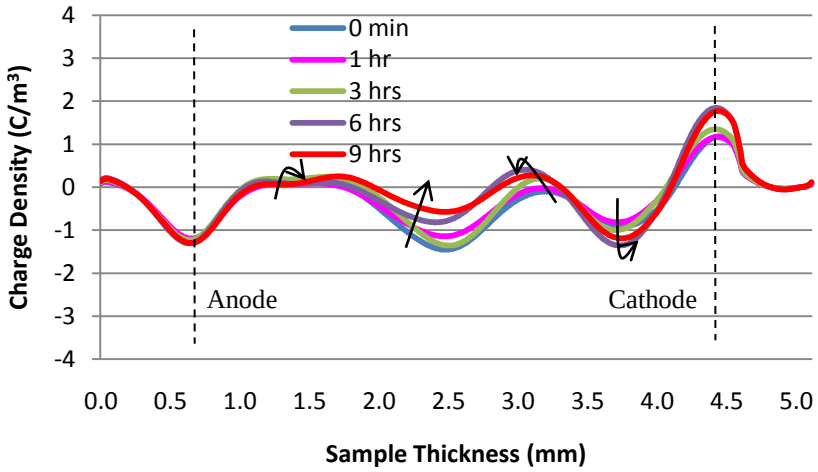

(c) 20 ^{0}C temperature gradient

Figure 8-9: Voltage on space charge profiles with aging time under the application of -80 kV

8.3.2.3 Polarity Reversal Test

After 9 hours of negative voltage stressing (-80 kV), voltage polarity was then switched towards positive (+80 kV) and space charge measurements were taken at different stressing period for each of the different temperature gradients, as illustrated in Figure 8-10. Similar phenomenon was observed in all three conditions where positive charges are widely distributed across the insulation immediately after polarity reversal. Thus, it shows that upon polarity reversal, the type of charges that are going to overrun across the insulation is determined by the sign (negative or positive) of the applied polarity

reversal voltage. In addition, it took less than a fraction of a second for the cancelling or recombination effect of initial accumulated charges to be replaced by the new polarity charge.

When the cable's XLPE insulation is under the condition of no temperature gradient, it can be observed there is a constant build up of negative charges across the material in the vicinity adjacent to the anode towards the centre of the bulk. These build up of negative charges throughout the stressing period are caused by the injection of electrons from the cathode where these electrons will interact and form a cancelling relationship with the preliminary positive charge, with further electrons being trapped when migrating towards the anode for extraction. Additionally, due to the injection of electrons after the polarity reversal, it can also be observed there is a decrease in positive charges in the region adjacent to the cathode within the first 30 minutes and followed by the saturation of positive charges at the region after 1 hour of stressing where more positive charges are being trapped after migrating from the anode.

Under the application of a 10 ^{0}C temperature gradient across the insulation, Figure 8-10b shows a similar trend adjacent to the cathode of decreasing positive charge in the first 30 minutes, followed by an increment towards saturation as mentioned earlier. In addition, a mirror image of charge can be seen within the 30 minutes of opposite polarity voltage which remained constant throughout the 2 hours of positive stressing.

Further increment of temperature gradient towards 20 ^{0}C across the insulation, as illustrated in Figure 8-10c, shows a rather similar charge formation as compared to condition of 10 ^{0}C where more charges are being accumulated and trapped across the sample and further towards the centre of the bulk. It can be observed that the shape of the accumulated charges starts to take shape immediately after voltage polarity reversal, subsequently, a "Mirror Image Effect" is obtained around 15 minutes of positive stressing. Moreover, the space charge measurements for negative to positive polarity voltage reversal, as shown in Figure 8-10c, have the same feature as the positive to negative polarity voltage reversal, as shown in Figure 8-5c, where fluctuation on the charge accumulations during stressing period are visible, especially from the bulk centre towards the cathode region. Firstly, this feature may be due to the increase mobility of both charges, as mentioned earlier, due to the increase temperature gradient across the

insulation where the injection and migrating of each charges (electrons and holes) towards its opposite polarity, constantly recombining and cancelling out each other. Secondly, the heterocharge formation will cause two high field regions in the vicinity of each electrode (anode and cathode) leading to the increase local currents and possibly assisting the charge recombination in the vicinity. Finally, the resultant measurements may be affected by the high temperature across the cable that creates the temperature gradient across the material as the influence of the divergence, attenuation and dispersion across the material would cause the scattering of the acoustic waves due to densely distributed inhomogeneities and frequency dependence of the material.

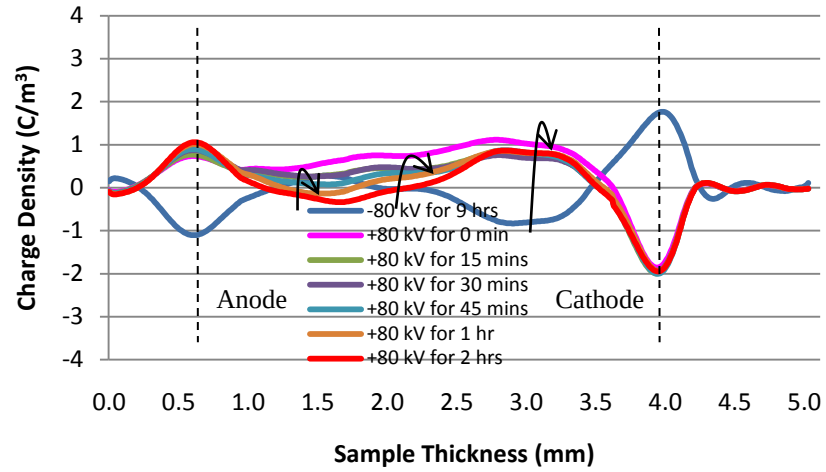

(a) No temperature gradient

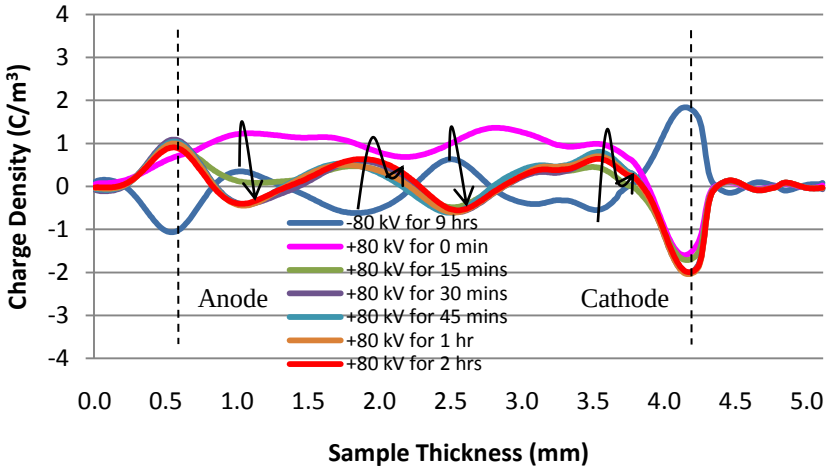

(b) 10 ^{0}C temperature gradient

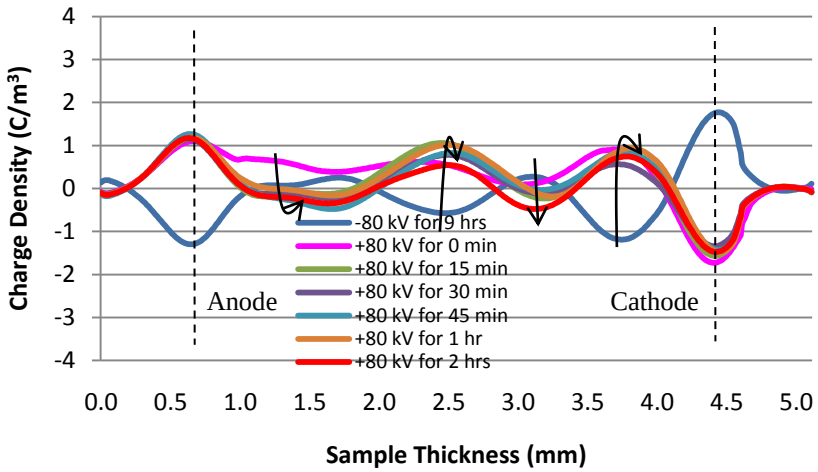

(c) 20 ^{0}C temperature gradient

Figure 8-10: Voltage on space charge profiles with aging time under the application of voltage reversal +80 kV

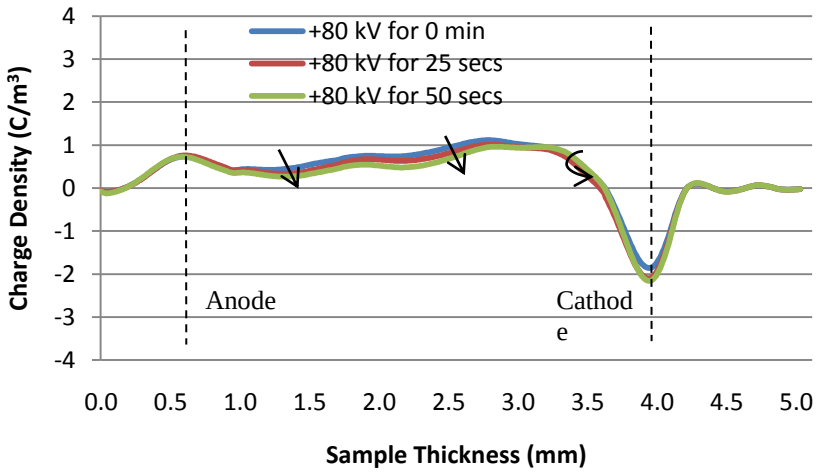

(a) No temperature gradient

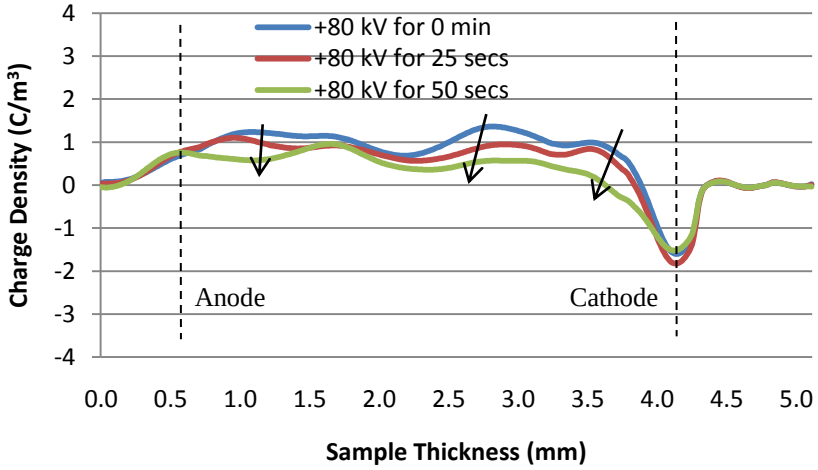

(b) 10 ^{0}C temperature gradient

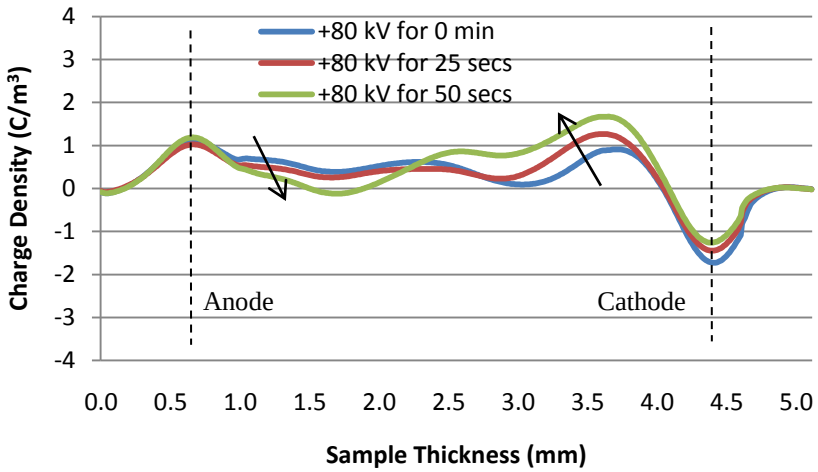

(c) 20 ^{0}C temperature gradient

Figure 8-11: Voltage on space charge profiles within a minute of aging time under the application of voltage reversal +80 kV

After voltage polarity reversal, two additional measurements were also taken within a minute for each of the different temperature gradient conditions as illustrated in Figure 8-11. This whole event correlates with the results obtained by demonstrating a higher temperature gradient influences the injection rate of the charges as well as the mobility of it where it influences the time for the formation of a "Mirror Image Effect".

8.3.2.4 Total Electric Field Distribution in Cable during Polarity Reversal

The results in Figure 8-12 are to realise the consequences of the total electric field deviation under different temperature gradient conditions across the insulation material based on the relocation of the accumulated space charge during voltage polarity reversal.

Figure 8-12a represents the total electric field distribution across the insulation under no temperature gradient where significant amounts of heterocharge are accumulated in the region adjacent to both electrodes under the application of -80 kV for 9 hours (before voltage reversal), consequently leading to the amplification of the interfacial stresses at both electrodes with values of -29.4 kV/mm at anode and -43.5 kV/mm at cathode interfaces. At the moment voltage polarity reversal (+80 kV) was implemented (0

minutes), both anode and cathode interfaces stress plunges to 5.4 kV/mm and rockets to 57.6 kV/mm respectively, subsequently reaching its final value of 24.2 kV/mm and 47.1 kV/mm at both anode and cathode interfaces respectively after 2 hours of stressing.

With a 10 ^{0}C temperature gradient applied across the insulation, the total electric field distribution is presented in Figure 8-12b which holds some similarities in shape as compared to the results obtained under no temperature gradient, as presented in Figure 8-12a. The dissimilarity lies on the 10 ^{0}C temperature gradient space charge accumulations between the centre section of the bulk towards the anode region where two additional packets of negative and positive charges were located. These additional charges increase the electric stress towards -37.3 kV/mm in the centre of the insulation when under 9 hours of positive voltage stressing. In addition, extremely high electric stresses of -51.6 kV/mm and 93.4 kV/mm were observed at the interfaces of both inner and outer electrode respectively under the event of voltage polarity reversal (0 minutes). The high interfacial electric stresses situated at both electrodes tend to decrease with the stressing duration, reaching its final value of 25.7 kV/mm and 43.2 kV/mm for inner and outer interfaces respectively after 2 hours of positive stressing.

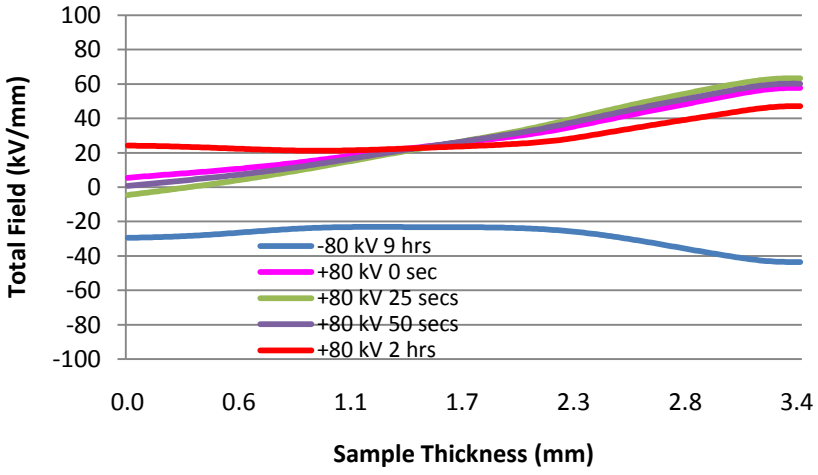

(a) No temperature gradient

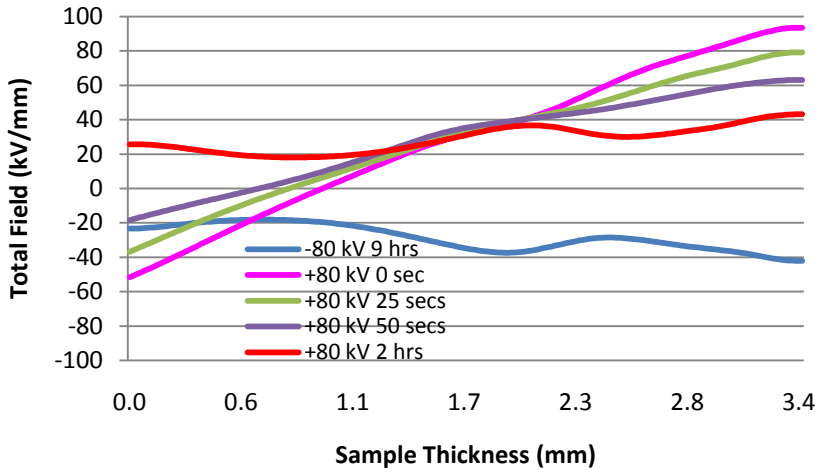

(b) 10 ^{0}C temperature gradient

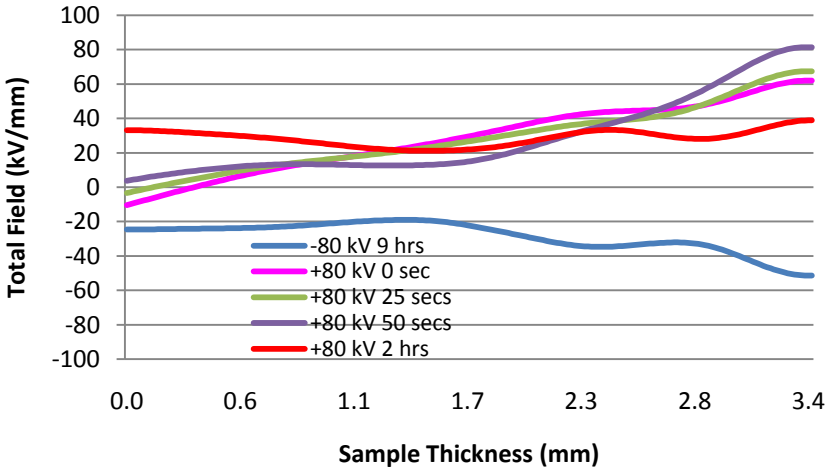

(c) 20 ^{0}C temperature gradient

Figure 8-12: Total electric field distribution during polarity reversal in cable based on own parameter (Negative to Positive)

Subsequently, comparisons were also done between Figure 8-12b and Figure 8-12c where a 20 ^{0}C temperature gradient is applied across the insulation material. The electric stress profiles between them show similarity in shape with only differences in the value of the interfacial electric stresses. This similarity of the electric stress profiles are due to space charge formation occurring under the applied voltage. Furthermore, it can be observed that under a higher temperature gradient of 20 ^{0}C, charges have migrated toward the cathode, leading to the -37.3 kV/mm electric stresses that was found previously in the centre of the insulation at 10 ^{0}C temperature gradient, as shown in Figure 8-12b, moving towards the cathode region, as presented in Figure 8-12c. The electric stresses before polarity reversal at 9 hours of stressing were -24.5 kV/mm and -

51.3 kV/mm for the inner and outer interface respectively. Instantaneously during voltage reversal (0 minutes), the inner interface stress decreases to -10.5 kV/mm and increases to 61.9 kV/mm at the outer interface, which further increases in value to 3.7 kV/mm for inner and 67.4 kV/mm for the outer interface after 50 seconds of +80 kV applied voltage. These stress increments at both interfaces can be explained through the build up of heterocharge in the vicinity adjacent to both electrodes, as illustrated in Figure 8-11c. Thus, after 2 hours of positive stressing the total electric stress values are 33.1 kV/mm and 38.9 kV/mm for both inner and outer interfaces respectively.

8.3.3 Degassed Cable (Positive to Negative Voltage Polarity Reversal)

8.3.3.1 Ramp Test

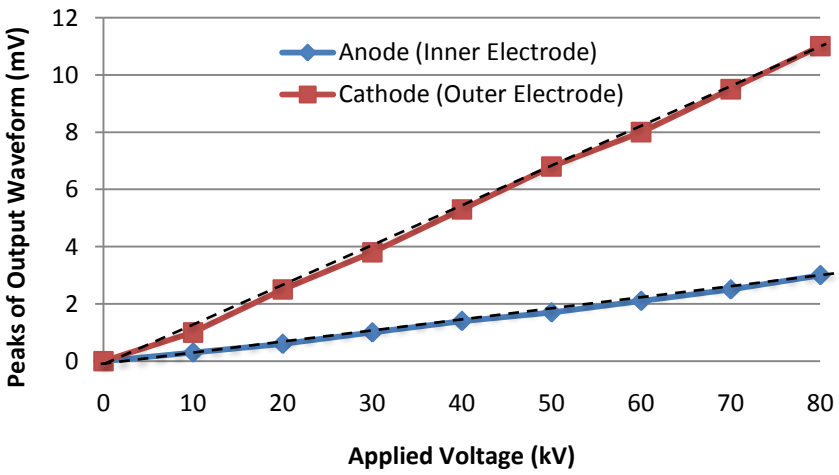

Figure 8-13: Ramp test profiles for no temperature gradient of degassed cable

Using the same technique as mentioned in section 8.3.1.1, a ramp test was been applied onto the degassed cable only under no temperature gradient condition due to experimental failure on the remaining conditions which will be clarified in Chapter 9. A linear proportional relationship is obtained between the induced charge at the electrode and the applied voltage between the application voltages of 0 V to +80 kV, as presented in Figure 8-13. Therefore, no space charges are formed across the insulation during the process of ramping up the voltage.

8.3.3.2 DC Aging Test

With the application of +80 kV DC voltage, space charge measurements were taken over a period of 9 hours on the degassed cable under no temperature gradient condition across its insulation material. The space charge profiles for the DC aging are illustrated in Figure 8-14. Immediately after the application of +80 kV at 0 minutes, there is no space charge formation across the sample which corresponded with the ramp test result. The result differs from the earlier un-degassed cables result, as this cable has its by-products, that are being left after the manufacturing process removed through a degassing process. It is well known that space charge distribution across XLPE polymeric material depends strongly on additives, oxidation products and by-products from the cross-linking reaction. In general, heterocharge formation is the result of by-products that ionic carriers attained from the impurities.

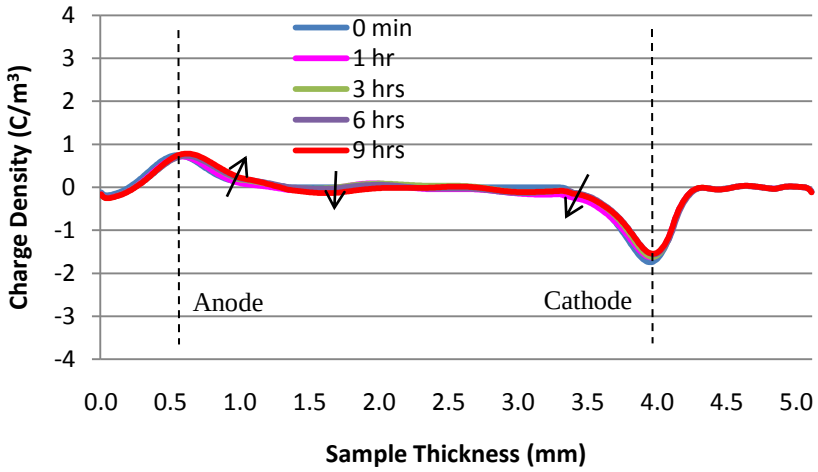

Figure 8-14: Voltage on space charge profiles with aging time under the application of +80 kV (Degassed Cable)

Under the DC aging test for 9 hours, it was observed a very small amount of homocharge was formed in the vicinities adjacent to both electrodes in view of the fact that the cable has been degassed. The formation of homocharge took approximately 6 hours to form, thus, suggesting the time required for a small homocharge to be developed in the degassed XLPE sample. This may suggest that the formation of homocharge is more difficult than heterocharge [Tanaka and Greenwood 1983b; Sanden, Ildstad et al. 1996]. Therefore, for the formation of homocharge it may require a higher electric stress or a longer stressing period under the same electrode and dielectric

preparation for the developing of the same amount of space charge accumulation as compared with the heterocharge.

8.3.3.3 Polarity Reversal Test

Under the procedure of a polarity voltage reversal, DC aging was applied under a negative 80 kV for 2 hours. Instantaneously after polarity voltage reversal, small packets of negative charges could be observed across the insulation material and tends to decrease within the first minute of aging, as illustrated in Figure 8-16. In Figure 8-15, it was observed that the homocharge accumulation in the vicinity adjacent to both the anode and cathode tend to decrease after 15 minutes of stressing. In all probability, this may be due to the increase of the bulk stress due to the homocharge formation during the aging test. The consequence of the increment of the bulk stress will lead to the ionisation of the remaining by-products in the middle of the bulk, which is most likely the vicinity where it is least susceptible to the degassing process that was conducted prior to the experiment. For that reason, generated heterocharge through the ionic dissociation will cancel out or recombine with the initial homocharge located at both the electrodes.

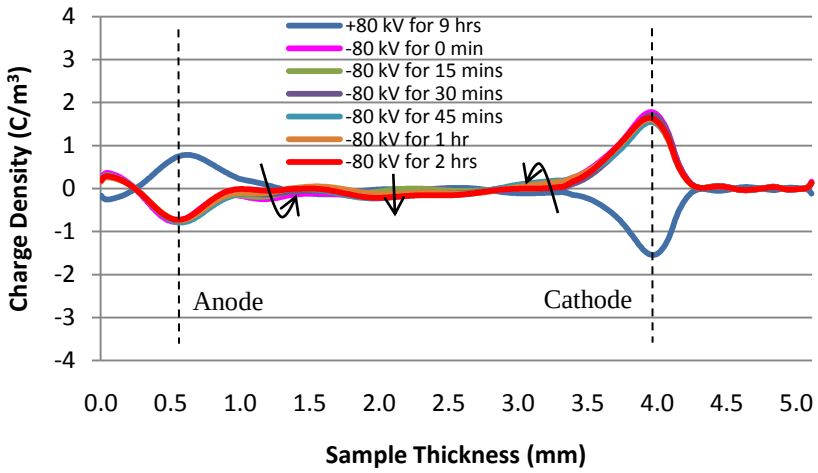

Figure 8-15: Voltage on space charge profiles with aging time under the application of voltage reversal -80 kV (Degassed Cable)

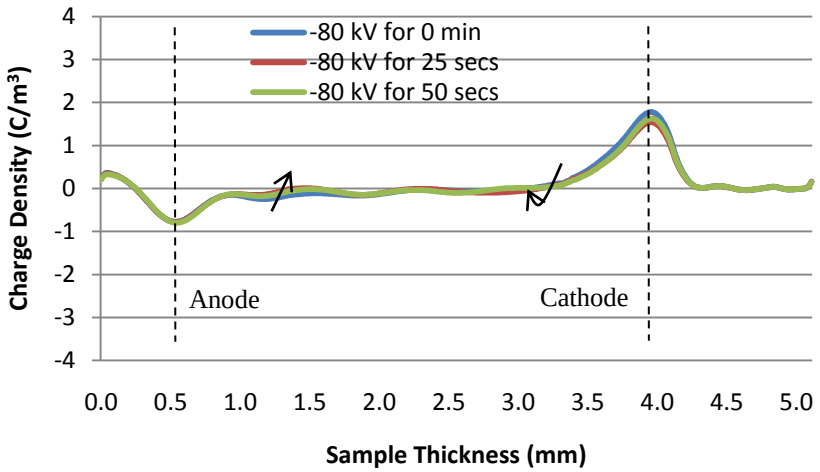

Figure 8-16: Voltage on space charge profiles within a minute of aging time under the application of voltage reversal -80 kV (Degassed Cable)

8.3.3.4 Total Electric Field Distribution in Cable during Polarity Reversal

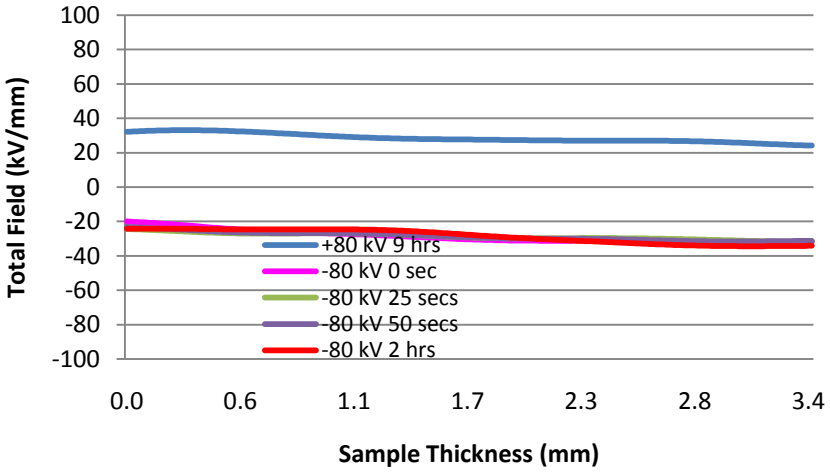

Figure 8-17: Total electric field distribution during polarity reversal in degassed cable based on own parameter (Positive to Negative)

The total electric field distribution in a degassed cable is less dependent on the electric field produced by the space charge due to the very small amount of space charge formed throughout the stressing period. Under the first 9 hours of positive stressing, the interfacial stress across the anode towards the cathode is approximately 32.2 kV/mm to 24.1 kV/mm respectively. After polarity reversal, it can be observed that there is a small increment of interfacial stresses at both electrodes as well as a decrease in the electric stress in the centre of the bulk. This small adjustment in electric stress during polarity

voltage reversal aging is due to a reduction of homocharge at the region adjacent to the electrodes as mentioned earlier.

8.3.4 Comparisons on the Interfacial Stresses under each Condition

The interfacial stresses of both un-degassed and degassed cables at different temperature gradient conditions under polarity reversal are summarised in Table 8-1. The values of the electric interfacial stresses at both interfaces were obtained from the stressing duration of 9 hours prior to polarity reversal, immediately after polarity reversal and under reversed polarity stressing periods of 25 seconds, 50 seconds and 2 hours.

With the significant increase of interfacial stresses due to the accumulation of space charges across the insulation, this high interfacial stress will result the degradation of the insulation material and possibly premature breakdown of the cable. Estimation on the cable's insulation life can be made using the inverse power law that follows the empirical expression:

$$E^n t = Constant \tag{E8-1}$$

where E is the electric stress, n is the voltage endurance coefficient whose value depends on the material quality and t is the expected lifetime of the material.

Table 8-1: Inner and outer interfacial stress at different temperature gradient conditions under polarity reversal

			No Temperature Gradient		**10 ^{0}C Temperature Gradient**		**20 ^{0}C Temperature Gradient**	
		Time	**Inner Interface (kV/mm)**	**Outer Interface (kV/mm)**	**Inner Interface (kV/mm)**	**Outer Interface (kV/mm)**	**Inner Interface (kV/mm)**	**Outer Interface (kV/mm)**
Positive to Negative	**+80 kV**	**9 hrs**	35.7	41.7	27.7	47.6	37.1	32.8
	-80 kV	**0 sec**	20.9	-77.4	16.8	-88.6	-8.2	-41.6
		25 secs	8.6	-68.9	-5	-66.7	-25.9	-29
		50 secs	-5	-54.9	-8.5	-65.1	-24.4	-42
		2 hrs	-34.3	-44.6	-16.5	-65.6	-35.6	-30.8
Negative to Positive	**-80 kV**	**9 hrs**	-29.4	-43.5	-23.3	-42	-24.5	-51.3
	+80 kV	**0 sec**	5.4	57.6	-51.6	93.4	-10.5	61.9
		25 secs	-4.6	63.3	-36.8	79.2	-3.3	67.4
		50 secs	0.7	60.2	-18.4	63.2	3.7	81.4
		2 hrs	24.2	47.1	25.7	43.2	33.1	38.9
Positive to Negative (Degassed)	**+80 kV**	**9 hrs**	32.2	24.1	N/A	N/A	N/A	N/A
	-80 kV	**0 sec**	-20	-31.8	N/A	N/A	N/A	N/A
		25 secs	-24.3	-31.6	N/A	N/A	N/A	N/A
		50 secs	-23.1	-31.2	N/A	N/A	N/A	N/A
		2 hrs	-24.1	-34.1	N/A	N/A	N/A	N/A

Table 8-2: Estimation of cable life time with n=8

			No Temperature Gradient	10 ^{0}C Temperature Gradient	20 ^{0}C Temperature Gradient
		Time	**Life Time Towards of the Original (%)**		
Positive to Negative	**+80 kV**	**9 hrs**	7.176	2.01	51.7
	-80 kV	**0 sec**	0.053	0.014	8.06
		25 secs	0.128	0.137	138.6
		50 secs	0.842	0.152	7.18
		2 hrs	4.18	0.164	26.6
Negative to Positive	**-80 kV**	**9 hrs**	5.12	5.41	1.43
	+80 kV	**0 sec**	0.54	9.1×10^{-3}	0.32
		25 secs	0.255	0.035	0.164
		50 secs	0.375	0.211	0.035
		2 hrs	2.71	4.34	13
Positive to Negative (Degassed)	**+80 kV**	**9 hrs**	56.9	N/A	N/A
	-80 kV	**0 sec**	62.7	N/A	N/A
		25 secs	66.2	N/A	N/A
		50 secs	100	N/A	N/A
		2 hrs	35.89	N/A	N/A

Table 8-3: Estimation of cable life time with n=15

			No Temperature Gradient	10 ^{0}C Temperature Gradient	20 ^{0}C Temperature Gradient
		Time	**Life Time Towards of the Original (%)**		
Positive to Negative	**+80 kV**	**9 hrs**	0.716	0.066	29
	-80 kV	**0 sec**	7.1×10^{-5}	6×10^{-6}	0.9
		25 secs	3.75×10^{-4}	4.28×10^{-4}	184
		50 secs	0.013	5.96×10^{-4}	0.72
		2 hrs	0.26	5.215×10^{-4}	8.35
Negative to Positive	**-80 kV**	**9 hrs**	0.38	0.42	0.035
	+80 kV	**0 sec**	5.63×10^{-3}	2.65×10^{-6}	2.11×10^{-3}
		25 secs	1.37×10^{-3}	3.4×10^{-5}	5.96×10^{-4}
		50 secs	2.83×10^{-3}	9.6×10^{-4}	3.38×10^{-5}
		2 hrs	0.12	0.28	2.2
Positive to Negative (Degassed)	**+80 kV**	**9 hrs**	34.75	N/A	N/A
	-80 kV	**0 sec**	41.73	N/A	N/A
		25 secs	46.1	N/A	N/A
		50 secs	100	N/A	N/A
		2 hrs	14.64	N/A	N/A

The voltage endurance coefficient, *n*, values were chosen based from a conservative value of 8 and a value of 15 due to a XLPE insulation being stress under an application of DC [Lalam and Hoang 2000; Maruyama, Ishii et al. 2004; Chen, Fu et al. 2005]. Under the applied field when no space charges are accumulated across the insulation

during no temperature gradient, 10 ^{0}C and 20 ^{0}C temperature gradients, the maximum electric stress experienced by the insulation are 30 kV/mm, 29.2 kV/mm and 30.2 kV/mm respectively.

With the voltage endurance coefficient value n=8 and n=15, the lifetime reduction from the original lifespan is shown in both Table 8-2 and Table 8-3 respectively. For illustration, as shown in Table 8-2, with space charges accumulated for 9 hours under no temperature gradient across the insulation, the electric stress (41.7 kV/mm) showed an increase of 39%, hence the lifetime is reduced to 7.176%.

In view of the above estimation for both n=8 and n=15, the most significant reduction in lifetime for the insulation of the un-degassed cable is in the sequence of when the insulation is having a 10 ^{0}C temperature gradient followed by no temperature gradient and lastly a 20 ^{0}C temperature gradient across it. The lifetime analysis for extreme cases under the application of polarity reversal during 0 to 50 seconds are also calculated with results showing the lifetime of the insulation is extremely shortened when polarity reversal is immediately applied (0 seconds) under both scenarios of positive to negative and negative to positive.

The lowest lifetime reduction for the insulation is found to be in the degassed cable under no temperature gradient, where the electric stress has the least enhancement due to the minimum amount of space charge accumulated across the insulation. Therefore, this lifetime estimation shows the effect of space charge accumulation and the importance of degassing the cable for the removal of by-products that initiate a large portion of the formation.

8.4 Conclusion

Space charge measurements were performed across both un-degassed and degassed XLPE extruded cables to understand the dynamics of space charge injection/accumulation under conditions when rated voltage is applied on the cable during service, and also the response of it under bi-direction power flow during polarity

reversal when different temperature gradients are applied across the insulation. In addition, total electric field across the insulation has been calculated based on the space charge profiles obtained during the process of polarity reversal and also the stressing period after the polarity reversal. The following conclusions can be made:

Firstly, a polymeric insulated power cable is in a hazardous state, attributable to the complex distribution of electric stress across its insulation due to the accumulation of space charge. In addition, through the existence of increase temperature gradient across the insulation material, additional complexity is done on the space charge dynamics, especially under 20 ^{0}C of temperature gradient. It is observed that injection and transportation of charges increases with the increment of temperature gradient across the insulation of the power cable, due to the higher activation energy of negative charges than positive charge and also, by having a higher temperature gradient across the insulation, it enhances the mobility of both positive and negative charges. Based on our experimental results it was found that with a temperature gradient of 10 ^{0}C across the cable's insulation, an extremely high interfacial stress will be located at the cathode as compared with a 20 ^{0}C temperature gradient.

Secondly, "Mirror Image Effect" is observed and obtained within 15 minutes for all three test conditions when voltage polarity reversal is applied. The duration for the formation of this mirror image to stabilise does vary with the different types of cables used [Fu, Dissado et al. 2008]. In addition, due to the enhance properties of the charges led by the increment of temperature gradient across the insulation, it is observed that when 20 ^{0}C temperature gradient is applied across the insulation, both positive and negative charges are formed immediately upon polarity reversal. Whereas in the case of both no temperature and 10 ^{0}C temperature gradient, upon polarity reversal the negative charges will spread throughout the insulation first, followed by the slower positive charge.

Thirdly, reduction of space charge accumulation can be achieved by removing the residues of any cross-linking by-products within the cable insulation through a degassing process. An un-degassed cable would produce a heterocharge formation as it has been reported the accumulation is influenced by additives, fillers, etc. [Khalil and Jevase 2000; Tanaka, Chen et al. 2003], whereas, a degassed cable would initiate a

homocharge formation. As degassed cable produces a very small amount of charge formation, therefore, a longer stressing duration or a higher amount of stressing voltage is required for the same amount of space charge as compared to the un-degassed cable.

Fourthly, it was found that space charge development between two different voltage polarities might have a different accumulation rate. As it can be seen from the results that by having a polarity voltage reversal stressing, the space charge profiles are similar or bigger in size when under the same stressing time when consideration are made to the neutralisation of previous charges upon polarity reversal.

Finally, with the inverse power law it clearly shows that the cable's life can be reduced by the enhancement on the electric stress across its insulation. This enhancement of electric stress is due to the presence of space charges that are deeply trapped across the cable's insulation. In addition, different temperature gradients across the insulation may have a different effect on the lifetime of the cable due to its support towards the movement of charges.

Chapter 9 Investigation of Problems Encountered in Space Charge Measurement of Cable when under Temperature Gradient

9.1 Introduction

In power cables a temperature gradient normally exists across the insulation due to the joule heating in the central conductor and the cooling effect by the surrounding ground on the outer insulation. Through this increment of temperature, it increases the mobility of the charges, promotes diffusion and thus increases viscosity within the material. As a result, it causes the variation of location of the inner electrode due to the decreasing speed of sound with temperature.

It has been reported that the field strength at the inner electrode is normally 2.5 times greater as compared to the outer electrode. Therefore, assuming there is an unchanged pressure pulse profile across the insulation, the amplitude of the anode (inner electrode) signal should be 2.5 times that of the cathode (outer electrode). However, attenuation of the pulse reduces the anode signal amplitude by ~20 % at room temperature and by 60 % at 80 ^{0}C. The speed of the pressure pulse decreases from 2100 m/s to 1500 m/s at room

temperature and 80 ^{0}C respectively [Lim and Fleming 1999]. This causes a conditioning effect on the insulation material where a decreasing effect of the charge density is observed.

9.2 Description of Problems

9.2.1 Apparent Shift of the Inner Electrode under Higher Temperature Condition

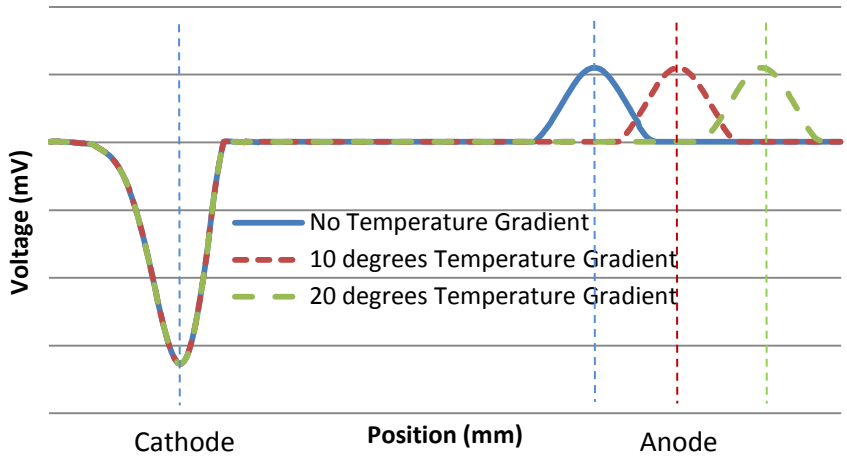

Figure 9-1: Inner electrode apparent shifting due to temperature

With the increase of temperature across the insulation the speed of the pressure pulse propagating through this medium is reduced, therefore the measured signal will arrive at later time in a sample with temperature gradient applied than a sample without any temperature gradient. This phenomenon is visible in the measured signals displayed by the oscilloscope as shown in Figure 9-1. It was found that for every 10 ^{0}C increase in temperature gradient, the pressure pulse speed will be reduced by a value of 250 m/s, which means at both 10 ^{0}C and 20 ^{0}C temperature gradients, the pressure pulse speeds were reduced to 1950 m/s and 1700 m/s respectively. Hence, it is important to calibrate the measurements such that this apparent shift of the inner electrode due to the temperature gradient is correctly accounted for.

In our measurements we found that it is essential to do a 20 ^{0}C temperature gradient trial run space charge measurements for 9 hours to obtain the maximum apparent shift of the electrode. By doing a trial run, it will ensure that the inner electrode apparent

shift will not exceed the maximum shift for experiments with less than 20 ^{0}C temperature gradient across the insulation. In addition, all settings within the oscilloscope will remain the same for all three experiments when under different temperature gradients to ensure no discrepancy among results.

9.2.2 Apparent Shift of the Inner Electrode during Experimental Condition

Initially, space charge measurements were taken from the XLPE cable without the consideration of temperature gradient and no problems were encountered during the collection of data. However, by having a temperature gradient across the XLPE insulation, a certain degree of difficulty is encountered when experimental results showed again a certain increase in the apparent shift of the inner electrode with time. In response to the apparent change of the inner electrode position (anode) and by aligning them together at a same point, it can be observed from Figure 9-2 that a longer stretch of signal is captured by the acoustic transducer (PVDF).

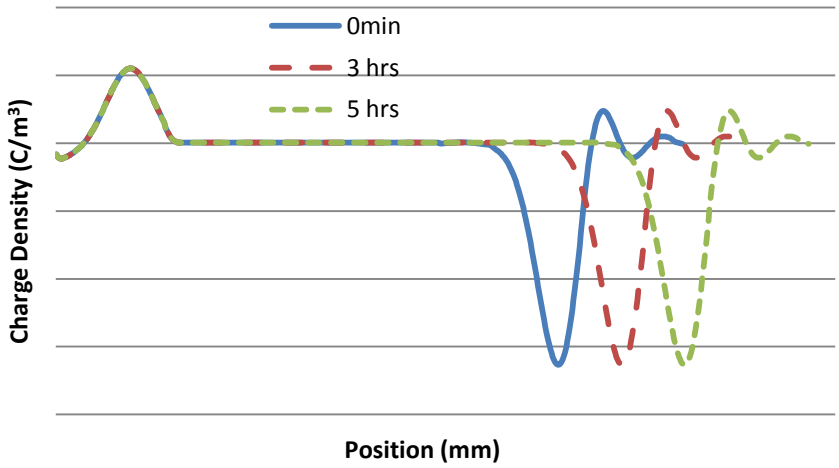

Figure 9-2: Inner electrode change of position during experiment

As mentioned earlier in Chapter 4.6, data processing is required in detecting the signal by calibrating it in the considerations of the divergence of acoustic waves due to the cylindrical geometry of cable, the attenuation and dispersion of the acoustic waves travelling through the lossy insulation material. Originally, the deconvolution technique was applied when no attenuation and dispersion were considered at the outer electrode when selected as the reference signal. This reference signal is then implemented

throughout the experiment for the calibration purposes. However, it was found that this reference signal will not be suitable for the calibration purposes when temperature gradient is applied across the cable's insulation, due to the longer stretch of captured data signal dependent on duration of time. Thus, if the original reference signal is used for the calibration of results obtained when temperature gradient is applied across the cable, the results obtained will not be accurate as a fluctuation of induced surface charge phenomenon will be observed at the outer electrode (cathode) as shown in Figure 9-3.

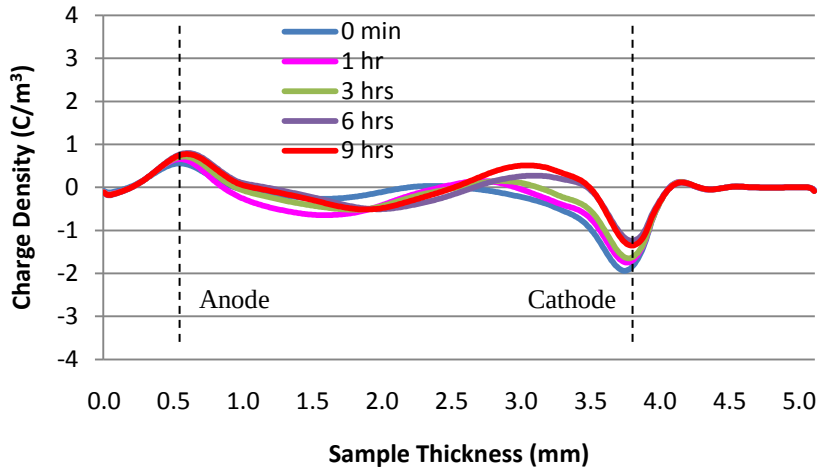

Figure 9-3: Original reference signal used on the application of temperature gradient

9.2.2.1 Polarity Solution for the Encountered Problem

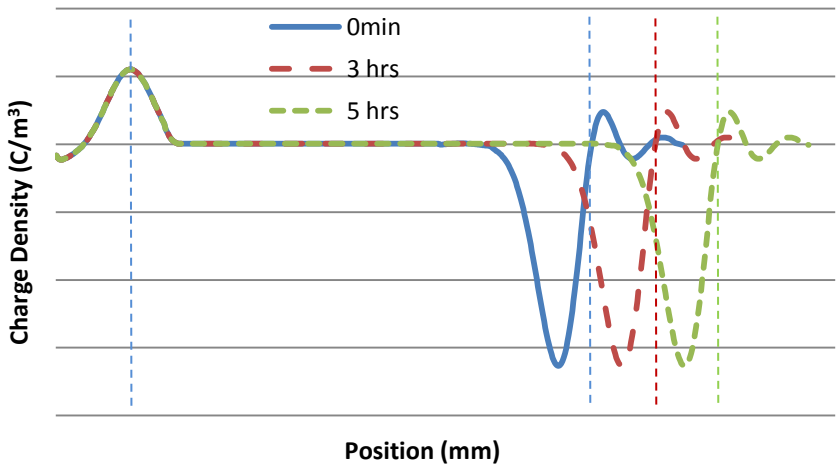

Figure 9-4: Illustration of lengthening the reference signal

Accurate space charge measurements from the experiments are needed especially when

temperature gradients across the cable's insulation material are considered. Therefore, results of the fluctuations of induced surface charges at the outer electrode can be eliminated by having the divergence, attenuation and dispersion of the acoustic waves put into consideration. This is simply done by lengthening the original signal and using this lengthened signal as the reference signal for accommodating the factors of divergence, attenuation and dispersion when there is change in the position of the inner electrode, as illustrated in Figure 9-4.

Through lengthening the reference signal we are able to control the area, which contains the features of the whole system response where important factors are considered during the introduction of temperature towards the experiments. As a result, a more accurate space charge measurement on the cable's insulation could be obtained, as shown below in Figure 9-5.

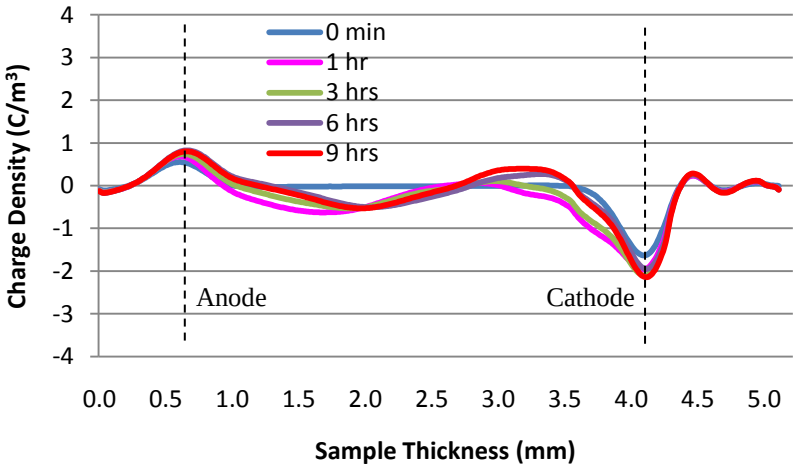

Figure 9-5: Lengthened reference signal used on the application of temperature gradient

9.2.3 Degassed Cable Samples for Temperature Gradient Conditions

For the cable to undergo a degassing process, it has to be fitted into a vacuum sealed oven under a heated temperature and pressure condition. As a result, the cable sample was cut into half in order to fit the sample into the laboratory vacuum sealed oven, where it was degassed at 90 ^{0}C temperature and 101.325 kPa for 120 hours.

After the degassing process has been done, the two sections of the cable were rejoined

together by a screw as its support and electrical paste is applied on the sections between the screw, cable aluminium core and the thin aluminium ferrule to improve its conductivity, as illustrated in Figure 9-6. To end the joining procedure, the whole joined section was then wrapped under an electrical self bonding tape to cover the exposed aluminium ferrule and also minimising any possible gaps between the joint.

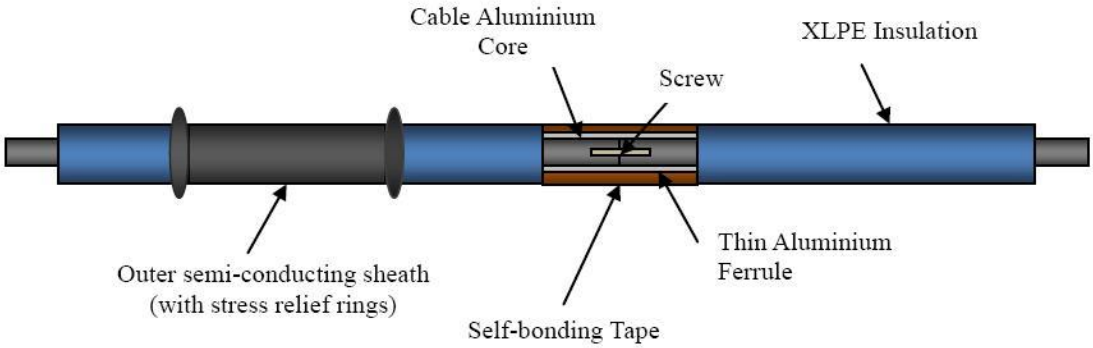

Figure 9-6: Illustration of a rejoined degassed cable

Figure 9-7: Rejoined degassed cable's self bonding wrap meltdown

The degassed jointed cable performed perfectly under no temperature gradient condition but was unable to fulfil the temperature gradient conditions when induction heating is applied on the cable core through the current transformer. Under the application of 250 A induced current through the current transformer for the creation of a 10 ^{0}C temperature gradient across the XLPE insulation, the result is the melting of the electrical self bonding wrap within 15 minutes of induction heating application due to

the increased resistance from the joint, as shown Figure 9-7. With the specification of the electrical self bonding tape stating the maximum operating temperature is 130 ^{0}C, therefore, it is deduced that the temperature situated at the joint is much higher than the maximum operating temperature it can withstand. For that reason, the electrical self bonding tape was removed and replaced with a fibreglass tape which has a maximum operating temperature at ~260 ^{0}C, as illustrated in Figure 9-8. However, through using the fibreglass tape and performing the induction heating through the jointed cable, white steam of smoke is detected emitting from the wrapping after 30 minutes of current application. This concludes that the temperature at the joint is much higher than we have expected.

Figure 9-8: Illustration of a rejoined degassed cable under fibreglass wrap

Therefore, due to the limited resources of high temperature tape within the laboratory and also the safety reasons due to the fire risk, along with the lengthy duration of stressing under high voltage and temperature (13 hours experiment), consequently, the experiments on degassed cable for temperature gradient conditions for both 10 ^{0}C and 20 ^{0}C were aborted.

9.3 Conclusion

In this chapter, a phenomenon is highlighted in showing that an apparent shift of the

inner electrode has been observed during space charge measurements across the insulation of a polymeric cable when temperature gradient is being applied. In addition, this apparent shift of inner electrode could not be controlled as it may shift at any moment of time during the experiment and the distance of this shift also tends to increases with the experiment duration.

The reason for this shift is due to the effect of temperature gradient across the insulation material as the applied temperature affects the divergence, attenuation and also the dispersion of the acoustic waves travelling across the insulation material. Thus, leading to a longer length of captured measurement signals, while having a shorter initial reference signal taken during an earlier measurement for its signal processing. Under this problem, the shorter reference signal is not being able to provide the correct length of data to undergo the signal processing, consequently, leading to the reduction of induced surface charge phenomenon on the space charge measurements.

This phenomenon can be rectified by a simple process of lengthening the reference signal to the same length of signal as compared to the measurement signal. Subsequently, this lengthened reference signal is then used for the signal processing of the corresponded measured signal in order to obtain the final space charge density across the insulation material. Therefore, allowing a more accurate result on the space charge measurement across the insulation of the cable when a temperature gradient is being considered.

In addition, the reason for the abortion of experiments on degassed cable under temperature gradient conditions of both 10 ^{0}C and 20 ^{0}C is due to the increase of resistance between the jointed sections of the degassed cable. This problem can be rectified by degassing the cable in a larger vacuum oven by keeping the cable intact and not splitting it into half and rejoining them in a later phase. Nevertheless, the jointed cable is still considered a success due to we were able to apply a high voltage of 80 kV and obtain space charge measurements throughout the 13 hours stressing duration, under no temperature gradient, via an improvised joining technique and without using any assisted commercial available product.

Chapter 10 Conclusion and Suggested Future Work

10.1 Conclusion

This thesis provides a report on the research done on space charge phenomenon within the insulation of an XLPE power cable. A newly modified PEA system with a current transformer attached is used for the investigation of space charge formation, migration and accumulation within a power cable's polymeric insulation. Under the application of this new PEA system, temperature gradient conditions can be applied across the polymeric insulation of the cable replicating its service conditions and its response to it.

1. **Electric Field Determination in the Presence of Space Charge and Temperature Gradient using COMSOL**

It is recognised that in direct current (DC) power cable, the electric field is affected by conductivity of the material, which is a function of both temperature and electric field. Applying high voltage in DC cable results in a temperature gradient across the insulation and hence a radial distribution of the insulation conductivity. With the consequence of a high voltage application, space charge is accumulated within the insulation bulk which will modify the electric field across the insulation. The coupled problems of electric field and temperature inflict difficulties to identify the electric field distribution in HVDC cables, which therefore poses a threat to the reliability in operation of DC power cables. Consequently, the design of future EHV DC cable encounters many challenges relating to the temperature and field-dependent properties

of polymeric dielectric materials.

Investigations have been made on the determination of electric field within the insulation of an XLPE power cable with the presence of space charge accumulated across the insulation. We have also developed an analytical basis for predicting the total electric stress within the insulation through using numerical simulation software, COMSOL, which provides us a tool to have an overview on the underlying theoretical principles and phenomenon of space charge through the determination of results obtained from the polymeric material.

2. Space Charge Measurements on XLPE Cable with and without Temperature Gradient

In the area of research on dielectric polymeric insulated cables, lots of publications on space charge distribution on cables samples had been made. However, space charge behaviours of the insulated polymeric materials under high temperature were not investigated. The service temperature gradients across the insulation, which exist when rated voltage is applied on the cables, are not being considered in most published results.

Therefore, in our current study we have obtained some initial results on space charge distribution and evolution within the insulation of the XLPE power cable, both with and without temperature gradient. The results show that space charge measurements in a group of cables with different temperature gradient applied across them have obtained almost similar space charge profiles with one another. The only difference is with the increased temperature gradient application, the charges tend to move further towards opposite electrodes, leading to a larger accumulation of charges adjacent to the electrodes. These results have confirmed that with an increase of temperature, injection is enhanced, leading to a higher amount of charges being injected and accumulate across the insulation. The temperature gradient also enhanced the mobility of the charges leading to a much more rapid accumulation of space charge and not to mention also a higher neutralisation rate of space charge.

3. Conductivity of the DC Power Cable's XLPE Insulation Material

Electric conduction current is being measured from the polymeric XLPE peeling of a power cable. The influence of temperature on electric conduction under the application of DC voltage has been studied and it shows the complexity of electric conduction in the XLPE peel where this conduction relies strongly on both the high electric field application and temperature.

During the application of high field and temperature, a well defined current peak is observed and this may be the link towards the accumulation of charges within the insulation through the injection of carriers by the electrodes. Carrier mobility can be obtained from this current peak and this mobility is dependent on the applied field and the temperature. Movement of crystallinity could have been initiated with the increment of temperature along 60 ^{0}C to 90 ^{0}C, causing obstruction towards the movement of the charge carriers.

Through these experiments, we are able to determine the conductivity parameters through the hopping model of conduction in dielectric. Subsequently, these parameters were used in the conductivity equation to determine the electric field distribution across the cable's XLPE insulation.

4. Effects of Temperature Gradient and Polarity Reversal on Space Charge Accumulation in XLPE Cable

In most HVDC transmission systems, a bi-direction flow of electricity is necessary in its daily operation. The presence of space charge across the insulation of the polymeric XLPE cable is especially dangerous during polarity reversal as the charges tend to be deeply trapped adjacent to the electrodes. Therefore, when an application of polarity reversal is applied across the system, this will lead to a sudden enhancement of the electric field piloting to the reason for breakdown.

In our experiments, space charge measurements were performed across both degassed and un-degassed XLPE extruded cables, showing its responses in polarity reversal under different temperature gradients across its insulation. In addition, total electric

field across the insulation have been calculated based on the insulation's own parameters and from the space charge profiles obtained during the process of polarity reversal and also the stressing period after the polarity reversal. It is observed that the charges accumulated under polarity reversal holds on to the same position and density across the insulation prior to the reversal in the exception of different polarity sign. In addition, existences of these charges across the insulation do pose a threat towards the stability of cable as, based from the total electric field calculation, a much higher interfacial stress is observed at the outer interface immediately after polarity reversal. Results have shown that the interfacial charge is dependent on the space charge accumulation across the insulation and also on the amount of heterocharge accumulated adjacent to the electrode. Based on our experimental results, it was concluded that a temperature gradient of 10 ^{0}C across the cable's insulation has a higher interfacial stress located at the cathode as compared with a 20 ^{0}C temperature gradient.

The increment of temperature gradient across the insulation will enhance the mobility of the charges. As it has been observed that when 20 ^{0}C temperature gradient is applied across the insulation, both positive and negative charges are formed immediately upon polarity reversal. Whereas in the case of both no temperature and 10 ^{0}C temperature gradient, upon polarity reversal the negative charges will spread throughout the insulation first, followed by the slower positive charge.

The process of degassing a cable could have a space charge accumulation reduction through the removal of by-product residues within the insulation and introduces a homocharge accumulation. A very small amount of charge formation is observed in a degassed cable; therefore, suggesting a longer stressing period or a higher stressing voltage is required for the same amount of space charge to accumulate as compared to an un-degassed cable.

It was also found that space charge development between two different voltage polarities have a different accumulation rate. As it can be seen from the results, the space charge profiles are comparable or greater in size when under the same stressing duration when consideration are made to the neutralisation of previous charges upon polarity reversal.

Finally, by having the enhancement of the electric field due to the accumulated space charge under service temperature and the event during a polarity reversal identified. The reduction of the cable's lifetime is deduced from the inverse power law. This lifetime prediction is vital towards the cable designers and power companies.

5. **Investigation of Problems Encountered in Space Charge Measurement of Cable when under Temperature Gradient**

The phenomenon showing an apparent shifting effect of the inner electrode is observed during space charge measurements across the insulation of a polymeric cable when temperature gradient is being applied. The reason for this apparent shifting effect is due to the application of temperature gradient across the insulation, leading to the effect of acoustic wave's dispersion while travelling across the insulation material. Consideration on this phenomenon effect is needed to obtain a truthful space charge density across an insulation material when under temperature gradient application. Therefore, it is being rectified by a simple process of lengthening the reference signal to enable a more accurate result on space charge measurement when temperature gradient is being considered. Furthermore, an improvised joining technique is utilised on the joining of a degassed cable without using any assisted commercial available product. This technique is proven feasible, if only when no force temperature gradient is created across its insulation.

10.2 Suggested Future Works

In this thesis, through using the newly modified PEA system with the current transformer attached, we are able to examine space charge distribution of the XLPE insulated power cables with temperature gradient occurring within the insulation material.

Studies have shown that rapid space charge evolution is often observed within the XLPE insulation of a power cable. This rapid space charge evolution arises basically from both the separation of species under the application of electric field and the

injection of carriers from the electrodes. There are reports showing charge carriers have been injected and transported across the polymeric insulation within a second. Therefore, investigation is needed to look upon this fast space charge associated process by having faster sampling rate signal averager equipment. With this equipment, further investigation can be carried out to promote the understanding of space charge evolution.

In addition, a new method based on the Maxwell-Wagner model can be proposed to calculate electric field distribution across polymeric DC power cable insulation in the presence of space charge. According to Maxwell-Wagner theory, space charge will be formed in the sample if the material is heterogeneous. So the space charge distribution actually reflects the in-homogeneity of the material. To calculate the electric field in the bulk dielectric, considering the effect of conductivity, the cable's dielectric material is divided into many portions with different values of conductivity and permittivity in each portion, reflecting the local difference in electrical properties with respect to the consideration on the cable's geometry. The electric flux in two adjacent portions will have different values, since the conductivity attributed by the presence space charge differ in each slab with respect to the cable's geometry. The difference in electric flux will produce charge contained in this subdivision. Therefore, by inputting the conductivity, based on the hopping theory model of conduction in dielectric, into the equation of the electric flux, we are able to obtain the resulting electric field distribution solved, taking into consideration the temperature and field effects on the conductivity. Finally, this result could be used to make comparison on the accuracy of electric field determination using the Maxwell-Wagner model.

References

Abou-Dakka, M., A.T. Bulinski and S.S. Bamji (2006). Space Charge Evolution in XLPE with Long-term Aging under DC Voltage - the Effect of Temperature and Polarity Reversals. Annual Report, Conference on Electrical Insulation and Dielectric Phenomena.

Agnel, S. and A. Toureille (1997). Two complementary techniques : the Thermal Step technique and the Thermally Stimulated Currents technique. Study of polycrystalline Al_2O_3. Annual Report, Conference on Electrical Insulation and Dielectric Phenomena.

Ahmed, N. H and N. N. Srinivas (1997). "Review of space charge measurements in dielectrics". IEEE Transactions on Dielectrics and Electrical Insulation, **4**(5): pp. 644-656.

Ando, N. and F. Numajiri (1979). "Experimental Investigation of Space Charge in XLPE Cable Using Dust Figures". IEEE Transactions on Dielectrics and Electrical Insulation, **14**(1): pp. 36-42.

Andrews, T., R. N. Hampton, A. Smedberg, D. Wald, V. Waschk and W. Weissenberg (2006). "The role of degassing in XLPE cable manufacture". IEEE Electrical Insulation Magazine, **22**(6): pp. 5-16.

Bahrman, M. P. and B. K. Johnson (2007). "The ABC of HVDC transmission technologies". IEEE Power and Energy Magazine, **5**(2): pp. 32-44.

Bambery, K. R. and R. J. Fleming (1998). "Space Charge Accumulation in Two Power Cable Grades of XLPE". IEEE Transactions on Dielectrics and Electrical Insulation, **5**(1): pp. 103-109.

Bambery, K. R., R. J. Fleming and J. T. Holböll (2001). "Space charge profiles in low density polyethylene samples containing Permittivity/conductivity gradient". Journal of Applied Physics D, **34**(20): pp. 3071-3077.

Bamji, S. S. and A. T. Bulinski (1995). An optical technique for in situ measurement of the concentration of the crosslinking by products in XLPE cables. JICABLE95: pp. 158-161.

Bartnkias, R. and R. M. Eichhorn (1983). "Engineering Dielectrics, Volume IIA Electrical Properties of Solid Insulating Materials: Molecular Structure and Electrical Behavior". American Society for Testing and Materials.

Beltzer, A. I. (1988). "Acoustic of Solids". Spriner-verlag, Berlin Heidelberg.

Blaise, G. (1995). "Space-charge physics and the breakdown process". Journal of Applied Physics, **77**: pp. 2916-2927.

Blythe, A. R. and D . Bloor. (2005). "Electrical properties of Polymers". 2nd Edition, Cambridge University Press.

Boggs, S., D. Damon, J. Hjerrild, J. Holbol and M. Henriksen (2001). "Effect of Insulation Properties on the Field Grading of Solid Dielectric DC Cable". IEEE Transactions on Power Delivery, **16**(4): pp. 456-461.

Boukezzi, L., A. Boubakeur and M. Lallouani (2007). Effect of Artificial Thermal Aging on the Crystallinity of XLPE Insulation Cables: X-ray Study. Annual Report, Conference on Electrical Insulation and Dielectric Phenomena.

Burns, N., R. Eichhorn and C. Reid (1992). "Stress Controlling Semiconductive Shields in Medium Voltage Power Distribution Cables". IEEE Electrical Insulation Magazine, **8**(5): pp. 8-24.

Carstensen, P., A. A. Farkas, A. Campus and U. H. Nilsson (2005). The Effect of the Thermal History on the Space Charge Accumulation in HVDC Crosslinked Polyethylene Cables. Annual Report, Conference on Electrical Insulation and Dielectric Phenomena: pp. 381-388.

CENELEC HD620. Distribution cables with extruded insulation for rated voltages from 3,6/6 (7,2)kV to 20,8/36 (42)kV.

Chen, G., Y. L. Chong and M. Fu (2006). "Calibration of the pulsed electroacoustic technique in the presence of trapped charge". Measurement Science and Technology, **17**: pp. 1974-1980.

Chen, G., M. Fu, X. Z. Liu and L. S. Zhong (2005). "ac aging and space-charge characteristics in low-density polyethylene polymeric insulation". Journal of Applied Physics, **97**: 083713.

Chen, G., Y. Tanaka, T. Takada and L. Zhong (2004). "Effect of Polyethylene Interface on Space Charge Formation". IEEE Transactions on Dielectrics and Electrical Insulation, **11**(1): pp. 113-121.

Chong, Y. L., G. Chen, I. L. Hosier, A. S. Vaughan and Y. F. F. Ho (2005). "Heat treatment of cross-linked polyethylene and its effect on morphology and space charge evolution". IEEE Transactions on Dielectrics and Electrical Insulation, **12**(6): pp. 1209-1221.

Choo, W. and G. Chen (2008). Electric Field Determination in DC Polymeric Power Cable in the Presence of Space Charge and Temperature Gradient under dc Conditions. In: Proceeding of 2008 International Conference on Condition Monitoring and Diagnosis: pp. 321-324.

Christen, T (2004). A simple model for DC-conduction and space-charge formation in insulation material. In: Proceeding of The International Conference on Solid Dielectrics: pp. 513-516.

Delpino, S., D. Fabiani, G. C. Montanari, L. A. Dissado, C. Laurent and G. Teyssedre (2007). Fast charge packet dynamics in XLPE insulated cable models. Annual Report, Conference on Electrical Insulation and Dielectric Phenomena: pp. 421-424.

Dissado, L. A. and J. H. Fothergill (1992). "Electrical Degradation and Breakdown in Polymers". Peter Peregrinus Ltd., London, United Kingdom.

Donald, B. et al (1978). "Standard Handbook for Electrical Engineers (11th Edition)". McGraw Hill.

Fabiani, F., G. C. Montanari, R. Bodega, P. H. F. Morshuis, C. Laurent and L. A. Dissado (2006). The Effect of Temperature Gradient on Space Charge and Electric Field Distribution of HVDC Cable Models. In: Proceeding of 8th International Conference on Properties and Applications of Dielectric Materials: pp. 65-68.

Fabiani, F., G. C. Montanari, C. Laurent, G. Teyssedre, P. H. F. Morshuis, R. Bodega, L. A. Dissado, A. Campus and U. H. Nilsson (2007). "Polymeric HVDC Cable Design and Space Charge Accumulation. Part 1: Insulation/Semicon Interface".

IEEE Electrical Insulation Magazine, **23**(6): pp. 11-19.
Fleming, R. J. (2005). "Space Charge Profiles Measurement Techniques: Recent Advances and Future Directions". IEEE Transactions on Dielectrics and Electrical Insulation, **12**(5): pp. 967-978.
Fothergill, J. C., G. C. Montanari, G. C. Stevens, C. Laurent, G. Teyssedre, L. A. Dissado, U. H. Nilsson and G. Platbrood (2003). "Electrical, Microstructural, Physical and Chemical Characterization of HV XLPE Cable Peelings for an Electrical Aging Diagnostic Data Base". IEEE Transactions on Dielectrics and Electrical Insulation, **10**(3): pp. 514-527.
Frutos, F., M. Acedo, M. Mudarra, J. Belana, J. Òrrit, J. A. Diego, J. C. Cañadas and J. Sellarès (2007). "Effect of annealing on conductivity in XLPE mid-voltage cable insulation". Journal of Electrostatics, **65**(2): pp. 122-131.
Fu, M. (2002). "Space Charge Measurement in Polymer Insulated Power Cables Using the PEA Method". PhD Thesis, University of Southampton, United Kingdom.
Fu, M., G. Chen, A. E. Davies and J. G. Head (2000a). Space Charge Measurements in Power Cables using a Modified PEA System. In: Proceeding of 8th International Conference on Dielectric Materials, Measurements and Applications: pp. 74-79.
Fu, M., G. Chen, A. E. Davies and J. Head (2001b). Space charge measurements in cables using the PEA method:-signal data processing considerations. In: Proceedings of the International Conference on Solid Dielectrics: pp. 219-222.
Fu, M., G. Chen, L.A Dissado, J.C. Fothergill (2007). "Influence of Thermal treatment and Residues on Space Charge Accumulation in XLPE for DC Power Cable Application". IEEE Transactions on Dielectrics and Electrical Insulation, **14**(1): pp. 53-64.
Fu, M., L. A. Dissado, G. Chen and J. C. Fothergill (2008). "Space Charge Formation and its Modified Electric Field under Applied Voltage Reversal and Temperature Gradient in XLPE Cable". IEEE Transactions on Dielectrics and Electrical Insulation, **15**(3): 851-860.
Fukuda, F., S. Irie, Y. Asada, M. Maeda, H. Nakagawa and N. Yamada (2002). "The Effect of Morphology on the Impulse Voltage Breakdown in XLPE Cable Insulation". IEEE Transactions on Dielectrics and Electrical Insulation, **17**(5): pp. 386-391.
Fukunaga, K., H. Miyata, M. Sugimori and T. Takada (1990). "Measurement of Charge Distribution in the Insulation of CAbles Using Pulsed Electroacoustic Method". IEE Transactions Japan, **110-A**(9): pp. 647-648.
Fukunaga, K., H. Miyata, T. Takahaashi, S. Yoshida and T. Niwa (1991). Measurement of Space Charge Distribution in Cable Insulation Using the Pulsed Electroacoustic Method. In: Proceeding of 3rd International Conference on Polymeric Insulated Power Cables (JICABLE 1991): pp. 520-525.
Gallot-lavallee, O. and G. Teyssedre (2004). Space charge measurement in solid dielectrics by pulsed electro-acoustic technique. In: Proceeding of 2004 IEEE International Conference Solid Dielectrics: pp. 268-271.
Garton, A., J. H. Groeger and J. L. Henry. (1990). "Ionic impurities in crosslinked polyethylene cable insulation". IEEE Transactions on Electrical Insulation, **25**(2): pp. 427-434.
Goshowaki, M., I. Endoh, K. Noguchi, U. Kawabe and Y. Sekii (2007). "Influence of antioxidants on electrical conduction in LDPE and XLPE". Journal of Electrostatics, **65**(9): pp. 551-554.
Hampton, N. (1995). Insulations for polymeric supertension cables. In: Proceeding of IEE Two Day Colloquium Supertension: pp. 511-515.
Hampton, N., R. Hartlein, H. Lennartsson, H. Orton and R. Ramachandran (2007).

"Long-life XLPE Insulated Power Cable". JiCable07.
Hanley, T. L., R. P. Burford, R. J. Fleming and K. W. Barber (2003). "A general review of polymeric insulation for use in HVDC cables". IEEE Electrical Insulation Magazine, **19**(1): pp. 13-24.
Ho, Y. F. F., G. Chen, A. E. Davies, S. G. Swingler, S. J. Sutton and R. N. Hampton (2003). "Effect of semiconducting screen on the space charge dynamic in XLPE and Polyolefin Insulation under dc and 50 Hz AC electric stresses conditions". IEEE Transactions on Dielectrics and Electrical Insulation, **10**(3): pp. 393-403.
Holbøll, J. T., M. Henriksen and J. Hjerrild (2000). Space Charge Build-up in XLPE-Cable with Temperature Gradient. Annual Report, Conference on Electrical Insulation and Dielectric Phenomena: pp. 157-160.
Holé, S., T. Ditchi and J. Lewiner (2003). "Non-destructive Methods for Space Charge Distribution Measurements: What are the Differences?". IEEE Transactions on Dielectrics and Electrical Insulation, **10**(4): pp. 670-677.
Hozumi, N., T. Okamoto and T. Imajo (1992). Space Charge Distribution Measurement In A Long Size XLPE Cable Using The Pulse Electroacoustic Method. IEEE International Symposium on Electrical Insulation: pp. 294-297.
Hozumi, N., T. Takeda, H. Suzuki and T. Okamoto (1998). "Space Charge Behavior in XLPE under 0.2-1.2 MV/cm DC Fields". IEEE Transactions on Dielectrics and Electrical Insulation, **5**(1): pp. 82-90.
ICEA Publication S-97-682 (1999). Standard for Utility Power Cables Rated 5 through 46 kV.
Ida, N. (2004). "Engineering Electromagnetics". Springer-Verlag New York, LLC.
Ieda, M. (1984). "Electrical Conduction and Carrier Traps in Polymeric Materials". IEEE Transactions on Dielectrics and Electrical Insulation, **19**(3): pp. 162-175.
Ishikawa, I., S. Nakamura, S. Utsunomiya, S. Yamamoto and T. Niwa (1994). The Research of Peroxide Decomposition in XLPE Cables. Annual Report, Conference on Electrical Insulation and Dielectric Phenomena.
Jones, J. P., J.P. Llewellyn and T.J. Lewis (2005). "The contribution of Field-Induced Morphological Change to the Electrical Aging and Breakdown of Polyethylene". IEEE Transactions on Dielectrics and Electrical Insulation, **12**(5): pp. 951-966.
Kao, K. C. and W. Hwang (1981). "Electrical Transport in Solids". Pergamon Press.
Kawasaki, K., Y. Arai and T. Takada (1991). "Two-Dimensional Measurement of Electrical Surface Charge Distribution on Insulating Material by Electrooptic Pockels Effect". Japanese Journal of Applied Physics, **30**(6): pp. 1262-1265.
Kon, H., T. Mizutani, Y. Suzuoki and H. Shigetsugu (1994). High-Field Conduction and Space Charge in Polyethylene. In: Proceeding of Annual Report, Conference on Electrical Insulation and Dielectric Phenomena: pp. 268-273.
Salah Khalil, M. (1997). "International research and development trends and problems of HVDC cables with polymeric insulation". IEEE Electrical Insulation Magazine, **13**(6): pp. 35-47.
Khalil, M. S. and J. A. Jevase (2000). Development of Polymeric Insulating Materials for HVDC Using Additives: Evidence from a Multitude of Experiments using Different Techniques. IEEE International Symposium on Electrical Insulation. pp 485-488
Khalil, M. S. and B. S. Hansen (1988). "Investigation of Space Charge in Low-Density Polyethylene Using a Field Probe Technique". IEEE Transactions on Dielectrics and Electrical Insulation, **23**(3): 441-445.
Lalam, F and Hoang. (2000). "Pressure effect on the electrical ageing of polyethylene". Journal of Applied Physics D, **33**: pp. L133-L136.
Lang, S. B. and D. K. Das-Gupta (1981). "A Technique for Determination the

Polarization Distribution in Thin Polymer Electrets Using Periodic Heating," Ferroelectrics **39**(1): pp. 1249-1252.

Lau, W. S. and G. Chen (2006). Simultaneous space charge and conduction current measurements in solid dielectrics under high dc electric field. In: Proceeding of 2008 International Conference on Condition Monitoring and Diagnosis.

Lee, D. C., N. H. Lee, T. Mizutani and M. Ieda (1988). Thermally Stimulated Current Due to Ionic Carriers in Polysulfone. In: Proceeding of 2nd International Conference on Properties and Applications of Dielectric Materials: pp. 363-366.

Levy, R. A. (1968). "Principles of Solid State Physics". Academic Press.

Lewiner, J. (1986). "Evolution of Experimental Techniques for the Study of the Electrical Properties of Insulating Materials". IEEE Transactions on Dielectrics and Electrical Insulation, **EI-21**(3):pp. 351-360.

Lewis, T. J. (1955a). Some Factors Influencing Field Emission and Fowler-Nordheim Law. In: Proceeding of the Physical Society, Section B **68**(11): pp. 938-943.

Lewis, T. J. (2002b). "Polyethylene under Electrical Stress". IEEE Transactions on Dielectrics and Electrical Insulation, **9**(5): pp. 717-729.

Li, K. C., K. C. Tang, J. S. Lee, C. L. Chao and R. K. Chang (1997). "Thermal Stimulated Current Study of Core-Shell Impact Modifier/PVC Blends". Journal of Vinyl and Additive Technology, **3**(1): 17-20.

Li, Y. and T. Takada (1992). "Experimental Observation of Charge Transport and Injection in XLPE at Polarity Reversal". Journal of Applied Physics D, **25**: pp. 704-716.

Li, Y. and T. Takada (1994). "Progress in space charge measurement of solid insulating materials in Japan". IEEE Electrical Insulation Magazine, **10**(5): pp. 16-28.

Li, Y., M. Yasuda and T. Takada (1994). "Pulsed Electroacoustic Method for Measurement of Charge Accumulation in Solid Dielectrics". IEEE Transactions on Dielectrics and Electrical Insulation, **1**(2): pp. 188-195.

Lim, F. N. and R. J. Fleming (1999). The Temperature Dependence of Space Charge Accumulation and DC Current in XLPE Power Cable Insulation. In: Proceeding of Annual Report, Conference on Electrical Insulation and Dielectric Phenomena: pp. 66-69.

Lim, F. N., R. J. Fleming and R. D. Naybour (1999). "Space Charge Accumulation in Power Cable XLPE Insulation". IEEE Transactions on Dielectrics and Electrical Insulation, **6**(3): pp. 273-281.

Long, W. and S. Nilsson (2007). "HVDC transmission: yesterday and today". IEEE Power and Energy Magazine, **5**(2): pp. 22-31.

Liu, R., T. Takada and N. Takasu (1993). "Pulsed Electoacoustic Method for Measurement of Space Charge Distribution in Power Cables under Both Dc and Ac Eletric Field". Journal of Physics D: Applied Physics, **26**: pp. 986-993.

Liu, Z., R. Liu, H. Wang and W. Liu (1989). "Space Charges and Initiation of Electrical Trees". IEEE Transactions on Dielectrics and Electrical Insulation, **24**(1): pp. 83-90.

Maeno, T., T. Futami, H. Kushibe, T. Takada and C. M. Cooke (1988). "Measurement of Spatial Charge Distribution in Thick Dielectrics using the Pulsed Electroacoustic Method". IEEE Transactions on Dielectrics and Electrical Insulation, **23**(3): pp. 433-439.

Maeno, T., H. Kushibe, T. Takada and C. M. Cooke (1985). Pulsed Electro-Acoustic Method for the Measurement of Volume Charges in E-Beam Irradiated PMMA. Annual Report, Conference on Electrical Insulation and Dielectric Phenomena.

Maeno, Y., N. Hirai, Y. Ohki, T. Tanaka, M. Okashita and T. Maeno (2005). "Effects of Crosslinking Byproducts on Space Charge Formation in Crosslinked

Polyethylene". IEEE Transactions on Dielectrics and Electrical Insulation, **12**(1): pp. 90-97.
Malec, D. (2000). "Technical Problems Encountered with the Laser Induced Pressure Pulse Method in Studies of High Voltage Cable Insulators". Measurement Science and Technology, **11**(5): pp. N76-N80.
Many, A. and G. Rakavy (1962). "Theory of Transient Space-Charge-Limited Currents in Solids in the Presence of Trapping". Physical Review, **126**(6): pp. 1980-1988.
Maruyama, S., N. Ishii, M. Shimada, S. Kojima, H. Tanaka, M. Asano, T. Yamanaka and S. Kawakami (2004). "Development of a 500-kV DC XLPE Cable System", Furukawa Review, **25**: pp. 47-52.
Mellinger, A., R. Singh and R. Gerhard-Multhaupt (2005). "Fast Thermal-Pulse Measurements of Space Charge Distributions in Electret Polymers". Review of Scientific Instruments, **76**: 013903.
Meunier, M., N. Quirke and A. Aslanides (2001). "Molecular modeling of electron traps in polymer insulators: Chemical defects and impurities". Journal of Chemical Physics, **115**(6): pp. 2876-2881.
Migliori, A. and T. Hofler (1982). "Use of Laser-Generated Acoustic Pulses to Measure the Electric Field inside a Solid Dielectric". Review of Scientific Instruments, **53**(5): pp. 662-666.
Mizutani, T. (1994). "Space Charge Measurement Techniques and Space Charge in Polyethylene". IEEE Transactions on Dielectrics and Electrical Insulation, **1**(5): pp. 923-933.
Molinié, P. (2005). "Measuring and modeling transient insulator response to charging: the contribution of surface potential studies". IEEE Transactions on Dielectrics and Electrical Insulation, **12**(5): pp. 939-950.
Montanari, G. C., C. Laurent, G.Teyssedre, A. Campus and U.H. Nilsson (2005). "From LDPE to XLPE: Investigating the Change of Electrical Properties. Part I: Space Charge, Conduction and Lifetime". IEEE Transactions on Dielectrics and Electrical Insulation, **12**(3): pp. 438-444.
Montanari, G. C., G. Mazzanti, F. Palmieri, A. Motori, G. Perego and S. Serra (2001). "Space-charge trapping and conduction in LDPE, HDPE and XLPE". Journal of Applied Physics D, **34**: pp. 2902-2911.
Montanari, G. C., G. Mazzanti, F. Palmieri, G. Perego and S. Serra (2001). Dependence of Space-Charge trapping Threshold on Temperature in Polymeric DC Cables. In: Proceeding of The International Conference On Solid Dielectrics: pp. 81- 84.
Morse, P. M. and K. U. Ingrad (1968). "Theoretical Acoustic". McGraw-Hill Book Company, New York.
Morshuis, P. H. F. and M. Jeroense (1997). "Space Charge Measurements on Impregnated paper: A Review of the PEA Method and A Discussion of the Results". IEEE Electrical Insulation Magazine, **13**(3): pp. 26-35.
Muronaka, T., Y. Tanaka, T. Takada, S. Maruyama and H. Mutou (1996). Measurement of Space Charge Distribution in XLPE using PEA system with Flat Electrode. In: Proceeding of Annual Report, Conference on Electrical Insulation and Dielectric Phenomena: pp. 266-269.
Murooka, Y., T. Takada and K. Hidaka (2001). "Nanosecond Surface Discharge and Charge Density Evaluation Part I: Review and Experiments". IEEE Electrical Insulation Magazine, **17**(2): 6-16.
Neagu, E. R., and C. J. Dias (2009). "Charge Injection/extraction at a Metal-dielectric Interface: Experimental Validation". IEEE Electrical Insulation Magazine, **25**(1): pp. 15-22.
Notingher jr, P., S. Agnel and A. Toureille (2001). "Thermal step method for space

charge measurements under applied dc field". IEEE Transactions on Dielectrics and Electrical Insulation, **8**(6): pp. 985 – 994.
Orton, H. E and R. Hartlein (2006). Long-life XLPE-insulated Power Cables.
Pascoe, K. J. (1973). "Properties of Materials for Electrical Engineers". J. Wiley and Sons.
Pollock, D. D. (1993). "Physical Properties of Materials for Engineers." CRC Press.
Precopio, F. and A. Gilbert (1999). "The Invention of Chemically Crosslinked Polyethylene". IEEE Electrical Insulation Magazine, **15**(1): pp. 23-25.
Roland, C. (1979). "Physics of Dielectrics for the Engineer". Elsevier Scientific Publishing Company.
Roy, S. Le., P. Segur, G. Teyssedre and C. Laurent (2003) "Description of bipolar charge transport in polyethylene using a fluid model with a constant mobility: model prediction". Journal of Applied Physics D, **37**: pp. 298-305.
Rudervall, R., J. Charpentier, and R. Sharma (2000). "High voltage direct current (HVDC) transmission systems technology review paper". In Energy Week, Washington, D.C, USA.
Sanden. B, E. Ildstad and R. Hegergerg (1996). Space Charge Accumulation and Conduction Current in XLPE Insulation. Conference on Dielectric Materials, Measurements and Applications: pp. 368-373.
See. A, L. A. Dissado and J. C. Fothergill (2001). "Electric field criteria for charge packet formation and movement in XLPE". IEEE Transactions on Dielectrics and Electrical Insulation, **8**(6): pp. 859-866.
Sekii, Y., T. Ohbayashi, T. Uchimura, K. Mochizuki, and T. Maeno (2002). The Effects of Material Properties and Inclusions on the Space Charge Profiles of LDPE and XLPE. Annual Report, Conference on Electrical Insulation and Dielectric Phenomena: pp. 635-639.
Serra, S., E. Tosatti, S. Iarlori, S. Scandolo, G. Santoro and M. Albertini (1998). Interchain States and the Negative Electron Affinity of Polyethylene. Annual Report, Conference on Electrical Insulation and Dielectric Phenomena: pp. 19-22.
Sessler, G. M. (1982a). "Nondestructive Laser Method for Measuring Chrage Profiles in Irradiated Polymer Films". IEEE Transactions on Nuclear Science, **NS-29**: pp. 1644-1649.
Sessler, G. M. (1997b). "Charge distribution and transport in polymers". IEEE Transactions on Dielectrics and Electrical Insulation, **4**(5): pp. 614-628.
Sessler, G. M., J. E. West and R. Gerhard (1982). "High-resolution Laser-pulse Method for Measuring Charge Distribution in Dielectrics". Physical Review Letters, **48**: pp. 563-566.
Sessler, G. M., J. E. West and R. Gerhard (1981). "Measurement of Charge Distribution in Polymer Electrets by a New Pressure-Pulse Method," Polymer Bulletin **6**(1-2): pp. 109-111.
Solymar, L. and D. Walsh (1999) "Electrical Properties of Materials". Oxford University Press.
Suh, K. S., S. J. Hwang, J. S. Noh and T. Takada (1994). "Effects of Constituents of XLPE on the Formation of Space Charge". IEEE Transactions on Dielectrics and Electrical Insulation, **1**(6): pp. 1077-1083.
Sze, S. M. (1981) "Physics of Semiconductor Devices". J. Wiley and Sons.
Takada, T. (1999). "Acoustic and Optical Methods for Measuring Electric Charge Distributions in Dielectrics". IEEE Transactions on Dielectrics and Electrical Insulation, **6**(5): pp. 519-547.
Takada, T. and N. Hozumi (2000). "Space Charge Measurements as a Diagnostic Tool

for Power Cables". IEEE Power Engineering Society Winter Meeting, **3**: pp. 1609-1614.

Takada, T. and T. Sakai (1983). "Measurement of Electric Fields at a Dielectric/electrode Interface Using an Acoustic Transducer Technique". IEEE Transactions on Dielectrics and Electrical Insulation, **EI-18**(6): pp. 619-628.

Takeda, T., N. Hozumi, H. Suzuki, K. Fujii, K. Terashima, M. Hara, Y. Murata, K. Watanabe and M. Yoshida (1998). "Space charge behavior in full-size 250 kV DC XLPE cables". IEEE Transactions on Power Delivery, **13**(1): 28-39.

Tanaka, T. and A. Greenwood (1983a). "Advanced Power Cable Technology Volume I". CRC Press Inc. USA.

Tanaka, T. and A. Greenwood (1983b). "Advanced Power Cable Technology Volume II". CRC Press Inc. USA.

Tanaka, Y., G. Chen, Y. Zhao, A. E. Davies, A. S. Vaughan and T. Takada (2003). "Effect of addictives on morphology and space charge accumulation in low density polyethylene". IEEE Transactions on Dielectrics and Electrical Insulation, **10**(1): 148-154.

Tanaka, Y., T. Takada, C. Shinoda and T. Hashizume (1994). Temperature Dependence of Space Charge Distribution in XLPE Cable. Annual Report, Conference on Electrical Insulation and Dielectric Phenomena.

Toriyama, Y. (1961). "Dust Figure of Surface Discharge and Its Application". Kinokuniya Bookstore.

Turton, R. (2000). "The Physics of Solids". Oxford University Press.

Vlastós, A. E. (1989). DC conduction of polymeric insulation of medium voltage cables. In: Proceeding of the 3rd International Conference on Conduction and Breakdown in Solid Dielectrics: pp. 287-293.

Wang, X., D. Tu, Y. Tanaka, T. Muronaka, T. Takada, C. Shinoda and T. Hashizumi (1995). "Space charge in XLPE power cable under dc electrical Stress and heat treatment". IEEE Transactions on Dielectrics and Electrical Insulation, **2**(3): pp. 467-474.

Weedy, B. M. (1980). "Underground Transmission of Electric Power". J. Wiley and Sons.

Weedy, B. M. and D. Chu (1984). "HVDC extruded cables – Parameters for determination of stresses". IEEE Transactions on Power Apparatus and Systems Insulation, **PAS-103**(3): 662-667.

Wu, X., G. Chen, A. E. Davies, R. N. Hampton, S. J. Sutton and S. G. Swingler (2001). "Space charge measurements in polymeric HV Insulation Materials". IEEE Transactions on Dielectrics and Electrical Insulation, **8**(4): pp. 725-730.

Xu, Z., W. Choo and G. Chen (2007). DC electric field distribution in planar dielectric in the presence of space charge. In: Proceedings of the International Conference on Solid Dielectrics: pp. 514-517

Yamanaka, T., S. Maruyama and T. Tanaka (2003). The Development of DC +/- 500 kV XLPE Cable in Consideration of the Space Charge Accumulation. In: Proceeding of 7th International Conference on Properties and Applications of Dielectric Materials: pp. 689-694.

Zhang, Y., J. Lewiner, C. Alquie and N. Hampton (1996). "Evidence of Strong Correlation Between Space-charge Buildup and Breakdown in Cable Insulation". IEEE Transactions on Dielectrics and Electrical Insulation, **3**(6): pp. 778-783.

Appendix A Numerical Model

The aim of this appendix is to provide the reader a detailed description on the numerical model used to solve the coupled problem (electrostatic and thermal) encounter in this work. COMSOL Multiphysics software was used in this thesis.

Drawing the profile of the cable is the first step in the geometry sequence. By using the **Draw** menu, select **Specify Objects** and with **Circle** option selected**.** The cable's aluminium core is drawn by inserting the radius value of the core.

From the space charge measurement PEA system we can get a charge density distribution across the thickness of the cable insulation. The PEA system will provide this data in a vector of 500 elements. Knowing the thickness of the sample being measured and the distribution within the insulation one can determine the distribution of charge across the sample.

For different conditions and thickness of the cable we found out that using a smaller number of data points we can correctly recreate the charge distributions across the sample, hence we used a smaller number of data points in creating the numerical model. For example in one of the cases studied we have used 105 data points, hence for an insulation thickness of 3.4 mm one can calculate the thickness of the partition to be used in the model as thickness divided by the number of data points, in this case the partition thickness was 0.03238 mm. The whole insulation is then portioned in 105 concentric equal thickness parts, and the charge in each of them is assigned accordingly such that

the measured distribution is well approximated.

Using the **Create Composite Objects** from the **Draw** menu and setting the **Formula** (Larger circle – Smaller circle), ring of each individual insulation partition are created based on the cable geometry, as illustrated in Figure A-1.

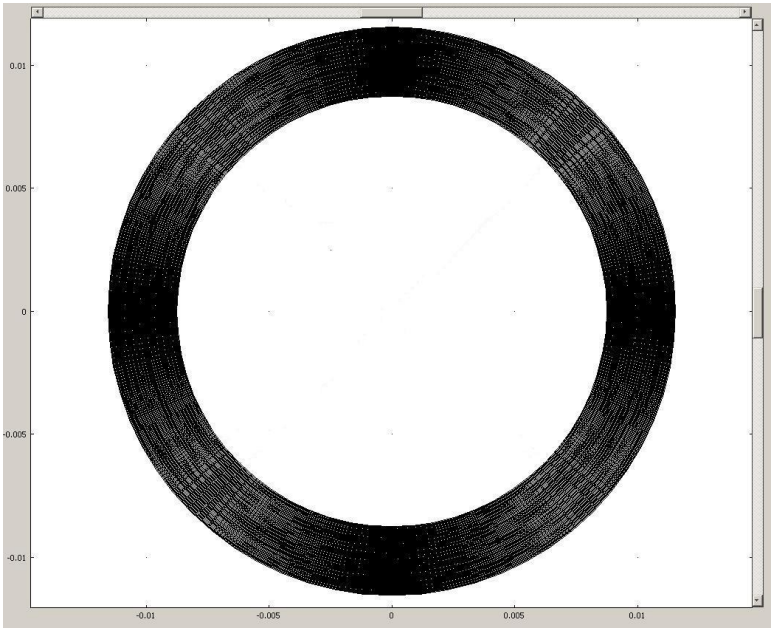

Figure A-1: The drawing of the cable geometry

This procedure results in creating model for the whole cross-section of the cable. Due to the high aspect ratio of the model – diameter of the cable much bigger than the thickness of each partition, the mesh generated will be very large as being controlled by the smallest feature in the modelled. For example the mesh for the test case described above had almost one million elements. With the computers at hand we could not solve such a large size problems; however it is not necessary to solve such a large model because the problem has an inherent symmetry. Actually the 2D problem to be solved can be simplified to a 1D case. We did not go all the way to the extreme 1D case but we have reduced the size of the problem to 1/32. This reduction can be applied providing that the correct boundary conditions are set. The resulting model needed only a mesh of about 22000 elements, which a huge reduction in the size of the problem that needed to be solved. Such a problem it is easily handled by desktop computer. The reduced model is shown in Figure A-2.

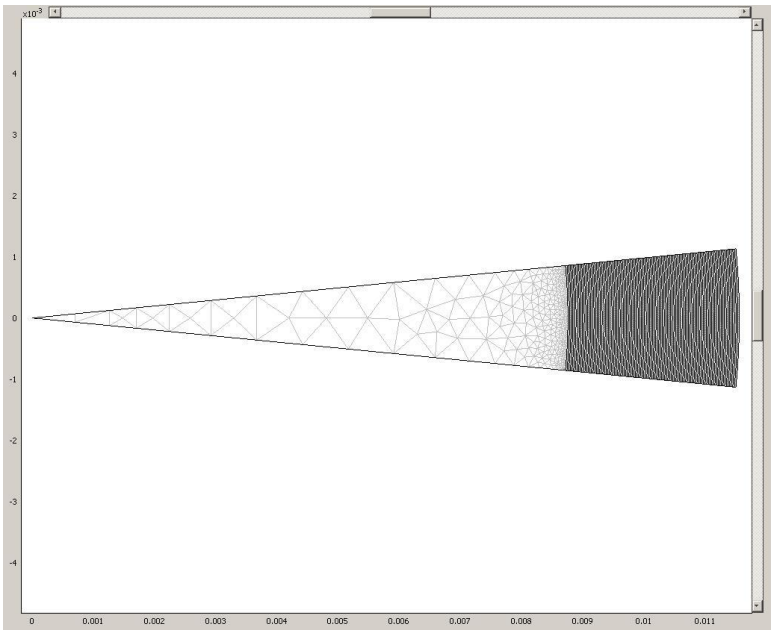

Figure A-2: The drawing of a scaled down cable geometry

Heat Transfer Module by Conduction

To build up the heat transfer module, the **Subdomain Settings (F8)** was selected and through the **Physics Tab > Library material** both aluminium and polyethylene (XLPE) were chosen from the materials list based on the drawing's subdomain group respectively as shown in the example in Figure A-3.

In the **Initial Tab**, **Initial value** is selected and the value, Ta, is inserted as the initial temperature value for subdomain selection 1 (aluminium) as shown in the above Figure. The remaining subdomain selection group will have the value, Tb, inserted as the initial temperature value. The temperature values of Ta and Tb are inserted at **Options > Contants** window as these values will create the temperature gradient effect.

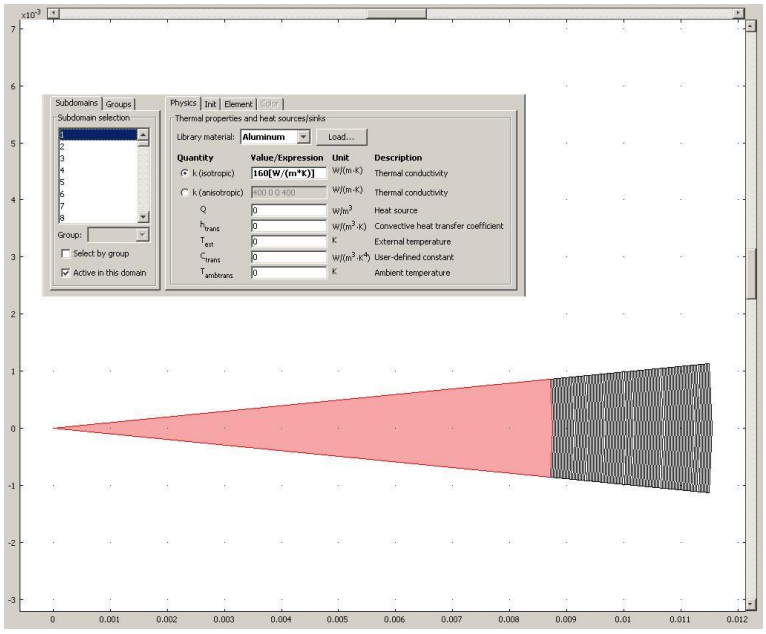

Figure A-3: Heat transfer module subdomain setting

Boundary conditions were then set up in **Boundary Setting (F7)**. As shown in Figure A-4, the boundary conditions surrounding the cable's core is set as Temperature with T_0 = Ta in the **Conditions** Tab. The boundary conditions across the insulation (partitions) were all set as Continuity and with the last boundary at the end of the insulation set as Temperature with T_0 = Tb in the **Conditions Tab**.

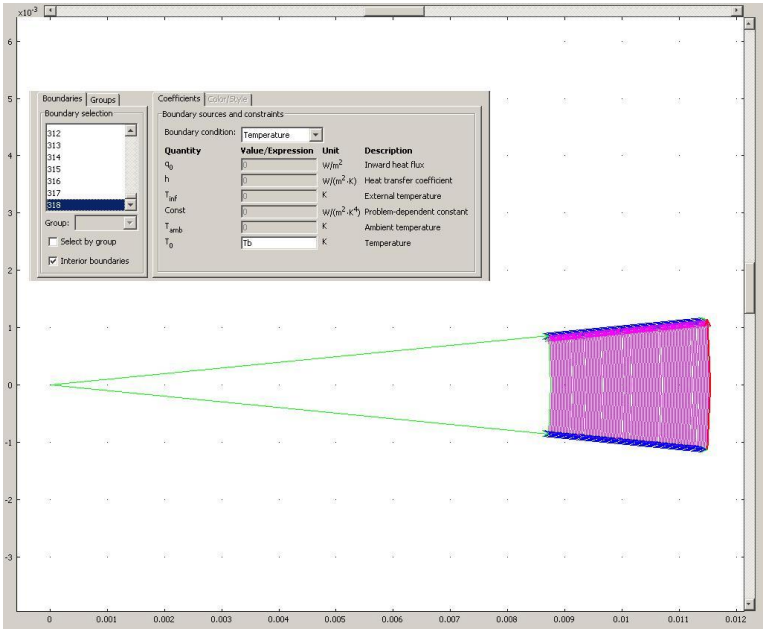

Figure A-4: Heat transfer module boundary setting

Electrostatic Module

In this module, two sets of electrostatic modules were used, namely for the calculation of applied field and space charge field respectively. Subsequently, by summing both fields together the total electric field across the insulation can be obtained.

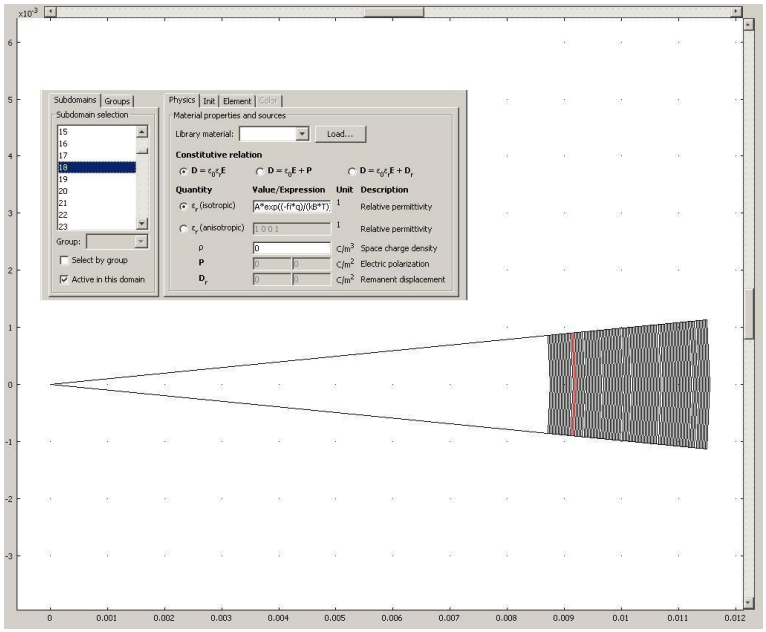

Figure A-5: Electrostatic module for applied field subdomain setting

In the electrostatic module for applied field, the conductivity equation was inserted to the system by replacing permittivity slot in the **Subdomain Settings (F8)** window for the insulation's subdomain group as shown in Figure A-5. For the cable's core, aluminium was selected from the **Physics Tab > Library material**, where the value of 1 is automatically inserted to the slot based from the aluminium's properties.

In the **Boundary Setting (F7)** window under the **Conditions Tab** as shown in Figure A-6, **Symmetry** was chosen for the selected boundary group. For the boundaries within the insulation, **Continuity** was chosen. Lastly, **Electric potential** and **Ground** was chosen for the inner and outer insulation boundaries respectively.

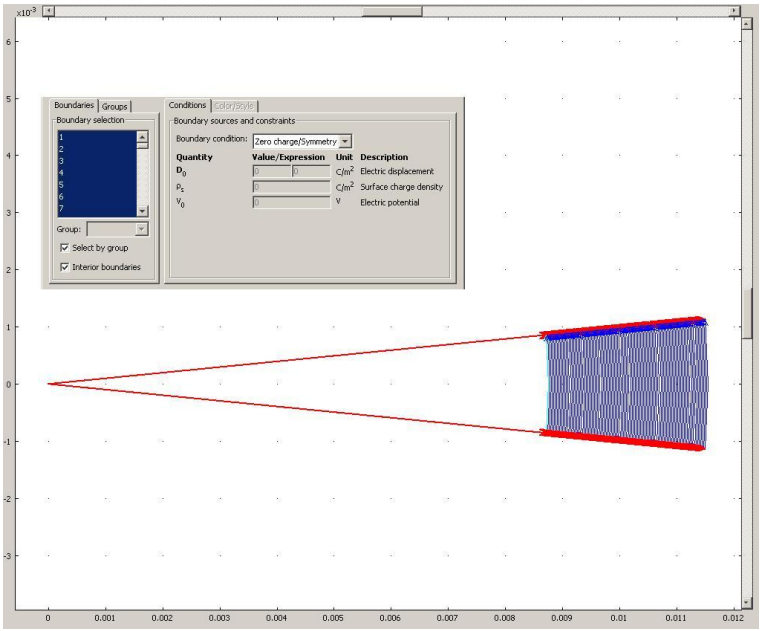

Figure A-6: Electrostatic module for applied field boundary setting

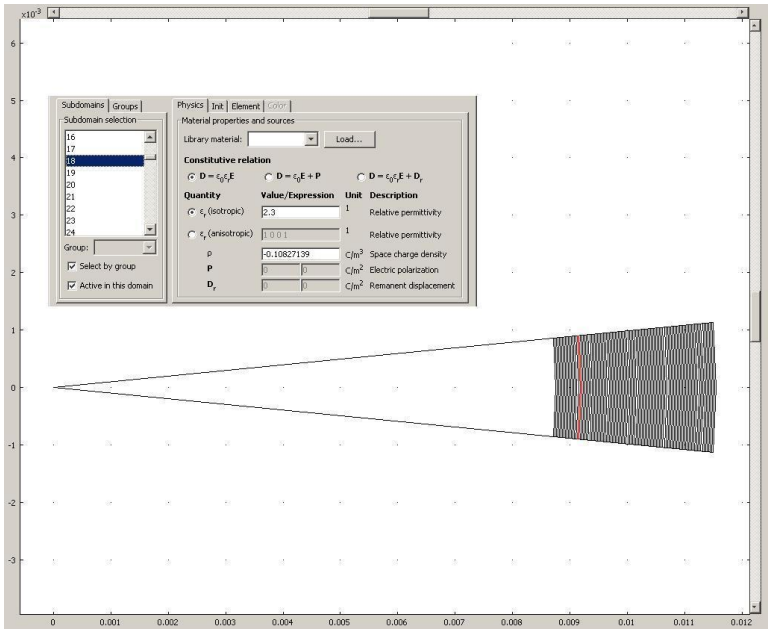

Figure A-7: Electrostatic module for space charge field subdomain setting

In the electrostatic module for space charge field, the **Boundary Setting (F7)** and the cable's aluminium core **Subdomain Settings (F8)** was set up in the same manner as mentioned earlier. In addition, the individual values of space charge measurements obtained across the insulation were inserted to their respective **Space charge density**

slot as shown in Figure A-7.

With all modules set up, the value of the dependent variables were then inserted to the **Options > Constants** window as shown below

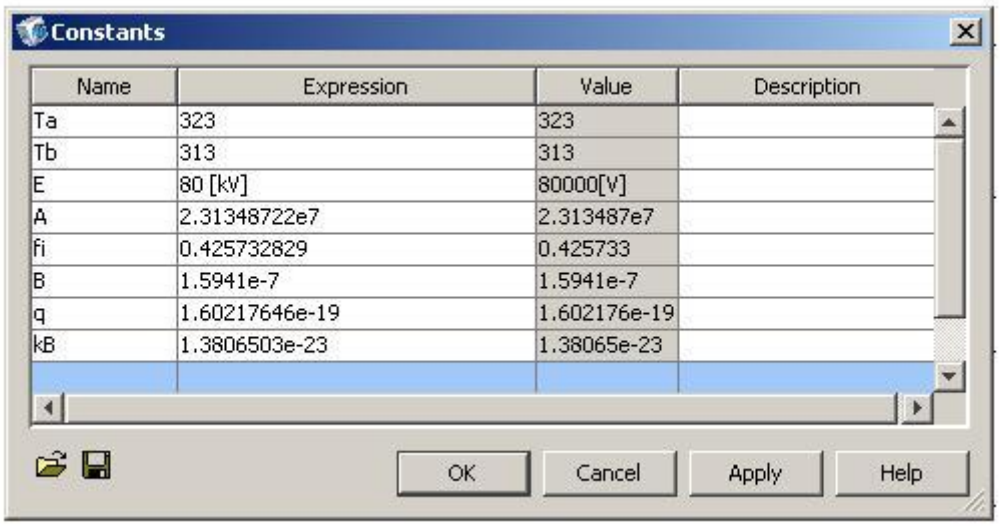

Figure A-8: Value of the dependent variables inserted to the constants window

The values for the insulation's inner temperature, Ta, outer temperature, Tb, constant values A and B are dependent on the temperature gradient conditions set towards the experiments.

Finally, to solve the multiphysics model, go to **Solve** menu > **Solver Manager** and click **Solve** button.

Appendix B Calculation of Constant B in the Hopping Model

The purpose of this appendix is to provide the computational details used to calculate constant B for the hopping model in Chapter 7.4. A MATLAB code has been written for this purpose. The code is listed below:

```
% y = f(B) = sinh(B*E1) - k sinh(B*E2)
% Obtain value of B when y=0

E1=2.344e7;                    % Applied field in V/m
E2=3.456e7;                    % Applied field in V/m
sig1=8.042e-7;                 % Conductivity value for E1
sig2=1.686e-6;                 % Conductivity value for E2

k=(sig1/sig2)*(E1/E2)          % Ratio value of k

u=2e-8;                        % Estimation region of B [u ≤ B ≤ v]
v=1.1e-7;                      % Estimation region of B [u ≤ B ≤ v]

y1=sinh(u*E1)-k*sinh(u*E2)     % f(u)
y2=sinh(v*E1)-k*sinh(v*E2)     % f(v) where f(u)*f(v) < 0
```

```
t=(u+v)/2;                          % Getting the estimated value of B through
                                    division of two
y=sinh(t*E1)-k*sinh(t*E2);          % f(t)

while abs(y)>1e-7                   % Setting the error as 1e-7
if y*y1<0
v=t;                                % Replace v with t as Bϵ[u,t]
elseif y*y1>0
u=t;                                % Replace u with t as Bϵ[t,v]
end

t=(u+v)/2;                          % Repeat t until the values of f(u) and f(v)
                                    are almost equal and obtaining the last
                                    value
y=sinh(t*E1)-k*sinh(t*E2);          % New f(t)
y1=sinh(u*E1)-k*sinh(u*E2);         % New f(u)
y2=sinh(v*E1)-k*sinh(v*E2);         % New f(v)
end

B=t                                 % Final value of B when y=0
```